

NIPTERK P-32 SPRAY ICE ISLAND

ABLATION PROTECTION EXPERIMENT

BY

J.P. POPLIN

ERCLRS.89.24

PROPRIETARY

**To
Oct 15, 1994**

JANUARY 1990

SUMMARY

This report documents results of the Nipterk P-32 Spray Ice Island Ablation Protection Experiment. The experiment was carried out by Esso Resources Canada Limited as a joint-industry project. The other original participants are Chevron Resources Canada Ltd., Canada Oil and Gas Lands Administration/ U.S. Minerals Management Service, and Mobil Research and Development Corporation.

The experiment was undertaken to assess the feasibility of various methods for extending the use of exploration spray ice platforms through breakup and into the summer season. The objective of this research was to develop technology that could contribute toward providing significant increases in available drilling and testing time as well as the feasibility to offset construction and/or drilling problems by demobilizing the rig after landfast ice breakup. Additionally, the technology developed from this study could offer the potential benefit of extending the application of spray ice platforms into deeper waters.

Nipterk Spray Ice Island was constructed during the 1988/1989 winter in the southern Canadian Beaufort Sea off the MacKenzie River Delta at Latitude N60° 41' 46.9" and Longitude W135° 22' 42.5" in a water depth of 6.5 m. The ice island originally had a 320 m grounded diameter and a 3.5 to 4.5 m freeboard.

Test plots consisting of different configurations and thicknesses of sawdust, various thicknesses of gravel, fabric sheets, and wood were constructed atop the spray ice to assess the degree of ablation protection each afforded. All of these materials provided at least some measure of ablation protection. The most effective materials were 15 cm thick sawdust bags, 20 cm thick timbers, and a layer of gravel greater than 0.6 m thick. Each of these materials drastically limited the magnitude of cumulative spray ice surface ablation to amounts less than 20 cm over the duration of the experiment.

Above-freezing air temperatures were prevalent from late-May until the island broke up. This condition along with solar radiation were most responsible for the average of 2.25 m of spray ice ablation documented in the unprotected portion of

the island through July . However, even relatively thin layers of materials on the surface provided substantial ablation protection leading to the conclusion that surface ablation can be effectively mitigated and managed in a cost effective manner with the use of coatings.

A portion of the experiment was designed to evaluate the performance of impermeable sheets draped over the edge of the island to protect the edges from mechanical and thermal wave erosion due to wave action and currents. Open water conditions persisted after breakup until the island completely disintegrated two and one-half weeks later. The island appeared to break up predominantly due to lack of freeboard rather than from wave erosion. Still the degree of stabilization afforded by the edge protection system both in regard to edge erosion and surface ablation protection was readily apparent leading to the conclusion that the rate of edge erosion can be significantly decreased by deploying a system of impermeable fabric sheets and nets.

Breakup of the landfast ice occurred by June 24. The island withstood ice forces imposed on it during breakup without undergoing any apparent sliding along the seafloor. A thermal equilibrium condition in the spray ice was reached by June 10 when the temperature throughout the island was very close to 0°C. The island mass decreased rapidly following the advent of landfast ice breakup due to an instability condition resulting from loss of freeboard and mechanical and thermal wave and current erosion. The final island remnant broke up on July 10, some two and one-half weeks following breakup of the surrounding ice sheet. The water temperature measured the day following complete island disintegration was 12°C.

Studies relating to barge docking and trafficability were not fully addressed as part of the experiment due to the relatively early breakup of the island. However, based on a supplemental study drawing upon operational experiences of spray ice features in western Alaska by a subcontractor, the edge of a spray ice island can be shaped by excavating with a backhoe or crane and wheelwashing with a tugboat to provide a barge docking area. The method of rig demobilization would be similar to that used for sand islands.

As a result of this experiment it is concluded that drilling operations on a spray ice platform can be extended to at least June 1 and potentially beyond. It is also

concluded that marine demobilization of a drilling rig is feasible. Even with the relatively early breakup of Nipterk, ice conditions would have enabled sufficient time to complete the rig demobilization effort.

The most promising materials for surface ablation protection are gravel, sawdust, and rig mats in areas where minimal ablation is needed and tarps and extra spray ice (i.e. higher freeboard) where ablation only need be reduced. Similarly, the most promising method of edge protection against waves and currents is covering the island edge with impermeable fabric sheets.

TABLE OF CONTENTS

	PAGE
SUMMARY	ii
INTRODUCTION	1
PRIOR FIELD EXPERIENCE	1
EXPERIMENT OBJECTIVES	2
BACKGROUND	3
GEOGRAPHIC LOCATION, OCEANOGRAPHIC AND LANDFAST	
ICE CONDITIONS	3
ISLAND CONSTRUCTION OVERVIEW	5
EXPERIMENT INSTALLATION	8
EXPERIMENT SITE SELECTION	8
INSTALLATION SCHEDULE AND LOCATION	11
EDGE EROSION PROTECTION SYSTEM	13
ABLATION TEST PLOTS	18
Surface Ablation Measurement Stakes	20
Additional Instrumentation	20
MONITORING SURVEYS	22
RESULTS	24
METEOROLOGICAL CONDITIONS	24
ICE TEMPERATURE	26
WATER TEMPERATURE	29
SURFACE ABLATION	30
Unprotected Spray Ice	32
Ablation Test Plot Measurements	36
Sheets and Insulated Tarp	37
Sawdust Plots	38
Gravel Plots	42
Simulated Rig Mat Plot	45
Ablation Test Plot Comparisons	46
Spray Ice Temperatures Beneath Ablation Plots	46

Additional Spray Ice Ablation Observations	49
ABLATION SUMMARY AND IMPLICATIONS	52
ISLAND EROSION	54
EROSION RATES	63
Previous Information	63
Numerical Simulation	64
Background	64
Overview	64
ISLAND BREAKUP	69
DEMOBILIZATION OF THE EDGE PROTECTION SYSTEM	72
ISLAND SETTLEMENT	72
ISLAND HORIZONTAL MOVEMENT	75
EXTENDED SPRAY ICE OPERATIONS	79
Overview	79
CONCLUSIONS	83
RECOMMENDATIONS	86
ACKNOWLEDGMENTS	87
REFERENCES	88
APPENDIX A: METEOROLOGICAL MEASUREMENTS	A
APPENDIX B: ICE TEMPERATURE MEASUREMENTS	B
APPENDIX C: ABLATION MEASUREMENTS	C
APPENDIX D: ANNOTATED SLIDE SET	D
APPENDIX E: ABLATION AND EROSION NUMERICAL SIMULATION	E
APPENDIX F: SETTLEMENT MEASUREMENTS	F
APPENDIX G: ISLAND HORIZONTAL MOVEMENT MEASUREMENTS	G

APPENDIX H: EXTENDED OPERATIONS ON SPRAY ICE

H

LIST OF FIGURES

FIGURE		PAGE
1	Nipterk P-32 Location Plan	4
2	Site Bathymetry and Initial Ice Thickness as Measured in Mid-November, 1988	6
3	Island Design Geometry	7
4	As-Built Contour Map of Island	10
5	Island Edge Protection System and Ablation Plot Layouts	14
6	Layout of Sawdust Ablation Test Plots	19
7	Locations of Sondex Settlement and Slope Indicator Survey Stations	21
8	Experiment Timetable	23
9	Comparison of 1989 and Historical Air Temperatures	25
10	Configuration of Spray Ice/Seabed Thermistor String	27
11	Spray Ice/Seabed Temperature Profiles	28
12	Energy Transfer Parameters	31
13	Cumulative Ablation of Unprotected Spray Ice	32
14	Sheet/Tarp Ablation Mitigation Comparisons	37
15	Sawdust Ablation Test Plot Comparisons	40
16	Gravel Ablation Test Plot Comparisons	43
17	Selected Ablation Test Plot Data Comparisons	47
18	Sprayed Ice Temperatures Beneath Gravel Plots	48
19	Spray Ice Temperatures Beneath Selected Ablation Plots	49
20	Comparison of Original and Remaining Island Area on July 5	59
21	Comparison of Original and Remnant Island Areas on July 8	61
22	Ablation of the Top Surface of the Ice Island Compared with Measured Data	66
23	Comparison Between Measured and Modeled Ice Meltback Under 1 cm of Sawdust	67

FIGURE

PAGE

24	Results of the Use of Different Wave Parameters in the Perimeter Erosion Model	68
25	Spray Ice Settlement at the Southwest Survey Station	74
26	Southwest Slope Indicator Station Deformation Profiles (North- South Direction)	78
27	Southwest Slope Indicator Station Deformation Profiles (East-West Direction)	78

LIST OF PLATES

PLATE		PAGE
1a	Oblique Aerial View of Nipterk on April 21	9
1b	View of Island From Ice Level	9
2	Island Edge View of Erosion Protection System Shortly After Installation	16
3	Close-up of Sandbag Attachment	16
4	Front End Loader Equipped with Auger Shown Drilling An Anchor Hole	17
5	Hummocks Created by Differential Ablation of the Spray Ice Surface as Observed on June 10	35
6	Water Collected on Sheets as Observed on June 10	39
7a	Sawdust Ablation Plot on April 23	41
7b	Sawdust Ablation Plot on July 5	41
8	Ablation Differences Between Spray Ice Covered with Spent Drilling Mud and Unprotected Spray Ice	51
9a	Aerial View of Nipterk on June 22	56
9b	Aerial View of Nipterk on July 5	57
9c	Aerial View of Nipterk on July 8	57

LIST OF TABLES

TABLE		PAGE
1	Spray Ice Island Summary	1
2	Experiment Installation Schedule	12
3	Comparison of Observed and Predicted Thaw Beneath Gravel Pads	45

INTRODUCTION

PRIOR FIELD EXPERIENCE

The use of grounded spray ice platforms for exploration drilling in shallow waters of the Beaufort Sea has been successfully demonstrated. To date, two spray ice platforms have been constructed in Canada by Esso and two have been built in Alaska, one by Amoco and the other by Chevron (see table 1).

Table 1. Spray Ice Island Summary

Year	1986	1987	1989	1989
Operator	Amoco	Esso	Esso	Chevron
Name	Mars	Angasak L-03	Nipterk P-32	Karluk
Location	U.S.	Canadian	Canadian	U.S.
	Beaufort Sea	Beaufort Sea	Beaufort Sea	Beaufort Sea
Water Depth	7.6 m	5.6 m	6.5 m	7.6 m

There are three major advantages for using spray ice platforms. First, they are less costly to construct and drill from than other platforms such as steel or concrete structures and dredged sand and/or gravel islands, particularly in instances when borrow materials are not available nearby. Second, they are more attractive from an environmental standpoint than sand islands since manmade ice islands are constructed with the local water supply and break up during the summer season. Third, because of their size and the relative degree of ductility they afford, spray ice islands are capable of protecting the drilling rig from ice forces which are the major design criterion in the Beaufort Sea. These advantages provide strong motivation to advance the technology of spray ice and thereby extend the applicability of spray ice platforms.

To date, the use of spray ice islands has been limited to water depths 7.6 m and shallower. Moreover, the drilling and testing window has been restricted to about 75 days. Extension of spray ice platforms into deeper waters would reduce the length of drilling window even further.

EXPERIMENT OBJECTIVES

Over the past few years, Esso Resources Canada Limited (ERCL) has been active in researching methods to extend spray ice technology into deeper waters and to increase the length of the drilling and testing period available with the use of these structures. Useful improvements have been made and opportunities for "breakthrough" advances identified. One such advance would be to demobilize the rig onto barges in late June after landfast ice breakup rather than via floating ice road in late April which is the current method. This approach would enable drilling operations to continue through May and potentially longer, leading to a 50 to 100% increase in the drilling and testing period and/or water depth range. However, before such an approach could be applied, confirmatory research was deemed necessary.

Towards this end, the Nipterk Spray Ice Island Ablation Protection Experiment was undertaken to assess the feasibility of various methods for extending the use of exploration spray ice platforms through breakup and possibly into the summer season. The objective of this research was to develop technology that could contribute toward providing significant additional drilling and testing time as well as the flexibility to offset construction and/or drilling problems by demobilizing the rig after breakup. Additionally, the technology developed from this study could offer the potential benefit of extending the application of spray ice platforms into deeper water.

The overall goal of this project was to develop sufficient knowledge of ablation, erosion rates, and protective methods to allow the marine demobilization option to be included in the plans for future spray ice islands. Specific objectives were to:

- monitor surface ablation and edge erosion rates until early summer,
- assess the effectiveness of various methods toward mitigating ablation and erosion,
- assess surface trafficability and edge stability in relation to docking and off-loading,
- investigate methods of improving surface trafficability and edge stability, and

- assess how methods of providing edge protection could be developed to extend the operational life of spray ice islands into the open-water season.

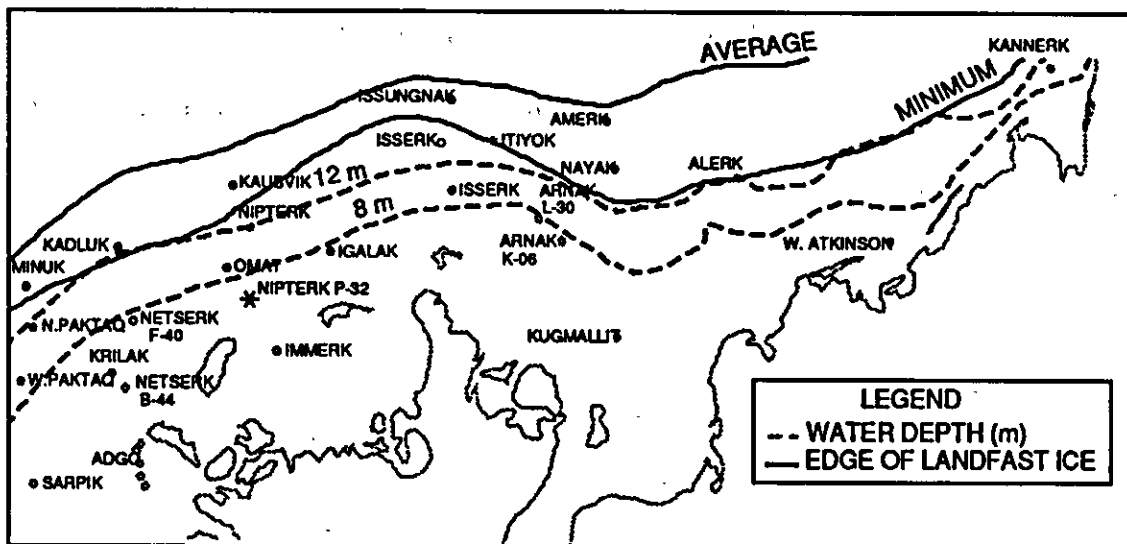
These objectives were accomplished by covering sections of the island with various thicknesses and configurations of gravel, sawdust, timbers, and white tarpaulins. Spray ice surface ablation was measured for each of these areas during the study period. Impermeable fabric sheets and netting were also used over a portion of the island in an attempt to reduce wave erosion after breakup of the surrounding ice sheet. Measurements of edge erosion were carried out from late-June until the island broke up in July.

Tasks addressing surface trafficability, edge stability, and docking were not fully addressed as part of the field experiment due to the relatively early breakup of the island. Consequently, a supplemental study drawing upon operational experiences of spray ice features in western Alaska was performed by a subcontractor and the pertinent results included in this report.

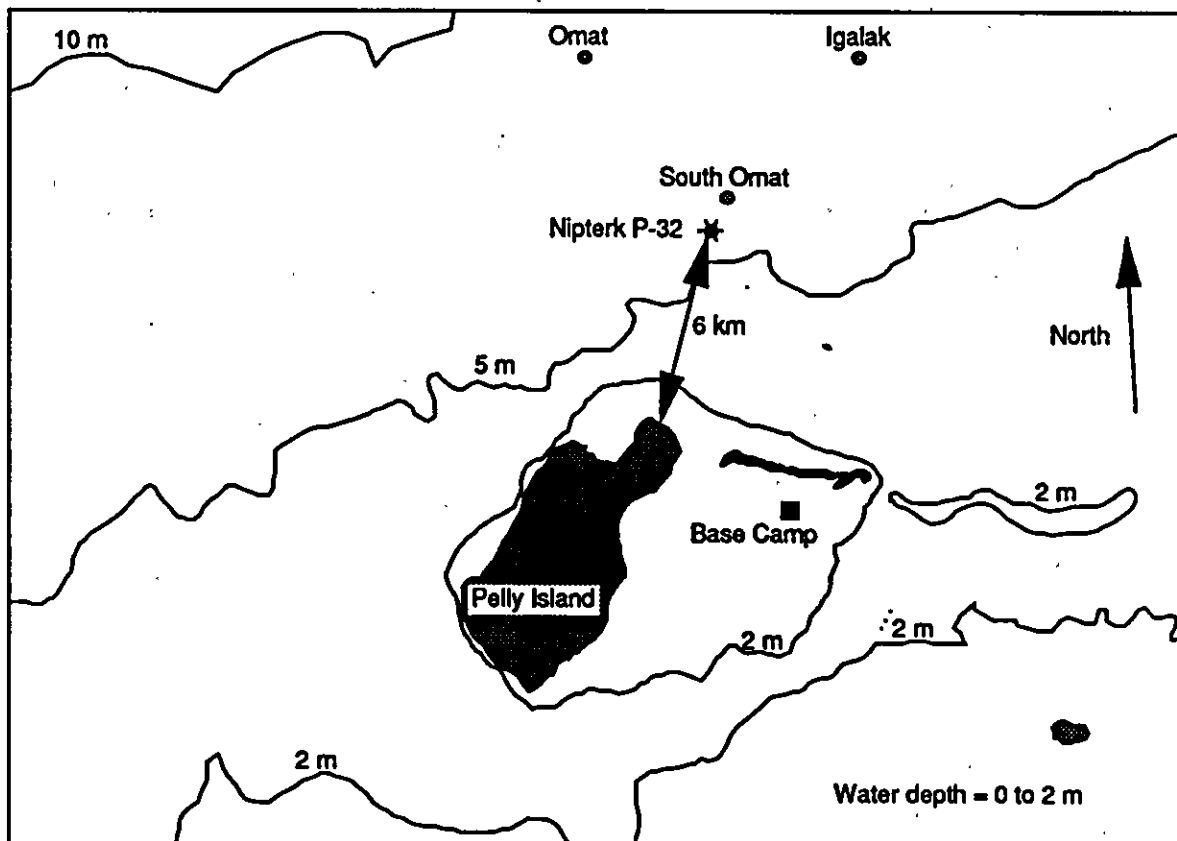
BACKGROUND

GEOGRAPHIC LOCATION, OCEANOGRAPHIC AND LANDFAST ICE CONDITIONS

Nipterk P-32 Spray Ice Island was constructed during the 1988/89 winter. The well location was off the MacKenzie River Delta, 6 km north-northeast of Pelly Island at Latitude N60° 41' 46.9" and Longitude W135° 22' 42.5". The island location is indicated in Figure 1. Dashed lines in Figure 1a denote the 8 and 12 m water depth contours. Average and minimum extents of the landfast ice are depicted by solid lines. As can be seen, the island was well within a relatively stable ice regime. A number of other Beaufort Sea wells drilled from sand islands and/or caissons are also shown. Figure 1b is a map which provides a more detailed view of the island location. The camp, construction equipment, and drilling consumables were transported aboard ice-strengthened barges deployed in September 1988 behind the Pelly Island Spit. The link to the island was via a 10 km long floating ice road.



(a)



(b)

Figure 1. Nipterk P-32 Location Plan

Bathymetry was measured at the site prior to island construction and found to average 6.5 m with a range of 6.38 to 6.65 m, inclusive. A map showing water depth measurements at the site is presented as Figure 2. Included in the figure are ice thicknesses measured in mid-November. Note that the first-year ice sheet was rubbled and rafted.

Ice and water column salinity and temperature profiles were measured in mid-November, 1988. At the time, fresh water was present to a depth 4 m below the surface. The remainder of the water column consisted of saline (15 ppt) water. Water temperatures ranged from about 0°C in the freshwater layer to about -1°C in the saline layer.

ISLAND CONSTRUCTION OVERVIEW

In response to an early freezeup, full-scale spray ice construction operations commenced November 28, 1988 and were completed 53 days later on January 20, 1989. Island construction involved four identical spray units enclosed in skid-mounted containers. Each unit consisted of a diesel engine, a 12,000 liters per minute capacity suction pump, and a spray monitor that could be programmed to sweep from side to side. Several nozzle configurations were used to optimize spray ice productivity at the different air temperatures and wind speeds experienced during the construction period.

A diagram showing the island design geometry is presented as Figure 3. Several environmental conditions necessitated that the design of Nipterk be different than previously constructed spray ice islands. First, Nipterk was built at a more exposed location. Second, the seabed soils were relatively weak which necessitated that the size of the island be greater. Third, due to its proximity to the MacKenzie River, source water used to construct the island was essentially fresh, resulting in warmer underwater spray ice.

Island construction was performed in three phases. The submerged portion of the island was largely built during the initial phase in layers 1 to 3 m thick. Spray pumps were frequently repositioned to provide total island coverage. The working surface drilling pad (150 m diameter) was built to final grade in Phase II by

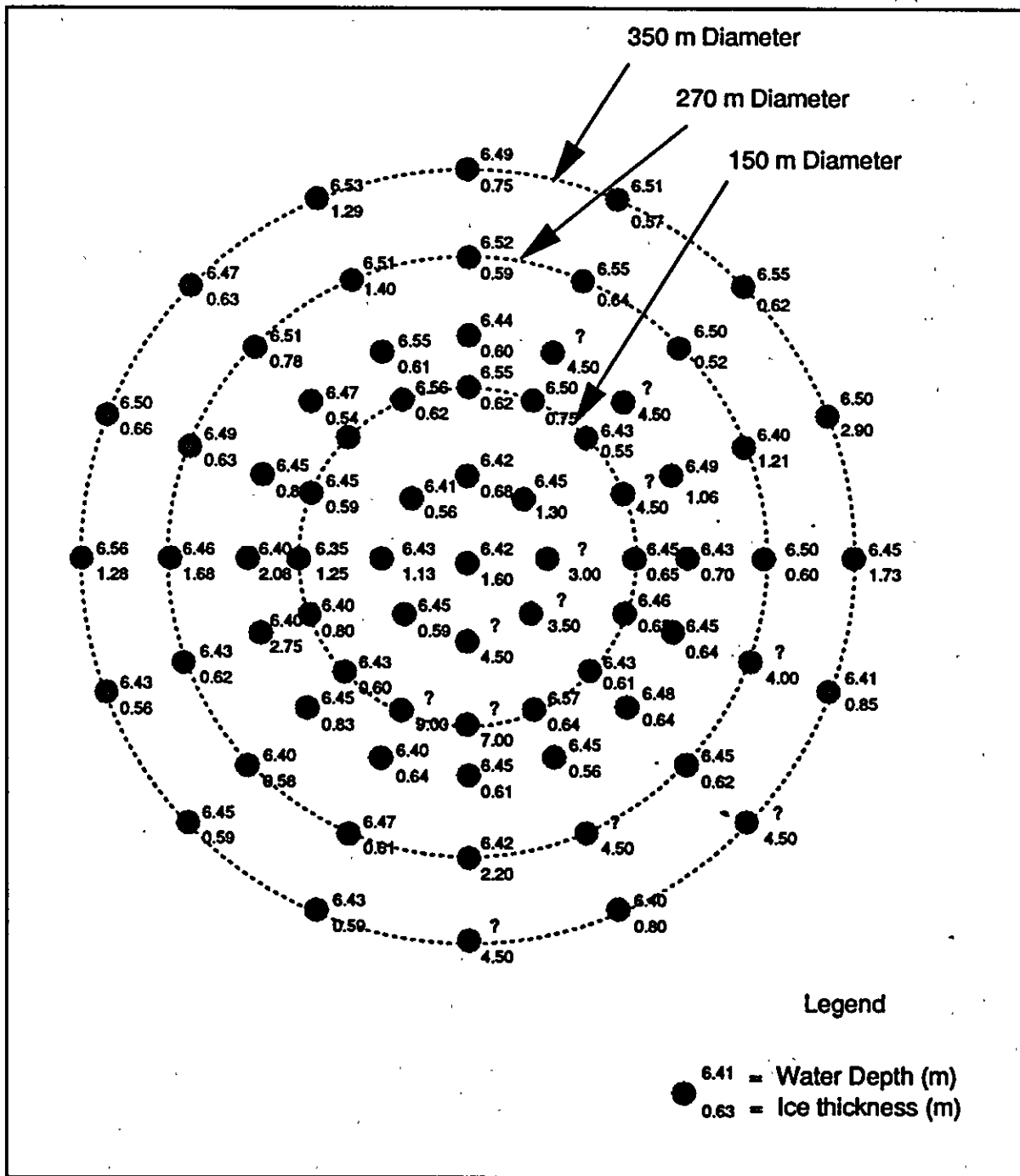


Figure 2. Site Bathymetry and Initial Ice Thicknesses as Measured in Mid-November, 1988.

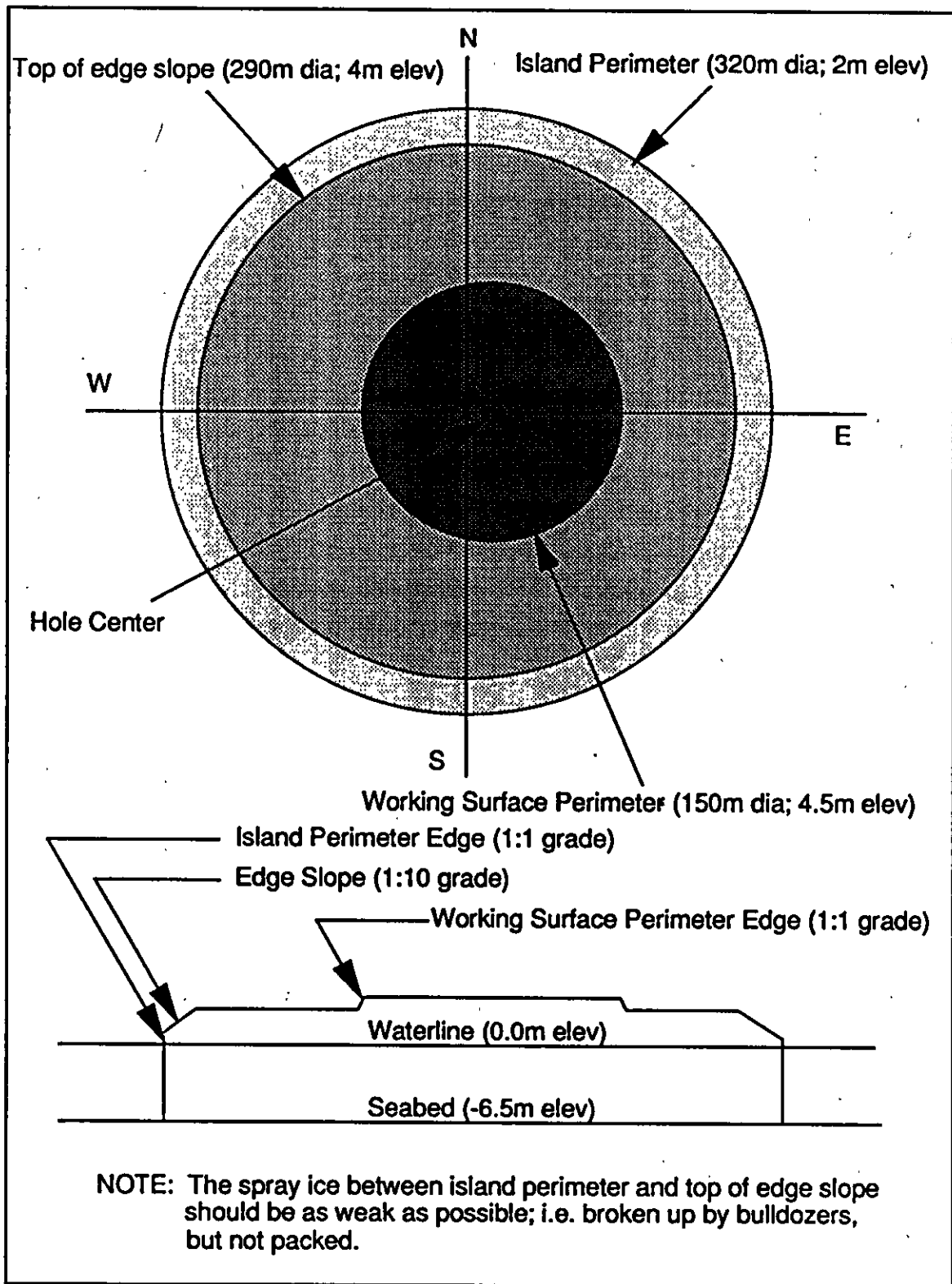


Figure 3. Island Design Geometry

positioning the pumps about 100 m from island center, directing spray toward the center and using bulldozers (Caterpillars) to both pack and level the spray ice. Due to the roughness of the first-year ice sheet, the island grounded unevenly. This condition resulted in the formation of cracks which were subsequently filled with reworked spray ice. Finally, the remainder of the island was built to grade during the last phase of construction. Oblique aerial and ground-based island photographs are shown in Plate 1.

A spray ice volume of approximately 825,000 m³ was required to complete the island. The island seabed contact (or grounded) area was estimated from about 125 thermally drilled holes, 21 gravity penetrometer tests, and 13 cone penetrometer tests. An as-built contour map of the island is presented as Figure 4. The average freeboard over the 150 m diameter island working surface was 4.15 m. The remainder of the grounded region had an average freeboard of 3.73 m. Freeboard gradually diminished as the island settled. The amount of settlement between the end of construction (January 20) and the time of maximum design ice load (May 1) was estimated to be less than 0.5 m.

EXPERIMENT INSTALLATION

EXPERIMENT SITE SELECTION

Two site selection options were considered during the early planning stages of the experiment. One option investigated was to protect a portion of the Nipterk island. The other option evaluated was to protect the relief well pad, a 125 m diameter spray ice feature built over a five day period in March, about 500 m east of Nipterk P-32.

There were a number of disadvantages identified with using the relief well pad. First, a road to the site was required. Second, bulldozers would have been needed to flatten the island surface since, unlike Nipterk, the relief pad was not leveled after construction. Third, between two and three times more tarpaulin material would have been necessary to protect the relief pad than for a test section on Nipterk. And fourth, ablation measurements on the relief pad would have been unrealistic because the spray ice surface had not been soiled as a result of use.

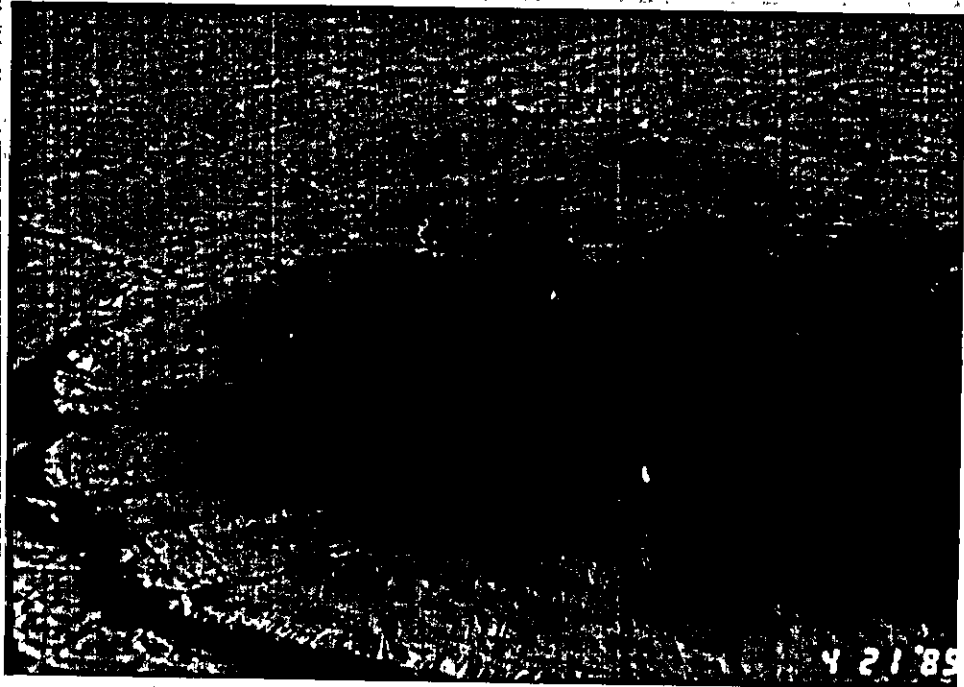


Plate 1a. Oblique Aerial View of Nipterk on April 21

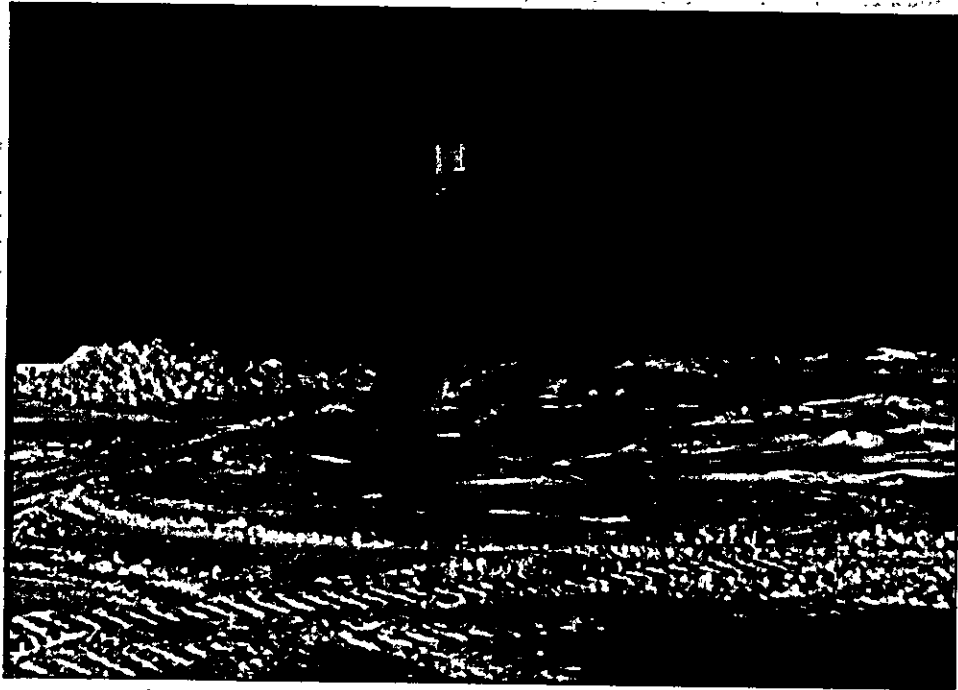


Plate 1b. View of Island From Ice Level

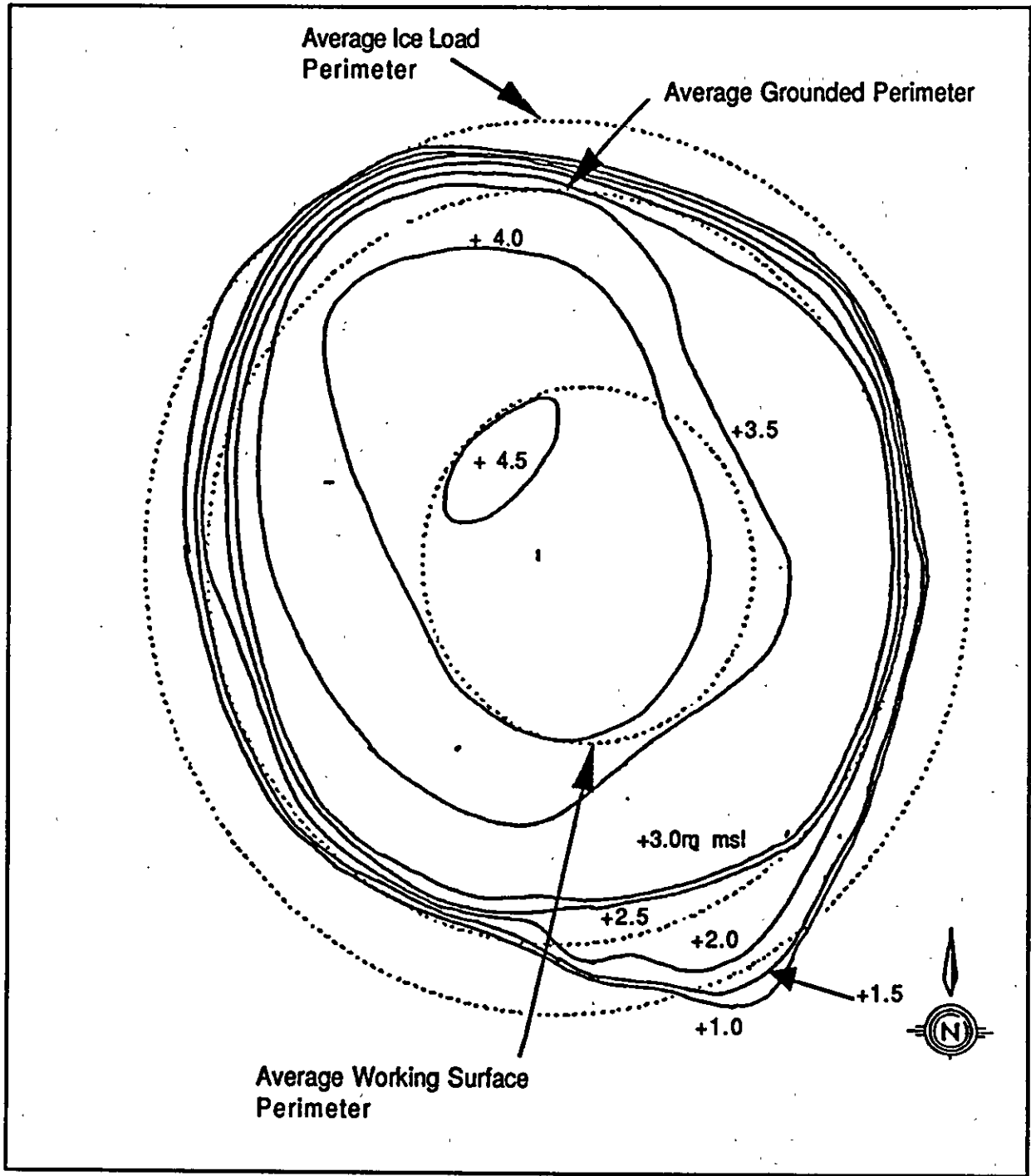


Figure 4. As-Built Contour Map of Island

Utilization of the Nipterk Spray Ice Island offered the following advantages. First, because of the island's size, different edge protection materials could be evaluated. Second, any benefit afforded by the edge protection system could be more easily assessed because most of the island edge was not protected. Third, personnel and equipment necessary for the experiment setup were more readily available and could be drawn upon on an as-needed basis, thus minimizing costs. Finally, instrumentation was already available on Nipterk from the winter monitoring program, enabling measurements of island sliding, settlement, and spray ice temperature to be continued. For these reasons, a decision was made to undertake the experiment on the main island.

INSTALLATION SCHEDULE AND LOCATION

A relatively short lead-time existed for planning, procurement of materials and instrumentation, and experiment installation. These time constraints were imposed by impending ice road closures both north and south of Inuvik as well as demobilization of the drilling rig along with support equipment and personnel. Table 2 is a schedule identifying the major milestones pertaining to the experiment installation.

A proposal describing the study was transmitted to industry and government on March 15. In the meantime, project planning was initiated, equipment suppliers contacted, and competitive bids obtained. Authorization to proceed with the project was received on April 5. Orders were placed immediately thereafter for all of the equipment required. Edge protection sheets were purchased from three suppliers to expedite delivery. Nets were assembled at the Esso Research Lab because they were not available commercially in the time frame required. Approximately 50% of the sandbags were filled in Calgary because gravel availability on the island could not be guaranteed at the time of edge protection system installation. Installation of the island edge protection systems and surface ablation test plots commenced on April 20 and was completed on April 25.

Any side of the island with the possible exception of the north would have been suitable to set up the experiment from a representative environmental condition standpoint. However, the area least affected by drilling operations was the

TABLE 2. EXPERIMENT INSTALLATION SCHEDULE

- MARCH 15 - PROJECT PROPOSAL**
- MARCH 27 - DETAILED PLANNING STARTS
- TARP SUPPLIERS CONTACTED,
- COMPETITIVE BIDS OBTAINED**
- APRIL 5 - PARTICIPANTS COMMITMENT -
- PROJECT GO AHEAD**
- APRIL 6 - ORDER ROPE FOR NETTING
- ORDERS PLACED FOR 3 TARPS
(3 SUPPLIERS)**
- APRIL 10 - INITIATED NET FABRICATION AND
- SANDBAG FILLING AT ESSO LAB**
- APRIL 14 - TRUCK LOADED AND SENT NORTH
- WITH ALL NETS, TARPS & SANDBAGS**
- APRIL 20 - COMMENCE FIELD INSTALLATION**
- APRIL 23 - GRAVEL AND SAWDUST DELIVERED TO
- ISLAND**
- APRIL 25 - INSTALLATION COMPLETE WITH
- EXCEPTION OF ELECTRONIC
- INSTRUMENTATION**

island's west-southwest side. Equipment not essential for the experiment set up was removed from this location prior to April 20. The surface was smoothed and the snowbanks at the island edge leveled to facilitate deployment of the edge protection system.

EDGE EROSION PROTECTION SYSTEM

As illustrated in Figure 5, four edge protection systems were placed along the west-southwest perimeter of the island. They were installed to shield the island edge against thermal and mechanical erosion induced by wave action after break-up of the surrounding ice sheet and to mitigate surface ablation. These consisted of the following:

- Net - a 50 m by 60 m, 1.5 m mesh size net consisting of 13 mm diameter white nylon rope.
- Sheet 1 - 35 m by 50 m, 18 oz. per square yard white polyester reinforced vinyl with roped hems and D-rings on edges.
- Sheet 2 - 35 m by 50 m, 13 oz. per square yard white polyester reinforced vinyl with roped hems and D-rings on edges.
- Sheet 3 - 50 m by 60 m Rufco SB 12 white reinforced polyethylene tarpaulin (pit liner).

The net was designed to hold back fragments of the island once they calved, thus mitigating at least for a while, the affects of wave erosion against the still intact spray ice. This system offered dual advantages of facilitated installation and potentially significantly lower cost especially if polypropylene rope were used and the net mesh spacing increased.

White 13 mm diameter nylon rope was used to manufacture the 50 by 60 m net. Even though the nylon rope was twice as expensive as polypropylene rope, its use

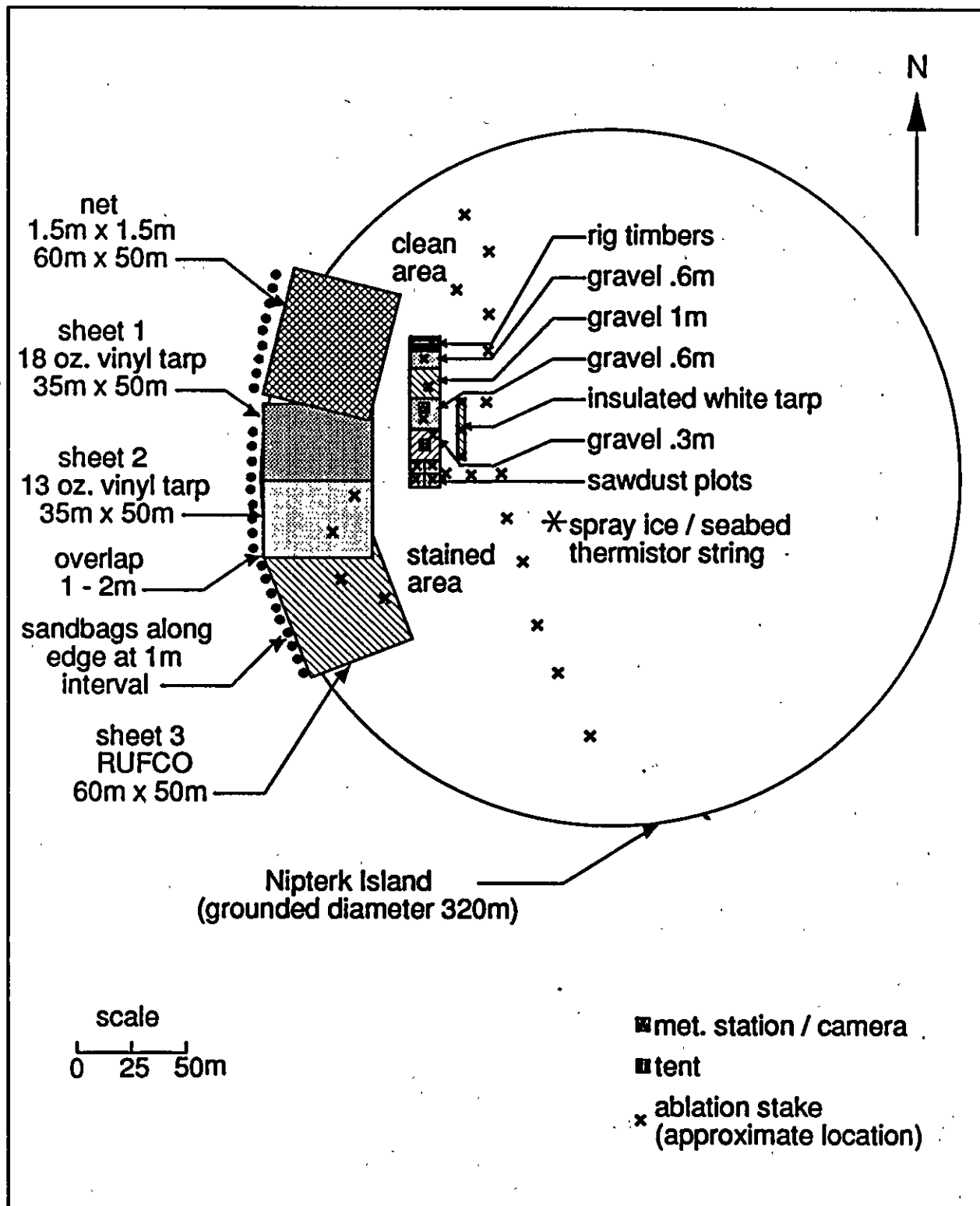


Figure 5. Island Protection System and Ablation Plot Layouts

was justified at the time based on ablation concerns regarding colored material. No white polypropylene rope was available.

The purpose of the sheets was to isolate the island even further from wave erosion by placing an impervious barrier between the island and the sea. Two different weights of polyester were used to evaluate the abrasion resistance of the material (which was identified as an area of concern). A third type of sheet, the Rufco pit liner, was used to evaluate a less expensive option.

Both the sheets and net edge protection systems were extended just beyond the grounded edge of the island perimeter which was denoted by a crack (see Plate 2). The net was relatively easy to deploy with five or six men. Contrastingly, because of their weight and stiffness characteristics in the cold, installation of the sheets required the assistance of a front end loader for handling and unrolling as well as an additional three to six men. Sheet installation took place during a period when winds were less than 10 to 15 knots. One factor which greatly facilitated stretching the sheets over the ice was the presence of entrapped air between the ice and the sheet.

Sheets were overlapped several meters inward of the island and 1 to 2 m outward of the island edge. Nets, consisting of 19 mm polypropylene rope forming 5 m by 5 m mesh were placed atop each protection sheet. Sandbags, each weighing about 14 kg were attached loosely to the radial portion of the net, one at each node (see Plate 3) to help hold the sheet in place. Sandbags were originally placed at about 2.5 m intervals along the island edge.

The inner edge (island-center side) of the net was anchored into the spray ice. This was accomplished by attaching 10 m long ropes to the net and 0.5 m by 0.3 m by 0.3 m wooden timbers to the free end of each rope. A front end loader having an auger attachment (Plate 4) was utilized to drill out 0.3 m diameter, 2-3 m deep holes into which the timbers (anchors) were lowered. The deadmen were subsequently covered with snow which was in turn saturated with water to create ice. To further reduce the potential for premature melt out, anchors were either buried beneath ablation plots or covered with 1 to 1.5 m high piles of snow. The deadmen served as anchors that were designed to melt out before the island broke



**Plate 2. Island Edge View of Erosion Protection System
Shortly After Installation**



Plate 3. Close-up of Sandbag Attachment

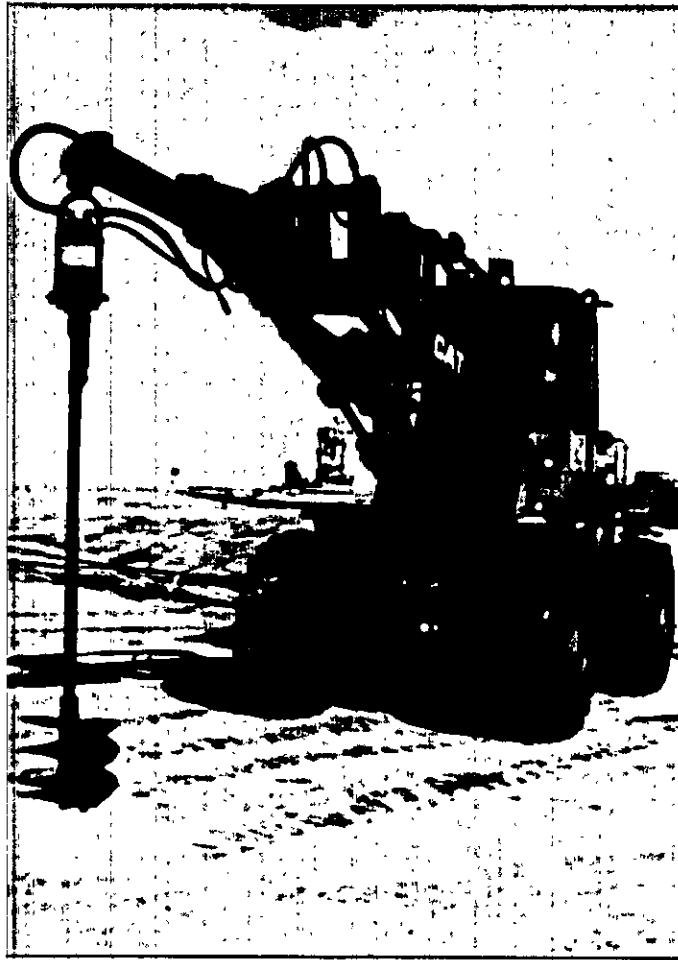


**Plate 4. Front End Loader Equipped With Auger Shown
Drilling an Anchor Hole**

up to facilitate recovery of the sheets. Mounds of snow were also placed along the south edge of the Rufco sheet and atop edges of the other sheets.

ABLATION TEST PLOTS

Test plots designed to assess spray ice ablation were constructed following deployment of the island edge protection systems. A number of different plots of various sizes and configurations were created at the inner edge of the sheets and net (see Fig. 5). These consisted of the following:

- Sawdust 1 cm, 1.5 cm, 2 cm, 3 cm and 15 cm thick bags.
- Gravel Thicknesses of 0.3 m, 0.6 m, and about 1 m. Each plot was approximately 180 m².
- Simulated Rig Mats 20 cm by 20 cm timbers placed side by side to simulate rig mats.
- Insulated Tarp Reinforced white vinyl having dimensions 30.5 m by 2.4 m.
- Sheets Rufco and 13 oz. per square yard polyester reinforced vinyl.
- Ice Unprotected spray ice; both clean and stained.

Approximately 425 m³ of gravel was hauled to the island from a surplus stockpile located about 30 km to the southwest on Garry Island. Once dumped onto the island surface, the gravel was leveled by a front end loader to the desired thicknesses (0.3, 0.6, and 1 m) over areas of about 12 by 15 m.

A 15 m by 15 m sawdust ablation plot was constructed by hand using four pallet boxes of sawdust available from the drilling program. A number of subplots were created (see Fig. 6) to evaluate the degree of surface ablation protection afforded by

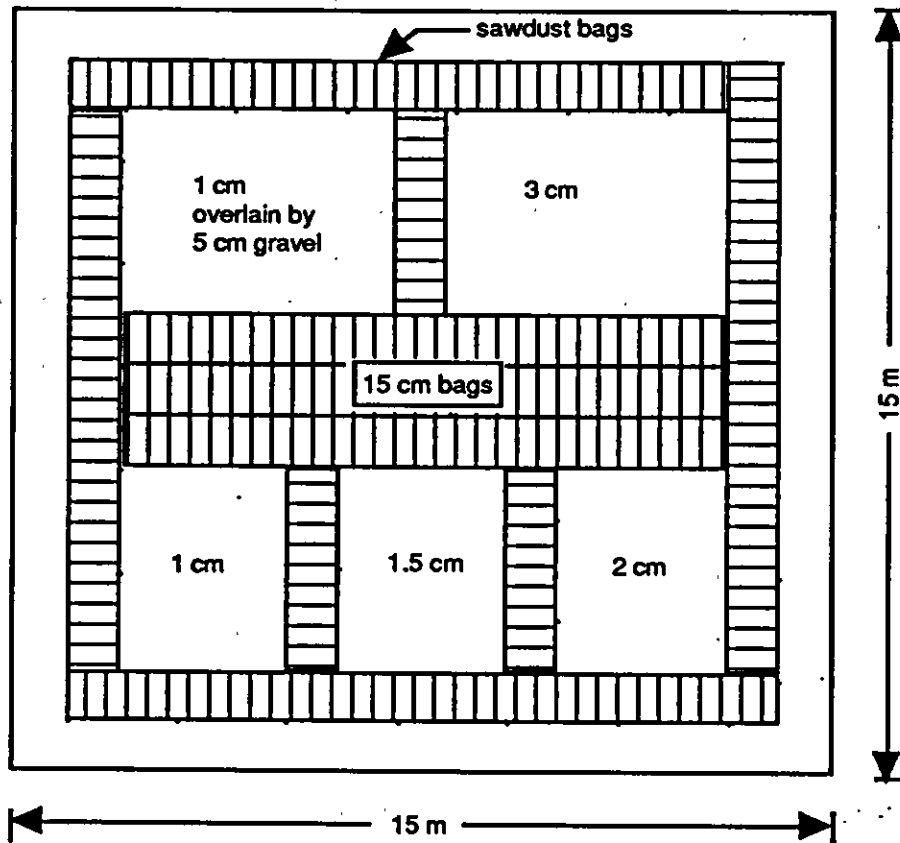


Figure 6. Layout of Sawdust Ablation Test Plots

different thicknesses of sawdust ranging from 1 to 15 cm. At the time the subplots were being constructed, the extent to which the sawdust would be blown away by wind was not known. To gain an understanding of the insulating qualities of the sawdust even in the event plots were adversely affected by wind, two subplots were constructed in a different manner. In one subplot, the sawdust was retained in bags while in the other, a 1 cm veneer of sawdust was held in place by 5 cm of gravel.

The insulating capabilities of rig mats were simulated in another surface ablation test plot prepared adjacent to the gravel plots. Rig mats were not used due to costs and environmental (recovery) concerns. Rather, the rig cellar which consisted of 20 by 20 cm timbers was dismantled and the timbers placed side by side atop the

spray ice. At the conclusion of the project it was planned to dispose of the timbers by burning them on site.

Lastly, the ablation protection afforded by a white insulated tarpaulin having dimensions 30.5 m by 2.4 m was evaluated. This tarpaulin was placed atop the spray ice in front of the gravel ablation plots and held in place by sandbags.

Surface Ablation Measurement Stakes

Once the island edge protection system and surface ablation test plots were in place, 35 - 5 cm by 5 cm by 4.9 m long graduated wooden ablation stakes were inserted into the island using a thermal ice drill to create the 5 cm diameter hole required. Attempts were made to install the stakes so that they extended between 0.25 and 0.75 m above the island surface. In some instances, the holes created for the ablation stakes were too deep. For these cases, snow and/or gravel was dropped down the hole to shorten it. A level survey was performed to ensure that the stakes did not slip into the hole. Subsequent surveys confirmed that no stake slippage had occurred.

A total of 15 ablation stakes were placed into the unprotected spray ice. Roughly one-half of these were in clean spray ice whereas the remaining stakes were placed in spray ice where the surface had been stained as a result of previous activity on the island. The remaining 20 stakes were placed in ablation plots and beneath the Rufco and 13 oz. per square yard vinyl edge protection sheets.

Additional Instrumentation

Several types of instrumentation were deployed and/or utilized from the winter island stability alert program. A 24 bead thermistor string which measured the spray ice and seabed temperature profile was left in place and read manually. Another 12 bead string previously used to measure spray ice temperature under the rig was placed beneath a number of ablation plots to monitor warming. Ice temperatures measured by this string were collected automatically by a Campbell Scientific 21X Data Logger at a sampling frequency of one hour. Data collected

from this thermistor string were used to further assess the insulating characteristics of the materials used in the ablation plots.

An environmental enclosure housed a time-lapse video camera system that was set up, but not turned on due to the cold ambient air temperature prevalent at the time. The purpose of the camera was to document surrounding ice conditions, wave state, and performance of the edge protection sheets following breakup of the surrounding ice sheet. A meteorological station was erected to measure wind speed, wind direction, air temperature, and incoming solar radiation, but was not hooked up to a data logger at this time.

Finally, the five Sondex settlement and slope indicator stations originally installed in January were left in place so that measurements could be continued. Locations of these stations are shown in Figure 7. Initial (baseline) settlement and inclinometer surveys were performed on April 22.

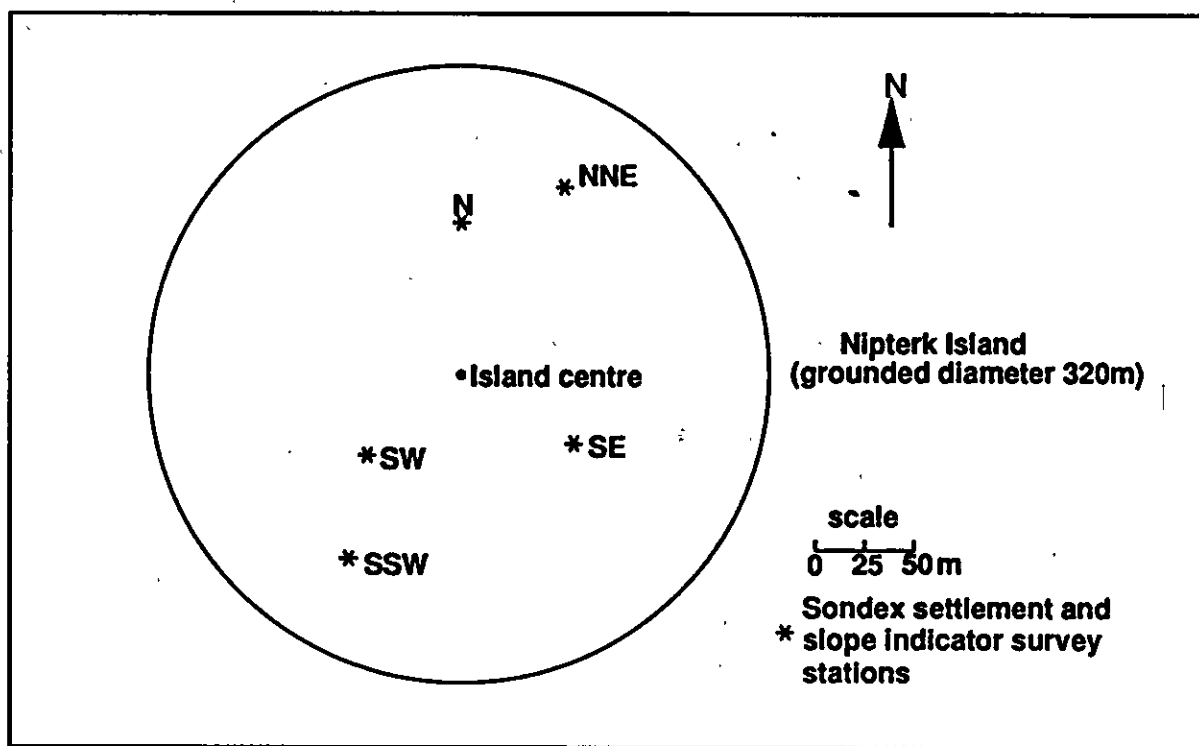


Figure 7. Locations of Sondex Settlement and Slope Indicator Survey Stations

MONITORING SURVEYS

Field monitoring surveys were carried out primarily by Esso personnel with occasional assistance provided by participating company's representatives. One survey of limited scope was undertaken for us by our helicopter pilot. The aerial photography survey was performed by Inuvik-based Photo Script Limited.

A timetable showing the dates of the monitoring surveys as well as those for other experiment milestones is presented as Figure 8. Six comprehensive surveys were undertaken between April 22 and July 5, inclusive. Except for the initial (reference) survey which was undertaken over the course of three days, monitoring surveys typically consisted of an 8-10 hour period on the island during which the following information was collected:

- General documentation of the surrounding ice conditions
- Measurement of island settlement (Sondex) and horizontal deformation (inclinometer readings)
- Surface ablation measurements in the unprotected spray ice and ablation test plots
- Performance evaluation and erosion rate observations associated with the island edge protection system
- Spray ice/seabed temperature profile
- Spray ice temperature measurements beneath ablation plots
- Meteorological conditions (wind speed, wind direction, air temperature, and solar radiation)
- General description of the spray ice surface (size, extent, and orientation of cracks, trafficability, degree of deformation)
- Aerial and surface photographs, and
- Condition of the ice road

Shorter duration visits to the island during which general conditions were described and/or the functionality of various instrumentation confirmed are identified in the figure as brief surveys. Several of these trips were combined with island cleanup and inspection trips to minimize costs.

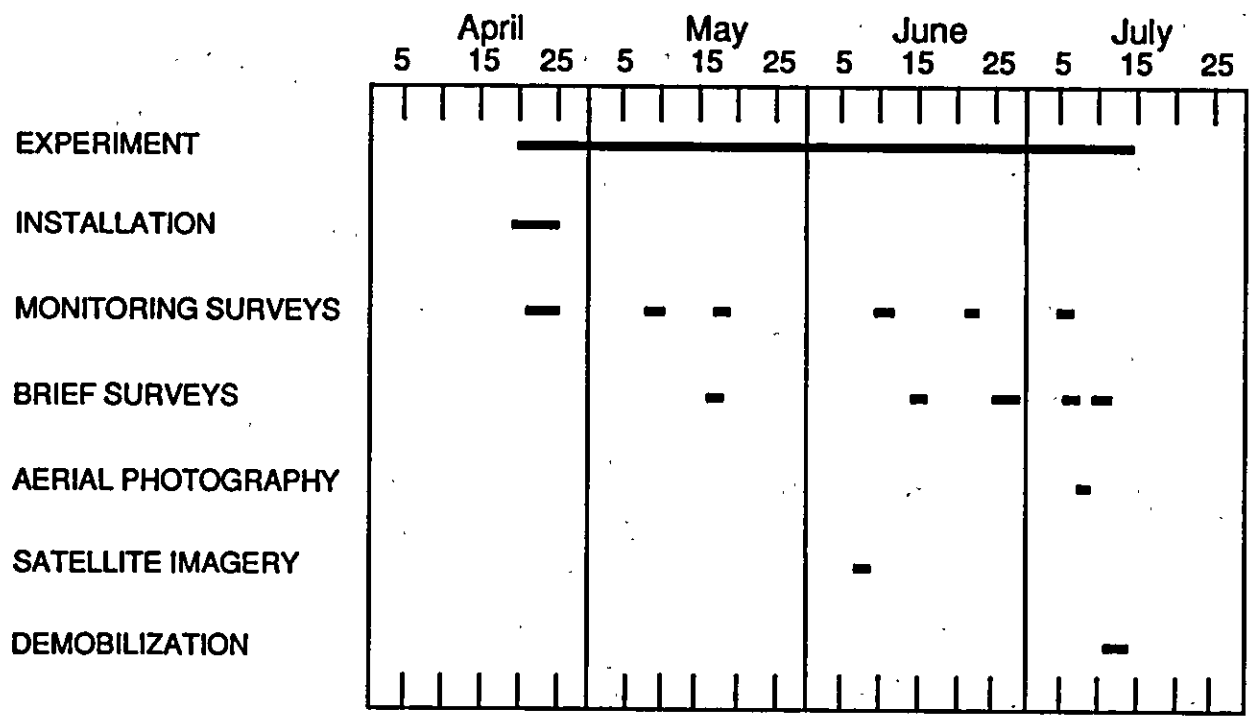


Figure 8. Experiment Timetable

RESULTS

METEOROLOGICAL CONDITIONS

Meteorological data (i.e. wind speed, wind direction, air temperature, and solar radiation) are important because they are used in the analysis of surface ablation and island erosion. During the course of the experiment, meteorological data were gathered from two sources. These were: Tuktoyaktuk, some 140 km to the east of Nitperk and from measurements taken on the island. These data are provided in Appendix A.

Tuktoyaktuk wind speed, wind direction, and air temperature data were relied upon exclusively when our met station was not yet in operation early in the program and between the period July 5 until island breakup. Tuk wind speed and direction data are recorded at six hour intervals whereas maximum and minimum air temperatures represent a 24 hour period. From June 7 through July 5, wind speed, wind direction, air temperature, and solar radiation were measured on the island at 15 minute intervals. These data were recorded by a Campbell Scientific 21X Data Logger.

Wind speed and direction were monitored by a RM Young 05103 wind monitor. The wind speed sensor is an injection molded helicoid-shaped propeller. Vane positioning was transmitted to a precision conductive plastic potentiometer located in a sealed chamber just below the wind speed transducer coil. Air temperature was measured by three thermistors and the data logger's sensor at hourly intervals. These data were also collected by the data logger. The air temperatures were then averaged.

A LI-COR LI-200SZ pyranometer sensor was used to measure solar radiation. The instrument is suitable for measuring global sun plus sky radiation. Output from the sensor to the logger was in terms of voltage (millivolts). This output was eventually converted to units of kWm^{-2} .

A comparison of Tuk and island wind speed data revealed that they were reasonably similar. There did however appear to be a time lag between the two data sets which is attributed to the relative distance between stations. In addition,

the Tuk wind speed data tended to be somewhat higher especially after mid-June. Island wind directions were also found to compare favorably with those measured in Tuk. Plots of wind speed and direction are provided in Appendix A.

Figure 9 is a plot of average daily air temperature. The data set utilizes air temperatures measured on the island whenever they are available. Prior to landfast ice sheet breakup, air temperatures measured on the island were generally similar to those observed in Tuk. Following breakup, island air temperatures were usually less than those recorded in Tuk due to the influence of the water and in some cases ice near the island. Another factor which contributed to the differences observed between Tuk and island measured air temperatures is that the island was not subjected to the the degree of warming experienced at Tuk as a result of land-derived winds due to its distance offshore.

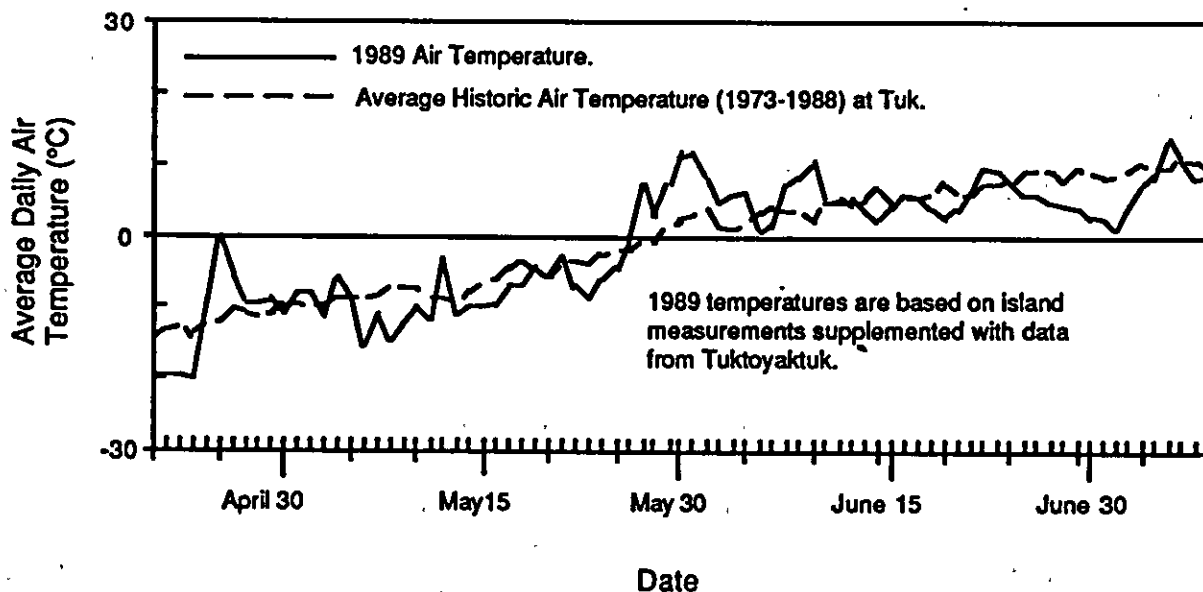


Figure 9. Comparison of 1989 and Historical Air Temperatures

As can be seen from the figure, average daily air temperatures rose above 0°C on May 25 and consistently remained above freezing thereafter. The arrival of above-freezing air temperatures was associated with a warming of the spray ice surface which eventually manifested itself in the onset of significant surface ablation. Historical daily average temperatures for Tuk are shown in the figure for

comparison. From these data, it is apparent that the temperatures observed on the island were typical. Therefore, when planning future operations it is reasonable to expect that spray ice surface ablation will commence sometime during the latter part of May.

A plot of solar radiation over time is shown in Appendix A. Solar radiation varied for a number of reasons, including cloud extent and thickness, surface albedo, and solar zenith angle. Solar radiation along with air temperature were the two factors which most influenced spray ice ablation.

ICE TEMPERATURE

Spray ice/seabed temperatures were measured by an 11 m long thermistor string deployed adjacent to the southwest Sondex/Slope Indicator survey station (75 m from island center). The thermistor string was installed in January as part of the winter island performance monitoring program undertaken in support of exploration drilling. The configuration of the string is illustrated in Figure 10. As can be seen the string was made up of 24 thermistors whose spacings varied.

The lowermost portion of the string consisted of a plastic cone tip which was driven 1 m into the soft seabed. For this portion of the string, 11 thermistors were spaced at 10 cm intervals. Contrastingly, temperature of the submerged spray ice was measured at 1 m intervals whereas in most of the freeboard, thermistor spacing was 0.5 m.

Yellow Springs Instrument Company (YSI) Model 44007 thermistors were used. These thermistors, sensitive to temperatures over the range -80° ($3684\text{K}\Omega$) to 150°C ($92.70\text{K}\Omega$) had an interchangeability of $\pm 0.2^{\circ}\text{C}$.

Thermistor resistance readings were taken on April 22, May 9, May 18, June 10, and June 22 (Appendix B). Temperature profiles (for all but June 22) are shown in Figure 11. The abscissa represents ice temperature in degrees Celsius and the ordinate represents the depth in meters measured from the ice surface at the time

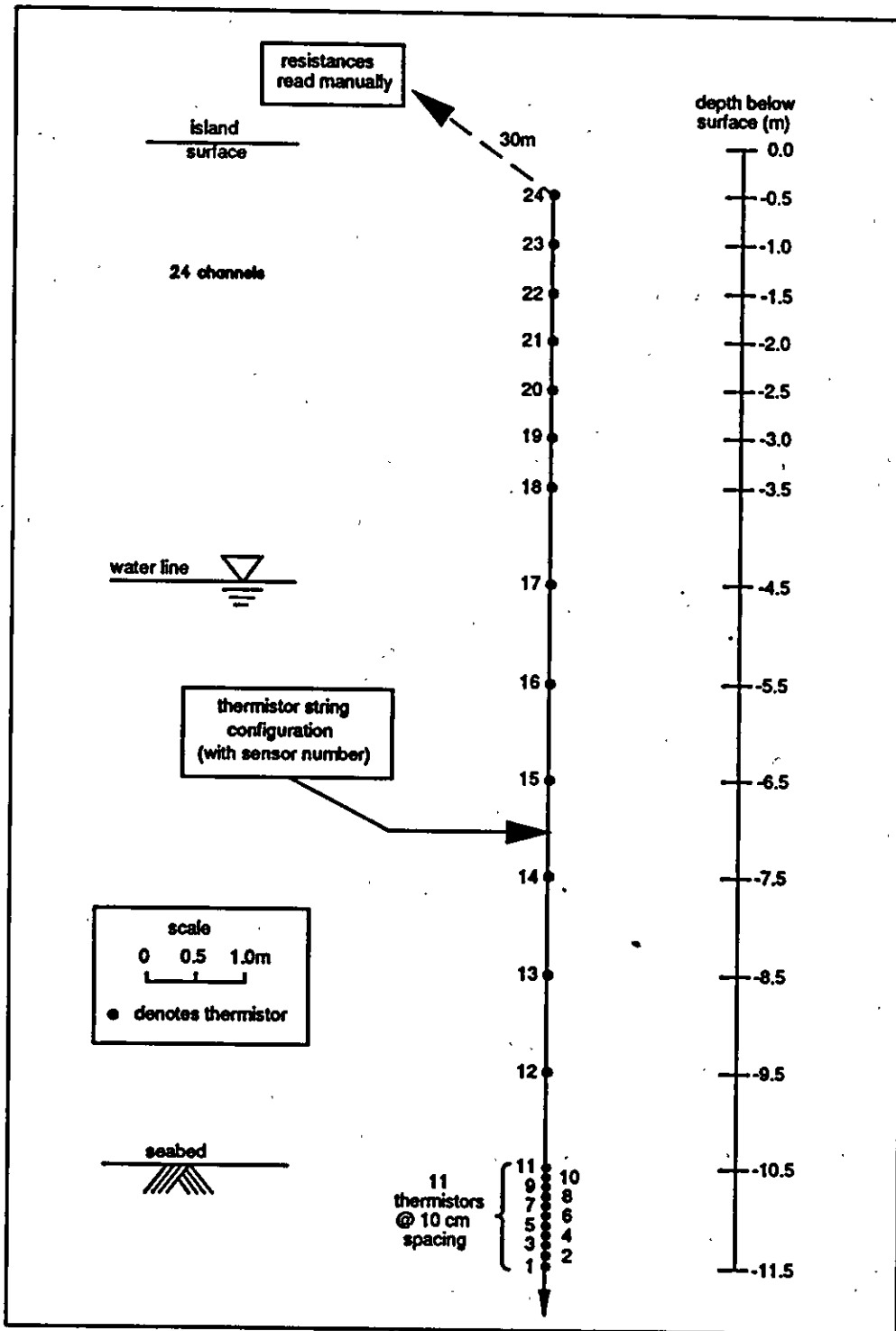


Figure 10. Configuration of Spray Ice/Seabed Thermistor String

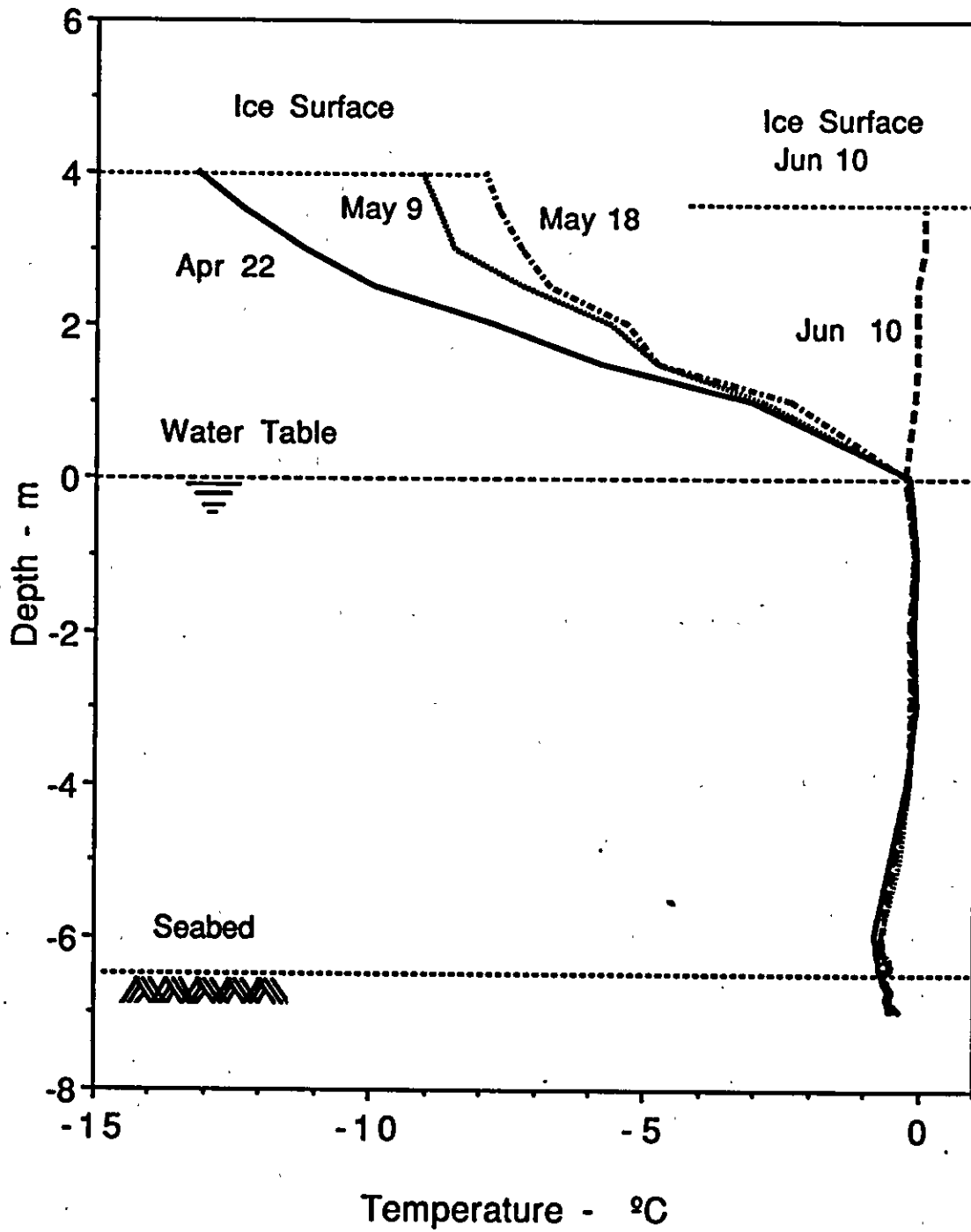


Figure 11. Spray Ice/Seabed Temperature Profiles

of thermistor string installation. The ice surface locations at the time of subsequent measurements are also plotted.

Three thermal regions can be distinguished from the profiles: the above-water ice, submerged ice, and seabed. Up until June 10, the lowest ice temperatures were associated with the above-water ice. Over the period April 22 to June 10, the ice in this zone increased from a minimum of about -13°C (at a depth 0.5 m below the surface) to near 0°C on June 10 in response to increased levels of solar radiation, warmer air temperatures, and the ablated ice surface. The average temperature rise for this period was $0.28^{\circ}\text{C day}^{-1}$.

The submerged ice temperature remained reasonably constant with time. At the water table to a depth of nearly 4 m below it, the ice temperature was about 0°C . Below this level to the seabed, the ice temperature decreased to about -1°C probably in response to the presence of brine. Seabed temperatures tended to remain constant over time. Near the surface of the seabed, the temperature was about -1°C increasing to -0.5°C , 1 m below the seabed.

WATER TEMPERATURE

The water column temperature profile was measured in mid-November, 1988 whereas the surface water temperature was measured on July 11, 1989, one day after island breakup. At the time of the November survey, water temperatures ranged from about 0°C in the freshwater layer (surface to a depth of 4 m below the surface) to about -1°C in the underlying saline (15 ppt) layer. For comparison, the water temperature at a depth of 0.3 m was 12°C on July 11 which is attributed to MacKenzie River outflow. It is anticipated that much of the water column was at or near this temperature due to the degree of mixing associated with the Mackenzie outflow. The effects of the relatively high water temperature on the island are discussed under the section: Island Erosion.

SURFACE ABLATION

Net ablation experienced by a spray ice island during the melt season can be characterized by solving an energy balance equation such as the following:

$$F_r + F_l + F_s + F_e + F_w + F_c + F_i = F_a \quad (1)$$

Where:

- F_r = net solar radiative flux
- F_l = net long wave radiative flux
- F_s = sensible heat flux
- F_e = evaporative heat flux
- F_w = heat flux from wave action
- F_c = heat flux from forced convection
- F_i = conductive heat flux, and
- F_a = heat absorbed by melting ice

This equation was adapted for spray ice islands by Connolly [1], based on a solution to the energy balance equation developed by Maykut and Untersteiner [2] for natural growth of sea ice in the central Arctic and adding terms used by El-Tahan et al. [3] in modeling iceberg detection. The evaporative heat flux term represents heat either released or absorbed as a result of water evaporating, ice sublimating, or to condensation. According to Connolly [1], this term can be essentially ignored during the melt season since these processes are much slower than others associated with ablation processes. Forced convection and wave action are processes described in the section entitled: Island Erosion.

Figure 12 is a diagram showing the energy transfer parameters. Processes responsible for energy transfer in only one direction are denoted by an arrow pointing in that direction whereas processes responsible for incoming and outgoing energy are denoted by arrows in both directions. Note that outgoing fluxes are negative.

Albedo is defined as the ratio of reflected to incident shortwave radiation. Spray ice albedo decreases after construction and as the melt season progresses due to the accumulation of dust and debris on the surface, largely from the drilling operation. However, the addition of foreign materials on the island surface does

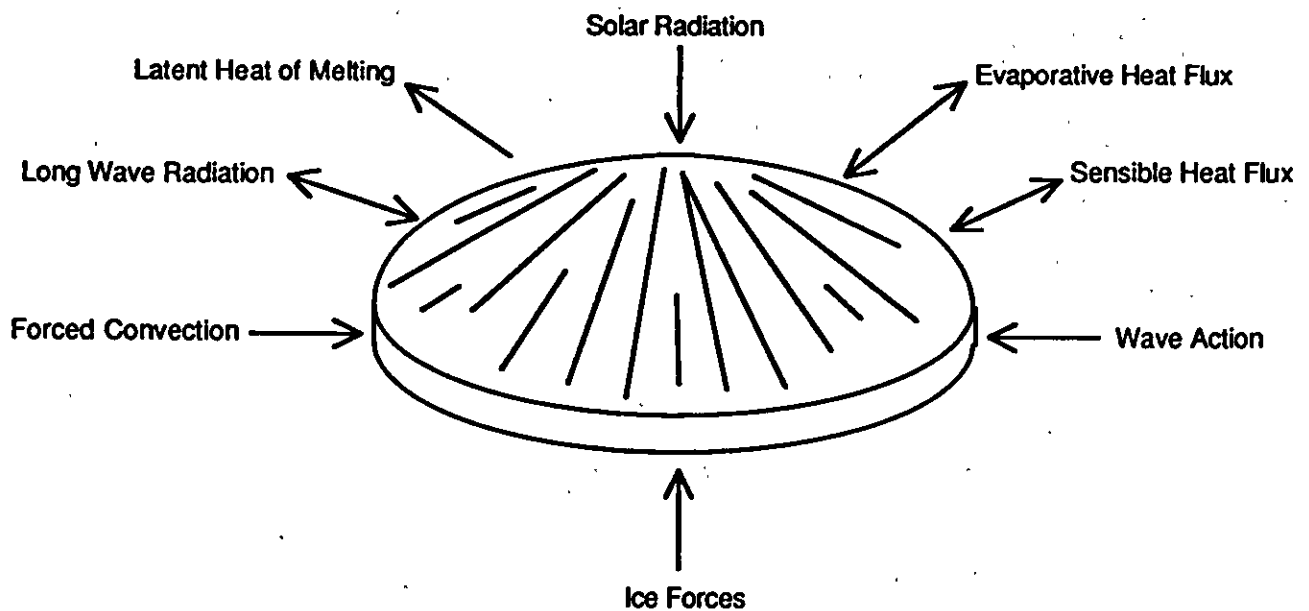


Figure 12. Energy Transfer Parameters. From Connolly [1].

not necessarily increase the melt rate since an insulating layer can be formed that actually protects the surface. Consequently, materials, debris, etc. on the island surface will act to reduce the melt rate below its naturally occurring value if sufficient material is present as demonstrated in the surface ablation studies.

Loss of island freeboard was monitored with ablation stakes. Stakes were placed at locations in the "clean" and "soiled" unprotected spray ice, in ablation test plots, as well as in two of three edge protection sheets. Ablation stakes were confined to the west half of the island so that they would not be destroyed during the ensuing rig demobilization and subsequent island cleanups.

Stakes were graduated at 10 cm intervals starting from the top. The visible stake length from the top of the stake to the spray ice surface was measured during each site survey. Initial baseline measurements were recorded on April 23 and subsequent surveys were undertaken on May 9, June 10, June 22, and July 5. (Measurements were not taken during the May 18 survey due to extensive drifting snow which had accumulated over the western half of the island, obscuring many of the stakes). The differences between initial and subsequent measurements yielded the magnitude of ice surface ablation at a particular location.

Unprotected Spray Ice

Average cumulative surface ablation of the unprotected spray ice (in centimeters) as a function of time is plotted in Figure 13. Individual ablation stake measurements are provided in Appendix C. Ablation was computed from measurements at 15 unprotected spray ice survey stake locations. Also shown are the average daily temperatures for the study period.

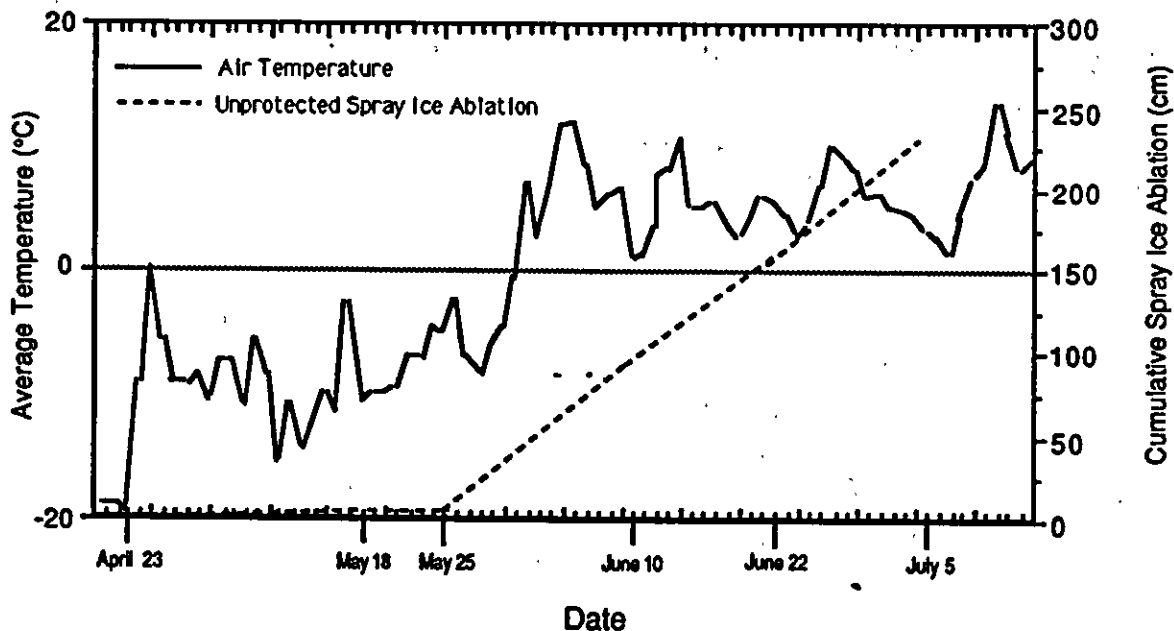


Figure 13. Cumulative Ablation of Unprotected Spray Ice

Up until air temperatures consistently exceeded 0°C (the last week of May) the most significant spray ice ablation was observed in areas where the surface had been soiled such as in vicinity of the rig and heavily trafficked areas. This was due to the absorption of solar radiation by debris-laden spray ice which hastened ablation.

Similar observations have been reported in published literature. Warren and Wiscombe in Colbeck [4] noted that small highly absorbent particles are capable of reducing snow albedo from 5 to 15% even in quantities as low as 1 part per million. According to Colbeck [4], there appears to be a consensus among

investigators that the persistence of the effect of albedo reduction decreases with time, but that the rate appears to vary significantly depending on several factors such as the size of material used and the surface over which it is spread. Snow (spray ice) surfaces would be expected to retain the effect longer, especially for smaller particles.

Ashwell and Hannell [5] noted that ablation was weather-dependent from a standpoint of conditions being overcast with winds or calm and sunny. This distinction according to Colbeck [4] correlates well from the mechanisms involved. That is, either mostly convective heating in the former case or radiative heating in the latter. Rhodes et al. [6] reported that when solar input is restricted, the optimum thickness of the dark layer required to enhance melting is only about 1 mm depending on the nature of the controlling parameters including the type of material. The optimum thickness of the dark layer to enhance ablation was reported to range from 3 to 24 mm by a number of other investigators cited in Colbeck [4]. The optimum thickness to enhance melt was influenced by weather conditions and the type of material used. Finer materials appear to insulate better than coarser materials as they can be more finely dispersed. According to Colbeck [4], the optimum thickness of the dark layer required to promote melting increases absorption much more than it increases thermal insulation. Once a sufficient thickness is obtained, the insulative effects become more important than increased solar absorption resulting in a melt rate that decreases below its natural value.

One means of reducing the amount of surface meltback in heavily soiled areas that was demonstrated to be extremely effective on Nipterk when air temperatures periodically exceeded 0°C was to cover the spray ice with a thin layer of clean snow. This operation was performed routinely in the vicinity of the drilling rig in early April during a warm period when air temperatures exceeded 0°C, skies were cloud-free, and winds calm. Addition of the snow layer was accomplished by a loader with a bucket. Snow was first dumped over a large area and smeared to a 3 to 5 cm thickness.

Covering the spray ice with a clean layer of snow to slow melting even worked well in highly trafficked areas though the snow required grooming at periodic

intervals. The benefit of using fresh snow to eliminate the effect of dark materials has been previously reported in public literature (see Colbeck [4]).

In addition to retarding the meltback rate, coatings placed on snow and spray ice features were reported to strengthen the surface and thereby increase its durability from a trafficability standpoint [7]. According to St. Lawrence [7], a 15 to 30 cm thick layer of gravel deposited on the spray ice was sufficient to harden its surface sufficiently to undertake gravel haul operations when the air temperature rose near and eventually slightly above freezing.

By early June, the debris-layer on Nipterk which earlier had promoted melting, reached sufficient thickness that it proved to be an effective insulator, thereby mitigating spray ice ablation. Areas overlain with as little as 0.5 cm of soiled material were observed to have reduced surface meltback by up to 1 m on June 10 as evidenced by a number of hummocks (see Plate 5). A set of annotated slides showing examples of ablation and erosion is provided in Appendix D.

Cumulative average ablation prior to May 18 was only 3 cm which represents an ablation rate of less than 1 cm per week for the period April 23 to May 18. Significant ablation occurred sometime after May 18 (probably commencing May 25 based on air temperature data) as the average ablation rate for the period May 18 to June 10 was 25.3 cmwk^{-1} . Ablation intensity increased to an average of 35.0 cmwk^{-1} during the interval June 10 to July 22. The most severe ablation was documented for the period June 22 through July 5 when the average ablation rate was 45.2 cmwk^{-1} . This increase in the rate of surface meltback may have been partly attributable to rain which was observed to have fallen over a prolonged period in late-June.

Colbeck [4] reported that the dominant energy fluxes are at the upper surface for glacial firn and deep snow covers. This is also the case for the ice island during the winter. These fluxes are dominated by radiation as well as sensible and latent heat fluxes. On the other hand, Colbeck suggested that for shallow snow covers, ground heating needs to be considered and input from rain can be important. It is apparent that this is the case for the spray ice island as temperatures approach

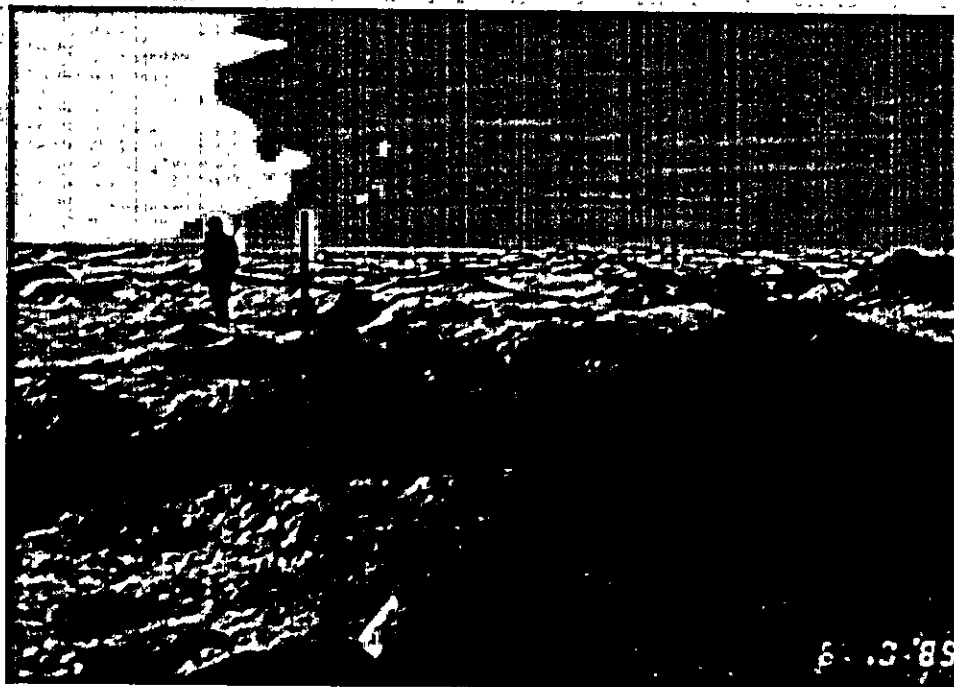


**Plate 5. Hummocks Created by Differential Ablation of the
Spray Ice Surface as Observed on June 10**

and then rise above freezing. Ground heating though would be dominated by the temperature of the surrounding water which would manifest itself in accelerated ablation along the island perimeter.

The average cumulative ablation of the unprotected spray ice was 2.3 m. The maximum cumulative ablation at one location was 2.8 m in an area where the island surface was soiled. Although the highest magnitude of ablation was identified at one ablation stake in this area, the average cumulative ablation measured at a number of locations in this dirt-contaminated region was essentially the same as that measured for the "clean" spray ice. The least amount of ablation of the unprotected spray ice, 1.8 m, was measured near the base of the sawdust test plots.

With the onset of warmer air temperatures and ablation, changes were noted in spray ice surface characteristics. Through the early part of the experiment when below freezing air temperatures predominated, the spray ice surface was hard and crusty. Because of its permeability, the spray ice surface allowed melt water to drain vertically. Due to the effects of warming especially by late-afternoon, the uppermost island surface softened to the extent that it could be dislodged with a boot into particles typically less than 5 mm in diameter.

Over time, surface cracks which at the time of island construction had been filled with reworked spray ice were visible. Most of the major cracks were located near the edge or outside the working surface. Once surface ablation became so extensive that less than 1 m of freeboard remained, new cracks developed as parts of the island became buoyant.

Ablation Test Plot Measurements

As previously mentioned, in addition to documenting ablation of the unprotected spray ice, ablation was measured in the test sections of a variety of materials to assess their effectiveness with regard to mitigating surface meltback. These materials included sheets, a tarpaulin, timbers, and various thicknesses of sawdust and gravel. Ablation stake measurements from each of these test plots are provided in Appendix C.

Sheets and Insulated Tarp

The effectiveness of the sheets and insulated tarpaulin in protecting the spray ice is demonstrated in Figure 14 which compares cumulative spray ice ablation with time. Surface ablation of the unprotected spray ice is also shown. Both the 13 oz. nylon sheet and the Rufco sheet had the effect of cutting the ablation rate by about one-half that measured for unprotected spray ice. The insulated tarpaulin further enhanced protection of the spray ice. Over the course of the measurement period, the average cumulative ablation was only 0.5 m, compared to 0.85 m for the Rufco sheet and 1.25 m for the vinyl sheet. The ablation reduction benefits afforded by the sheets are attributed to a combination of their relatively high albedo and the insulating effects provided by the entrapped air layer between the surface of the ice and the sheet.

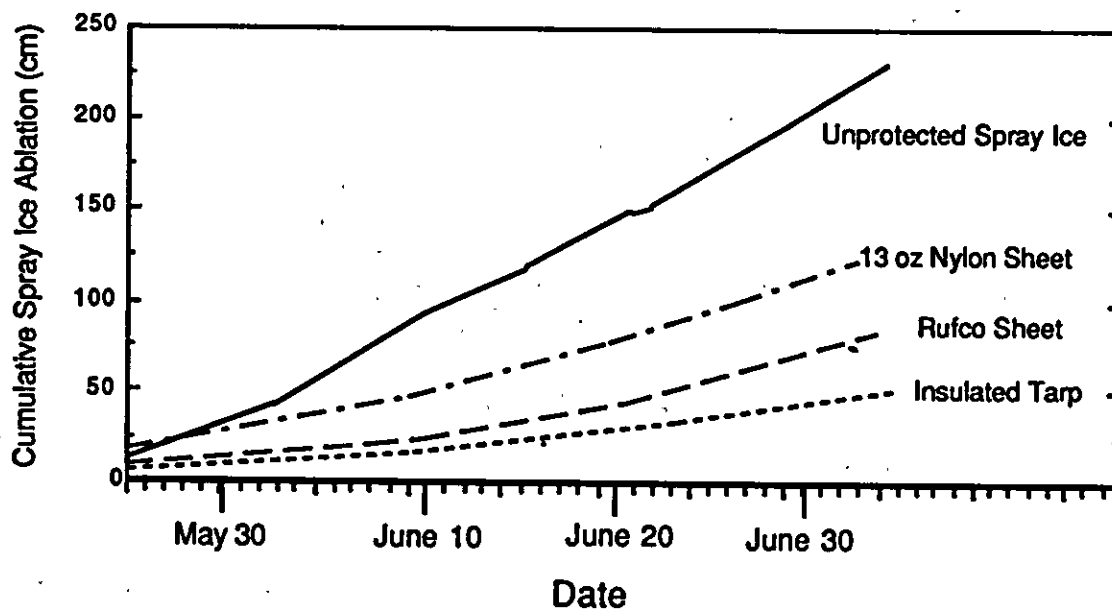


Figure 14. Sheet/Tarp Ablation Mitigation Comparisons

Because ablation data were collected at only two locations in areas covered by each sheet, it is not possible to establish with certainty whether the Rufco sheet actually provided insulating qualities superior to those of the 13 oz. vinyl sheet. Although the two spray ice ablation stakes beneath the Rufco sheet revealed less overall surface meltback than was observed under the vinyl sheet, there was a greater degree of variability between locations. Up to a 30 cm difference was found

between the Rufco ablation stakes compared to a total ablation difference of 10 cm exhibited by measurement locations beneath the two vinyl sheets. On the other hand, the superiority of the insulated tarpaulin at mitigating ablation was supported by nearly identical measurements at three locations. Moreover, the ablation rate associated with the insulated tarpaulin remained more uniform with time than the sheets. And finally, the average ablation rate associated with the insulated tarpaulin (1.5 cm day^{-1}) during the latter stages of the measurement period was less than half that (3.1 to 3.5 cm day^{-1}) measured beneath the sheets.

By June 10, all of the snow which had accumulated on the sheets had melted. Snow meltwater and subsequent rainfall accumulated in depressions which grew in size throughout the program (see Plate 6) as the underlying spray ice thawed. No attempt was made to drain the water as it served to further hold the sheets in place. With the progression of the melt season, the degree of spray ice degradation became so extensive that pools developed. The largest depression was roughly 15 m in diameter, 4 m deep, and contained two meters of water. Thus, it is evident from an operational and an island stability context that draining the water at some point in time is desirable.

Sawdust Plots

Six subplots were constructed as part of the 15 m by 15 m sawdust ablation plot system to quantify the effectiveness of sawdust as an insulating material. Under operational conditions, wood chips rather than sawdust would likely be the form of wood product used. However, sawdust was utilized in this study since it was available on-site at minimal cost to the project.

Subplots consisting of 1, 1.5, 2 and 3 cm thick layers of sawdust were constructed. The remaining two subplots consisted of 15 cm thick sawdust bags and 1 cm of sawdust blanketed by approximately 5 cm of gravel to insure that the sawdust remained in place. The latter configuration was investigated because a more durable surface would be required to support even limited island operations. Sawdust bags were placed around each subplot and ablation stakes positioned in



Plate 6. Water Collected on Sheets as Observed on June 10

the center of each subplot to isolate to the extent possible, the impact of ablation at one subplot from that of a neighboring plot. Sawdust bags were also placed along the outside edge of the ablation plot to retard spray ice meltback in this region with the onset of summer. Comparative photographs of the test plot taken on April 23 and July 5 are shown in Plate 7.

A comparison of cumulative spray ice ablation beneath the sawdust ablation plots with time is presented as Figure 15. One can see from the plot that the magnitude

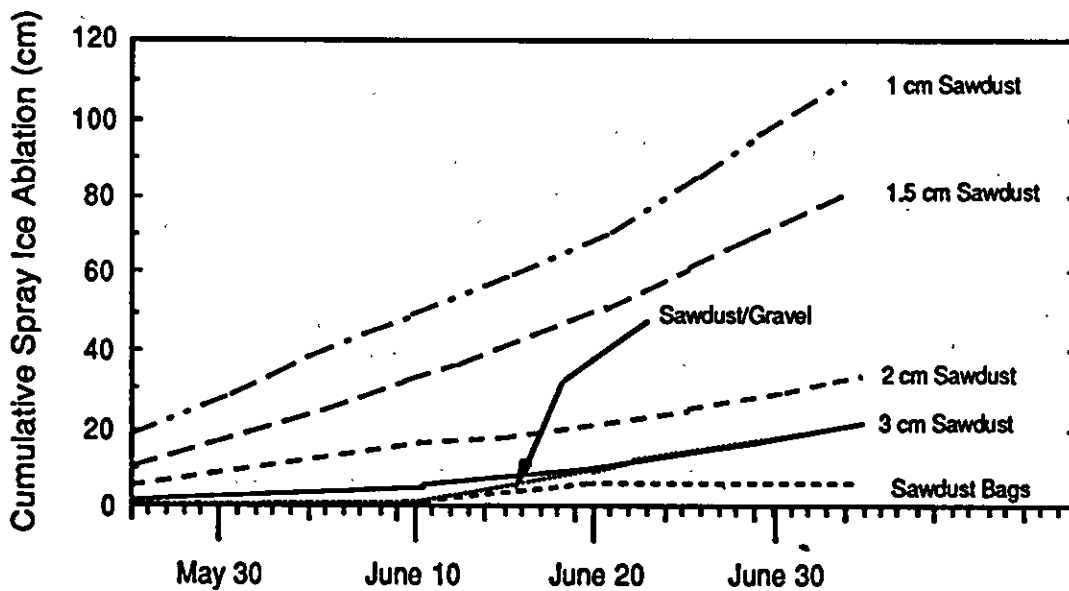
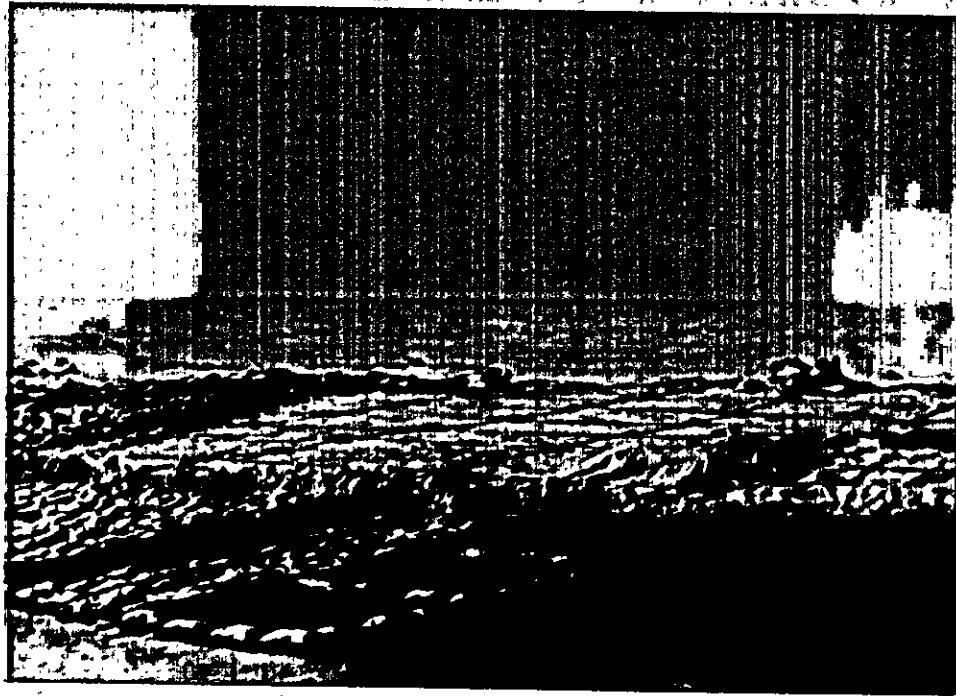
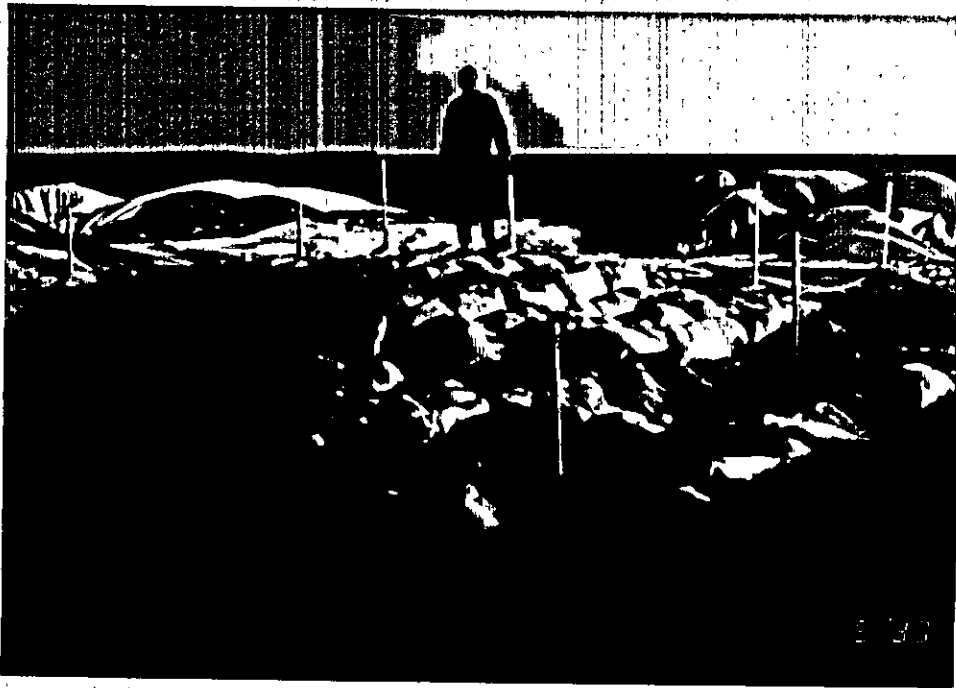


Figure 15. Sawdust Ablation Test Plot Comparisons

of ablation decreased with increasing thickness of sawdust. A 1 cm veneer of sawdust was sufficient to reduce the ablation by over 50% from an average of 2.25 m for unprotected spray ice to only 1.07 m on July 5. Doubling the thickness of the sawdust cover had a dramatic impact on reducing the magnitude of ablation. Over the same evaluation period, the magnitude of ablation associated with 2 cm of sawdust was only 30 cm. Increasing the thickness of sawdust resulted in nominal reductions in the amount of spray ice ablation measured. A 3 cm thick blanket of sawdust limited cumulative ablation to 20 cm on July 5; the same amount as for a 1 cm thick layer of sawdust overlain by 5 cm of gravel.



(a) April 23



(b) July 5

Plate 7. Sawdust Ablation Plots

Finally, the most effective subplot examined was 15 cm thick sawdust bags. As with the sawdust/gravel subplot, virtually no ablation was apparent until the June 22 survey. Total spray ice ablation measured beneath the sawdust bags was only 5 cm over the entire measurement program.

During the period June 22 to July 5, the rate of ablation increased substantially particularly in subplots having a thin layer of sawdust. This increase in ablation rate was also observed at other surface ablation measurement locations in both permeable and impermeable plots. A factor which accelerated melting of the spray ice is rain. It tended to accelerate ablation beneath permeable and impermeable test plots alike. In permeable test plots, rain water percolated through the coating material to erode and melt the spray ice. On the other hand in impermeable sheets, rain water collected at the surface causing the underlying spray ice to thaw.

Gravel Plots

Spray ice ablation was measured beneath three thicknesses of gravel, each test plot covering a 15 m by 12 m area. Gravel was studied not only to investigate its insulating qualities with regard to ablation protection, but also as a base material to operate on during the rig marine demobilization. Construction experience with the use of gravel coatings for heavy equipment operations has been gained on other projects. Polar Alpine used this technology during a construction project which is described in the section detailing extended operations on spray ice.

Figure 16 is a comparison of cumulative spray ice ablation over time for each of the gravel test plots. The baseline from which subsequent ablation is compared was adjusted to be on May 25 rather than April 23 due to spray ice creep which occurred following placement of the gravel. Evidence for creep (as opposed to ablation) accounting for the change in stake stick-up observed above ground was that almost no ablation of the unprotected spray ice was documented prior to this period.

Cumulative spray ice ablation associated with the 0.3 m thick gravel cover totaled 65 cm. This magnitude of ablation was similar to that recorded for an equivalent

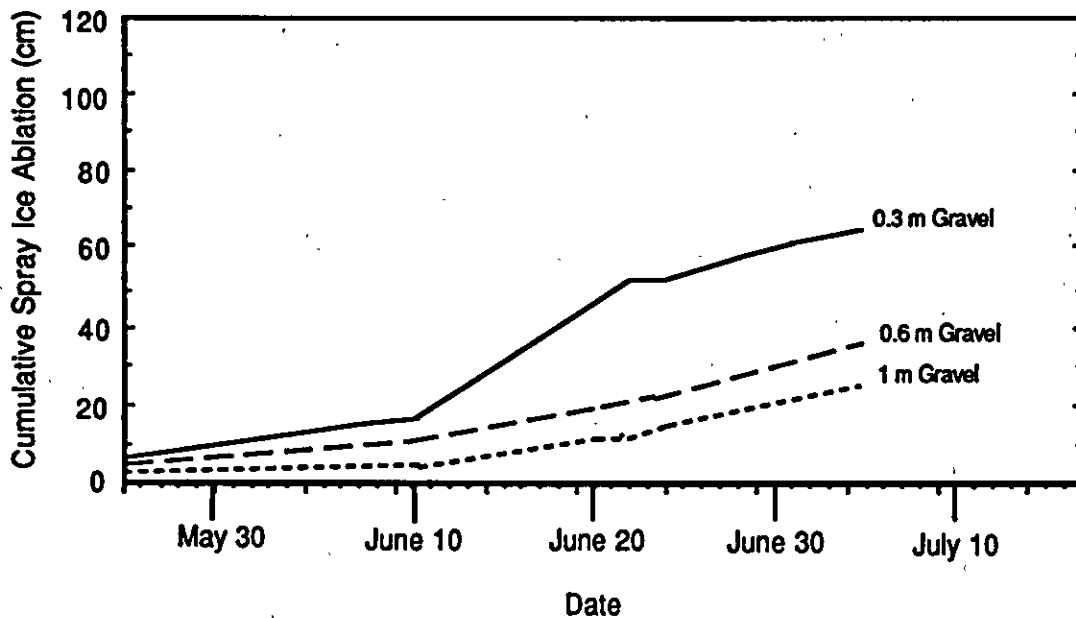


Figure 16. Gravel Ablation Test Plot Comparisons

1.5 to 2 cm thickness of sawdust and somewhat less than that associated with the Rufco sheet (85 cm), but more than was measured under the insulated tarpaulin (50 cm). Doubling the gravel cover thickness had the effect of cutting spray ice ablation by nearly one-half. A 1 m thick gravel cover was only marginally better at reducing ablation than a 0.6 m thick cover. Identification of the optimum gravel thickness required for maximum thermal insulation qualities is important to minimize the amount of material required and thereby transportation and material costs. The ablation protection provided by the thicker gravel plots was superior to that provided by any tarpaulin and comparable to that of a 2 to 3 cm blanket of sawdust and a thin veneer of sawdust held in place by gravel.

Ablation rates varied for each of the gravel test plots throughout the monitoring period. The highest average ablation rate (2.92 cm day^{-1}) was associated with the 0.3 m gravel plot for the period June 10-22. This rate was 3.5 to over 4 times those observed for the other two gravel ablation plots. Average ablation rates before and after this time period were substantially lower. Contrastingly, average ablation rates associated with the 0.6 and 1 m thick gravel plots increased over time. The average ablation rates documented for the two thicknesses of gravel were similar during the periods June 10-22 and June 22-July 5. The average ablation rates

measured at all three plots near the end of the study were also similar (1.04 cmday^{-1} to 1.15 cmday^{-1}).

Spray ice ablation beneath the gravel was predicted using an in-house finite difference thermal model developed by Dr. J. Nixon of ERCL. This model is quite rigorous yet sufficiently versatile to accommodate a non-linear surface temperature-time relationship. In brief, the model was used to predict the onset of ablation and the depth of spray ice thaw beneath the gravel pads. The following assumptions and material properties were found to yield a very good fit of the observed data:

- a 5% (by weight) ice content of gravel
- a gravel bulk density of 1.8 Mg/m^3
- unfrozen thermal conductivity of gravel is 2.1 w/mC
- frozen thermal conductivity of gravel is 2.0 w/mC
- "n" factor for gravel is 1.5
- zero snow cover
- specific heat of soil grains is 0.2 cal/gmC
- bulk density of spray ice is 0.65 Mg/m^3
- temperature of spray ice at sea level is fixed at 0°C
- initial temperature profile varies linearly from -8.5°C at gravel surface to 0°C at sea level
- Computations start on Julian Day 116 (April 26)

The above gravel properties are very reasonable for the gravel used at Nipterk. A comparison of the observed and predicted thaw is presented in Table 3.

The 0°C isotherm quickly penetrates the gravel layer. The mean daily air temperature rose above 0°C on May 25 (Figure 13) and the time to melt the gravel was 7, 16, and 25 days for the 0.3, 0.6 and 1.0 m pads, respectively. Consequently, the time to thaw out the gravel is approximately proportional to the latent heat (or ice content) of the gravel. This suggests that a 0.5 m gravel pad of ice content 10%

Table 3. Comparison of Observed and Predicted Thaw Beneath Gravel Pads

Gravel Thickness	Onset of Spray Ice Ablation	Depth of Spray Ice Thaw on July 5	
		Observed	Predicted
0.3 m	June 2	0.65 m	0.56 m
0.6 m	June 11	0.23 m	0.28 m
1.0 m	June 20	0.15 m	0.12 m

is just as effective at preventing spray ice thaw as a 1 m gravel pad having an ice content of 5%.

Therefore in the future, perhaps more emphasis should be placed on increasing the ice content rather than the thickness of the gravel pad at least in areas that will not be subjected to extensive over-ice operations. This could be achieved by flooding the gravel after placement. Increasing the ice content without providing for adequate drainage of meltwater could, however potentially pose trafficability problems.

In light of the reasonable agreement in Table 3 it is concluded that Nixon's thermal model can be reliably used to predict spray ice thaw beneath gravel pads.

Simulated Rig Mat Plot

One test plot was constructed out of 20 cm by 20 cm by 4 m long timbers removed from the rig cellar. Rig mats were not left on the island because of the high cost associated with their removal. Instead, rig timbers were used. The advantage of using rig timbers is that they could be burned on-site as part of the island cleanup. Therefore, to minimize costs, the cellar was dismantled and the timbers used to build the simulated rig mat ablation plot. Under an operating scenario, rig mats could be placed beneath relatively heavy rig loads awaiting marine

demobilization and along the access road to the barge to reduce the potential for spray ice degradation associated with the rig demobilization operation.

Following the June 22 site survey, the simulated rig mat test plot was accidentally burned during the general island cleanup. Even so, extremely encouraging data were collected until that time. Total cumulative spray ice ablation measured beneath the timbers through June 22 was only 8 cm, a mere 3 cm greater than that measured beneath the sawdust bags.

Under operational conditions, rig mats may be a superior alternative to sawdust bags for several reasons. First, rig mats would likely already be on site since they are used in the drilling operation. Thus additional materials would not have to be purchased and transported to the island. Second, rig mats could be placed along the barge access way once the rig component they formally supported is transported aboard the barge. This scenario would reduce the likelihood of trafficability problems. Third, rig mats could be easily picked up during the marine demobilization, thus avoiding potential environmental concerns associated with the use of either sawdust or wood chips which would probably be left on site. And fourth, rig mats can be reused whereas sawdust and/or wood chips must be considered expendable.

Ablation Test Plot Comparisons

Figure 17 is a plot comparing the ablation protection performance of some of the most beneficial insulating materials identified from each of the categories evaluated. As can be seen, wood products (i.e. a 15 cm thick blanket of sawdust and 20 cm thick timbers) provided the highest degree of protection followed by gravel and to a lesser extent, the insulated tarpaulin.

Spray Ice Temperatures Beneath Ablation Plots

Spray ice temperatures were measured beneath most of the sawdust ablation subplots and all of the gravel ablation plots for a one month period beginning in

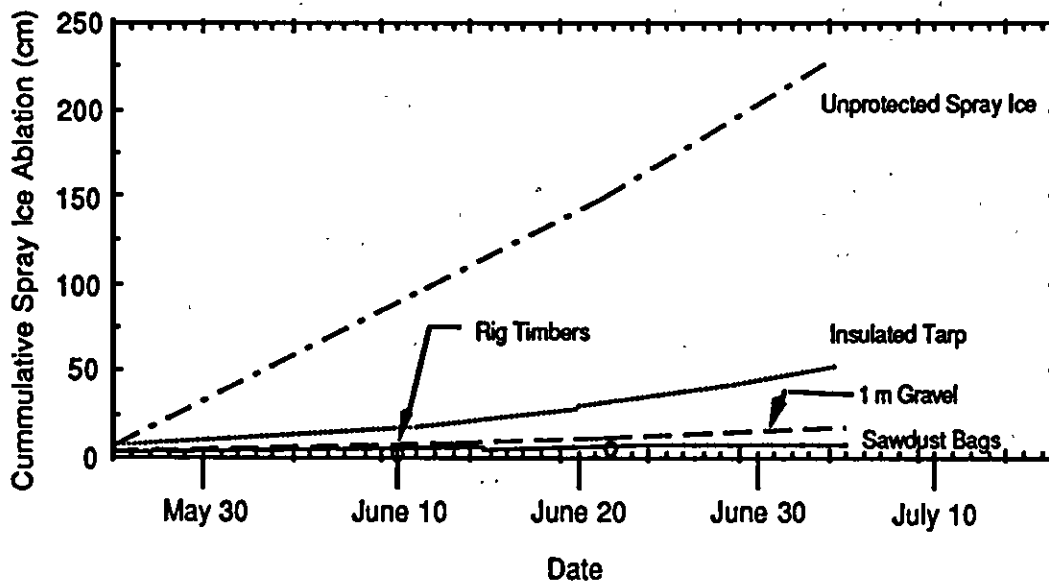


Figure 17. Selected Ablation Test Plot Data Comparisons

early June. These data are useful in further evaluating the insulating qualities of the overlying materials.

Average daily temperature-time series plots were prepared for each of the ablation plots and subplots for which these data are available. Obscured by averaging the data at one day intervals were the diurnal temperature fluctuations apparent in all of the data. However, the effectiveness of various materials with regard to mitigating ablation is readily apparent.

Figure 18 is a time series plot of surface spray ice temperature measurements collected beneath the gravel ablation plots. Also included in the figure are averaged daily air temperatures recorded on the island during the same period. One can see from the figure that a 1 m thickness of gravel offered the best degree of insulation, limiting the average temperature to about 0.3°C throughout most of the measurement period. Minimal fluctuation from day to day is documented, except in early July where a slight warming trend is observed. Similarly, average spray ice temperature data from the 0.6 m thick gravel ablation plot show the

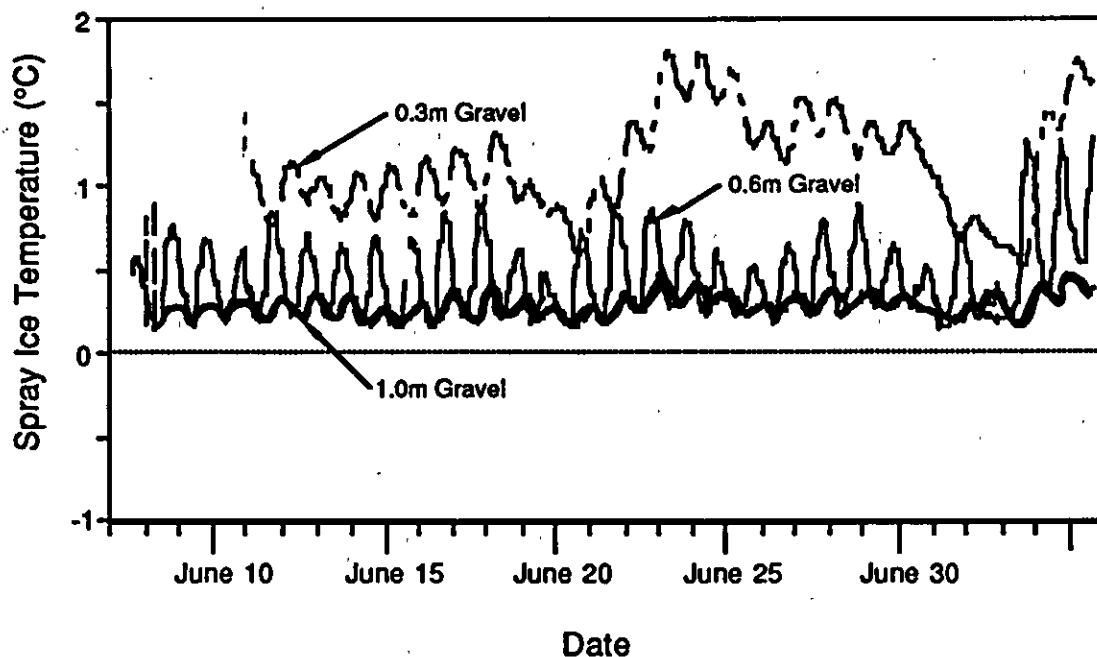


Figure 18. Spray Ice Temperatures Beneath Gravel Plots

same trend. However, the average daily temperature is typically warmer by 0.1 to 0.2°C. Spray ice ablation measured at these two sites was nevertheless similar.

Contrastingly, spray ice temperatures associated with the 0.3 m thick gravel ablation plot were higher than the thicker gravel plots by amounts ranging from 0.5 to 1°C. Moreover, ice temperatures appeared to be influenced to a greater degree by air temperatures. This warming was responsible for the greater degree of spray ice ablation observed.

Comparisons of spray ice temperatures measured beneath the sawdust ablation subplots are indicated by the temperature - time series plots shown in Figure 19. Again, both the spray ice and air temperatures were averaged on a daily basis. Like the gravel ablation plots, there was a strong correlation between spray ice temperature and ablation. The thicker the sawdust layer, the lower the spray ice temperature, and the less ablation observed. One anomaly was noted in the spray ice temperature data beneath the sawdust bags at the end of June. Meteorological data cannot adequately account for the rise in spray ice temperature observed

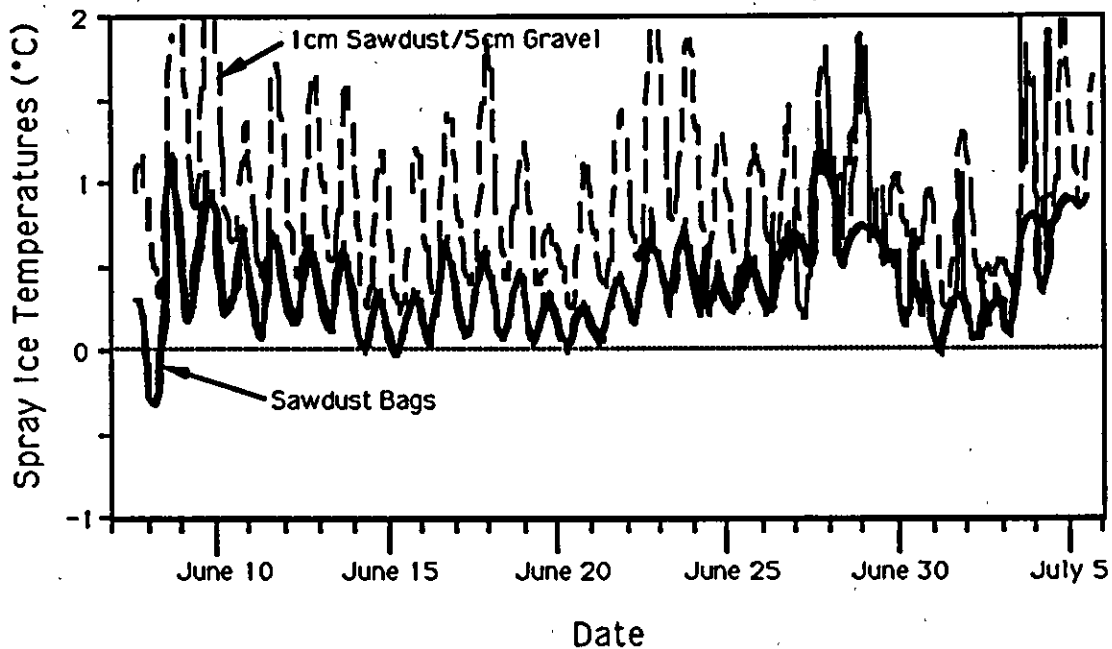


Figure 19. Spray Ice Temperatures Beneath Selected Ablation Plots

beneath the sawdust bags. On the other hand, spray ice temperature increases documented in July for each of the sawdust subplots appeared to be directly attributable to warm air temperatures.

Additional Spray Ice Ablation Observations

Significant spray ice ablation was documented during the first month of the experiment at locations where the island surface had been soiled. This is attributed to the albedo reduction and absorption of solar radiation by dark colored materials.

Ablation of clean spray ice commenced in earnest with the onset of above-freezing air temperatures in late-May. After late-May, the ablation rate of soiled areas was drastically diminished, due to the fact that the layer of dark materials had reached sufficient thickness such that it now served to thermally insulate the spray ice surface. This resulted in the formation of a number of mounds and hummocks which grew higher with time as the relatively cleaner surrounding spray ice ablated at a comparatively more rapid rate.

The insulating layer thickness necessary to retard ablation varied with material (i.e. sawdust, sand, cement, pit liner, etc.). However, except for foam insulation it was seldom over 1 to 2 cm thick. One portion of the island not part of our ablation experiment, but from which ablation data could be collected nonetheless was the used drilling mud discharge area on the northeast side. A photograph of this area is shown as Plate 8. The thickness of the drilling mud, insulating the spray ice ranged from 10 to 20 cm. Because of the insulating quality afforded by the mud, island freeboard was maintained in this area.

The central portion of the island where the drilling rig had operated was another area that experienced relatively limited spray ice ablation due to the presence of debris (especially before the late-June cleanup). Cumulative ablation in this area was estimated to be less than 0.5 m where the spray ice had been covered. Hummocks 2.5 to 3.5 m higher than the surrounding ice were observed to be covered with 1 to 2 cm of sawdust and/or cement and mud.

Sand also proved to be effective in slowing the rate of spray ice ablation. Evidence to support this claim was collected at the inclinometer stations and at several isolated sites where hummocks had been created as a result of a thin (2 cm) layer of sand covering the spray ice. Sand was originally packed around the inclinometer casing at the time of installation in January. As spray ice meltback progressed, inclinometer stickup increased, exposing a greater quantity of sand. This sand was eventually spread atop the spray ice surface in the vicinity of the inclinometer casing.

During subsequent visits, spray ice beneath the sand had not ablated appreciably whereas that beyond the cover of the sand ablated to the extent that a mound was created. Over time, it was impossible to reach the top of the casing from the unprotected spray ice due to differential ablation. Therefore, the sand and spray ice protected by the sand which surrounded the casing had to be removed. At the time it was found to be hard and competent and could only be dislodged by chipping with a sharp object. This observation provides additional support to the claim that surface coatings tend to provide additional benefits by hardening the spray ice surface.

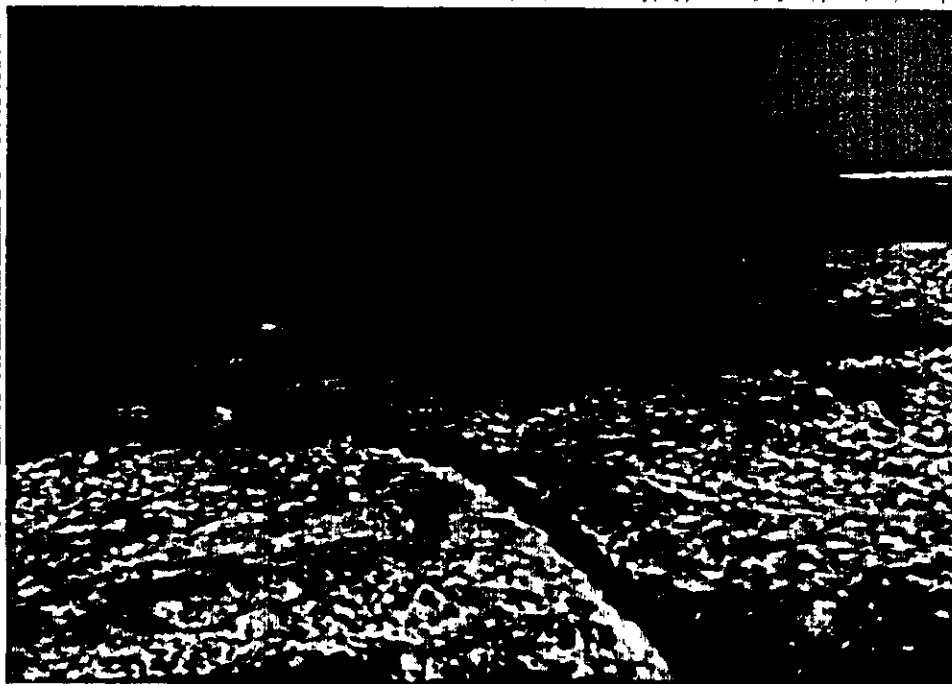


**Plate 8. Ablation Differences Between Spray Ice Covered With
Spent Drilling Mud and Unprotected Spray Ice**

ABLATION SUMMARY AND IMPLICATIONS

Based on an assessment of the ablation data collected over the course of the experiment, it appears that protecting the spray ice island from excessive ablation is feasible from both technical and economic standpoints. The following comments and observations pertaining to spray ice ablation are provided toward the development of a scenario that would enable drilling to continue until June and the drill rig to be demobilized by barge after breakup of the landfast ice sheet.

- Island design should take into account that between 2.5 m and 4 m of freeboard will be ablated from the unprotected spray ice (depending upon the timing of rig marine demobilization). The design freeboard of a spray ice island should be at least several meters higher than the expected ablation to ensure that the island does not break up due to loss of freeboard before the demobilization operation is completed.
- A 3 cm thick layer of sawdust or wood chips placed on the working surface in the vicinity of the rig prior to deployment of rig mats and mobilization of the rig would be beneficial to guard against undue warming of the spray ice. This is especially true later in the season when increasing air temperatures prevalent in April and May could result in unacceptable settlement or differential settlement rates.
- Rig mats or sawdust/wood chips placed atop the spray ice in the vicinity of warm rig buildings and radiators will mitigate undue warming of the spray ice.
- One potentially cost effective method of reducing spray ice ablation (environmental regulations permitting) is to save and stockpile used drilling mud for subsequent spreading atop the ice surface later in the season.
- Floor temperatures of rig buildings should be closely monitored and kept as cool as possible, especially with the onset of warmer air temperatures later in the drilling season. Undue warming may be at least partially prevented by opening access doors and vents and redirecting radiator airflow.

- A thin cover of clean snow smeared over soiled spray ice surfaces during short periods of near or above freezing temperatures and/or intense solar radiation and calm winds is an effective means of mitigating ablation.
- It may be advisable to ascertain the extent and density of hidden cracks in that portion of the island eventually underlying the stacked rig to minimize the potential for operational problems associated with the marine demobilization.
- A thin (3 cm) veneer of sawdust/wood chips should be spread over the spray ice near the stacked rig to minimize surface ablation. Rig components should be placed atop rig mats whenever possible.
- It may be necessary to place ablation protection materials as much as 15-20 m beyond rig components to avoid the formation of a scarp too close to the stacked rig. A gentle slope could be created by gradually reducing the thickness of ablation protection materials with distance from rig components.
- To minimize costs, application of ablation protection materials could be limited to the vicinity of the stacked rig and along routes allowing access to the edge of the island. The remainder of the island could be considered sacrificial and thereby left unprotected.
- It may be worthwhile to consider constructing primary and secondary access routes from the stacked rig to the barge docking location. This scenario could potentially minimize barge standby time in the event of persistent adverse weather conditions during the planned demobilization.
- Barge access routes should be constructed wide enough to allow vehicles and equipment to pass side by side.
- Spray ice along the access routes could temporarily be protected with sawdust or wood chips until the barge docking point is identified. Then, the spray ice could be covered with sand, gravel, and rig mats to reduce

disturbance to the spray ice. Materials such as sand and gravel appear to offer an additional benefit of hardening the surface and thereby minimizing the disturbance to the spray ice as a result of over-ice operations associated with the demobilization effort. It is speculated that sawdust would also provide a degree of surface hardening, but probably less than that of either sand or gravel.

- Rig mats should first be placed near the barge, gradually working toward island center to minimize the risk and consequences of encountering a crack near the edge of the island.
- Cracks could be spanned by rig mats used in conjunction with timbers.
- Ablation of the protected and unprotected spray ice should be monitored until the rig has been demobilized to the barges. Routine maintenance of ablation protection materials will probably be required.
- Stacking the drilling rig on or near the edge of the working surface rather than the edge of the island minimizes the consequences imposed by a prolonged intense storm severely eroding the island.
- The access route from the staging area to the loading dock may need to be continually groomed so that the underlying spray ice is not overly degraded.

ISLAND EROSION

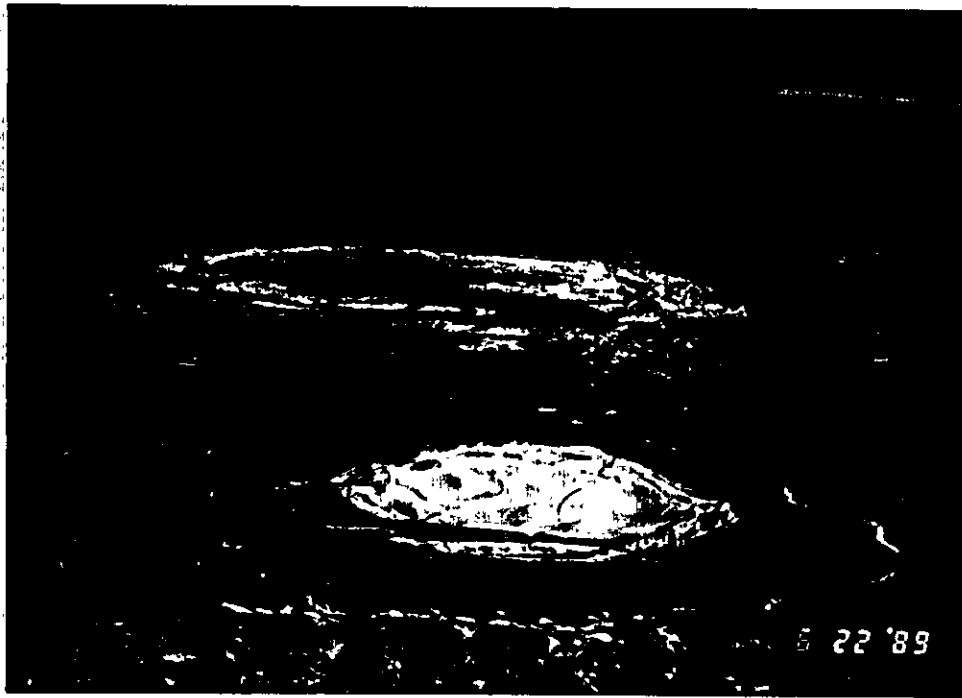
A portion of the experiment was designed to evaluate the performance of the edge protection system to protect the island edges from thermal and mechanical erosion due to wave action and currents. (An evaluation of the edge protection system with regard to protecting the island surface from ablation was presented in the section entitled: Surface Ablation). A knowledge of spray ice erosion rates is an essential part of a marine demobilization in that the island needs to be protected long enough into the open water season to allow for the demobilization operation to be completed.

Island erosional processes, rates, and patterns were monitored from the time of island breakup (on June 23 or 24) through final island breakup on July 10. Two forms of wave erosion were evident - thermal and mechanical.

The affects of thermal wave erosion were probably most readily observed on the relief pad and on portions of the island outside of the experiment setup area having a relatively high freeboard. These regions appeared to be breaking up predominantly as a result of thermal wave erosion which is similar to that observed for previously constructed spray ice features Jahns, et al. [8]. In this mode, wave action produces high local water velocities which cause a high effective heat transfer rate between the near-surface water and the ice edge. Wave induced heat transfer tends to undercut the island edges creating notches. As the notches grow inward at the waterline, ice overhangs and underwater terraces are created. In time, the overhangs collapse due to gravity forces and the terraces either break upward because of buoyancy or possibly disintegrate in place depending on the degree of cohesion at the seabed [7].

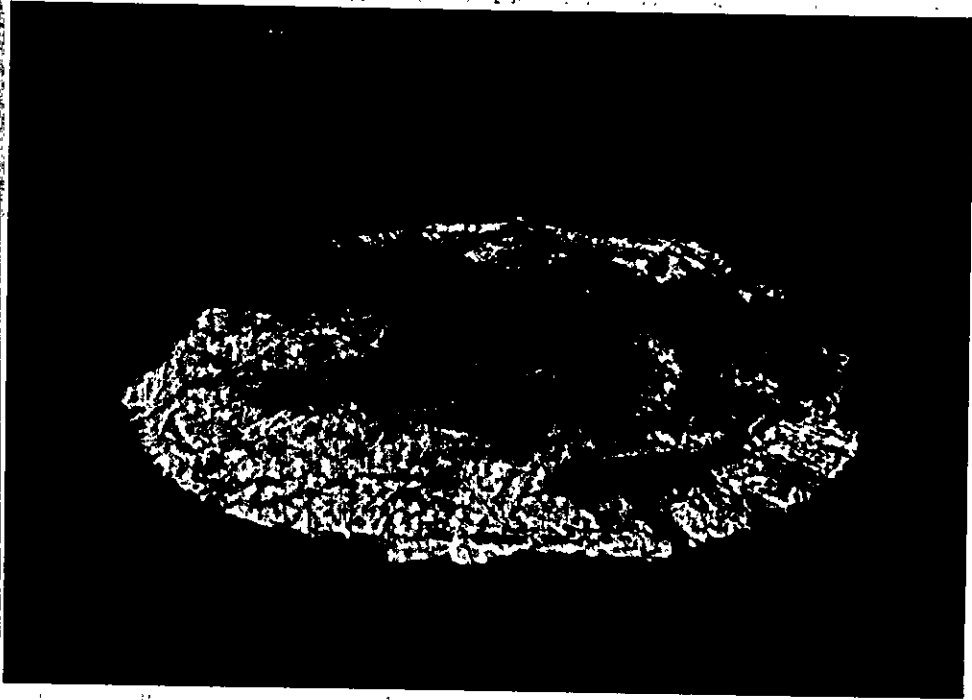
Nipterk appeared to break up predominantly due to a lack of freeboard rather than from wave erosion. Except for the experiment setup area and other regions in which the spray ice was protected, ablation reduced the freeboard to between 0.5 and 1 m on July 5. A network of newly formed cracks, the largest of which could readily be seen from the air (see Plate 9b and 9c) were probably due to an instability condition created by the lack of freeboard as a part of the island became buoyant. Small sections of the island tended to periodically lift up off the bottom. These eventually drifted away from the island as a result of mechanical wave action and currents. The wholesale breakup of the island on July 10 is further evidence that it broke up mainly due to a lack of freeboard. Once dislodged from the seabed, fragments were carried away by currents.

Composites of oblique and vertical aerial photographs of the island taken on June 22, July 5, and July 8 are shown in Plate 9. These photographs graphically illustrate the succession of island breakup. On June 22, the island diameter was 320 m (area = 80,500 m²) as complete landfast ice breakup had not yet occurred.



(a) June 22

Plate 9. Aerial Views of Nipterk.



(b) July 5



(c) July 8

Plate 9 (cont'd). Aerial Views of Nipterk

Open water conditions persisted on July 5 and the edge protection system was draped over the edge as per design. Based on an assessment of ice and weather conditions, barges could have been mobilized to the island from Tuktoyaktuk for the rig demobilization by this time.

An analysis of a July 5 aerial photograph to determine island area was performed by VTA Photogrammetric Consults. Island area was estimated to be 58,000 m² at this time. An error estimated to be within $\pm 10\%$ was introduced in the calculation because the photograph was taken at an oblique rather than vertical orientation. The effectiveness of the island edge protection system at mitigating edge erosion is clearly visible from the photo. A 25 m protrusion was created due to the presence of the system. An outline showing the original island diameter is shown in Figure 20 so that the location and extent of erosion can be identified. As can be seen from the figure, erosion was most intense on the south half of the island which is attributed to the outflow from the MacKenzie River.

During the July 5 site survey, 20 cm by 20 cm by 3 m long wooden timbers were placed at the southwest, southeast, north, and north-northeast slope indicator stations in such a manner that they would serve as ground reference points in aerial photographs. Ground reference points were required to accurately determine island area. Distances between the storage tent and southwest and north survey stations were also measured. The hole center (cellar) was another known reference point which could be used. The distances between the hole center and slope indicator survey stations had been measured in January.

Vertical aerial photographs of the island were taken the morning of July 8 by Inuvik-based Photo Script Ltd. using a Twin Otter aircraft chartered from Aklak Air Ltd. The aircraft had a camera mounting hatch on the underside of its fuselage which facilitated the collection of vertical photographs.

The negative of one color image was analyzed by VTA to determine island area. Using the control points which we provided, a scale factor was computed such that a conversion from the instrument units to true ground units was performed. A perimeter was digitized from which the polygon area was calculated. Three areas were computed: 1) the main ice island excluding the four fragments which appear to have already calved, 2) the area covered by the four fragments, and 3)

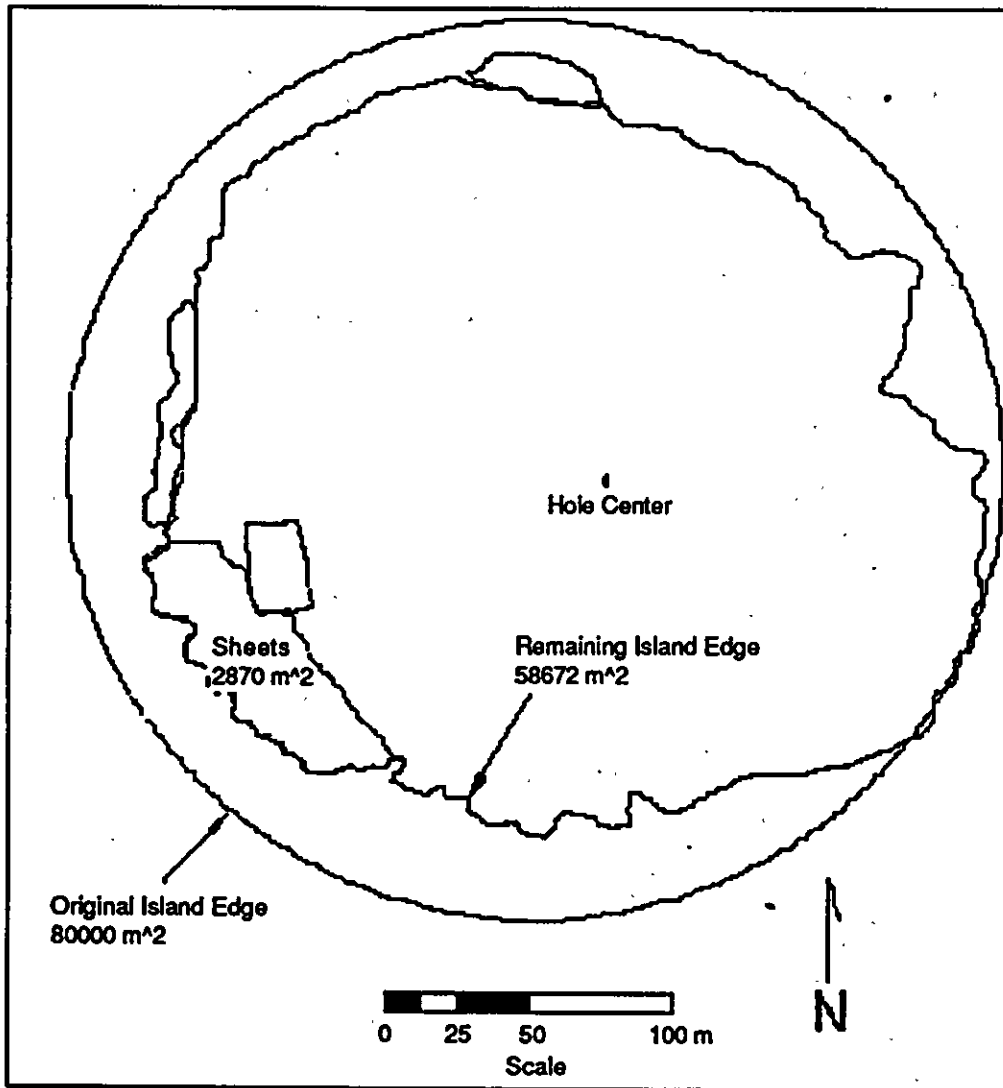


Figure 20. Comparison of Original and Remaining Island Area on July 5

the area covered by the edge protection system. Figure 21 shows the digitized island perimeter used to calculate the area and the original island area.

Prior to the initiation of erosion, the original island area was about 80,500 m². According to calculations performed by VTA, the island area was between 28,600 - 29,400 m² (the latter value including fragments which had already calved) on July 8. Thus, about 36% of the original island area was still intact.

The actual area covered by the sheets and net was initially about 8,000 m². This value takes into account overlap and extension of the system beyond the grounded portion of the island which was estimated at 1,500 m². VTA calculated that 790 m² or 10% of the sheet protection system was still covering the island surface on July 8.

At the time, the net protection system was no longer in place due to insufficient anchoring. This factor in conjunction with minimal freeboard induced by ablation were responsible for that portion of the island protected by the net calving as soon as it did. Omitting the original island area covered by the net resulted in an island area of 5,600 m² originally protected by the sheets. Utilizing this value, it was calculated that 14% of the area originally covered by the sheets was still in place.

The degree of stabilization afforded by the edge protection system is readily apparent from Figure 21 which is a diagram comparing the original and remnant (July 8) island areas. The next least amount of radial erosion documented at a different location was more than twice that observed at the sheets. Also evident from the figure is that erosion was most pronounced on the south and east sides of the island which is attributed to the warm outflow from the MacKenzie River.

It is not possible to determine with any degree of certainty whether one type of sheet was more effective in retarding erosion than another. Collectively through, the sheets appeared to be significantly better at slowing erosion than the net system. However, at least a portion of the success attributed to the sheets in this regard was due to spray ice ablation protection provided by them.

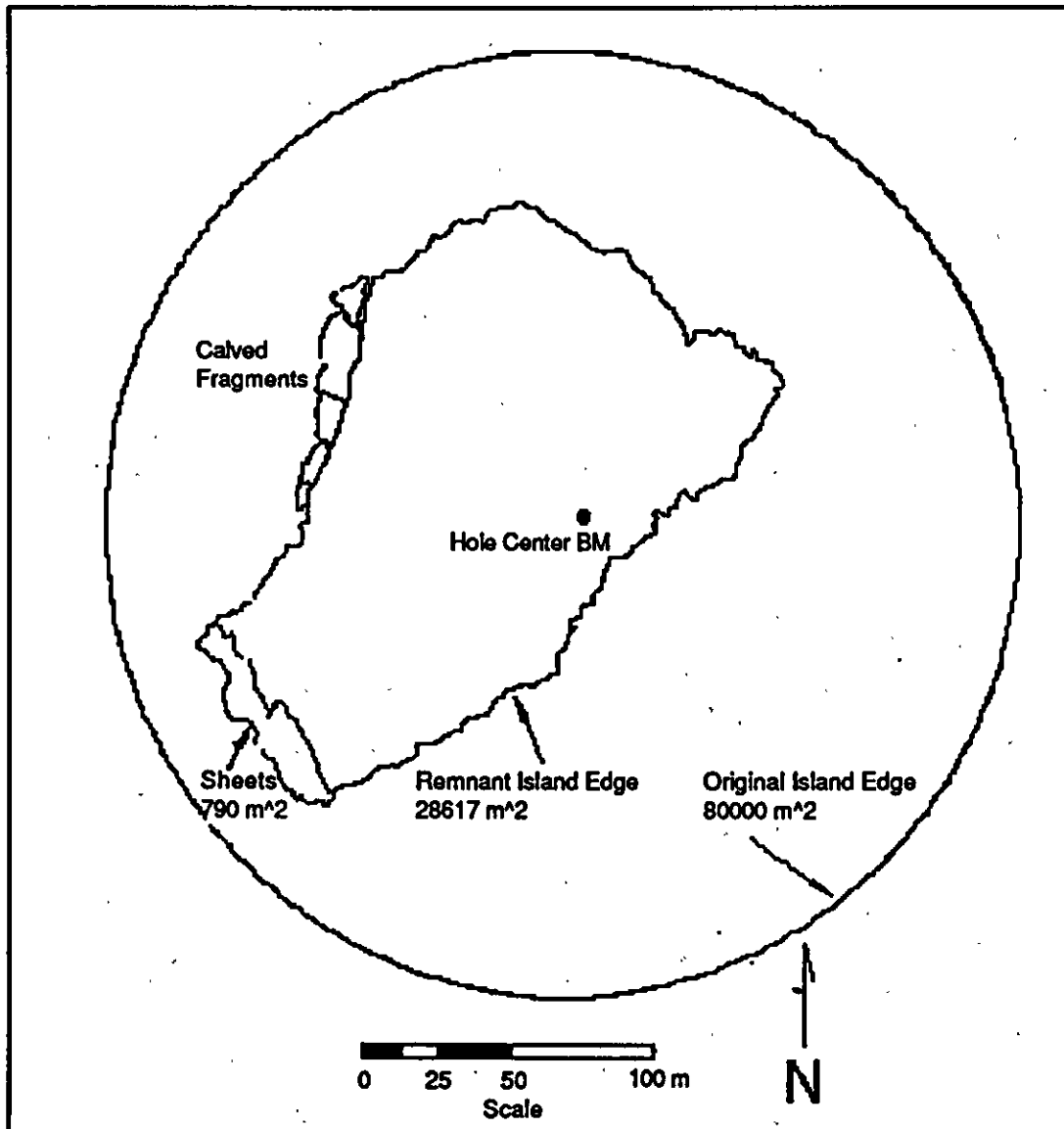


Figure 21. Comparison of Original and Remnant Island Areas on July 8

As of July 5, there had been only minor tearing of the sheets due to abrasion of the spray ice. The degree of fabric sheet abrasion resistance was an area of concern identified during the planning stages of the experiment. With time however, this concern was alleviated. None of the sheets appeared to have been more susceptible to the effects of abrasion than the others. This is an important finding because the Rufco sheet costs only half the amount of the vinyl sheets. Moreover, the Rufco sheet was also easier to install resulting in even greater cost savings.

Unlike the sheets, the nylon reinforced sandbags at the edge of the island experienced a high degree of abrasion due to being in contact with the spray ice. A number of bags were abraded to the extent that their gravel contents spilled out onto the ice. Still others became dislodged from their tie down points. In light of these shortcomings other materials should be considered for sandbag fabrication in future operations.

Another problem connected with sandbags pertains to the degree of sheet anchoring capability they provided. Westerly component winds in excess of 20 knots tended to push the sheets back on to the island. Only after additional sandbags were placed at 1 m intervals along the island edge were the sheets held securely in place. The weight associated with the placement of additional sandbags would have made it even more difficult to retrieve the sheets from the island prior to complete island disintegration had this option been exercised.

Contrastingly, the number and spacing of sandbags used to retain the net protection system was adequate. Because ablation exposed most of the anchors and the spray ice beneath the net disintegrated due to lack of freeboard, it is not possible to accurately assess whether the net edge erosion system by itself would have been sufficient to mitigate erosion long enough to enable the rig to be demobilized by barge. Consequently, the edge protection system designed for future islands should rely predominantly on sheets. Nets could be placed on both sides of the sheets to further mitigate erosion. One way to decrease the overall cost of the net is to use polypropylene rope and increase the mesh spacing. In light of the data collected from this program, neither of these modifications are anticipated to have a significant adverse effect on the performance of the net protection system.

EROSION RATES

Previous Information

To date, few data are available regarding the erosion rate of unprotected spray ice. One if not the earliest account of erosion rate data was collected during the Exxon Ice Island Experiment. The maximum degree of radial erosion measured during the experiment was 7.9 m day^{-1} in August whereas average radial erosion was less than 3 m day^{-1} [9]. However, due to differing construction techniques, much of the island was built out of ice that was significantly more dense and thus less porous than typical spray ice islands. Therefore, the aforementioned erosion rates may be considered low compared to those which can be expected for spray ice features.

Additional insight into spray ice erosion rates is provided in Jahns et al. [8]. The information presented is based on data acquired from a large spray ice barrier surrounding Global Marine's Concrete Island Drilling System (CIDS) at the Exxon Antares drill site in 14.9 water depth in the Alaskan Beaufort Sea. Jahns et al. [8] reported that following breakup, thermal erosion associated with wave action was more detrimental to the barrier than spray ice ablation. Wave undercutting was observed to be particularly severe during storms and resulted in calving of large pieces of spray ice from above and below water. Breakup of the landfast ice sheet occurred on July 3. From an analysis of time-lapse camera data collected during the open water season, the rate of barrier retreat was as high as 30 m day^{-1} . Nearly 50% of the barrier was reported to be still intact when the structure was towed out on August 17. A small portion of the barrier was still in place in early September.

Numerical Simulation

Background

Connolly [1] developed a numerical model to calculate the amount of spray ice that would be lost by a spray ice island due to surface melting and erosion from waves and currents during the open water season for a site in the landfast ice region of the Alaskan Beaufort Sea. The simulation was refined and rerun as part of this study.

Overview

In order to explain the physics behind the ablation and erosion processes on the spray ice island, an effort has been made to model these processes. The model was developed from earlier work done by Connolly [1] in which a hypothetical ice island was used to determine the survivability of a spray ice island through a summer melt season in the Alaskan Beaufort Sea. For that study, climatological data were parameterized in order to determine the average energy balance of a spray ice island.

For the current study, the models were modified to incorporate data collected by Esso directly on the ice island. A more detailed account of this modeling effort undertaken by Analytic Applications, Inc. is provided as Appendix E. By incorporating the data collected into physically meaningful models, the deterioration processes of the island can be observed independently and the capability of predicting the behavior of future islands can be enhanced.

The modeling effort was broken into two parts; the ablation of the top surface of the island, and the erosion of the perimeter. The ablation of the top surface involves the energy transfer between the ice and the atmosphere. In this case the standard energy balance equation was used. This equation is given as:

$$F_s + F_l + L + S = \gamma p D + C \quad (2)$$

where F_s is the net short wave radiation, F_l is the net long wave radiation, L is the latent heat flux, S is the sensible heat flux, γ is the latent heat of fusion, ρ is the spray ice density, D is the depth to which the ice has melted, and C is the heat conducted through the ice. All of these quantities are averaged over the surface of the island.

Erosion of the island perimeter begins when the natural ice breaks up, leaving the spray ice exposed to the action of waves and currents. Although the currents erode over the entire vertical cross section of the perimeter and the wave action is only at the waterline, the wave action term dominates because of the greater amount of heat transferred. White et al. [10] used the following Reynolds analogy to compute heat transfer to an iceberg as a function of wave friction:

$$F_w = 0.000219 \left(\frac{R}{H}\right)^{0.2} \left(\frac{H}{P}\right) \rho \gamma (T_w - 273) \quad (3)$$

where F_w is the heat flux due to wave action, R is the roughness length of the ice, H is the average wave height, P is the average wave period, and T_w is the water surface temperature.

Equations (2) and (3) were used in separate models and run independently. For the ablation model, data were taken from the island data set from June 10, 1989 to July 5, 1989. From the measured ablation data and spray ice temperature data June 10 is slightly after the onset of significant ablation. Data from the instruments were not collected after July 5 and the island broke up July 10. The ablation model was first run to simulate unprotected spray ice. In this case the albedo is high, reflecting much of the incoming solar radiation. The island is assumed to be isothermal at 0° C, so that any addition of heat at the surface is converted into melting ice.

The sensible and latent heat flux terms were calculated from the measured temperature gradients and energy transfer coefficients. The coefficients are dependent predominantly upon wind speed, stability, and roughness length. Because the differences between the sensible and latent heat flux coefficients are within measurement error, they were taken to be equal for this study. A number of different coefficients were tried in the model to determine the model sensitivity.

Figure 22 shows some of these results compared with the data measured on the island. From this figure it appears that 0.0014 provides the best fit to the measured data.

The flat parts in the ablation curves correspond to the night time periods when net heat flux is away from the island. Since there is no heat entering the island surface, no ice is melted. Instead, some of the liquid water present in the surface can then be refrozen which requires subsequent energy absorption to melt again. This accounts for the hard crust on the island surface in the mornings.

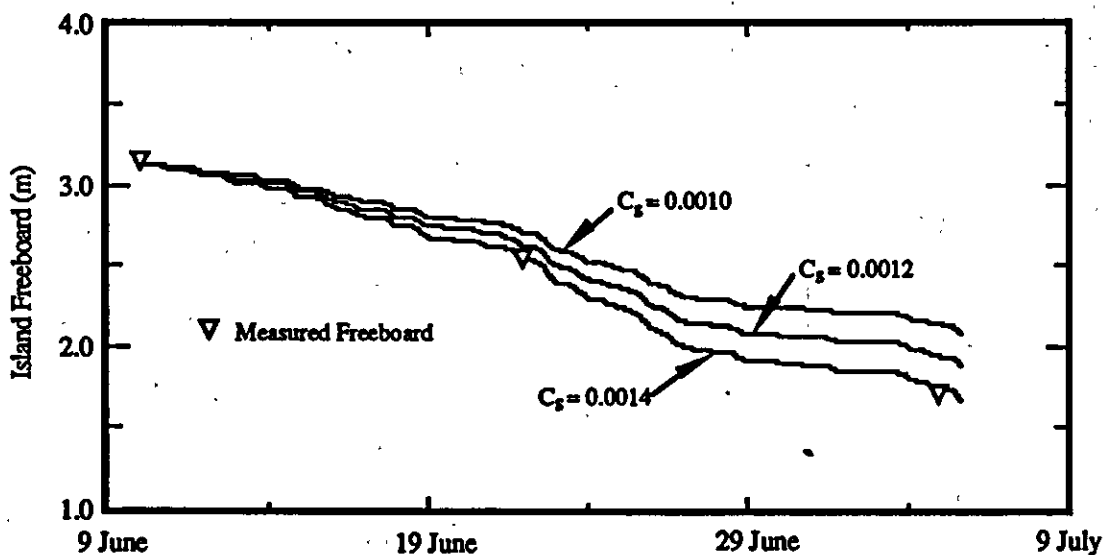


Figure 22. Ablation of the Top Surface of the Ice Island Compared With Measured Data.

The model was changed in order to simulate the presence of various ablation protection materials. These materials consisted of gravel pads of various thickness, sawdust layers, and fabric sheets. A protective material spread over the ice serves to insulate the ice from solar and longwave radiation, and sensible and latent heat flux. The approach taken by Connolly was to calculate the energy transfer between the material and the atmosphere and then to calculate the heat

conducted through the material to the ice. The resultant heat transferred through the protection material was used to melt the ice.

The results from the sawdust model are shown in Figure 23. Although the results compare favorably, some discrepancies arise due to the fact that the sawdust was modeled as a material of homogeneous thermal conductivity. This may not be the case due to an inhomogeneous distribution of ice or water in the sawdust, which would lead to changes in the thermal conductivity of the material. These thermal conductivity inhomogeneities could also change with time since water is added with rainfall, percolates out the bottom, refreezes or thaws.

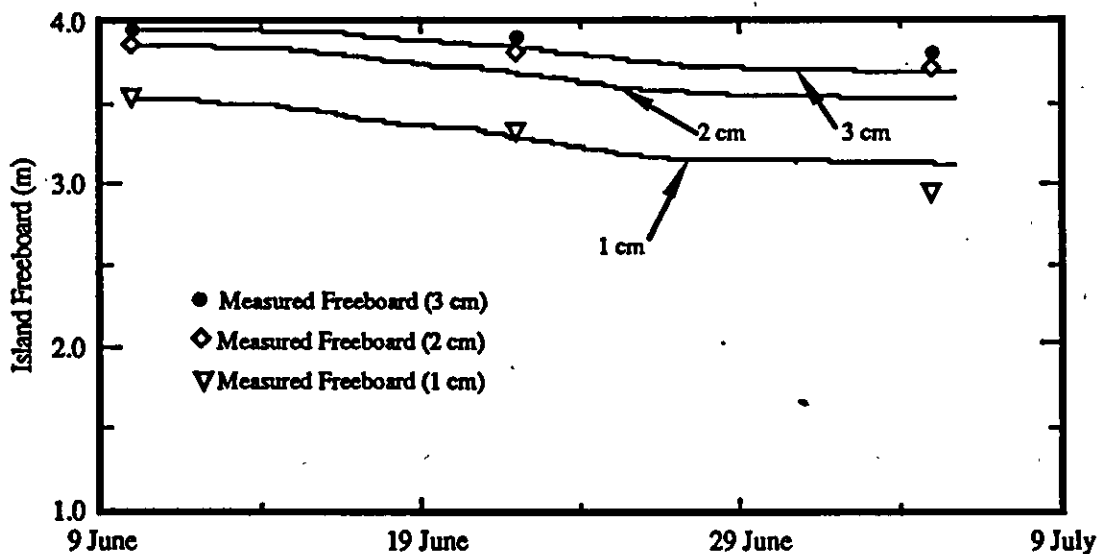


Figure 23. Comparison Between Measured and Modeled Meltback Under 1 cm of Sawdust

Wave erosion was modelled as being distributed evenly around the perimeter of the island so that the island retains the shape of a disc. In reality the erosional forces are directional and the island quickly becomes asymmetrical depending on the predominant directions of the forces. However, one of the most important factors in island survivability is sliding friction between the ice and the seabed.

Since the sliding friction is a function of area of contact, the shape of the island is not as critical of a term.

Wave height, period, and water temperature are important factors in the erosion model. Since data concerning these terms were sparse, a variety of different wave heights and periods were input into the model to determine the sensitivity of the model. The results are shown in Figure 24. Waves of 0.25 m, 0.5 m, and 1.0 m were input along with periods of 3 and 4 seconds. The model was run from the first day of open water, June 23, until July 5.

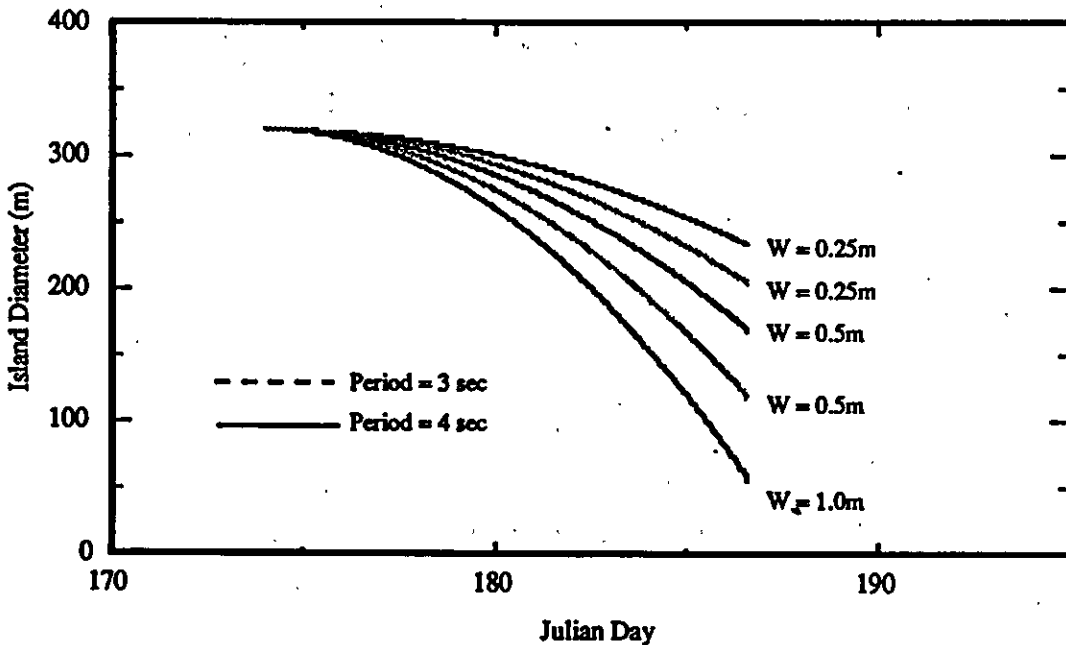


Figure 24. Results of the Use of Different Wave Parameters in the Perimeter Erosion Model.

As can be expected, the higher wave heights and shorter periods cause the greatest amount of erosion. The closest fit to the data is achieved with an average wave height of 0.5 m and a period of 4 seconds.

The use of various island edge protection materials has shown definite value in protecting the perimeter of the island from erosion. Although a number of

different protective materials were used, it was difficult to determine from the aerial photos if any showed better results than the others. Another comparison problem arose due to the fact that the protective sheets were only used on a portion of the island. Since perimeter erosion was asymmetric it was difficult to determine what erosion would be for an unprotected edge with the same exposure. Nevertheless, the island radius was observed to decrease from 160 m to 135 m where the edge protection was used. The edge protection is seen as a baffle between the waves and the ice, in effect damping out the amplitude of the waves. From the model a diameter of 260 m corresponds to an average wave height of 0.2 m if the period remains at 4 seconds. Thus, the edge protection effectively attenuates the waves by 40% of their original height.

The results of the modeling effort have provided some new information on the behavior of a spray ice island during the melt season. The results of the ablation and erosion protection experiments have also added valuable information along the lines of protecting an island and extending its operating period. Of significant importance are results of the sensitivity studies which have shown the response of the model to differing environmental conditions.

ISLAND BREAKUP

Breakup of the landfast ice sheet occurred sometime between June 23 and June 24. The island withstood the lateral ice forces imposed on it during breakup. As indicated in the section entitled "Monitoring Surveys", the last complete site survey was carried out on July 5. At the time, the island was surrounded by open water which extended several kilometers in all directions. Only isolated, relatively small first-year ice floes were observed to drift over the island during the 12 hour site survey.

Most of the grounded portion of the spray ice relief pad located about 500 m to the east was also intact on July 5. Because of its higher freeboard, the relief pad appeared to be diminishing in size predominantly as a result of calving induced by wave thermal and mechanical erosion along the edges. This form of behavior is similar to that observed for other spray ice features [8]. Wave action produces high local water velocities causing a high effective heat transfer rate between the

near-surface water and the ice edge. The wave-induced heat transfer undercuts the island edge creating notches which grow inward at the waterline. Eventually, these overhangs become sufficiently large that they break off as a result of gravity. The underwater terraces which tend to adhere to the seafloor [7] are eventually brought to the surface by buoyancy or are melted in place.

As of July 5, approximately 28% (by area) of the grounded portion of Nipterk (originally 320 m) had calved. Due to cumulative ablation, island freeboard was typically reduced to between 0.5 to 1 m except in areas where the surface had been protected. The island appeared to be disintegrating in a different manner than that observed at the relief pad. At Nipterk, calving appeared to occur due to an instability condition created as a result of insufficient freeboard. Small portions of the island periodically lifted off the bottom and were eventually carried away by winds and current.

After break out of the first-year ice sheet, the protection sheets draped over the island edge as per design. The south edge of the Rufco sheet was almost entirely in contact with open water on July 5.

Island breakup was anticipated in the near future due to the instability created by the lack of freeboard. Several new cracks had already developed where portions of the island became buoyant. However, even though the island was deteriorating at an accelerated pace, there was no evidence of significant horizontal sliding along the seabed at most of the slope indicator survey stations which may have been indicative of a precursor to eventual catastrophic breakup.

The performance of the sheets on mitigating edge erosion had, to date, only been evaluated for a brief period. Therefore, in order to continue collecting data for as long a period as possible, a decision was made not to terminate the experiment. Most of the nonessential equipment was removed from the island by helicopter on July 5.

To monitor the progression of island deterioration more closely, another site survey was scheduled for July 10. Based on an assessment of the condition of the island at that time, the option existed to immediately demobilize the edge protection system onto a barge as Arctic Transportation Ltd. (ATL) would be

undertaking salvage operations of equipment which had broken through the ice at the base of the island earlier in the year. Alternatively, another option available was to demobilize following completion of the salvage operation. The timing for retrieval of ablation and edge erosion monitoring instrumentation would also be assessed at the time. It was felt that this approach would enable a maximum data collection effort and still afford the opportunity for a quickly instituted complete demobilization in the event of imminent island breakup. Selection of this option also enabled us to go ahead with plans to dock a barge alongside the island since this operation would be required in demobilizing a drilling rig during the open water season.

The island was next visited on July 6 for a brief period by an Esso representative during a final cleanup site inspection. Small-scale calving was reported as was a newly formed crack in the vicinity of the gravel ablation plots. An aerial photography survey was undertaken on the morning of July 8 to determine the island area, effectiveness of the edge erosion protection sheets, and the general state of the island. By this time, only about 35% of the island (by area) remained.

The Nipterk site was next visited by Esso personnel on July 10. However, the remaining portion of the island had broken up into a number of small fragments prior to our arrival in only a matter of a few hours (according to ATL personnel). The date of complete island breakup was about 2.5 weeks after breakup of the surrounding ice sheet. Most of the fragments subsequently drifted westward under the influence of light easterly winds and currents.

From an ensuing aerial reconnaissance survey, it was determined that the island remnants were still located within 500 m of their original calving site. Several fragments appeared to have drifted only a short distance and temporarily grounded. Unfortunately, even after a thorough search, the island fragments containing the ablation plots and geotechnical instrumentation could not be spotted. These fragments probably rolled onto their side due to an instability condition created by the ablation protection materials (mainly gravel). ATL personnel confirmed that several island fragments rolled shortly after calving.

DEMOBILIZATION OF THE EDGE PROTECTION SYSTEM

After island break-up the edge protection system had to be recovered due to the potential environmental and navigation hazards it imposed. On the afternoon of July 10, two of the three edge protection sheets were visible just to the west of the former island site. Both the Rufco and 18 oz. per square yard nylon sheet had entrapped air beneath them so that a portion of each was raised out of the water.

The netting from all four protection systems was also easily identified by their wooden 20 cm by 20 cm deadmen which were now afloat. At the time of our survey, the location of the 13 oz. vinyl tarpaulin could not be identified though it was speculated that the sheet was still being held in place by the netting. Arrangements were made with ATL to recover the edge protection system as soon as the salvage operation was completed.

Another helicopter aerial reconnaissance survey was instituted the following day. The wind direction had reversed from the previous day and was now west-northwesterly. No island fragments were visible; the nearest ice being 10 km away. The sheets could no longer be seen in the heavily silted water, but the netting was known to still be on-site as evidenced by the floating anchors.

The entire edge protection system was successfully retrieved over a 12-hour period on July 12. To perform this operation, divers first determined the exact positions of the sheets. Then, the crane barge was moved into position so that sheets could be reached. A crane equipped with a clam bucket was used to lift the sheets onto the barge. After successfully completing the recovery operation, the barge was towed back to Tuktoyaktuk and the edge protection system disposed of.

ISLAND SETTLEMENT

The spray ice foundation beneath rig structures must not only provide an adequate bearing capacity for all dead and live loads, but also exhibit acceptable settlement. Since spray ice is viscoelastic, the allowable bearing pressure will be controlled by consideration of settlement rather than bearing capacity. Surface subsidence caused by time-dependent deformation of the spray ice mass is one of

the critical aspects of a spray ice drilling platform. The anticipated total and differential settlements are of particular interest for rig foundations. Predicted subsidence characteristics could potentially impact both planning of the drilling operation (by allowing time for initial settlement prior to rig up) or the type of rig and foundation mat used including special means for rig leveling.

During their operating period, drilling rigs are capable of withstanding a certain magnitude of creep settlement without a disruption in drilling activities. Surface settlement rates will likely increase as the spray ice temperature rises above -5°C .

Towards this end, measurements of surface settlement were performed at as many as five locations during the experiment. The survey locations shown in Figure 7 are the same as those in which inclinometer surveys were undertaken.

The Sondex settlement system utilized was installed in January as part of the winter island monitoring program. System components consisted of a Sondex probe, an electrical cable graduated in meters, a readout unit, and the flexible casing. A measurement stand was located above the casing to facilitate depth measurement. Over time, spray ice ablation progressed to the extent that the base of the stand melted out and the stand could no longer be utilized.

Sensing rings were originally mounted to the outside of the Sondex casing at approximately 0.5 m intervals. The precise location of the sensing points was determined by means of electrical induction. The sensor's meter peaked when the probe's internal coil was aligned with the sensing point. Probe depth was measured by picking off the depth indicated on the cable corresponding to a graduated measurement tape on the reader stand (or affixed to the inclinometer casing). Since the sensing rings move (or settle) with the surrounding ice, the change in elevation of each ring with time can be directly related to settlement.

Sondex settlement surveys were performed at varying frequencies and locations during the experiment for a number of reasons including time constraints, restricted access to the station or to the bottom of the casing, and in the case of the June 10 survey, lack of an alternative means to perform the measurements due to loss of the reader stands. Settlement data are available throughout the

experiment period for stations located near the edge of the island working surface.

Figure 25 is a representative settlement profile measured at the southwest edge of the island working surface. Settlement profiles for the other survey locations are presented along with the raw settlement data in Appendix F. The seabed is at a depth of about 10.5 to 11 m whereas the submerged spray ice is represented by the level 4.5 m below the surface to the seabed. As a result of spray ice ablation, the uppermost 2 m of Sondex casing was cut off on June 22 due to the height of stick up. An additional meter of casing was removed on July 5. Consequently, settlement data for the upper 3-4 m of the island were not collected after the June 10 survey.

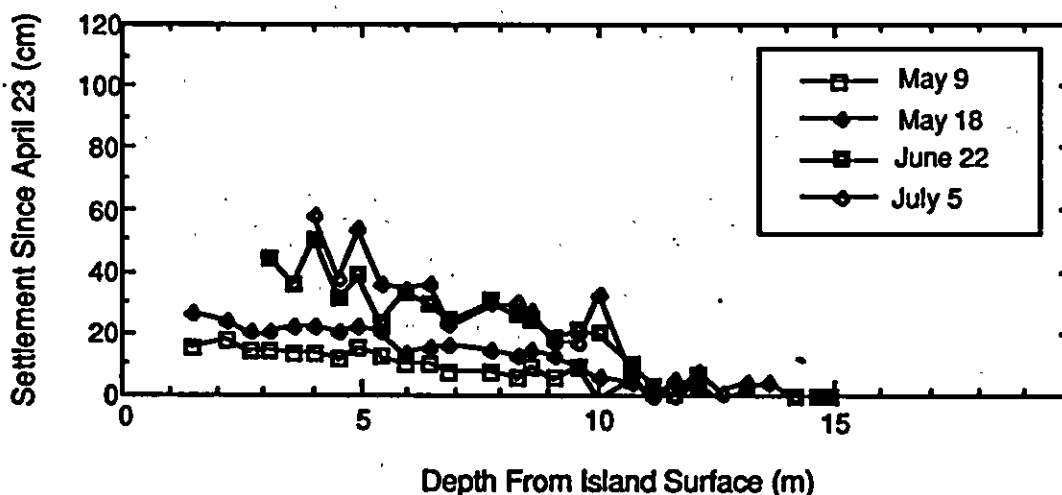


Figure 25. Spray Ice Settlement at Southwest Survey Station

An extrapolation of the settlement data on June 1 was performed for each of the three drilling pad settlement monitoring stations. The extrapolation may be a bit conservative in that it does not take into account the below freezing air temperatures prevalent throughout most of May. Based on the interpolation, maximum settlements ranged from 37 cm to 45 mm. Neither the magnitude nor rate of settlement documented would have posed any operational problems for a drilling rig. In fact, from a standpoint of total surface settlement, the drilling rig

could have operated through to at least July 5. Maximum differential settlement across the working surface was estimated to be less than 1 cm on June 1. Like total surface settlement, the maximum differential settlement estimated for June 1 is not expected to impose any restrictions on operating a drilling rig until this time. It appears from the profiles, that differential settlement would not have created any drilling restrictions until after at least June 22. By July 5, only the southeast station appears to be settling at an accelerated rate. However, this apparent trend may actually be at least partially due to casing bending.

Surface settlement near the southwest edge of the island was only measured on May 9 and 18. This is because the inclinometer casing had buckled at the seabed prior to the June 10 survey to the extent that the sensor could not be completely lowered down to the bottom. The maximum total surface settlement of 1 cm documented on May 18 was only one-half to one-third that measured on the drilling pad. In apparent contrast, total settlement observed at the north-northeast edge of the island on May 18 appeared to be significantly greater. It appears that most of the apparent settlement may have been due to localized failure. If this 50 to 60 mm offset is removed from the data, the total surface settlement observed is similar to that measured on the drilling pad.

ISLAND HORIZONTAL MOVEMENT

Nipterk was constructed at a site having relatively weak soils. In fact, the soil strength rather than the spray ice strength had the greatest impact on island design. The drilling rig can only withstand a certain magnitude of island lateral deformation before operations are adversely affected. Therefore, monitoring of lateral deformation is required throughout the drilling program as a means to assess island stability.

Five manually read inclinometers (slope indicators) were installed in January as part of the winter island stability monitoring program. Three of the five were at the periphery of the drilling pad whereas the other two were near the edge of the island (see Figure 7). Inclinometer casings were installed inside Sondex casings which in turn were anchored at different depths below the seabed. These stations

were left intact at the conclusion of the drilling program so that measurements could be continued.

Casing consisted of 7 cm (outside diameter) self-aligning 3.05 m (10 ft) long ABS plastic pipes. The inner surface of the casing was inscribed with four equispaced longitudinal grooves milled to control inclinometer orientation in a preselected direction (north-south or east-west). Casings were originally installed such that they projected about 0.3 m above the island surface. Propylene glycol was poured into the casing to prevent it from filling with water and eventually freezing.

A standard metric Digitilt Inclinometer probe manufactured by Slope Indicator Company (SINCO) was utilized. It consisted of a watertight aluminum cylinder that contained two servo-accelerometers mounted with the sensitive axes 90° apart which measure the angle of inclination of the longitudinal axis of the sensor in two orthogonal planes. The sensor was supported laterally in the casing by means of two sets of wheels which are guided by the casing grooves.

The inclinometer was supported by a heavy duty electrical cable graduated in one-half meter increments. To perform a survey, the probe was first lowered to the bottom of the casing and allowed to equilibrate. Then, the inclinometer was raised to the surface at 0.5 m increments and readings were collected in both the A and B (orthogonal) directions. After completion of the first survey, the probe was rotated 180° and a second survey was performed for greater accuracy.

Inclinometer data were collected using the SINCO Recorder Printer Processor (RPP) system. The RPP collected, stored, processed and displayed the digitilt data in terms of deflection vs. depth profiles.

Slope indicator surveys were undertaken during each complete site survey except at the south-southwest survey station where the casing deformed to the point that surveys could not be performed after May 18. An initial (reference) slope indicator survey was carried out on April 22 and data from subsequent surveys were compared relatively.

Inclinometer data and plots containing lateral deformation profiles for each of the stations in the north-south and east-west directions are provided in Appendix G.

Representative profiles from north-south and east-west directions for the survey station at the southwest edge of the drilling pad are shown in Figures 26 and 27. Deflections are given in millimeters and depths are shown in meters with regard to mean sea level which is denoted by a depth of 0 m. Positive depths correspond to the freeboard. Negative depths to as low as -6 to -6.5 m are associated with submerged spray ice whereas the seabed is below this depth. Relative changes in the surface of the island are also apparent from the profiles.

As can be seen from Figures 26-27 and those presented in Appendix G, total deflections measured at the stations near the edge of the drilling pad (i.e. southwest, southeast, and north) were typically small (maximum 13 mm in any one direction). Also note that most of the movement resulted from sliding along the seabed.

Up until June 10 or June 22 (depending upon the location), the island moved predominantly to the north. Then in late-June and early July the island movement direction reversed. Movements were greater in the north-south direction than in the east-west direction.

Due to the presence of cracks, both the magnitude and direction of horizontal displacements often varied among and between measurement locations. Horizontal movements were, however, typically much less in magnitude and more similar in direction on the working surface than near the island edge.

Deformation profiles from inclinometer stations near the island periphery are shown in figures provided in Appendix G. The magnitude of deformation was significantly greater at these sites than on the working surface. Most of the deformation at the south-southwest survey station occurred along the seabed. Over 6 cm of movement along the seabed was measured on May 18. Cumulative casing buckling became so great shortly after this time that the slope indicator probe could no longer be lowered to a level below the seabed.

Unlike any of the other survey sites, deformation at the north-northeast survey site appeared to be over a larger plane of failure in the saturated spray ice above the seabed at least in the north-south direction. The total magnitude of deflection

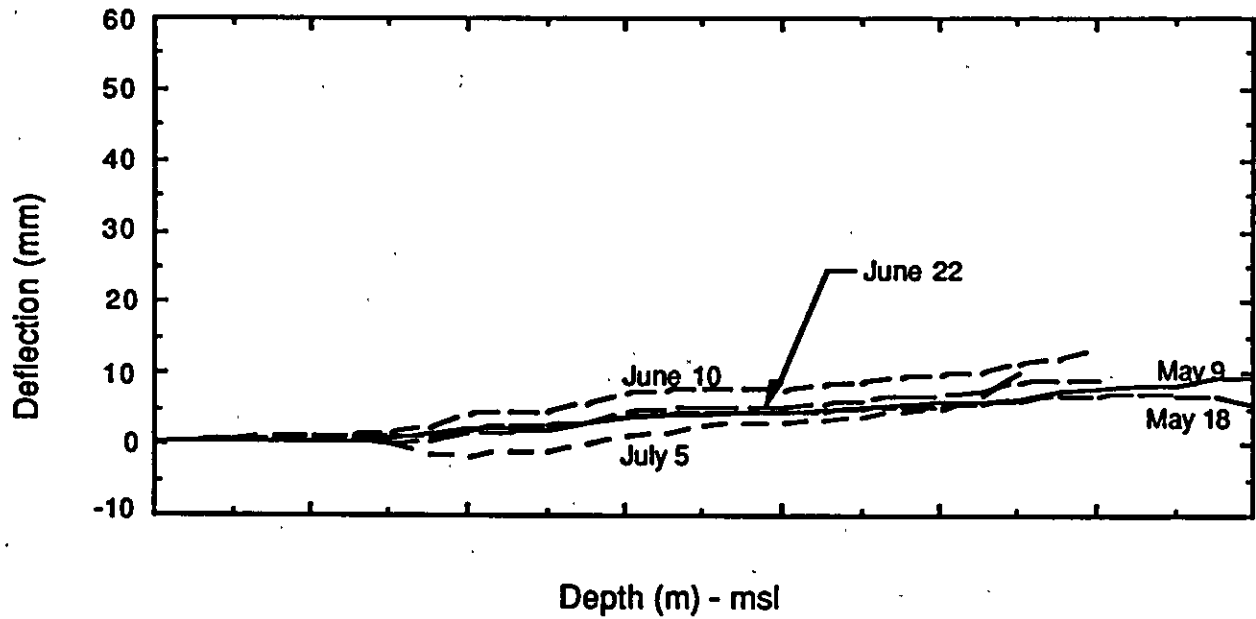


Figure 26. Southwest Slope Indicator Station Deformation Profiles (North-South Direction)

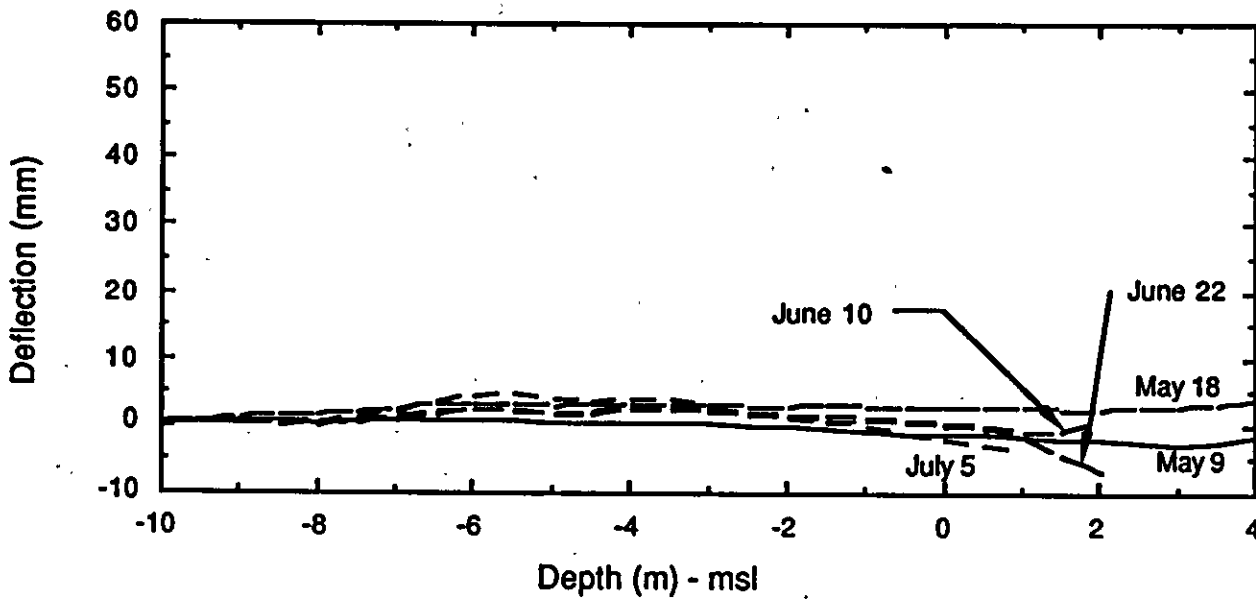


Figure 27. Southwest Slope Indicator Station Deformation Profiles (East-West Direction)

was 5.8 cm on July 5. By this time, the island had eroded to within 15 m of the station and several new cracks were apparent between the station and island center. The dominant movement direction was to the north throughout the measurement period. As with the other sites, east-west component deflections were substantially smaller than those measured in the north-south direction. Most of the movement (albeit small), was observed along the seabed. Movement directions changed from westerly to easterly over time.

EXTENDED OPERATIONS ON SPRAY ICE

Overview

This section addresses operations on spray ice in conditions and operating regimes that have not been generally considered for normal Arctic operations. The information presented was gained by Polar Alpine over two seasons of constructing spray ice structures in sub-arctic and marginally arctic conditions. A more detailed account of these operations is provided in Polar Alpine's report which is contained in Appendix H.

Two spray ice structures constructed by Polar Alpine were built at Nome, Alaska during the 1987/88 and 1988/89 winter seasons. The primary function of the spray ice barriers at Nome was to protect a gold dredge and tugboat that could not be moored in the inner harbor. As a result, the two vessels wintered over alongside the causeway that forms the Port of Nome. The Nome jetty is 600 m long and projects southward into Norton Sound. Vessels moored alongside the jetty are subjected to the force of ice movements as a result of movements of the active Norton Sound ice pack. For vessels required to winter alongside the Nome Jetty some type of protection against ice forces is mandatory. In addition to protection, the spray ice barrier at Nome also acted as a work platform from which heavy equipment could operate to repair and service the vessels through the winter. The spray ice barrier at Nome proved successful during the first season it was employed. A spray ice barrier was again constructed during the 1988-1989 winter season.

Special construction techniques were employed to construct the barrier at the relatively high ambient temperatures experienced at Nome. The construction also extended technology of operating on relatively warm spray ice surfaces, operating heavy equipment close to the edge of a spray ice feature and removing spray ice quickly and efficiently.

A spray ice structure was also built at the Red Dog Port Site 26 km south of Kivaline, Alaska, during the 1988-1989 winter. The purpose of this spray ice structure was to provide a jetty over which heavy equipment could be moved to construct a gravel-filled sheet pile sea cell. In addition to constructing a jetty for the movement of equipment, a barrier was constructed to protect the structure while it was being built.

The spray ice jetty and barrier at the Red Dog Site provided information regarding the extent to which operations can be safely carried out on spray ice. Polar Alpine's report includes an overview of the operations carried out at both Nome and the Red Dog Port Site. Their review considers: over-ice operations on spray ice with heavy equipment, a stress analysis of the loads imposed on spray ice, surface preparation and ablation protection of spray ice to increase its durability, and the removal and excavation of spray ice.

In terms of over-ice operations, the operation of various types of equipment over the spray ice at the two construction sites is considered. In general the main concern centers on the level of experience at moving heavy equipment over narrow spray ice structures at high ambient air temperatures. Often, the temperatures at both the Nome site and the Red Dog site were above freezing for extended periods of time. Also, since the spray ice structures were used as platforms for off-ice construction, it was necessary to operate the equipment close to the edge of the spray ice. To accommodate these operations extensive use was made of crane mats to lower the ground pressure of the equipment. Crane mats (rig mats) were used to effectively facilitate operations of high ground-pressure equipment on spray ice in proximity to the edge of the spray ice structures.

Stresses imposed on narrow spray ice structures by heavy equipment operations were also considered. The primary objective of the analysis was to look at loads that are causing failures in spray ice structures. To carry out this work,

information available on the state of stress at failure in spray ice was addressed. This information is used as the failure criteria in a four-material finite element stress analysis.

Several different types of spray ice loads are considered. In the first instance, a narrow spray ice structure is considered subjected only to body loadings. The primary objective of this analysis is to show that the magnitude of stresses due to gravitational forces are small and generally uniform, even over narrow structures.

The second type of load considered is the magnitude of the pressure required to induce an incipient failure in the spray ice and the pattern of failure within the spray ice. In this case a centrally located load was spread over a width of 6 m on a spray ice structure 16 m wide. This model reproduced typical situations encountered at the Nome and Red Dog Port Site. It was found that subsurface failure was induced when the ground pressure exceeded 276 kPa.

In the third case the situation was investigated where the load was moved to the vertical edge of the spray ice structure. Using the same load distribution considered in case two, Polar Alpine found that the upper edge of the spray ice failed when the ground pressure rose above 145 kPa. The analysis was consistent with observations of equipment that were made on spray ice while operating in the field.

Of considerable interest were investigations into hardening the surface of spray ice in the absence of low temperatures. Spray ice surfaces are typically hardened by spraying water on the surface and letting it soak in and freeze. At both Nome and the Red Dog Site the temperatures were too high to utilize this technique. To circumvent this limitation Polar Alpine found that coating the surface with a layer of gravel served to harden the surface sufficiently to enable the operation of heavy equipment over it continuously. They also found that a layer of material such as gravel spread over the surface tended to thermally insulate, thus slowing the rate at which surface melting occurred.

The final topic in Polar Alpine's report deals with methods for removing and excavating spray ice. In terms of excavating spray ice, Polar Alpine determined

that ordinary excavation techniques could be used to remove both above-and-below water spray-ice. Typically a backhoe and dragline can be used to effectively excavate spray ice at rates as fast if not faster as when similar equipment is used on gravel. When constructing docking facilities for barges and vessels, standard excavation techniques are applicable to spray ice. For completely removing spray ice structures, wheelwashing with tugboats or ice breakers proved extremely effective. In one instance, 150,000 m³ of spray ice was removed in a period of eight to ten hours.

The Polar Alpine report sums up a great deal of experience concerning extended operations on spray ice. As a means of further extending spray ice operations they offer suggestions for further work that could be carried out to improve our understanding of the limits to which operations on spray ice can be performed.

CONCLUSIONS

General

As a result of this study, the feasibility of protecting the edges and surface of a spray ice island against ablation to extend drilling operations through the breakup period and to demobilize drilling equipment from the island immediately after landfast ice breakup was demonstrated. The island provided a stable platform from which drilling operations could have continued until at least June 1 and probably longer.

More specific conclusions are detailed below under the headings of Surface Ablation, Edge Erosion, Island Stability, and Equipment Demobilization.

Surface Ablation

1. Ablation of clean spray ice commenced when the mean daily air temperature rose above 0°C, which in this experiment occurred on May 25. The average cumulative ablation of clean spray ice was 2.25 m by July 5.
2. Ablation of heavily soiled spray ice commenced in early April due to the low albedo of the dirty spray ice, increased solar radiation, and a period of near 0°C air temperatures. As the spray ice ablated, dirt concentrated as a thin surficial veneer. When this layer reached a critical thickness it served to thermally insulate the underlying spray ice and therefore mitigate further ablation. The critical thickness of this layer was not measured but it is estimated to be about 0.5 to 2 cm. The maximum measured ablation coincided with soiled spray ice and was found to be 2.8 m by July 5.
3. Spray ice ablation was effectively controlled with surface coatings. The following minimum thicknesses were required to effectively prevent ablation up until July 5:

- 0.6 m of gravel
- 0.15 m of sawdust

- 0.2 m of wood (i.e. rig matting)

Smaller thicknesses of the above materials were effective in reducing ablation. For example, areas covered with 1 cm of sawdust ablated only 0.8 m up until July 5.

4. Fabric sheets also mitigated ablation. Areas covered with uninsulated tarpaulins experienced about 1.0 m of ablation by July 5 whereas cumulative ablation was one-half this amount beneath an insulated tarpaulin.
5. Ablation also played a major role in edge erosion in that large portions of the island became buoyant and floated away when the freeboard was reduced (by ablation) to about 0.75 m.

Edge Erosion

1. Edge erosion resulted from *in situ* melting and calving after breakup of the landfast ice sheet. *In situ* melting was due to warm currents, air temperatures, and solar radiation. Calving occurred when either warm currents or waves undercut the island edge or the spray ice became buoyant due to loss of freeboard through surface ablation. Accelerated edge erosion was observed on the south side of the island following the arrival of warm water outflow from the Mackenzie River on June 23.
2. Impermeable sheets effectively limited edge erosion to about 25 m by July 8. Several types of fabric sheets were evaluated, but no one sheet appeared to be superior to the others in regard to erosion and ablation protection. The Rufco sheet was considered best overall however, by virtue of its lower cost and ease of installation.

Island Stability

1. Horizontal island movements within the working surface area were less than 15 mm up until the working surface disintegrated after July 5.

2. The average island surface settlement over the period April 23 to June 1 was about 45 mm. The maximum differential settlement across the working surface over the same period was estimated to be less than 10 mm.

Equipment Demobilization

1. A barge docking area can be created by shaping the spray ice at the island edge with a backhoe or a crane positioned near the island edge.
2. If necessary, wheelwash from a tugboat can be used to remove potentially unstable areas at the edge of the island.
3. A crane barge can be used to offload rig equipment from the island immediately prior to and immediately after landfast ice breakup.
4. Adequate surface trafficability can be assured by placing about 0.6 m of dry gravel on the island surface.

RECOMMENDATIONS

A logical follow-up to this investigation would be to perform a detailed design study for a drilling rig marine demobilization operation from a spray ice platform. Such an analysis should include an assessment of risks and costs.

Because a rig demobilization from a spray ice island has not yet been attempted, the initial effort would likely be undertaken in a conservative and not necessarily cost effective manner in order to guarantee its success as soon after landfast ice breakup as feasible. Some of the perceived risks presently associated with this operation could be minimized or better defined by performing another experiment on a future ice island demobilized prior to breakup utilizing the design and methodology identified in the design study.

ACKNOWLEDGEMENTS

The Nipterk P-32 Spray Ice Island Ablation Protection Experiment was undertaken as a team effort. Both the assistance and experience of a number of individuals were drawn upon to ensure the ultimate success of the Project. These consisted of personnel from different departments within Esso Resources Canada Ltd., personnel from participating companies and government agencies as well as independent contractors.

The following individuals are acknowledged for their contributions to this study: Ken Croasdale for his overall guidance and supervision, Jeff Weaver for his technical assistance, field support, and guidance, and Derrick Nixon for his technical assistance. Support was also received from a number of individuals in the Esso Drilling Department under the direction of Pete Meyer. These included: Ian Fraser, Les Gibbs, Cliff Miller, Rudy Muster, and John Pastega.

Technical and field assistance during the site investigations were provided by Ram Sisodiya (Chevron Corporation), and Kailash Gulati and Brian Woods (Mobil Research and Development Corporation). Encouragement was also provided by Ibrahim Konuk and Stephen Lord (Canada Oil and Gas Lands Administration and Charles Smith (U. S. Minerals Management Service). Financial support provided by each of these companies and government agencies was crucial toward undertaking the ambitious scope of work.

Finally, the assistance in a variety of different areas of the study by several contractors is acknowledged. These are: Steven Connolly (Arctic Applications, Inc.), Michel Metge (Canatec Consultants Ltd.), and William St. Lawrence (Polar Alpine, Inc.).

REFERENCES

1. Connolly, S.T., 1986: Artificial Ice Islands for Deep Water and Production Structures, In Proceedings Fourth International Conference on Cold Regions Engineering, Anchorage, Alaska, ASCE, pp. 58-68.
2. Maykut, G.A. and Untersteiner, N., 1976: Some Results from a Time-Dependent Thermo-Dynamic Model of Sea Ice, Journal of Geophysical Research, Vol. 76, No. 6.
3. El-Tahan, M., Venkatech, S., and El-Tahan, H., 1984: Validation and Quantitative Assessment of the Deterioration Mechanisms of Arctic Icebergs, in the Proceedings-ASME Offshore Mechanics/Arctic Engineering Symposium, New Orleans, LA., Feb. 1984, ASME, NY.
4. Colbeck, S.C., 1988: Snowmelt Increase Through Albedo Reduction, U.S. Army Corps. of Engineers Cold Regions Research and Engineering Laboratory Special Report 88-26, December, 11 p.
5. Ashwell, I.Y. and Hannell, F.G., 1966: Experiments on a Snow-Patch in the Mountains of Sweden, Journal of Glaciology, Vol. 6, No. 43, pp. 135-144.
6. Rhodes, J.J., Armstrong, R.L., and Waren, S.G., 1987: Mode of Formation of "Ablation Hollows" Controlled by Dirt Content of Snow, Journal of Glaciology, Vol. 33, No. 114, pp. 135-139.
7. Jahns, H.O., Petrie, D.H., and Lockett, A.V., 1986: CIDS Spray Ice Barrier, 18th Annual Offshore Technology Conference, Houston, Texas, pp. 575-584.
8. St. Lawrence, W., 1989: Extended Operations on Spray Ice, Proprietary Report Prepared by Polar Alpine, Inc., 31 p.
9. Prodanovic, A., 1981: Ice Island Experiment - Summer Monitoring Report, Exxon Production Research Company Production Operations Report EPR. 43 PS.81 prepared for AOGA 49, 89 p.

10. White, F.M., Spalding, M.L., and Gominho, L., 1980: Theoretical Estimates of the Various Mechanisms Involved in Iceberg Deterioration in the Open Environment, U.S. Coast Guard Report No. CG-0-62-80.

APPENDIX A

METEOROLOGICAL MEASUREMENTS

Meteorological data were gathered from the island during the period June 7 to July 5. Tuktoyaktuk data were used to supplement the island measurements during the first half of the study before the weather station was deployed and after the July 5 site survey through island breakup. Island-based data were utilized in the analysis whenever possible as these data are indicative of conditions on the island.

Date	Date Fraction (Julian Day)	Meteorological Data									
		Wind		Speed		Temperature		Solar			
		Direction (degrees) (N=0,360 S=180)	Speed (knots)	maximum (°C)	island (°C)	minimum (°C)	Radiation (kW/m ²)				
20-Apr	110.75	247	4	-14		-24					
21-Apr	111.00		0	-15		-23					
	111.25	90	12								
	111.50	67	10								
	111.75	22	2								
22-Apr	112.00	0	6	-15		-23					
	112.25	270	6								
	112.50		0								
	112.75										
23-Apr	113.00	67	14	-16		-23					
	113.25	67	10								
	113.50	90	8								
	113.75	90	8								
24-Apr	114.00	90	12	-1		-17					
	114.25	67	12								
	114.50	90	2								
	114.75	157	5								
25-Apr	115.00		0	7		-7					
	115.25		0								
	115.50	112	2								
	115.75	112	7								
26-Apr	116.00		0	-3		-8					
	116.25	292	10								
	116.50	0	6								
	116.75	270	12								
27-Apr	117.00	270	2	-7		-11					
	117.25	292	8								
	117.50	292	10								

Date	Date Fraction (Julian Day)	Meteorological Data						Solar Radiation (kW/m ²)		
		Wind		Temperature		Speed (knots)	maximum (°C)		island (°C)	minimum (°C)
		Direction (degrees) (N=0,360 S=180)	Speed	maximum	island					
	117.75	292	8							
28-Apr	118.00	292	20	-5					-13	
	118.25	292	18							
	118.50	339	10							
	118.75	135	8							
29-Apr	119.00	135	14	-5					-12	
	119.25	45	10							
	119.50	22	12							
	119.75	22	10							
30-Apr	120.00	339	12	-7					-14	
	120.25		0							
	120.50	225	4							
	120.75	270	8							
1-May	121.00	270	18	-3					-12	
	121.25	270	10							
	121.50	270	4							
	121.75	247	14							
2-May	122.00	247	10	-5					-10	
	122.25	339	5							
	122.50	292	6							
	122.75	270	6							
3-May	123.00	292	14	-8					-14	
	123.25	292	10							
	123.50	315	10							
	123.75	339	5							
4-May	124.00	180	8	2					-13	
	124.25	135	10							
	124.50	135	6							

		Meteorological Data							
		Wind			Temperature			Solar	
Date	Date Fraction (Julian Day)	Direction (degrees) (N=0,360 S=180)	Speed (knots)	maximum (°C)	island (°C)	minimum (°C)	Radiation (kW/m ²)		
	124.75	157	7						
5-May	125.00		0	-3		-14			
	125.25	45	8						
	125.50	0	15						
	125.75	315	13						
6-May	126.00	292	8	-12		-19			
	126.25	0	4						
	126.50	67	8						
	126.75	67	14						
7-May	127.00	67	14	-7		-15			
	127.25	67	2						
	127.50	67	8						
	127.75	67	10						
8-May	128.00	67	6	-10		-19			
	128.25	45	8						
	128.50	67	10						
	128.75	45	10						
9-May	129.00	292	12	-10		-14			
	129.25								
	129.50								
	129.75	22	10						
10-May	130.00	45	10	-8		-12			
	130.25	45	8						
	130.50	67	15						
	130.75	67	22						
11-May	131.00			-3		-20			
	131.25	67	6						
	131.50	45	6						

Date	Date Fraction (Julian Day)	Meteorological Data						Solar Radiation (kW/m ²)	
		Wind		Temperature		maximum (°C)	island (°C)		minimum (°C)
		Direction (degrees) (N=0,360 S=180)	Speed (knots)	Direction (degrees) (N=0,360 S=180)	Speed (knots)				
	131.75	90	4						
12-May	132.00		0	4				-10	
	132.25	67	9						
	132.50	67	20						
	132.75	67	14						
13-May	133.00	0	10	-7				-14	
	133.25	315	10						
	133.50	315	10						
	133.75	339	8						
14-May	134.00	315	5	-8				-12	
	134.25	67	5						
	134.50	90	10						
	134.75	90	10						
15-May	135.00	90	16	-5				-15	
	135.25	90	18						
	135.50	90	14						
	135.75	90	15						
16-May	136.00	67	12	-8				-11	
	136.25	45	12						
	136.50	0	10						
	136.75	315	12						
17-May	137.00	339	10	-5				-9	
	137.25	339	10						
	137.50	339	8						
	137.75	270	5						
18-May	138.00	112	6	-3				-11	
	138.25	90	5						
	138.50	90	10						

Date	Date Fraction (Julian Day)	Meteorological Data						Solar Radiation (kW/m ²)		
		Wind		Temperature		Speed (knots)	maximum (°C)		island (°C)	minimum (°C)
		Direction (degrees) (N=0,360 S=180)								
	138.75	45		5						
19-May	139.00				-3			-6		
	139.25	339		3						
	139.50	22		6						
	139.75	0		2						
20-May	140.00	315		5	-1			-9		
	140.25	45		4						
	140.50	90		4						
	140.75	90		4						
21-May	141.00	90		3	2			-7		
	141.25	90		6						
	141.50	90		2						
	141.75	67		4						
22-May	142.00	67		2	-7			-7		
	142.25	67		6						
	142.50	45		15						
	142.75	67		12						
23-May	143.00	67		15	-3			-14		
	143.25	67		12						
	143.50									
	143.75	90		14						
24-May	144.00	90		15	-1			-11		
	144.25	90		18						
	144.50	90		8						
	144.75	90		14						
25-May	145.00	67		10	1			-10		
	145.25	67		15						
	145.50	90		5						

		Meteorological Data								
		Wind			Temperature					
Date	Date Fraction (Julian Day)	Direction (degrees) (N=0,360 S=180)	Speed (knots)	maximum (°C)	Island (°C)	minimum (°C)	Solar Radiation (kW/m ²)			
	145.75	90	8							
26-May	146.00	90	8	6		-7				
	146.25	90	10							
	146.50	90	2							
	146.75	112	5							
27-May	147.00	90	8	12		2				
	147.25	112	5							
	147.50		0							
	147.75	157	6							
28-May	148.00	135	6	9		-3				
	148.25	157	2							
	148.50	0	4							
	148.75	339	4							
29-May	149.00	45	2	13		1				
	149.25	90	5							
	149.50	90	4							
	149.75	90	10							
30-May	150.00	90	10	19		4				
	150.25	90	10							
	150.50	90	10							
	150.75	90	10							
31-May	151.00		1	19		5				
	151.25	90	10							
	151.50	112	8							
	151.75	90	10							
1-Jun	152.00			14		3				
	152.25	45	6							
	152.50	270	8							

		Meteorological Data									
		Wind					Temperature				
Date	Date Fraction (Julian Day)	Direction (degrees) (N=0,360 S=180)	Speed (knots)	maximum (°C)	Island (°C)	minimum (°C)	Solar Radiation (kW/m ²)				
	152.75	270	4								
2-Jun	153.00	339	4	9		1					
	153.25	270	5								
	153.50	270	8								
	153.75	270	8								
3-Jun	154.00	292	10	11		1					
	154.25	270	5								
	154.50	90	4								
	154.75	112	4								
4-Jun	155.00	90	15	13		0					
	155.25	90	4								
	155.50	90	6								
	155.75		0								
5-Jun	156.00	270	10	3		-1					
	156.25	292	20								
	156.50	339	12								
	156.75	292	10								
6-Jun	157.00			3		0					
	157.25	339	6								
	157.50	0	6								
	157.75	0	8								
7-Jun	158.00			9		-2					
	158.25	45	5								
	158.50	45	4								
	158.67					7.11		0.684			
	158.71					7.61		0.649			
	158.75	90	5			8.21		0.591			
	158.79					8.53		0.516			

		Meteorological Data								
		Wind			Temperature				Solar	
Date	Date Fraction (Julian Day)	Direction (degrees) (N=0,360 S=180)	Speed (knots)	maximum (°C)	Island (°C)	minimum (°C)	Radiation (kW/m ²)			
9-Jun	160.00			21	12.95	8	0.101			
	160.04				11.2		0.041			
	160.08				9.24		0.028			
	160.13				8.01		0.040			
	160.17				6.92		0.050			
	160.21				6		0.042			
	160.25	112	6		5.65		0.127			
	160.29				5.81		0.183			
	160.33				6.24		0.255			
	160.38				6.85		0.352			
	160.42				7.43		0.414			
	160.46				8.4		0.519			
	160.50	157	10		9.34		0.577			
	160.54				10.35		0.559			
	160.58				11.34		0.619			
	160.63				12.34		0.669			
	160.67				13.44		0.659			
	160.71				14.29		0.634			
	160.75	157	6		15		0.566			
	160.79				15.51		0.443			
	160.83				15.26		0.405			
	160.88				14.63		0.168			
	160.92				13.76		0.227			
	160.96				12.45		0.098			
10-Jun	161.00	180	12	18	9.35	2	0.056			
	161.04				7.34		0.021			
	161.08				5.83		0.010			
	161.13				4.84		0.013			

Date	Meteorological Data										
	Wind					Temperature					Solar Radiation (kW/m ²)
	Date Fraction (Julian Day)	Direction (degrees) (N=0,360 S=180)	Speed (knots)	maximum (°C)	Island (°C)	minimum (°C)	Island (°C)	minimum (°C)	Solar Radiation (kW/m ²)		
	163.50	202	5		4.7				0.454		
	163.54				5.06				0.381		
	163.58				5.68				0.493		
	163.63				6.81				0.567		
	163.67				7.66				0.449		
	163.71				7.99				0.458		
	163.75	270	12		8.31				0.346		
	163.79				8.05				0.267		
	163.83				7.06				0.192		
	163.88				6.15				0.151		
	163.92				5.35				0.079		
	163.96				4.59				0.048		
13-Jun	164.00	270	4	3	3.88	0			0.035		
	164.04				3.26				0.016		
	164.08				2.7				0.013		
	164.13				2.29				0.011		
	164.17				1.96				0.019		
	164.21				-0.02				0.040		
	164.25				1.76				0.027		
	164.29	315	4		1.66				0.052		
	164.33				1.63				0.063		
	164.38				1.67				0.109		
	164.42				1.8				0.125		
	164.46				2.07				0.200		
	164.50				2.56				0.239		
	164.54	315	10		3.68				0.464		
	164.58				4.74				0.468		
	164.63				5.31				0.404		

		Meteorological Data								
		Wind			Temperature					
Date	Date Fraction (Julian Day)	Direction (degrees) (N=0,360 S=180)	Speed (knots)	maximum (°C)	Island (°C)	minimum (°C)	Radiation (kW/m ²)	Solar Radiation (kW/m ²)		
16-Jun	167.00	67	16	17	6.61	2	0.122	0.122		
	167.04				5.29		0.078	0.078		
	167.08				3.94		0.052	0.052		
	167.13				2.98		0.046	0.046		
	167.17				2.31		0.060	0.060		
	167.21				1.93		0.045	0.045		
	167.25	90	12		1.85		0.135	0.135		
	167.29				2.14		0.190	0.190		
	167.33				2.6		0.258	0.258		
	167.38				3.27		0.331	0.331		
	167.42				4.23		0.412	0.412		
	167.46				5.47		0.502	0.502		
	167.50	135	5		7.01		0.575	0.575		
	167.54				8.44		0.720	0.720		
	167.58				9.01		0.679	0.679		
	167.63				9.02		0.565	0.565		
	167.67				9.48		0.680	0.680		
	167.71				10.45		0.593	0.593		
	167.75	180	6		10.7		0.583	0.583		
	167.79				10.34		0.298	0.298		
	167.83				8.66		0.171	0.171		
	167.88				7.08		0.127	0.127		
	167.92				5.9		0.102	0.102		
	167.96				4.81		0.021	0.021		
17-Jun	168.00	270	14	15	3.71	1	0.017	0.017		
	168.04				2.91		0.020	0.020		
	168.08				2.3		0.008	0.008		
	168.13				1.83		0.007	0.007		

		Meteorological Data							
Date	Date Fraction (Julian Day)	Wind		Speed (knots)	Temperature		Solar Radiation (kW/m ²)		
		Direction (degrees) (N=0,360 S=180)	maximum (°C)		Island (°C)	minimum (°C)			
	169.33					1.11	0.113		
	169.38					1.07	0.250		
	169.42					1.33	0.337		
	169.46					1.85	0.405		
	169.50	0		25		2.26	0.344		
	169.54					2.61	0.391		
	169.58					3.09	0.338		
	169.63					3.47	0.403		
	169.67					4.33	0.461		
	169.71					5.02	0.400		
	169.75	339		16		5.57	0.421		
	169.79					7.04	0.522		
	169.83					8.14	0.273		
	169.88					7.77	0.184		
	169.92					7.1	0.133		
	169.96					6.4	0.124		
19-Jun	170.00				12	5.04	0.038		
	170.04					3.74	0.022		
	170.08					2.56	0.016		
	170.13					1.38	0.018		
	170.17					0.75	0.028		
	170.21					0.69	0.038		
	170.25	135		4		0.96	0.098		
	170.29					1.49	0.121		
	170.33					1.98	0.133		
	170.38					2.52	0.208		
	170.42					3.27	0.207		
	170.46					3.99	0.274		

		Meteorological Data								
		Wind			Temperature					
Date	Date Fraction (Julian Day)	Direction (degrees) (N=0,360 S=180)	Speed (knots)	maximum (°C)	Island (°C)	minimum (°C)	Solar Radiation (kW/m ²)			
	170.50	180	10		4.76		0.309			
	170.54				5.13		0.188			
	170.58				4.78		0.095			
	170.63				4.61		0.164			
	170.67				4.51		0.102			
	170.71				3.88		0.075			
	170.75	180	18		3.42		0.222			
	170.79				3.46		0.243			
	170.83				3.19		0.181			
	170.88				2.78		0.093			
	170.92				2.11		0.088			
	170.96				1.6		0.062			
20-Jun	171.00			7	1.11	-1	0.033			
	171.04				0.55		0.014			
	171.08				0.08		0.014			
	171.13				-0.44		0.031			
	171.17				-0.81		0.032			
	171.21				-1.07		0.050			
	171.25	315	20		-0.85		0.132			
	171.29				-0.42		0.160			
	171.33				0.18		0.254			
	171.38				0.72		0.339			
	171.42				1.29		0.428			
	171.46				2.02		0.523			
	171.50	45	5		2.93		0.584			
	171.54				3.92		0.636			
	171.58				4.74		0.670			
	171.63				5.3		0.684			

		Meteorological Data								
		Wind			Temperature					
Date	Date Fraction (Julian Day)	Direction (degrees) (N=0,360 S=180)	Speed (knots)	maximum (°C)	Island (°C)	minimum (°C)	Solar Radiation (kW/m^2)			
23-Jun	174.00	157	10	21	11.21	9	0.034			
	174.04				10		0.017			
	174.08				9.01		0.017			
	174.13				7.8		0.023			
	174.17				7.15		0.023			
	174.21				6.49		0.033			
	174.25	157	4		6.3		0.094			
	174.29				5.96		0.098			
	174.33				5.75		0.146			
	174.38				6.24		0.300			
	174.42				6.49		0.246			
	174.46				6.39		0.354			
	174.50	135	10		6.68		0.410			
	174.54				6.97		0.450			
	174.58				7.86		0.616			
	174.63				8.8		0.470			
	174.67				9.54		0.526			
	174.71				10.38		0.499			
	174.75	247	8		11.55		0.468			
	174.79				12.97		0.516			
	174.83				14.06		0.368			
	174.88				14.29		0.360			
	174.92				13.98		0.099			
	174.96				13.09		0.200			
24-Jun	175.00	339	6	26	12.74	9	0.118			
	175.04				11.36		0.075			
	175.08				9.79		0.049			
	175.13				8.39		0.028			

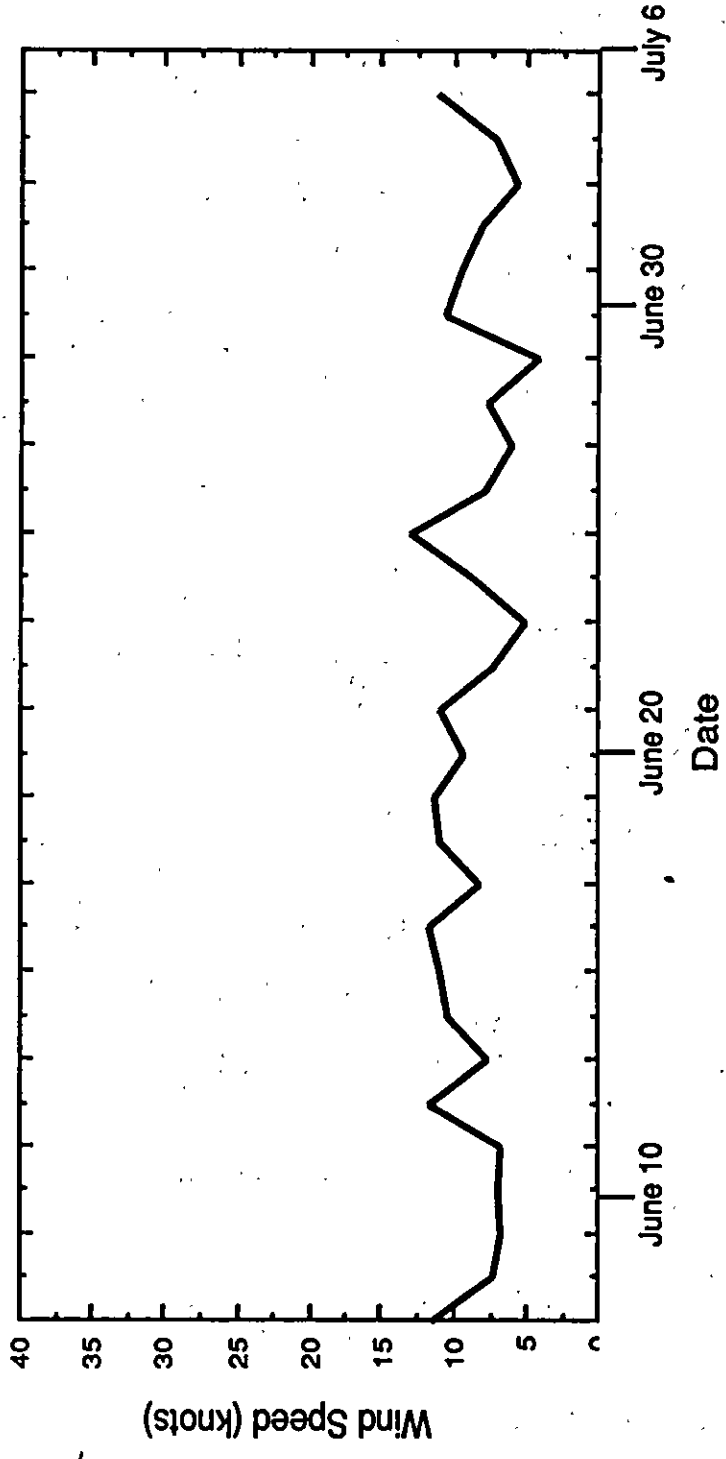
		Meteorological Data							
Date	Date Fraction (Julian Day)	Wind		Speed (knots)	Temperature		Solar Radiation (kW/m ²)		
		Direction (N=0,360 S=180)	maximum (°C)		Island (°C)	minimum (°C)			
	177.50	22		16		4.41	0.542		
	177.54					5	0.594		
	177.58					5.79	0.634		
	177.63					6.77	0.655		
	177.67					8.1	0.655		
	177.71					9.58	0.632		
	177.75	22		11		9.17	0.503		
	177.79					8.87	0.503		
	177.83					8.53	0.428		
	177.88					8.22	0.342		
	177.92					7.93	0.257		
	177.96					7.48	0.174		
27-Jun	178.00	45		12	20	6.85	0.109		
	178.04					6.01	0.069		
	178.08					5.37	0.030		
	178.13					4.61	0.014		
	178.17					4.02	0.017		
	178.21					3.62	0.021		
	178.25	45		8		3.3	0.033		
	178.29					3.05	0.099		
	178.33					3.25	0.221		
	178.38					3.67	0.305		
	178.42					3.98	0.378		
	178.46					4.52	0.412		
	178.50	90		4		4.83	0.408		
	178.54					4.91	0.367		
	178.58					5.09	0.520		
	178.63					5.35	0.436		

		Meteorological Data							
		Wind		Temperature					
Date	Date Fraction (Julian Day)	Direction (N=0,360 S=180)	Speed (knots)	maximum (°C)	Island (°C)	minimum (°C)	Solar Radiation (kW/m ²)		
30-Jun	181.00			12	4.55	2	0.045		
	181.04				3.99		0.021		
	181.08				3.58		0.007		
	181.13				3.26		0.007		
	181.17				2.96		0.013		
	181.21	90	5		2.75		0.021		
	181.25				2.7		0.039		
	181.29				2.85		0.040		
	181.33				3.06		0.066		
	181.38				3.35		0.137		
	181.42				3.44		0.061		
	181.46				3.03		0.052		
	181.50	315	3		2.7		0.167		
	181.54				2.64		0.260		
	181.58				2.68		0.225		
	181.63				2.62		0.306		
	181.67				2.92		0.431		
	181.71				3.31		0.408		
	181.75	315	18		3.29		0.323		
	181.79				3.18		0.223		
	181.83				2.99		0.234		
	181.88				2.94		0.150		
	181.92				2.82		0.163		
	181.96				2.77		0.121		
1-Jul	182.00	0	20	5	2.47	1	0.080		
	182.04				2.06		0.071		
	182.08				1.71		0.036		
	182.13				1.3		0.045		

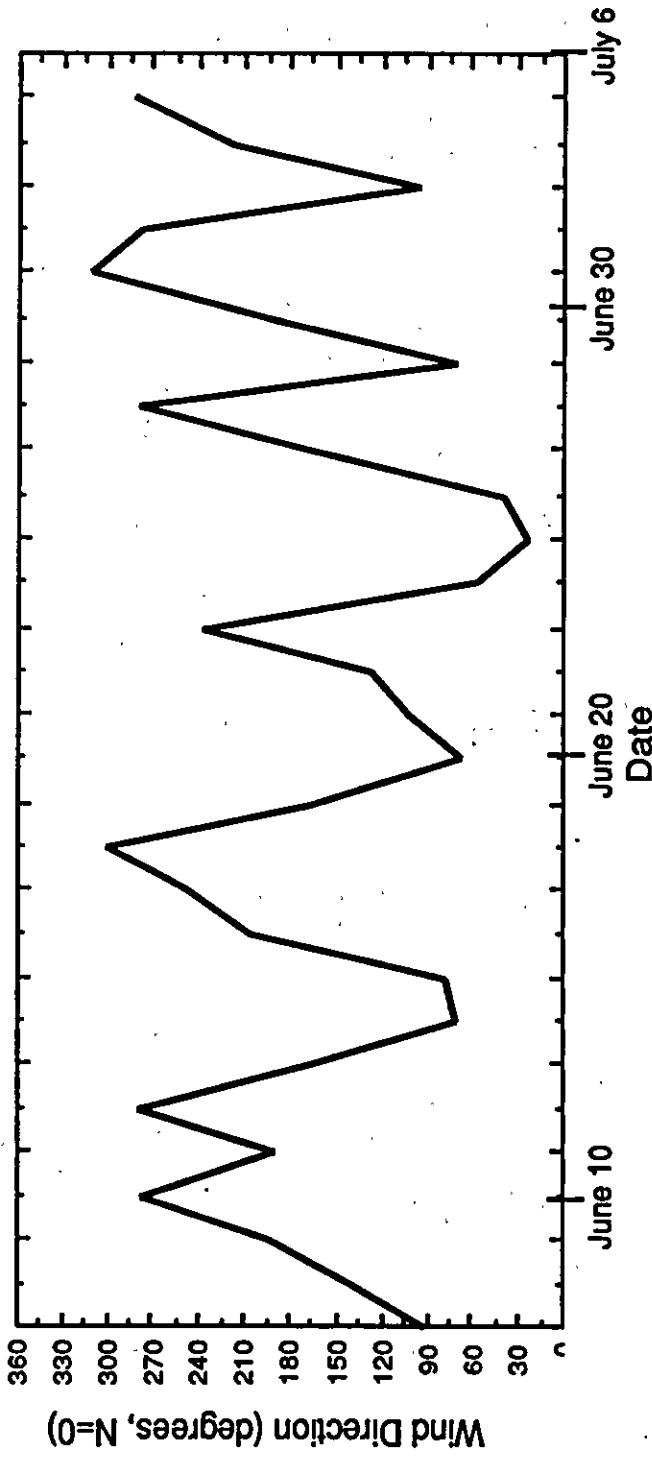
		Meteorological Data							
Date	Date Fraction (Julian Day)	Wind		Speed (knots)	Temperature		Solar Radiation (kW/m ²)		
		Direction (degrees) (N=0,360 S=180)	maximum (°C)		Island (°C)	minimum (°C)			
	182.17					1.15		0.051	
	182.21					1.1		0.041	
	182.25	339		12		1.1		0.108	
	182.29					1.13		0.151	
	182.33					1.17		0.185	
	182.38					1.15		0.266	
	182.42					1.33		0.301	
	182.46					1.65		0.339	
	182.50	0		10		1.91		0.285	
	182.54					2.15		0.362	
	182.58					2.49		0.451	
	182.63					2.92		0.556	
	182.67					3.51		0.490	
	182.71					3.9		0.495	
	182.75	0		10		4.41		0.534	
	182.79					4.93		0.419	
	182.83					5.16		0.263	
	182.88					4.61		0.144	
	182.92					3.91		0.080	
	182.96					3.18		0.043	
2-Jul	183.00	339		12	5	2.52	2	0.034	
	183.04					2.02		0.018	
	183.08					1.59		0.012	
	183.13					1.21		0.013	
	183.17					0.94		0.019	
	183.21					0.73		0.036	
	183.25	315		8		0.64		0.049	
	183.29					0.7		0.080	

		Meteorological Data							
Date	Date Fraction (Julian Day)	Wind		Speed (knots)	maximum (°C)	Temperature		Solar Radiation (kW/m ²)	
		Direction (degrees) (N=0,360 S=180)	Temperature island (°C)			minimum (°C)			
	183.33					0.81		0.082	
	183.38					0.92		0.094	
	183.42					1.04		0.139	
	183.46					1.24		0.127	
	183.50	292		10		1.25		0.103	
	183.54					1.1		0.099	
	183.58					0.99		0.097	
	183.63					0.93		0.109	
	183.67					0.99		0.110	
	183.71					1.12		0.114	
	183.75	339		10		1.3		0.150	
	183.79					1.52		0.115	
	183.83					1.56		0.085	
	183.88					1.53		0.093	
	183.92					1.51		0.064	
	183.96					1.44		0.051	
3-JUL	184.00	292		22	15	1.33	0	0.036	
	184.04					1.2		0.011	
	184.08					1.04		0.006	
	184.13					0.88		0.004	
	184.17					0.75		0.010	
	184.21					0.66		0.022	
	184.25	0		12		0.62		0.032	
	184.29					0.68		0.060	
	184.33					0.85		0.062	
	184.38					1		0.108	
	184.42					1.32		0.150	
	184.46					1.96		0.329	

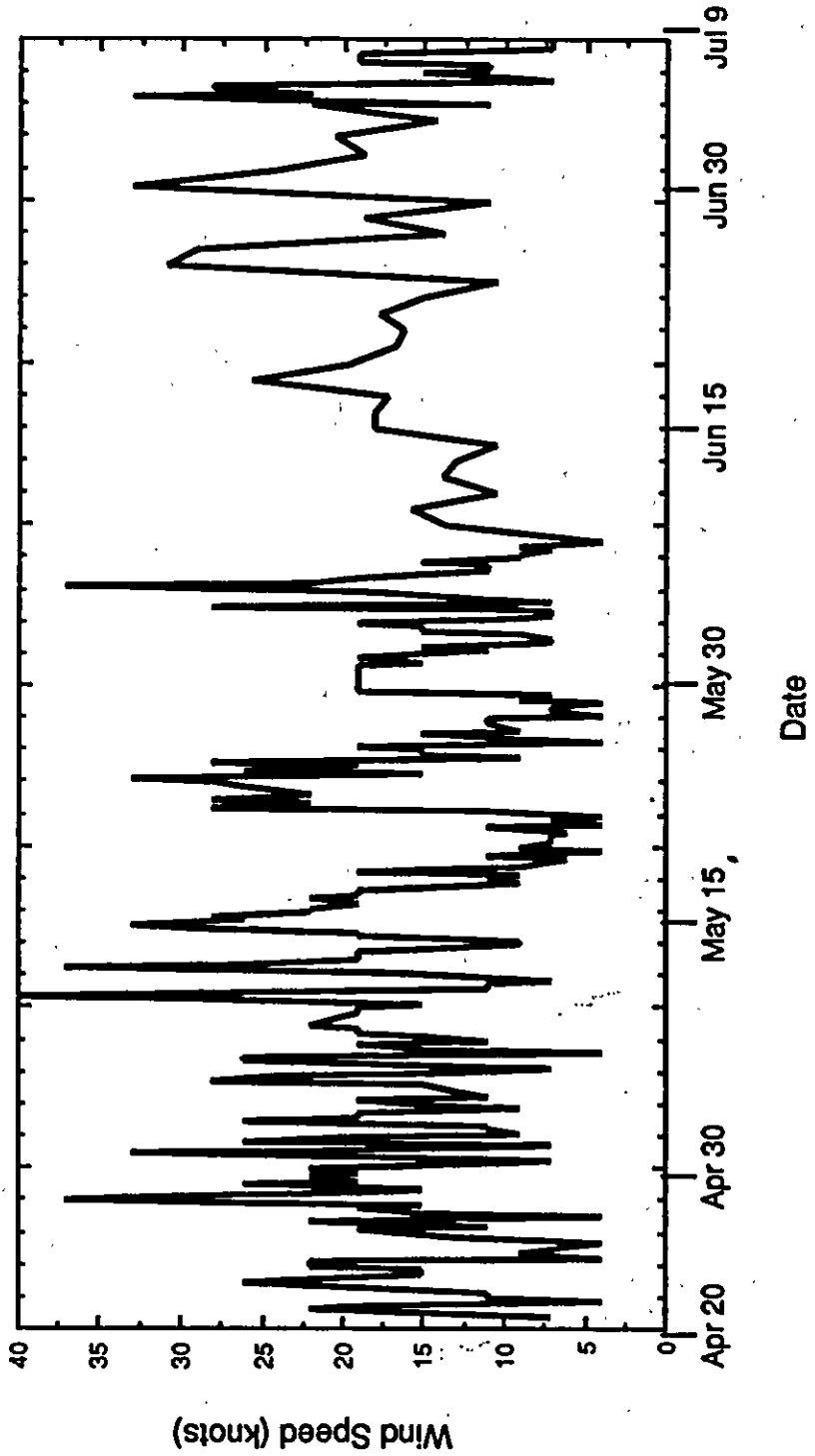
		Meteorological Data								
Date	Date Fraction (Julian Day)	Wind			Speed (knots)	maximum (°C)	Temperature		Solar Radiation (kW/m ²)	
		Direction (degrees) (N=0,360 S=180)	Island (°C)	minimum (°C)						
	185.67						8.97		0.636	
	185.71						9.35		0.619	
	185.75	270		4			9.39		0.497	
	185.79						8.96		0.198	
	185.83						8.18		0.306	
	185.88						8.01		0.212	
	185.92						7.85		0.294	
	185.96						8.09		0.144	
5-Jul	186.00	315		6	22		7.99	10	0.065	
	186.04						7.46		0.013	
	186.08						6.94		0.006	
	186.13						6.68		0.014	
	186.17						6.54		0.023	
	186.21						6.41		0.024	
	186.25	339		10			6.29		0.046	
	186.29						6.21		0.124	
	186.33						6.45		0.178	
	186.38						6.82		0.287	
	186.42						7.41		0.324	
	186.46						8.02		0.460	
	186.50	270		18			8.67		0.552	
	186.54						9.2		0.566	
	186.58						9.64		0.617	
	186.63						9.93		0.643	
	186.67						11.91		0.635	
	186.75	270		12						
6-Jul	187.00	225		15	18			9		
	187.25	339		15						



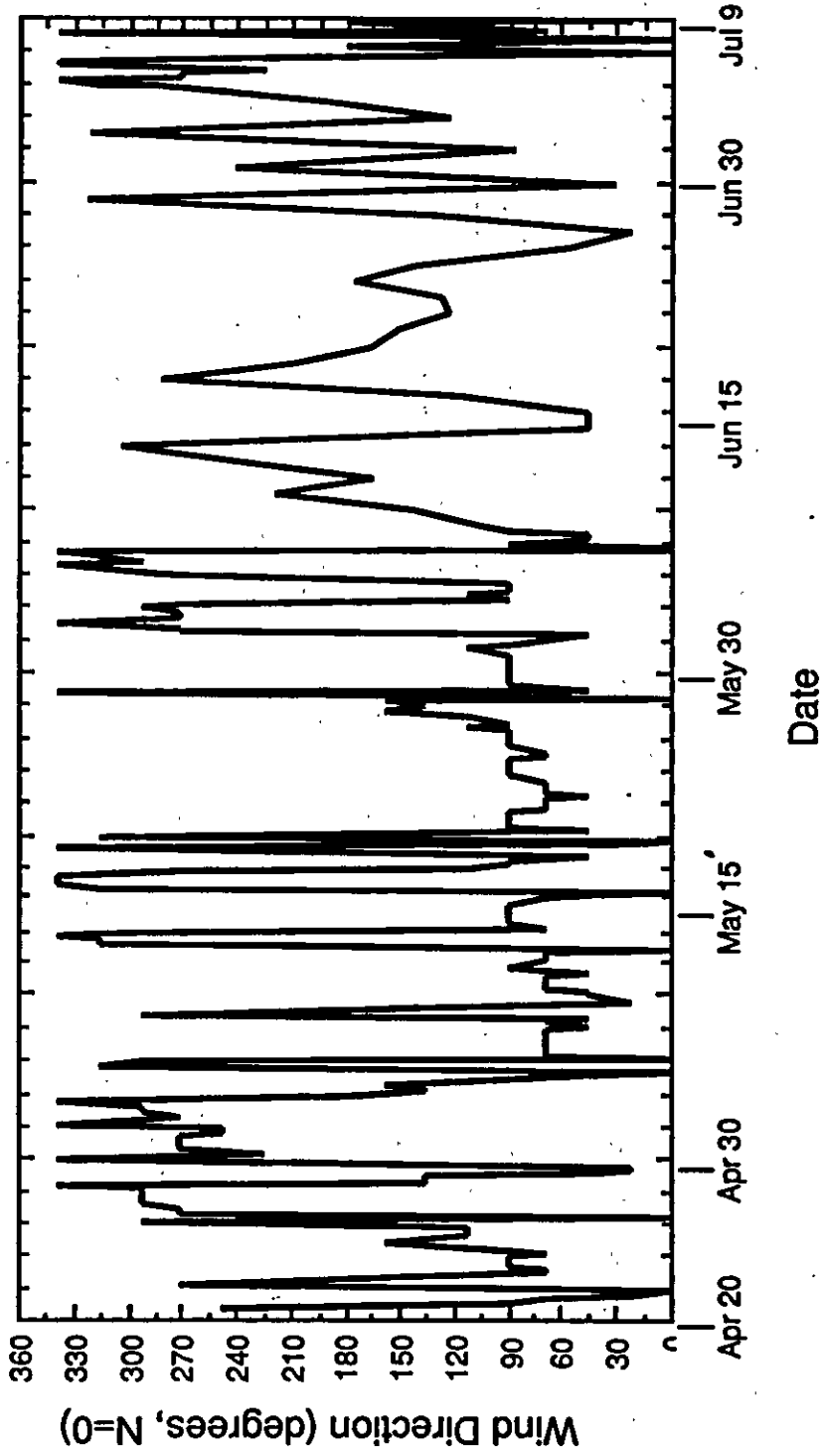
Wind Speed (on Island)



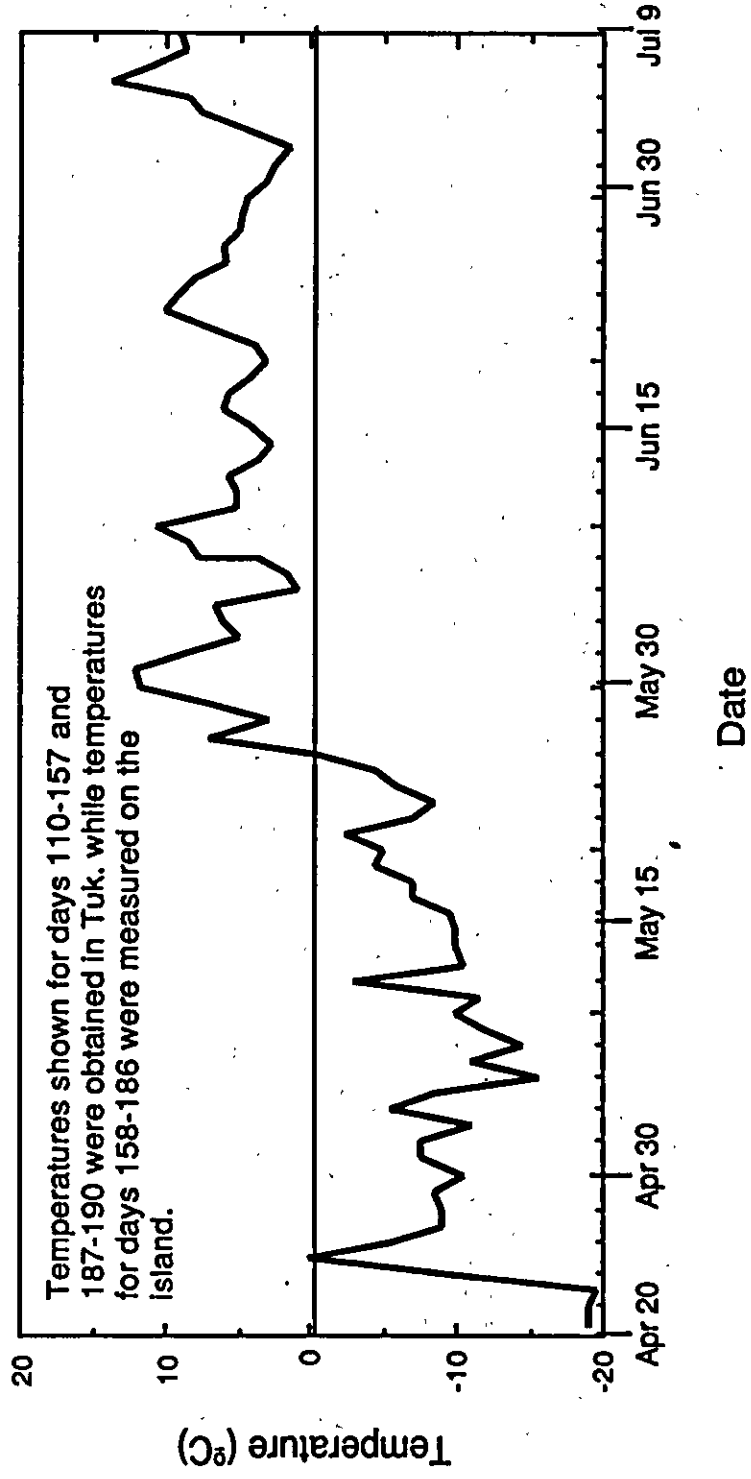
Wind Direction (on island)



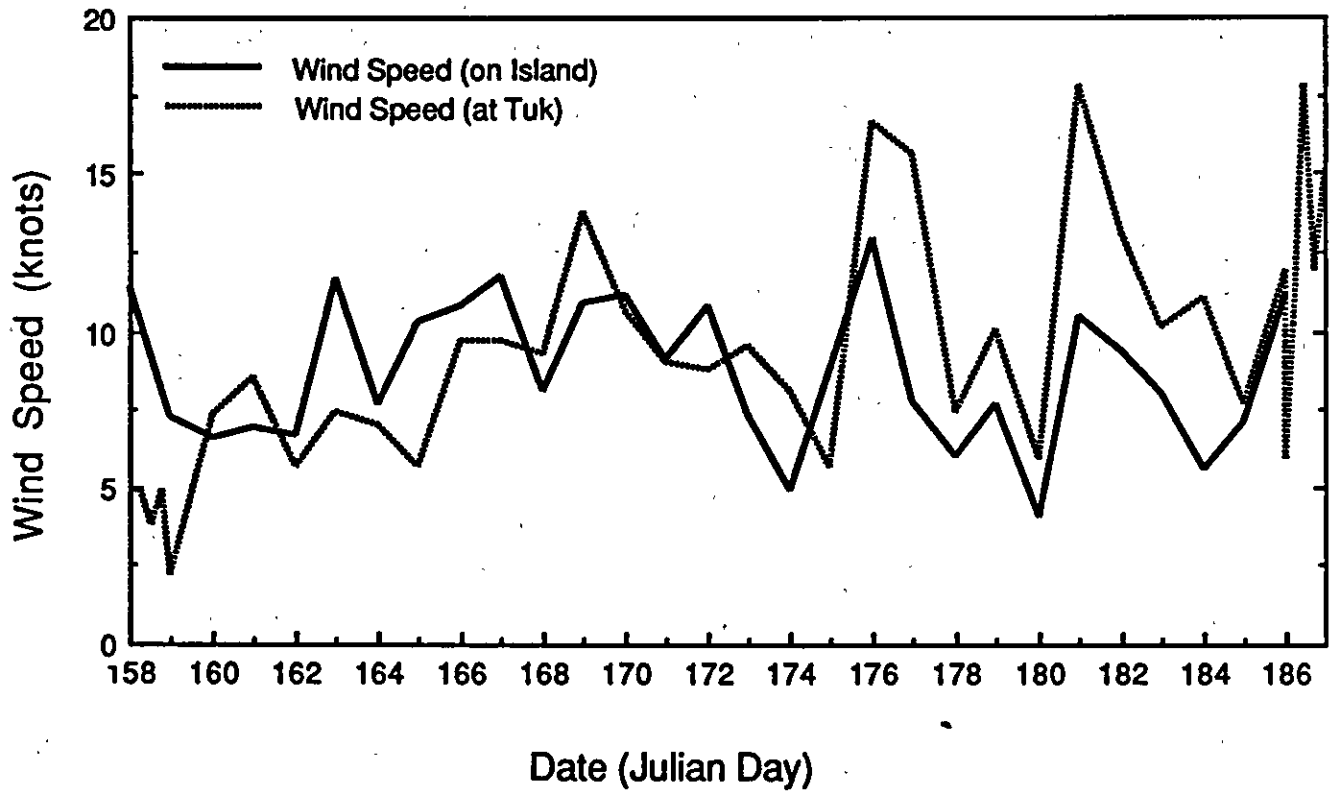
Wind Speed (at Tuk.)



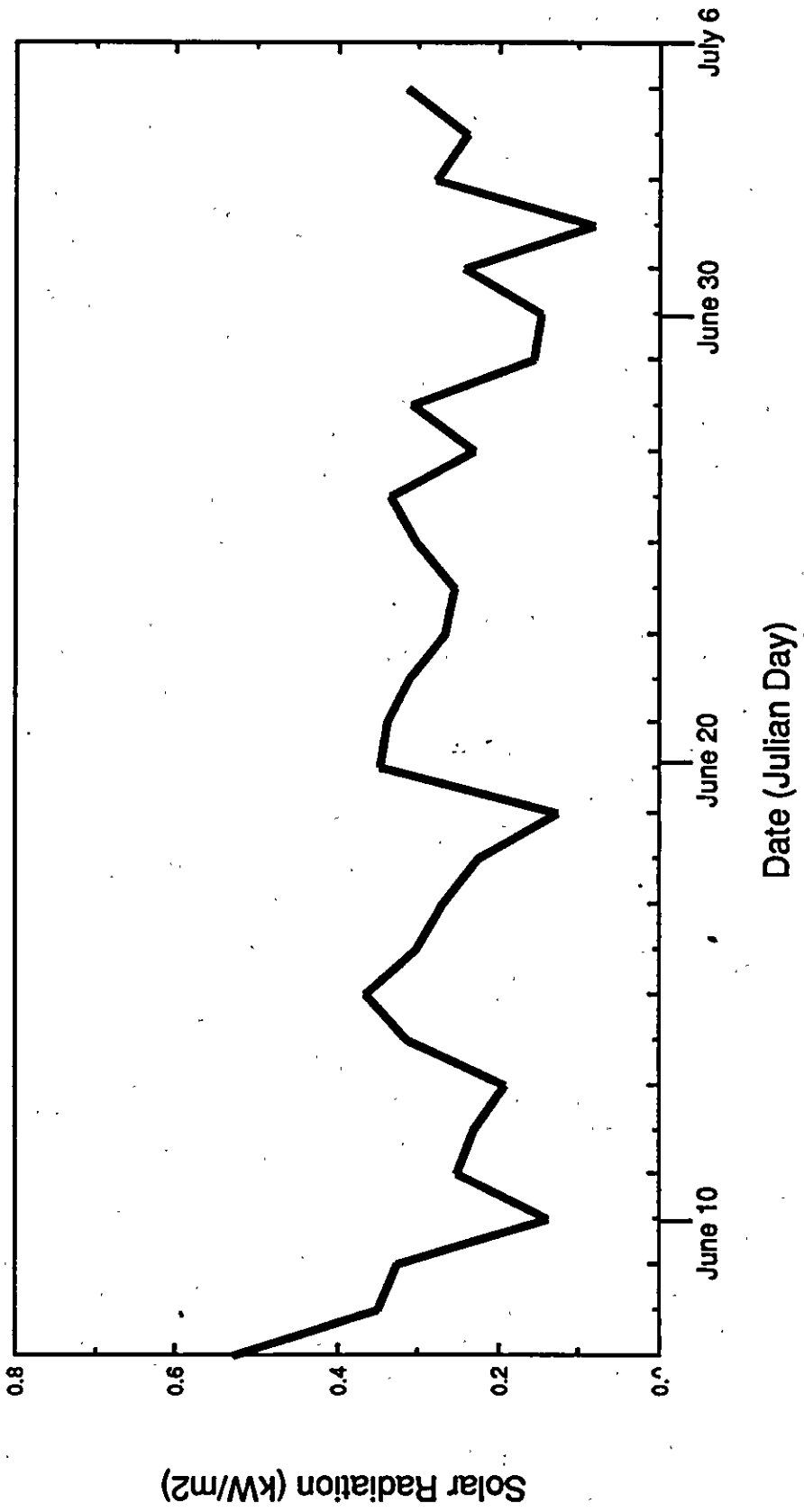
Wind Direction (at Tuk)



Temperature Averaged Daily



Wind Speed Comparison



Daily Averaged Solar Radiation

APPENDIX B

ICE TEMPERATURE MEASUREMENTS

Spray ice/seabed temperatures were measured by an 11 m long thermistor string deployed adjacent to the southwest Sondex/Slope Indicator survey station (75 m from island center). The string was made up of 24 thermistors whose spacings varied. Thermistor readings were performed on April 22, May 9, May 18, June 10, and June 22 and the corresponding temperatures are presented in this Appendix. Thermistor resistance readings were taken manually. The resistances in Kohms were then translated into degrees Celsius using information provided by the thermistor manufacturer.

		Island/Seabed Temperature Profile Data				Spray Ice/Seabed Temperature						
		Thermistor Conversion Table										
Temp. (C)	Resistance (kohm)	Therm. Number	4/23/89 Temp. (C)	5/9/89 Resistance (kohm)	Temp. (C)	Resistance (kohm)	5/18/89 Resistance (kohm)	Temp. (C)	6/10/89 Resistance (kohm)	Temp. (C)	Resistance (kohm)	6/22/89 Resistance (kohm)
-21	51.47	1	-0.510	16.70	-0.43	16.777	-0.52	16.59	-0.30	16.74	-0.48	
-20	48.56	2	-0.517	16.75	-0.49	16.756	-0.50			16.75	-0.49	
-19	45.83	3	-0.563	16.77	-0.51			16.78	-0.52	16.75	-0.49	
-18	43.27	4	-0.555	16.76	-0.50	16.792	-0.54	16.73	-0.47	16.75	-0.49	
-17	40.86	5	-0.641	16.78	-0.52			16.82	-0.57	16.75	-0.49	
-16	38.61	6	-0.659	16.87	-0.63	16.872	-0.63	16.87	-0.63	16.81	-0.56	
-15	36.49	7	-0.701	16.79	-0.53			16.73	-0.47	16.84	-0.59	
-14	34.50	8	-0.689	16.74	-0.48			16.81	-0.56	16.83	-0.58	
-13	32.63	9	-0.732	16.87	-0.63	16.908	-0.67	16.88	-0.64	16.83	-0.58	
-12	30.88	10	-0.765	16.88	-0.64			16.89	-0.65	16.86	-0.62	
-11	29.23	11	-0.812	16.89	-0.65			16.89	-0.65	16.9	-0.66	
-10	27.67	12	-0.506	16.60	-0.31	16.724	-0.46	16.68	-0.41	16.66	-0.38	
-9	26.21	13	-0.185	16.47	-0.16	16.472	-0.17	16.45	-0.14	16.47	-0.16	
-8	24.83	14	-0.028	16.40	-0.08			16.42	-0.10	16.42	-0.10	
-7	23.54	15	-0.064	16.43	-0.12	16.429	-0.12	16.47	-0.16	16.41	-0.09	
-6	22.32	16	-0.019	16.39	-0.07	16.393	-0.07	16.38	-0.06	16.36	-0.03	
-5	21.17	17	-0.156	16.50	-0.20	16.538	-0.24	16.52	-0.22	16.46	-0.15	
-4	20.08	18	-3.067	18.90	-2.83	18.4	-2.31	16.37	-0.05	16.35	-0.02	
-3	19.06	19	-5.766	20.90	-4.75	20.9	-4.75	16.36	-0.03	16.36	-0.03	
-2	18.10	20	-7.753	21.90	-5.63	21.53	-5.31	15.81	0.64	16.33	0.00	
-1	17.19	21	-9.942	23.80	-7.20	23.2	-6.72	16.36	-0.03	16.45	-0.14	
0	16.33	22	-11.194	25.50	-8.49	23.82	-7.22	16.21	0.15	16.39	-0.07	
1	15.52	23	-12.315	25.90	-8.78	24.39	-7.66	16.21	0.15			
2	14.75	24	-13.172	26.30	-9.06	24.74	-7.93	15.25	1.35			

Spray Ice Temperatures Beneath Ablation Plots (Hourly)																										
Date	Date Fraction (Julian Day)	Average Air Temp. (°C)	1.5 cm			2 cm			3 cm			Temperature (°C)														
			Sawdust	Gravel/	Sawdust	Gravel/	Sawdust	Gravel/																		
10-Jun	161.00	4.36	0.854	0.730	0.843	0.628	0.628	1.964	0.548	0.502	0.430	0.378	0.335	0.304	0.272	0.252	0.241	0.241	0.252	0.263	0.275	0.275	0.298	0.329	0.372	0.438
	161.04	4.07	0.684	0.650	0.479	0.524	1.817	0.502	0.430	0.378	0.335	0.304	0.272	0.252	0.241	0.241	0.252	0.263	0.275	0.275	0.298	0.329	0.372	0.438	0.502	0.548
	161.08	3.07	0.476	0.578	0.316	0.430	1.622	0.430	0.378	0.335	0.304	0.272	0.252	0.241	0.241	0.252	0.263	0.275	0.275	0.298	0.329	0.372	0.438	0.502	0.548	0.598
	161.13	3.17	0.492	0.651	0.264	0.356	1.446	0.356	0.378	0.335	0.304	0.272	0.252	0.241	0.241	0.252	0.263	0.275	0.275	0.298	0.329	0.372	0.438	0.502	0.548	0.598
	161.17	2.06	0.290	0.540	0.233	0.278	1.267	0.278	0.378	0.335	0.304	0.272	0.252	0.241	0.241	0.252	0.263	0.275	0.275	0.298	0.329	0.372	0.438	0.502	0.548	0.598
	161.21	3.09	0.589	0.657	0.224	0.270	1.111	0.270	0.378	0.335	0.304	0.272	0.252	0.241	0.241	0.252	0.263	0.275	0.275	0.298	0.329	0.372	0.438	0.502	0.548	0.598
	161.25	2.61	0.568	0.648	0.249	0.238	0.978	0.238	0.378	0.335	0.304	0.272	0.252	0.241	0.241	0.252	0.263	0.275	0.275	0.298	0.329	0.372	0.438	0.502	0.548	0.598
	161.29	2.51	0.639	0.696	0.275	0.206	0.867	0.206	0.378	0.335	0.304	0.272	0.252	0.241	0.241	0.252	0.263	0.275	0.275	0.298	0.329	0.372	0.438	0.502	0.548	0.598
	161.33	3.42	0.833	0.855	0.355	0.229	0.787	0.229	0.378	0.335	0.304	0.272	0.252	0.241	0.241	0.252	0.263	0.275	0.275	0.298	0.329	0.372	0.438	0.502	0.548	0.598
	161.38	3.96	0.992	0.958	0.457	0.241	0.719	0.241	0.378	0.335	0.304	0.272	0.252	0.241	0.241	0.252	0.263	0.275	0.275	0.298	0.329	0.372	0.438	0.502	0.548	0.598
	161.42	4.50	1.503	1.253	0.628	0.298	0.674	0.298	0.378	0.335	0.304	0.272	0.252	0.241	0.241	0.252	0.263	0.275	0.275	0.298	0.329	0.372	0.438	0.502	0.548	0.598
	161.46	3.07	0.890	1.003	0.674	0.263	0.662	0.263	0.378	0.335	0.304	0.272	0.252	0.241	0.241	0.252	0.263	0.275	0.275	0.298	0.329	0.372	0.438	0.502	0.548	0.598
	161.50	5.33	1.752	1.344	0.799	0.320	0.662	0.320	0.378	0.335	0.304	0.272	0.252	0.241	0.241	0.252	0.263	0.275	0.275	0.298	0.329	0.372	0.438	0.502	0.548	0.598
	161.54	5.61	1.775	1.435	0.981	0.366	0.662	0.366	0.378	0.335	0.304	0.272	0.252	0.241	0.241	0.252	0.263	0.275	0.275	0.298	0.329	0.372	0.438	0.502	0.548	0.598
	161.58	6.34	2.270	1.726	1.239	0.477	0.682	0.477	0.378	0.335	0.304	0.272	0.252	0.241	0.241	0.252	0.263	0.275	0.275	0.298	0.329	0.372	0.438	0.502	0.548	0.598
	161.63	7.81	2.606	1.893	1.463	0.543	0.748	0.543	0.378	0.335	0.304	0.272	0.252	0.241	0.241	0.252	0.263	0.275	0.275	0.298	0.329	0.372	0.438	0.502	0.548	0.598
	161.67	7.28	2.298	1.789	1.539	0.586	0.836	0.586	0.378	0.335	0.304	0.272	0.252	0.241	0.241	0.252	0.263	0.275	0.275	0.298	0.329	0.372	0.438	0.502	0.548	0.598
	161.71																									
	161.75	10.58	3.519	2.108	2.018	0.703	0.998	0.703	0.378	0.335	0.304	0.272	0.252	0.241	0.241	0.252	0.263	0.275	0.275	0.298	0.329	0.372	0.438	0.502	0.548	0.598
	161.79	10.32	2.968	1.964	2.235	0.729	1.115	0.729	0.378	0.335	0.304	0.272	0.252	0.241	0.241	0.252	0.263	0.275	0.275	0.298	0.329	0.372	0.438	0.502	0.548	0.598
	161.83	8.32	1.986	1.692	1.862	0.661	1.262	0.661	0.378	0.335	0.304	0.272	0.252	0.241	0.241	0.252	0.263	0.275	0.275	0.298	0.329	0.372	0.438	0.502	0.548	0.598
	161.88	4.78	1.106	1.197	1.412	0.595	1.333	0.595	0.378	0.335	0.304	0.272	0.252	0.241	0.241	0.252	0.263	0.275	0.275	0.298	0.329	0.372	0.438	0.502	0.548	0.598
	161.92	3.20	0.782	0.851	0.941	0.544	1.338	0.544	0.378	0.335	0.304	0.272	0.252	0.241	0.241	0.252	0.263	0.275	0.275	0.298	0.329	0.372	0.438	0.502	0.548	0.598
	161.96	1.81	0.572	0.697	0.640	0.469	1.253	0.469	0.378	0.335	0.304	0.272	0.252	0.241	0.241	0.252	0.263	0.275	0.275	0.298	0.329	0.372	0.438	0.502	0.548	0.598
11-Jun	162.00	1.31	0.301	0.563	0.427	0.392	1.131	0.392	0.378	0.335	0.304	0.272	0.252	0.241	0.241	0.252	0.263	0.275	0.275	0.298	0.329	0.372	0.438	0.502	0.548	0.598
	162.04	1.45	0.272	0.546	0.261	0.318	1.001	0.318	0.378	0.335	0.304	0.272	0.252	0.241	0.241	0.252	0.263	0.275	0.275	0.298	0.329	0.372	0.438	0.502	0.548	0.598
	162.08	1.41	0.261	0.523	0.192	0.272	0.876	0.272	0.378	0.335	0.304	0.272	0.252	0.241	0.241	0.252	0.263	0.275	0.275	0.298	0.329	0.372	0.438	0.502	0.548	0.598
	162.13	1.09	0.104	0.423	0.104	0.206	0.765	0.206	0.378	0.335	0.304	0.272	0.252	0.241	0.241	0.252	0.263	0.275	0.275	0.298	0.329	0.372	0.438	0.502	0.548	0.598

Spray Ice Temperatures Beneath Ablation Plots (Hourly)																
Date	Date Fraction (Julian Day)	Average Air Temp. (°C)	1.5 cm		2 cm		3 cm		Temperature (°C)		0.3m		0.6 m		1.0 m	
			Sawdust	Gravel/	Sawdust	Gravel	Gravel	Gravel	Gravel	Gravel						
17-Jun	168.00	1.22	0.224	0.475	0.384	0.304	0.998	1.145	0.475	0.384	0.475	0.384	0.475	0.384	0.475	0.384
	168.04	0.97	0.204	0.466	0.227	0.249	0.887	1.182	0.409	0.375	0.409	0.375	0.409	0.375	0.409	0.375
	168.08	0.69	0.138	0.446	0.149	0.206	0.787	1.196	0.343	0.366	0.343	0.366	0.343	0.366	0.343	0.366
	168.13	0.59	0.095	0.426	0.084	0.163	0.688	1.210	0.300	0.357	0.300	0.357	0.300	0.357	0.300	0.357
	168.17	0.54	0.075	0.428	0.052	0.120	0.611	1.213	0.269	0.337	0.269	0.337	0.269	0.337	0.269	0.337
	168.21	0.53	0.075	0.428	0.040	0.098	0.542	1.213	0.246	0.326	0.246	0.326	0.246	0.326	0.246	0.326
	168.25	0.73	0.169	0.465	0.054	0.089	0.488	1.193	0.226	0.306	0.226	0.306	0.226	0.306	0.226	0.306
	168.29	0.93	0.260	0.511	0.100	0.077	0.442	1.182	0.226	0.294	0.226	0.294	0.226	0.294	0.226	0.294
	168.33	1.70	0.477	0.613	0.180	0.077	0.408	1.159	0.226	0.271	0.226	0.271	0.226	0.271	0.226	0.271
	168.38	2.82	0.807	0.784	0.328	0.100	0.397	1.136	0.237	0.260	0.237	0.260	0.237	0.260	0.237	0.260
	168.42	4.16	1.273	1.102	0.533	0.134	0.397	1.102	0.248	0.237	0.248	0.237	0.248	0.237	0.248	0.237
	168.46	4.91	1.451	1.225	0.679	0.177	0.417	1.077	0.303	0.234	0.303	0.234	0.303	0.234	0.303	0.234
	168.50	6.49	1.834	1.426	0.904	0.232	0.460	1.040	0.346	0.220	0.346	0.220	0.346	0.220	0.346	0.220
	168.54	11.03	3.891	2.389	1.505	0.357	0.505	1.006	0.391	0.209	0.391	0.209	0.391	0.209	0.391	0.209
	168.58	15.48	5.211	3.103	2.538	0.497	0.600	0.964	0.475	0.201	0.475	0.201	0.475	0.201	0.475	0.201
	168.63	16.07	3.987	2.950	3.119	0.469	0.765	0.936	0.606	0.196	0.606	0.196	0.606	0.196	0.606	0.196
	168.67	17.81	4.184	2.887	3.406	0.521	0.998	0.907	0.726	0.202	0.726	0.202	0.726	0.202	0.726	0.202
	168.71	18.17	4.507	2.817	3.042	0.552	1.245	0.871	0.803	0.188	0.803	0.188	0.803	0.188	0.803	0.188
	168.75	17.95	4.782	2.641	2.574	0.593	1.477	0.865	0.843	0.206	0.843	0.206	0.843	0.206	0.843	0.206
	168.79	20.12	4.967	2.613	2.229	0.610	1.653	0.848	0.860	0.223	0.860	0.223	0.860	0.223	0.860	0.223
	168.83	18.33	5.928	2.663	1.884	0.593	1.783	0.866	0.854	0.241	0.866	0.241	0.854	0.241	0.866	0.241
	168.88	18.73	5.677	2.897	1.769	0.579	1.848	0.886	0.818	0.261	0.886	0.261	0.818	0.261	0.886	0.261
	168.92	14.50	4.489	2.463	1.492	0.540	1.853	0.937	0.767	0.279	0.937	0.279	0.767	0.279	0.937	0.279
	168.96	4.03	1.180	0.886	1.090	0.454	1.791	1.010	0.738	0.329	1.010	0.738	0.738	0.329	1.010	0.738
18-Jun	169.00	4.15	1.361	0.953	0.806	0.454	1.690	1.089	0.670	0.374	1.089	0.670	0.670	0.374	1.089	0.374
	169.04	2.26	0.825	0.814	0.768	0.405	1.494	1.143	0.564	0.393	1.143	0.564	0.564	0.393	1.143	0.393
	169.08	1.07	0.330	0.546	0.490	0.307	1.319	1.205	0.478	0.410	1.205	0.478	0.478	0.410	1.205	0.410
	169.13	0.60	0.176	0.461	0.256	0.244	1.143	1.245	0.392	0.415	1.245	0.392	0.392	0.415	1.245	0.415

		Spray Ice Temperatures Beneath Ablation Plots (Hourly)															
		1.5 cm			2 cm			3 cm			Temperature (°C)						
		Sawdust			Sawdust			Sawdust			Sawdust						
		Bags			Bags			Bags			Gravel/						
		Sawdust			Sawdust			Sawdust			Sawdust						
		0.3m			0.6 m			1.0 m									
		Gravel			Gravel			Gravel			Gravel						
Date	Date Fraction (Julian Day)	Average Air Temp. (°C)	1.5 cm Sawdust	2 cm Sawdust	3 cm Sawdust	3 cm Sawdust	3 cm Sawdust	3 cm Sawdust	3 cm Sawdust	3 cm Sawdust	3 cm Sawdust						
24-Jun	175.00	6.86	1.913	3.367	0.588	0.418	1.585	1.664	0.599	0.384							
	175.04	4.27	0.829	2.874	0.284	0.341	1.452	1.690	0.523	0.398							
	175.08	2.62	0.073	1.876	0.061	0.278	1.322	1.740	0.460	0.414							
	175.13	1.83	0.032	0.590	-0.025	0.226	1.169	1.757	0.397	0.431							
	175.17	2.24	0.402	0.607	-0.008	0.208	1.015	1.774	0.334	0.425							
	175.21	2.91	0.601	0.885	0.065	0.214	0.873	1.780	0.282	0.407							
	175.25	2.80	1.896	0.615	0.216	0.239	0.751	1.772	0.250	0.398							
	175.29	4.16	2.913	1.012	0.410	0.592	0.660	1.772	0.250	0.387							
	175.33	6.94	5.122	1.557	0.785	0.512	0.603	1.749	0.239	0.364							
	175.38	5.92	1.873	1.681	0.921	0.239	0.581	1.726	0.228	0.353							
	175.42	6.00	2.758	1.435	0.879	0.207	0.572	1.695	0.230	0.344							
	175.46	15.01	7.800	2.137	1.219	0.321	0.595	1.661	0.253	0.333							
	175.50	11.25	5.415	2.755	1.930	0.307	0.615	1.613	0.296	0.307							
	175.54	16.33	6.720	2.470	2.492	0.316	0.703	1.588	0.396	0.305							
	175.58	15.30	5.634	2.342	2.647	0.314	0.837	1.551	0.484	0.291							
	175.63	14.65	5.517	2.181	2.419	0.334	0.993	1.525	0.561	0.300							
	175.67	15.68	5.108	2.562	2.032	0.513	1.137	1.511	0.604	0.308							
	175.71	16.43	5.123	2.644	1.650	0.504	1.231	1.491	0.584	0.322							
	175.75	15.48	3.994	2.788	1.500	0.524	1.274	1.489	0.547	0.320							
	175.79	8.27	3.521	2.077	1.137	0.377	1.274	1.511	0.547	0.343							
	175.83	12.09	3.208	2.464	0.947	0.356	1.242	1.537	0.493	0.356							
	175.88	10.01	2.949	2.486	0.811	0.322	1.140	1.548	0.447	0.345							
	175.92	5.52	2.328	1.808	0.675	0.311	1.050	1.582	0.425	0.356							
	175.96	4.05	1.800	1.449	0.496	0.279	0.973	1.619	0.405	0.370							
25-Jun	176.00	3.08	1.576	1.304	0.396	0.248	0.885	1.644	0.362	0.373							
	176.04	2.32	1.353	1.069	0.319	0.262	0.785	1.670	0.342	0.376							
	176.08	2.09	1.290	1.018	0.256	0.267	0.700	1.675	0.301	0.370							
	176.13	1.73	1.066	0.907	0.224	0.224	0.623	1.678	0.281	0.361							

Spray Ice Temperatures Beneath Ablation Plots (Hourly)																		
Date	Date Fraction (Julian Day)	Average Air Temp. (°C)	1.5 cm			2 cm			3 cm			Temperature (°C)						
			Sawdust	Sawdust	Sawdust	Sawdust	Sawdust	Sawdust	Sawdust									
1-Jul	182.00	0.86	0.243	1.721	0.152	0.072	0.801	1.040	0.380	0.255								
	182.04	0.26	0.004	1.040	0.038	0.061	0.733	1.040	0.334	0.266								
	182.08	-0.39	-0.074	0.736	-0.005	0.018	0.645	1.031	0.280	0.257								
	182.13	-0.76	-0.131	0.349	-0.017	0.006	0.554	1.020	0.234	0.269								
	182.17	-0.89	-0.220	0.363	-0.026	-0.003	0.454	1.000	0.191	0.260								
	182.21	-0.79	-0.266	0.374	-0.014	-0.014	0.385	0.989	0.180	0.248								
	182.25	-0.47	0.602	0.351	-0.014	0.009	0.317	0.966	0.180	0.237								
	182.29	0.27	2.236	0.431	0.020	-0.026	0.283	0.943	0.169	0.237								
	182.33	2.23	4.991	0.511	0.123	0.123	0.260	0.909	0.169	0.226								
	182.38	3.21	5.544	0.511	0.226	0.214	0.260	0.886	0.169	0.214								
	182.42	4.88	6.607	0.579	0.465	0.283	0.294	0.852	0.169	0.214								
	182.46	5.04	4.958	0.693	0.773	0.260	0.351	0.818	0.169	0.203								
	182.50	5.62	4.886	0.918	1.020	0.303	0.451	0.793	0.246	0.200								
	182.54	5.32	3.995	1.304	1.043	0.257	0.554	0.759	0.337	0.200								
	182.58	6.78	4.774	2.154	1.179	0.326	0.645	0.724	0.394	0.189								
	182.63	10.83	5.594	1.970	1.471	0.312	0.744	0.710	0.460	0.198								
	182.67	11.57	6.257	2.973	2.035	0.457	0.855	0.696	0.537	0.206								
	182.71	9.49	5.229	3.086	1.729	0.491	1.015	0.674	0.639	0.206								
	182.75	10.49	4.256	3.219	1.590	0.534	1.159	0.659	0.694	0.204								
	182.79	11.86	3.452	4.422	1.282	1.043	1.259	0.668	0.714	0.213								
	182.83	12.62	2.956	4.884	1.123	0.861	1.304	0.657	0.714	0.213								
	182.88	5.81	2.843	2.527	0.770	0.372	1.304	0.668	0.714	0.235								
	182.92	3.60	1.973	1.610	0.611	0.281	1.282	0.702	0.680	0.258								
	182.96	1.93	1.023	0.955	0.443	0.204	1.205	0.728	0.614	0.272								
2-Jul	183.00	0.99	0.400	0.560	0.252	0.149	1.094	0.753	0.537	0.286								
	183.04	0.77	0.129	0.426	0.106	0.118	0.983	0.767	0.449	0.289								
	183.08	0.46	0.040	0.405	0.040	0.075	0.861	0.781	0.371	0.292								
	183.13	-0.02	-0.005	0.394	-0.005	0.063	0.759	0.793	0.326	0.303								

Spray Ice Temperatures Beneath Ablation Plots (Hourly)									
	Average	Temperature (°C)		Sawdust		Gravel/		Sawdust	
Date	Air Temp.	1.5 cm	2 cm	3 cm	Sawdust	Gravel	Sawdust	Gravel	Gravel
(Julian Day)	(°C)	Sawdust	Sawdust	Sawdust	Bags	Gravel	Gravel	Gravel	Gravel
186.67	22.33	10.910	4.801	3.788	5.116	1.837	1.622	1.361	0.397

APPENDIX C

ABLATION MEASUREMENTS

A total of 35 - 5 cm by 5 cm by 4.9 m long graduated wooden stakes were inserted into the island to measure spray ice ablation. Fifteen ablation stakes were placed into the unprotected spray ice. Roughly one-half of these were in clean spray ice whereas the remaining stakes were placed in spray ice where the surface had been stained as a result of previous activity on the island. The remaining 20 stakes were placed in ablation plots and beneath the Rufco and 13 oz. per square yard vinyl edge protection sheets.

Stakes were graduated at 10 cm intervals starting from the top. The visible stake length from the top of the stake to the spray ice surface was measured during each site survey. Initial baseline measurements were recorded on April 23 and subsequent surveys were undertaken on May 9, June 10, June 22, and July 5. (Measurements were not taken during the May 18 survey due to extensive drifting snow which had accumulated over the western half of the island, obscuring many of the stakes). This differences between initial and subsequent measurements yielded the magnitude of ice surface ablation at a particular location.

Raw Data

	Baseline	May 9.	May 18.	June 10.	June 22.	July 5.
Sawdust Bags 1	90	90	90	90	95	95
Sawdust Bags 2	80	80	80	80	85	85
1m Gravel 1	55	75	75	75	85	100
1m Gravel 2	10	14	14	21	28	40
0.6m Gravel	5	10	10	20	30	45
0.3m Gravel	35	50	50	65	100	115
Unprotected Spray Ice 1	50	52	52	130	185	230
Unprotected Spray Ice 2	50	53	53	140	200	290
Unprotected Spray Ice 3	40	44	44	140	200	285
Unprotected Spray Ice 4	40	46	46	150	215	
Unprotected Spray Ice 5	40	43	43	122	175	265
Unprotected Spray Ice 6	45	49	49	145	205	285
Unprotected Spray Ice 7	35	39	39	110	170	270
Unprotected Spray Ice 8	43	47	47	115	175	260
Unprotected Spray Ice 9	70	75	75	135	190	270
Unprotected Spray Ice 10	20	23	23	110	185	300
Unprotected Spray Ice 11	55	55	55	130	190	290
Unprotected Spray Ice 12	20	22	22	120	180	270
Unprotected Spray Ice 13	55	56	56	130	180	280
Unprotected Spray Ice 14	72	75	75	160	215	290
Unprotected Spray Ice 15	70	71	71	160	230	300
1cm Sawdust	3	4	4	50	72	110
1.5cm Sawdust	50	50	50	80	102	130
2cm Sawdust	50	50	50	65	70	80
3cm Sawdust	50	50	50	55	60	70
1cm Sawdust/5cm Gravel	50	50	50	50	60	70
Rufco Sheet 1	50	50	50	80	110	150
Rufco Sheet 2	50	50	50	65	80	120
13oz Nylon 1	50	50	50	90	125	170
13oz Nylon 2	50	50	50	100	135	180
Rig Timbers	72	72	72	75	80	
Insulated Tarp 1	195	195	195	210	225	
Insulated Tarp 2	40	40	40	50	70	90
Insulated Tarp 3	178	180	180	200	210	

Adjusted Raw Data

Material	Baseline	May 9.	May 18.	June 10.	June 22.	July 5.
Sawdust Bags 1	90	90	90	90	95	95
Sawdust Bags 2	80	80	80	80	85	85
* 1m Gravel 1	75	75	75	75	85	100
* 1m Gravel 2	14	14	14	21	28	40
* 0.6m Gravel	10	10	10	20	30	45
* 0.3m Gravel	50	50	50	65	100	115
Unprotected Spray Ice 1	50	52	52	130	185	230
Unprotected Spray Ice 2	50	53	53	140	200	290
Unprotected Spray Ice 3	40	44	44	140	200	285
Unprotected Spray Ice 4	40	46	46	150	215	
Unprotected Spray Ice 5	40	43	43	122	175	265
Unprotected Spray Ice 6	45	49	49	145	205	285
Unprotected Spray Ice 7	35	39	39	110	170	270
Unprotected Spray Ice 8	43	47	47	115	175	260
Unprotected Spray Ice 9	70	75	75	135	190	270
Unprotected Spray Ice 10	20	23	23	110	185	300
Unprotected Spray Ice 11	55	55	55	130	190	290
Unprotected Spray Ice 12	20	22	22	120	180	270
Unprotected Spray Ice 13	55	56	56	130	180	280
Unprotected Spray Ice 14	72	75	75	160	215	290
Unprotected Spray Ice 15	70	71	71	160	230	300
1cm Sawdust	3	4	4	50	72	110
1.5cm Sawdust	50	50	50	80	102	130
2cm Sawdust	50	50	50	65	70	80
3cm Sawdust	50	50	50	55	60	70
1cm Sawdust/5cm Gravel	50	50	50	50	60	70
Rufco Sheet 1	50	50	50	80	110	150
Rufco Sheet 2	50	50	50	65	80	120
13oz Nylon 1	50	50	50	90	125	170
13oz Nylon 2	50	50	50	100	135	180
Rig Timbers	72	72	72	75	80	
Insulated Tarp 1	195	195	195	210	225	
Insulated Tarp 2	40	40	40	50	70	90
Insulated Tarp 3	178	180	180	200	210	

* baseline is adjusted to be May 9 reading as opposed to April 23 due to misleading spray ice creep that took place during this period.

	Spray Ice Ablation Level					
Material	Measure of Ice Level (cm)					
	Baseline	May 9.	May 18.	June 10.	June 22.	July 5.
Sawdust Bags 1	90	90	90	90	95	95
Sawdust Bags 2	80	80	80	80	85	85
1m Gravel 1	55	75	75	75	85	100
1m Gravel 2	10	14	14	21	28	40
0.6m Gravel	5	10	10	20	30	45
0.3m Gravel	35	50	50	65	100	115
Unprotected Spray Ice 1	50	52	52	130	185	230
Unprotected Spray Ice 2	50	53	53	140	200	290
Unprotected Spray Ice 3	40	44	44	140	200	285
Unprotected Spray Ice 4	40	46	46	150	215	
Unprotected Spray Ice 5	40	43	43	122	175	265
Unprotected Spray Ice 6	45	49	49	145	205	285
Unprotected Spray Ice 7	35	39	39	110	170	270
Unprotected Spray Ice 8	43	47	47	115	175	260
Unprotected Spray Ice 9	70	75	75	135	190	270
Unprotected Spray Ice 10	20	23	23	110	185	300
Unprotected Spray Ice 11	55	55	55	130	190	290
Unprotected Spray Ice 12	20	22	22	120	180	270
Unprotected Spray Ice 13	55	56	56	130	180	280
Unprotected Spray Ice 14	72	75	75	160	215	290
Unprotected Spray Ice 15	70	71	71	160	230	300
1cm Sawdust	3	4	4	50	72	110
1.5cm Sawdust	50	50	50	80	102	130
2cm Sawdust	50	50	50	65	70	80
3cm Sawdust	50	50	50	55	60	70
1cm Sawdust/5cm Gravel	50	50	50	50	60	70
Rufco Sheet 1	50	50	50	80	110	150
Rufco Sheet 2	50	50	50	65	80	120
13oz Nylon 1	50	50	50	90	125	170
13oz Nylon 2	50	50	50	100	135	180
Rig Timbers	72	72	72	75	80	
Insulated Tarp 1	195	195	195	210	225	
Insulated Tarp 2	40	40	40	50	70	90
Insulated Tarp 3	178	180	180	200	210	

Averaged Data

	A	B	C	D	E	F	G
1				Rate of Ablation Data (cm/day)			
2							
3	Material			Time Period			
4			April 23-	May 9-	May 18-	June 10-	June 22-
5			May 9.	May 18.	June 10.	June 22.	July 5.
6							
7	Sawdust Bags		0	0	0	0.417	0
8	1m Gravel		0.25	0	0.304	0.708	0.923
9	0.6m Gravel		0.75	0	0.152	0.833	1.039
10	0.3m Gravel		0.312	0	0.435	2.917	1.154
11	Unprotected Spray Ice		0.188	0	3.615	4.989	6.621
12	1cm Sawdust		0.062	0	2	1.833	2.923
13	1.5cm Sawdust		0	0	1.304	1.833	2.154
14	2cm Sawdust		0	0	0.652	0.417	0.769
15	3cm Sawdust		0	0	0.217	0.417	0.769
16	1cm Sawdust/5cm Gravel		0	0	0	0.833	0.769
17	Rufco Sheet		0	0	0.978	1.875	3.077
18	13oz Nylon Sheet		0	0	1.957	2.917	3.462
19	Rig Timbers		0	0	0.13	0.417	
20	Insulated Tarp		0.042	0	0.652	1.25	1.538

Material	Cumulative Ablation to Date					
	(cm)					
	April 23	May 9.	May 18.	June 10.	June 22.	July 5.
Sawdust Bags 1	0	0	0	0	5	5
Sawdust Bags 2	0	0	0	0	5	5
Sawdust Bags Average	0	0	0	0	5	5
1m Gravel 1	0	20	20	20	30	45
1m Gravel 2	0	4	4	11	18	30
1m Gravel Average	0	12	12	15.5	24	37.5
0.6m Gravel	0	5	5	15	25	40
0.3m Gravel	0	15	25	30	65	80
Unprotected Spray Ice 1	0	2	2	80	135	180
Unprotected Spray Ice 2	0	3	3	90	150	240
Unprotected Spray Ice 3	0	4	4	100	160	245
Unprotected Spray Ice 4	0	6	6	110	175	
Unprotected Spray Ice 5	0	3	3	82	135	225
Unprotected Spray Ice 6	0	4	4	100	160	240
Unprotected Spray Ice 7	0	4	4	75	135	235
Unprotected Spray Ice 8	0	4	4	72	132	217
Unprotected Spray Ice 9	0	5	5	65	120	200
Unprotected Spray Ice 10	0	3	3	90	165	280
Unprotected Spray Ice 11	0	0	0	75	135	235
Unprotected Spray Ice 12	0	2	2	100	160	250
Unprotected Spray Ice 13	0	1	1	75	125	225
Unprotected Spray Ice 14	0	3	3	88	143	218
Unprotected Spray Ice 15	0	1	1	90	160	230
Unprotected Spray Ice Average	0	3	3	86.13	146	230
1cm Sawdust	0	1	1	47	69	107
1.5cm Sawdust	0	0	0	30	52	80
2cm Sawdust	0	0	0	15	20	30
3cm Sawdust	0	0	0	5	10	20
1cm Sawdust/5cm Gravel	0	0	0	0	10	20
Rufco Sheet 1	0	0	0	30	60	100
Rufco Sheet 2	0	0	0	15	30	70
Rufco Sheet Average	0	0	0	22.5	45	85

		Cumulative Ablation to Date					
		(cm)					
Material	April 23	May 9.	May 18.	June 10.	June 22.	July 5.	
13oz Nylon Sheet 1	0	0	0	40	75	120	
13oz Nylon Sheet 2	0	0	0	50	85	130	
13oz Nylon Sheet Average	0	0	0	45	80	125	
Rig Timbers	0	0	0	3	5		
Insulated Tarp 1	0	0	0	15	30		
Insulated Tarp 2	0	0	0	10	30	50	
Insulated Tarp 3	0	2	2	22	32		
Insulated Tarp Average	0	0.67	0.67	15.67	30.67	50	

Spray Ice Ablation Rates

Material	Spray Ice Ablation Rates (cm/day)				
	Time Period				
	April 23- May 9.	May 9- May 18.	May 18- June 10.	June 10- June 22.	June 22- July 5.
Sawdust 1	0	0	0	0.417	0
Sawdust 2	0	0	0	0.417	0
Sawdust Bags Average	0	0	0	0.417	0
* 1m Gravel 1	0	0	0	0.833	1.154
* 1m Gravel 2	0	0	0.304	0.583	0.923
* 1m Gravel Average	0	0	0.152	0.708	1.039
* 0.6m Gravel	0	0	0.435	0.833	1.154
* 0.3m Gravel	0	0	0.652	2.917	1.154
Unprotected Spray Ice 1	0.125	0	3.391	4.583	3.462
Unprotected Spray Ice 2	0.188	0	3.783	5	6.923
Unprotected Spray Ice 3	0.25	0	4.174	5	6.538
Unprotected Spray Ice 4	0.375	0	4.522	5.417	
Unprotected Spray Ice 5	0.188	0	3.435	4.417	6.923
Unprotected Spray Ice 6	0.25	0	4.174	5	6.154
Unprotected Spray Ice 7	0.25	0	3.087	5	3.226
Unprotected Spray Ice 8	0.25	0	2.957	5	6.538
Unprotected Spray Ice 9	0.312	0	2.609	4.583	6.154
Unprotected Spray Ice 10	0.188	0	3.783	6.25	8.846
Unprotected Spray Ice 11	0	0	3.261	5	7.692
Unprotected Spray Ice 12	0.125	0	4.261	5	6.923
Unprotected Spray Ice 13	0.062	0	3.217	4.167	7.692
Unprotected Spray Ice 14	0.188	0	3.696	4.583	5.769
Unprotected Spray Ice 15	0.062	0	3.87	5.833	5.385
Unprotected Spray Ice Average	0.188	0	3.615	4.989	6.302
1cm Sawdust	0.062	0	2	1.833	2.923
1.5cm Sawdust	0	0	1.304	1.833	2.154
2cm Sawdust	0	0	0.652	0.417	0.769
3cm Sawdust	0	0	0.217	0.417	0.769
1cm Sawdust/5cm Gravel	0	0	0	0.833	0.769
Rufco Sheet 1	0	0	1.304	2.5	3.077
Rufco Sheet 2	0	0	0.652	1.25	3.077

Spray Ice Ablation Rates

Material	Spray Ice Ablation Rates (cm/day)				
	Time Period				
	April 23- May 9.	May 9- May 18.	May 18- June 10.	June 10- June 22.	June 22- July 5.
Rufco Sheet Average	0	0	0.978	1.875	3.077
13oz Nylon 1	0	0	1.739	2.917	3.462
13oz Nylon 2	0	0	2.174	2.917	3.462
13oz Nylon Sheet Average	0	0	1.957	2.917	3.462
Rig Timbers	0	0	0.13	0.417	
Insulated Tarp 1	0	0	0.652	1.25	
Insulated Tarp 2	0	0	0.435	1.667	1.538
Insulated Tarp 3	0.125	0	0.87	0.833	
Insulated Tarp Average	0.042	0	0.652	1.25	1.538

Spray Ice Ablation Rates					
Material	Rate of Spray Ice Ablation (cm/day)				
	April 23- May 9.	May 9- May 18.	May 18- June 10.	June 10- June 22.	June 22- July 5.
Rufco Sheet Average	0	0	0.98	1.88	3.08
13oz Nylon Sheet 1	0	0	1.74	2.92	3.46
13oz Nylon Sheet 2	0	0	2.17	2.92	3.46
13oz Nylon Sheet Average	0	0	1.96	2.92	3.46
Rig Timbers	0	0	0.13	0.42	
Insulated Tarp 1	0	0	0.65	1.25	
Insulated Tarp 2	0	0	0.44	1.67	1.54
Insulated Tarp 3	0.13	0	0.87	0.83	
Insulated Tarp Average	0.04	0	0.65	1.25	1.54

Ablation Rates (not adj.)

A	B	C	D	E	F
1		Spray Ice Ablation Rates			
2					
3			Ablation (cm/day)		
4	Material				
5			Time Period		
6	April 23- May 9	May 9-May 18	May 18-June 10	June 10-June 22	June 22-July 5
7					
8	Sawdust 1	0	0	0.417	0
9	Sawdust 2	0	0	0.417	0
10	Sawdust Bags	0	0	0.417	0
11	1m Gravel 1	1.25	0	0.833	1.154
12	1m Gravel 2	0.25	0.304	0.583	0.923
13	1m Gravel	0.75	0.152	0.708	1.039
14	0.6m Gravel	0.3125	0.435	0.833	1.154
15	0.3m Gravel	0.9375	0.652	2.917	1.154
16	Unprotected Spray Ice 1	0.125	3.391	4.583	3.462
17	Unprotected Spray Ice 2	0.188	3.783	5	6.923
18	Unprotected Spray Ice 3	0.25	4.174	5	6.538
19	Unprotected Spray Ice 4	0.375	4.522	5.417	
20	Unprotected Spray Ice 5	0.188	3.435	4.417	6.923
21	Unprotected Spray Ice 6	0.25	4.174	5	6.154
22	Unprotected Spray Ice 7	0.25	3.087	5	7.692
23	Unprotected Spray Ice 8	0.25	2.957	5	6.538
24	Unprotected Spray Ice 9	0.312	2.609	4.583	6.154
25	Unprotected Spray Ice 10	0.188	3.783	6.25	8.846
26	Unprotected Spray Ice 11	0	3.261	5	7.692
27	Unprotected Spray Ice 12	0.125	4.261	5	6.923
28	Unprotected Spray Ice 13	0.062	3.217	4.167	7.692
29	Unprotected Spray Ice 14	0.188	3.696	4.583	5.769
30	Unprotected Spray Ice 15	0.062	3.87	5.833	5.385
31	Unprotected Spray Ice	0.188	3.615	4.989	6.302
32	1cm Sawdust	0.062	2	1.833	2.923
33	1.5cm Sawdust	0	1.304	1.833	2.154

Ablation Rates (not adj.)

	A	B	C	D	E	F
34	2cm Sawdust	0	0	0.652	0.417	0.769
35	3cm Sawdust	0	0	0.217	0.417	0.769
36	1cm Sawdust/5cm Gravel	0	0	0	0.833	0.769
37	Rufco Sheet 1	0	0	1.304	2.5	3.077
38	Rufco Sheet 2	0	0	0.652	1.25	3.077
39	Rufco Sheet	0	0	0.978	1.875	3.077
40	13oz Nylon 1	0	0	1.739	2.917	3.462
41	13oz Nylon 2	0	0	2.174	2.917	3.462
42	13oz Nylon Sheet	0	0	1.957	2.917	3.462
43	Rig Timbers	0	0	0.13	0.417	
44	Insulated Tarp 1	0	0	0.652	1.25	
45	Insulated Tarp 2	0	0	0.435	1.667	1.538
46	Insulated Tarp 3	0.125	0	0.87	0.833	
47	Insulated Tarp	0.042	0	0.652	1.25	1.538

Cumulative Ablation

Cumulative Ablation (averaged from samples available)						
Material	Cumulative Ablation to Date (cm)					
	Apr. 23.	May 9.	May 18.	Jun. 10.	Jun. 22.	Jul. 5.
Sawdust Bags	0	0	0	0	5	5
1m Gravel	0	0	0	3.5	12	25.5
0.6m Gravel	0	0	0	10	20	35
0.3m Gravel	0	0	0	15	50	65
Unprotected Spray Ice	0	3	3	86.13	146	230
1cm Sawdust	0	1	1	47	69	107
1.5cm Sawdust	0	0	0	30	52	80
2cm Sawdust	0	0	0	15	20	30
3cm Sawdust	0	0	0	5	10	20
1cm Sawdust/5cm Gravel	0	0	0	0	10	20
Rufco Sheet	0	0	0	22.5	45	85
13oz Nylon Sheet	0	0	0	45	80	125
Rig Timbers	0	0	0	3	5	
Insulated Tarp	0	0.667	0.667	15.67	30.67	50

Ablation Measures

Material	Measure of Ice Level (cm)					
	Baseline	May 9.	May 18.	June 10.	June 22.	July 5.
Sawdust Bags 1	90	90	90	90	95	95
Sawdust Bags 2	80	80	80	80	85	85
* 1m Gravel 1	75	75	75	75	85	100
* 1m Gravel 2	14	14	14	21	28	40
* 0.6m Gravel	10	10	10	20	30	45
* 0.3m Gravel	50	50	50	65	100	115
Unprotected Spray Ice 1	50	52	52	130	185	230
Unprotected Spray Ice 2	50	53	53	140	200	290
Unprotected Spray Ice 3	40	44	44	140	200	285
Unprotected Spray Ice 4	40	46	46	150	215	
Unprotected Spray Ice 5	40	43	43	122	175	265
Unprotected Spray Ice 6	45	49	49	145	205	285
Unprotected Spray Ice 7	35	39	39	110	170	270
Unprotected Spray Ice 8	43	47	47	115	175	260
Unprotected Spray Ice 9	70	75	75	135	190	270
Unprotected Spray Ice 10	20	23	23	110	185	300
Unprotected Spray Ice 11	55	55	55	130	190	290
Unprotected Spray Ice 12	20	22	22	120	180	270
Unprotected Spray Ice 13	55	56	56	130	180	280
Unprotected Spray Ice 14	72	75	75	160	215	290
Unprotected Spray Ice 15	70	71	71	160	230	300
1cm Sawdust	3	4	4	50	72	110
1.5cm Sawdust	50	50	50	80	102	130
2cm Sawdust	50	50	50	65	70	80
3cm Sawdust	50	50	50	55	60	70
1cm Sawdust/5cm Gravel	50	50	50	50	60	70
Rufco Sheet 1	50	50	50	80	110	150
Rufco Sheet 2	50	50	50	65	80	120
13oz Nylon 1	50	50	50	90	125	170
13oz Nylon 2	50	50	50	100	135	180
Rig Timbers	72	72	72	75	80	
Insulated Tarp 1	195	195	195	210	225	
Insulated Tarp 2	40	40	40	50	70	90
Insulated Tarp 3	178	180	180	200	210	
* baseline is adjusted to be May 9 reading as opposed to April 23 due to misleading spray ice creep that took place during this period.						

Cumulative Ablation (adj)

Material	Adjusted Cumulative Ablation					
	Cumulative Ablation to Date (cm)					
	April 23	May 9.	May 18.	June 10.	June 22.	July 5.
Sawdust Bags 1	0	0	0	0	5	5
Sawdust Bags 2	0	0	0	0	5	5
Sawdust Bags Average	0	0	0	0	5	5
* 1m Gravel 1	0	0	0	0	10	25
* 1m Gravel 2	0	0	0	7	14	26
* 1m Gravel Average	0	0	0	3.5	12	25.5
* 0.6m Gravel	0	0	0	10	20	35
* 0.3m Gravel	0	0	0	15	50	65
Unprotected Spray Ice 1	0	2	2	80	135	180
Unprotected Spray Ice 2	0	3	3	90	150	240
Unprotected Spray Ice 3	0	4	4	100	160	245
Unprotected Spray Ice 4	0	6	6	110	175	
Unprotected Spray Ice 5	0	3	3	82	135	225
Unprotected Spray Ice 6	0	4	4	100	160	240
Unprotected Spray Ice 7	0	4	4	75	135	235
Unprotected Spray Ice 8	0	4	4	72	132	217
Unprotected Spray Ice 9	0	5	5	65	120	200
Unprotected Spray Ice 10	0	3	3	90	165	280
Unprotected Spray Ice 11	0	0	0	75	135	235
Unprotected Spray Ice 12	0	2	2	100	160	250
Unprotected Spray Ice 13	0	1	1	75	125	225
Unprotected Spray Ice 14	0	3	3	88	143	218
Unprotected Spray Ice 15	0	1	1	90	160	230
Unprotected Spray Ice Average	0	3	3	86.133	146	230
1cm Sawdust	0	1	1	47	69	107
1.5cm Sawdust	0	0	0	30	52	80
2cm Sawdust	0	0	0	15	20	30
3cm Sawdust	0	0	0	5	10	20
1cm Sawdust/5cm Gravel	0	0	0	0	10	20
Rufco Sheet 1	0	0	0	30	60	100
Rufco Sheet 2	0	0	0	15	30	70
Rufco Sheet Average	0	0	0	22.5	45	85

Cumulative Ablation (adj)

Material	Adjusted Cumulative Ablation					
	Cumulative Ablation to Date (cm)					
	April 23	May 9.	May 18.	June 10.	June 22.	July 5.
13oz Nylon Sheet 1	0	0	0	40	75	120
13oz Nylon Sheet 2	0	0	0	50	85	130
13oz Nylon Sheet Average	0	0	0	45	80	125
Rig Timbers	0	0	0	3	5	
Insulated Tarp 1	0	0	0	15	30	
Insulated Tarp 2	0	0	0	10	30	50
Insulated Tarp 3	0	2	2	22	32	
Insulated Tarp Average	0	0.6667	0.6667	15.667	30.667	50

APPENDIX E

ABLATION AND EROSION NUMERICAL SIMULATION

**REPORT PREPARED BY S.L. CONNOLLY DOCUMENTING ANALYTICAL
APPLICATION'S ABLATION AND EROSION NUMERICAL SIMULATION.**

**FINAL REPORT TO:
ESSO RESOURCES RESEARCH LABORATORY**

**SPRAY ICE ISLAND ABLATION
MODELING**

February, 1990

**Submitted by:
Analytic Applications, Inc.
1705 14th St.
Suite 126
Boulder, CO 80302**

INTRODUCTION

As spray ice islands become an accepted structure for arctic exploratory drilling, the possibilities for expanding their operational capabilities should be explored. Some of these possibilities include the use of a single spray ice island for multi-year drilling operations, open water demobilization of the drilling rig, and even as an early production platform. Ice, although inexpensive and readily available in the arctic, is a very unstable construction material when compared to conventional materials and undergoes considerable deterioration during the arctic summer season. The degree to which this deterioration takes place and the ability to protect the island from ablation and erosional forces is the subject of this study.

The approach taken in this study was to simulate the meteorological and oceanographic conditions effecting the island as closely as possible. When possible, direct measurements have been included in the model and where these measurements have been lacking, the terms have been parameterized. One of the advantages of this technique is that the model can be used to simulate the behavior of a spray ice island under a variety of conditions. Predictions as to the feasibility of a spray ice island at certain locations can be made when climatological data are input into the model. Because of the wide fluctuations in meteorological conditions from the climatological averages in the arctic, a range of conditions can be fed into the model in order to determine the range of operating conditions for the island.

The effects of environmental conditions to the island were measured in terms of the ablation and erosion of the island. Ablation was considered to be the loss of ice mass due to melting of the top surface and erosion was considered to be loss of ice mass around the perimeter. Ablation was caused by the interaction of the island with the atmosphere and erosion was caused by the interaction between the island and the water. The island was modeled as an ice mass both protected and unprotected by other materials.

The results of the model were compared against measurements of ablation and erosion taken on the island. Sensitivity to changes in both environmental factors and island properties are observed and discussed.

THE MODEL

The modeling effort was broken into two parts; the ablation of the top surface of the island, and the erosion of the perimeter. Since these two parts operate independent of one another they will be modeled independently.

Ablation

The ablation of the top surface involves the energy transfer between the ice and the atmosphere. In this case the standard energy balance equation was used. This equation is given as:

$$F_s + F_l + L + S = \gamma \rho D + G \quad (1)$$

where F_s is the net shortwave radiation, F_l is the net longwave radiation, L is the latent heat flux, S is the sensible heat flux, γ is the latent heat of fusion, ρ is the spray ice density, D is the depth to which the ice has melted, and G is the heat conducted through the ice. All these quantities are averaged over the surface of the island. The convention used here is for the terms on the left side of (1) to be positive into the island surface and heat conduction to be positive away from the surface.

Incoming shortwave radiation is solar radiation whereas outgoing shortwave is solar radiation reflected from the surface. Incoming shortwave radiation has been measured hourly on the island with a pyranometer. The albedo of the spray ice, the ratio of outgoing radiation to incoming radiation, was taken as 0.9, approximately the same as that for snow. Hence the actual amount of absorbed radiation is relatively small.

Incoming longwave radiation originates mainly from water vapor in the air. Since no direct measurement of longwave radiation was taken, it will be estimated using an empirical relation developed by Idso and Jackson (1969):

$$F_l^i = \epsilon \sigma T_a^4 \left[1 - 0.261 \exp(-7.77 \times 10^{-4} (T_a - 273)^2) \right] \quad (2)$$

where ϵ is the surface emissivity, σ is the Stefan-Boltzman constant, and T_a is the near-surface air temperature in degrees Kelvin. The surface emissivity for spray ice is taken to be 0.95, the same as that for snow.

Longwave radiation emitted from the surface is given by the equation:

$$F_l^o = -\epsilon \sigma T_s^4 \quad (3)$$

where T_s is the temperature of the surface in Kelvin. Since the surface is first considered to be ice at the melting point this number will remain constant at 305 W m^{-2} .

Sensible heat flux is the energy transferred by the turbulent action of the wind. Although no sophisticated sensible heat flux measurements were taken on the island, the bulk aerodynamic method of calculating the sensible heat flux only requires wind speed and a temperature profile. This method is commonly used over the ocean (Kondo, 1975), where surfaces are fairly uniform and fetches are large. The sensible heat flux from this method is given by:

$$S = c_p \rho_a C_s (T_s - T_d) u \quad (4)$$

where c_p is the specific heat of air at constant pressure, ρ_a is the air density, C_s is the sensible heat transfer coefficient, and u is the near surface wind speed.

Latent heat flux becomes a significant term during the summer melt season when liquid water is plentiful at the surface. Energy is absorbed by the water at the surface when there is a phase change into vapor. This energy is then carried off by the vapor as it is transported into the atmosphere. The term can be measured by observing the humidity gradient above the surface and can be represented by the bulk aerodynamic method as:

$$L = \gamma_v \rho_a C_l (q_s - q) u \quad (5)$$

where γ_v is the latent heat of vaporization, C_l is the latent heat transfer coefficient, q_s is the surface vapor density, and q is the near-surface vapor density. Since humidity was not directly measured on the island we will use the assumptions commonly used in the bulk aerodynamic method over the ocean (Large and Pond, 1982) namely that the air is saturated with respect to water both at the surface and slightly above the surface. In this case the saturation vapor density is given by:

$$q = \frac{a}{R_v (T_a - 273)} \exp\left(\frac{b T_a}{T_a + c}\right) \quad (6)$$

where R_v is the gas constant for water vapor, and a , b , and c are constants given by Buck (1981) as 611.21, 17.502, and 240.97 respectively.

Latent heat can also be transferred to the island by water vapor condensing on the ice surface, rain falling and refreezing, or snow falling. Because of the low precipitation rates in the arctic this will not be considered as an important term.

The energy not reflected at the surface of the island is either conducted down into the ice, absorbed by melting the ice, or absorbed by evaporating liquid water. From the thermistor data the island was observed to be isothermal on 10 June and assumed to be isothermal on 7 June as well. This is to say that the average temperature was 0°C although some lower temperatures might be observed at night at the surface. Because the whole island is at the freezing temperature, there can be no heat conducted into the ice and so the term G in (1) becomes zero.

In addition to modeling the ablation of the unprotected spray ice, the model was modified to simulate the melt behavior a protective surface would have on the ice. When the ice surface is covered by any material, all the terms in (1) are changed to some degree. The energy transfer occurs between the atmosphere and the protection material providing heat which is conducted through the protection material to the ice below. Equation (1) is then modified for the protection material by eliminating the ice melt term on the right side and including the conduction term.

The heat absorbed by the protection material at $z = 0$ can be represented by the sine series:

$$G(0) = \sum_{n=0}^P A_n \sin \omega_n t \quad (7)$$

where A_n are the Fourier coefficients, P is the time period over which the time series is measured, and ω_n are the harmonic frequencies. At some depth, z , the heat flux through that layer can be expressed as:

$$G(z) = \sum_{n=0}^P A_n e^{-k_n z} \sin(\omega_n t - k_n z) \quad (8)$$

where

$$k_n = \sqrt{\frac{\omega_n}{2\kappa}} \quad (9)$$

and κ is the diffusivity of the protection material. If z is the depth of the protection material and the heat flux is positive, then the heat flux given by (8) is the amount of heat available for melting the ice.

Erosion

There are two terms which describe the erosional forces acting on the perimeter of the island. Forced convection is a result of a current forcing water passed the island melting the submarine portion of the island. The rate at which the melting takes place is a function of both water

temperature and velocity. The second term stems from the turbulence created by waves which aid to the melting process but is confined to the wave zone around the perimeter of the island. This process is responsible for undercutting the subaerial part of the island which calves off at the same rate as it is undercut. White et al. (1980) use a Reynolds analogy to compute heat transfer to an iceberg as a function of wave friction:

$$F_w = 0.000219 \left(\frac{R}{H}\right)^{0.2} \left(\frac{H}{P}\right) \rho \gamma (T_w - 273) \quad (10)$$

where F_w is the heat flux due to wave action, R is the roughness length of the ice, H is the average wave height, P is the average wave period, and T_w is the water surface temperature.

Forced convection, as applied to icebergs by El-Tahan et al. (1984), has been expressed as:

$$F_c = Nu \cdot K_w \cdot T_w / L \quad (11)$$

where Nu is the Nusselt number, K_w is the thermal conductivity of water, and L is the maximum water line length. The Nusselt number is usually given as:

$$Nu = 0.055 Re^{0.8} Pr^{0.4} \quad (12)$$

Re is the Reynold's number, and Pr is the Prandtl number.

Because turbulent energy transfer is so much more efficient than laminar energy transfer, the wave erosion term dominates the erosion above water island perimeter. The below water portion of the island perimeter erodes more slowly but, because the ice is buoyant, does not add to the weight on bottom and therefore contributes little to the resistance of the island to lateral forces.

FIELD EXPERIMENT

Air temperature and solar radiation data were collected on the island hourly from 7 June to 5 July, 1989. Wind data were collected at Tuk every 6 hours. Incoming solar radiation was measured with a LI-COR LI-200SZ pyranometer. This pyranometer is calibrated against a more sophisticated Eppley Precision Spectral Pyranometer to give an accuracy of $\pm 5\%$.

The solar energy absorbed at the island surface is the net solar radiation which is the difference between the incoming and outgoing shortwave radiation. In order to calculate the outgoing shortwave radiation, the albedo of spray ice must be known. In this case we take the albedo to be that of wet, clean snow which is approximately 0.8. The net shortwave radiation is then the incoming radiation multiplied by 0.2. This is plotted in Figure 1.

When ablation protection materials such as gravel or sawdust are used the albedo decreases resulting in greater solar radiation absorption. This could actually result in higher ablation rates if the albedo is raised without a corresponding rise in insulation.

The air temperature was measured with thermistors placed at 2 cm and 30 cm above a gravel surface and were unprotected against solar radiation. The thermistor temperatures will then show a temperature higher than the ambient air temperature during the daylight hours due to radiative heating from the sun. The temperatures will also be more representative of air temperatures over an ablation protection material than the air temperature over ice. Another temperature is the internal temperature of a datalogger. Although this does not represent a true air temperature either,

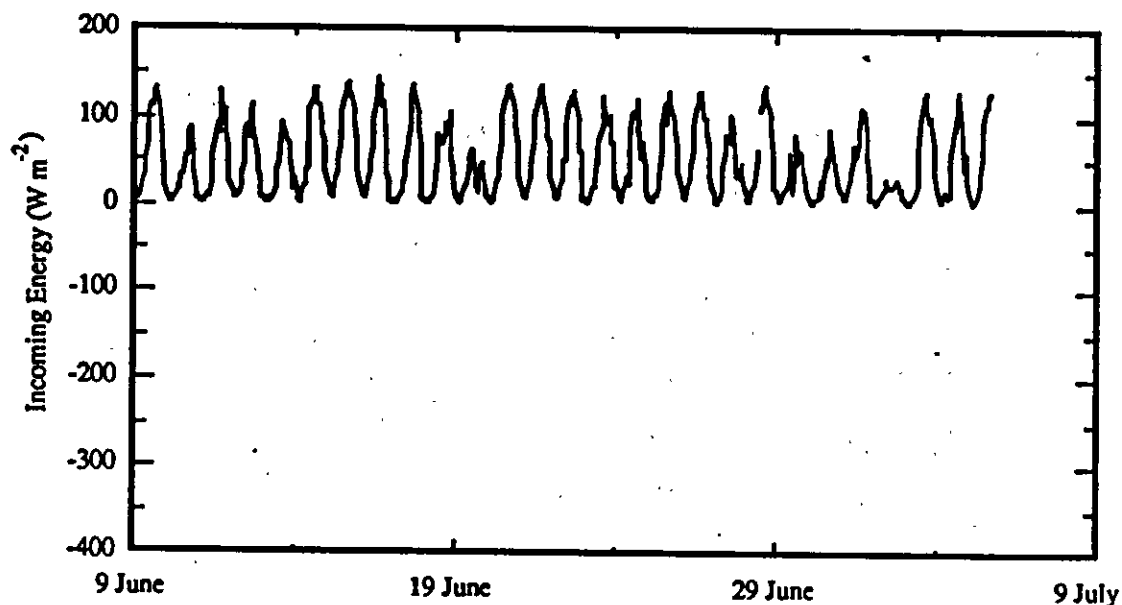


Figure 1. Net solar radiation over ice during the field experiment.

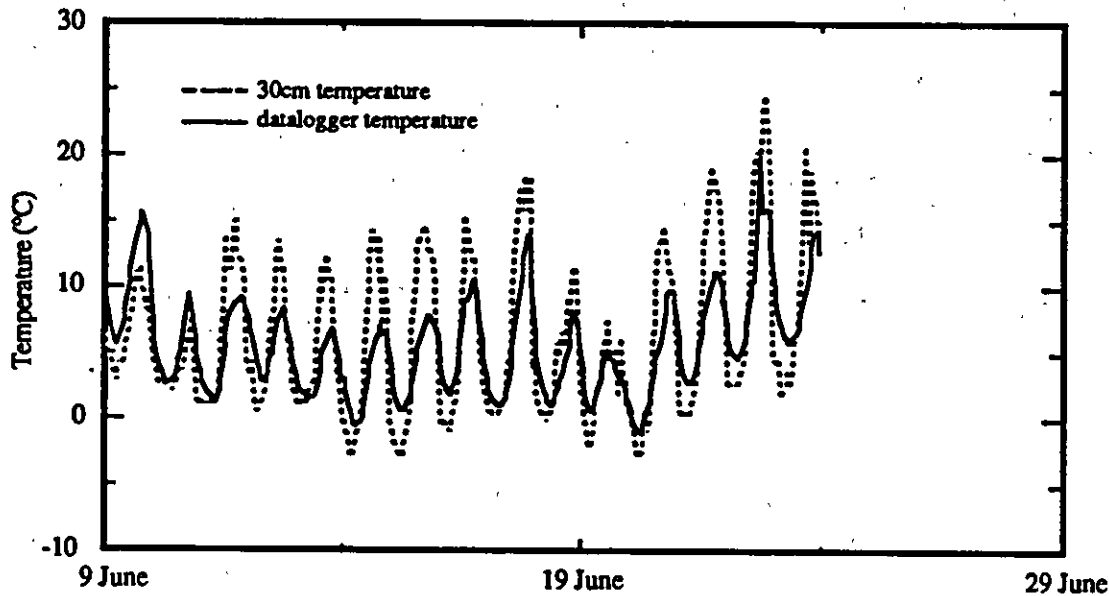


Figure 2. Comparison of two temperature time series gathered on Nipterk.

it has greater thermal mass so may resist rapid heating from the sun. In Figure 2, two temperature time series are plotted. One is the 30cm temperature and one is the datalogger temperature.

The two time series track fairly well, although there is more damping on the datalogger time series because it was located inside a tent and was insulated by its own hardware. The temperature amplitude fluctuations are higher at the surface since surface temperatures are more susceptible to solar radiation. The air is heated by the surface and, to a much lesser extent, direct solar radiation. In this way air temperatures farther away from the surface have smaller amplitude fluctuations and their fluctuations lag behind the surface fluctuations. This is what is observed in the datalogger temperature time series. Although the datalogger temperature might not duplicate the 10m air temperature, T_a in (2), it is taken to be an adequate approximation.

Since the ice is undergoing ablation we can assume it is at 0°C . For the calculation of heat flux over unprotected ice this will be used as the temperature, T_s , given in (3). When (2) and (3) are calculated in this way, and (3) is subtracted from (2) the result is the net longwave radiation and is shown in Figure 3.

Of course, when the surface of the island is covered with ablation protection material, the surface temperature is not limited to 0°C and will be more likely to be closer to those temperatures collected by the thermistor mounted above the gravel. For the ablation protection model, the temperature of the thermistor at 2 cm will be used. Because the surface is allowed to rise to a higher temperature, the outgoing longwave radiation will be higher as well.

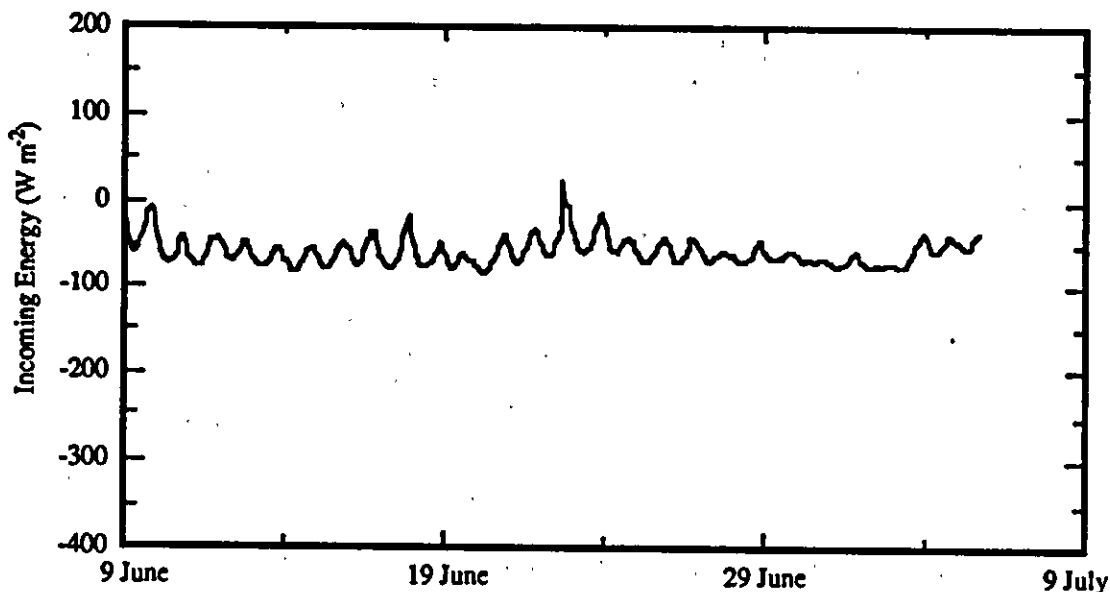


Figure 3. Net longwave radiation over the ice surface.

The temperature gradient used to calculate both the sensible and latent heat fluxes given in (4) and (5) is given by subtracting the surface temperature from the datalogger temperature. For the sensible heat flux over the ice this yields an almost constantly outgoing heat flux. In the Beaufort Sea near land, this situation will occur since warmer air will be moving off the land onto the ice creating an almost constant inversion.

Figure 4 shows both sensible and latent heat fluxes plotted together. Note that since latent heat flux was calculated from the air temperature using (6), the two fluxes follow each other closely.

When an ablation material is used, quite a different situation occurs. Since the ablation material can rise to higher temperatures than the ice can, the temperature of the surface can become much warmer than the air resulting in a reversal of the heat flux. Despite the higher surface temperatures of the protection material, it can dissipate more heat thus preventing heat from flowing to the ice.

Because of the lack of oceanographic data, some assumptions were made in order to calculate the erosion of the island perimeter. The average wave height was assumed to be 0.5m and the period to be 4 sec. Since the wave heights are constantly changing, making an assumption like this may lead to major errors. For this reason the wave height and period were varied in the model to determine the sensitivity to this term. The first day of open water, when the island perimeter began eroding, was set to 23 June.

Surface water temperature was measured once during the field experiment. The temperature taken was 12°C. This was shortly before the island broke up and the region in which the island was located was under

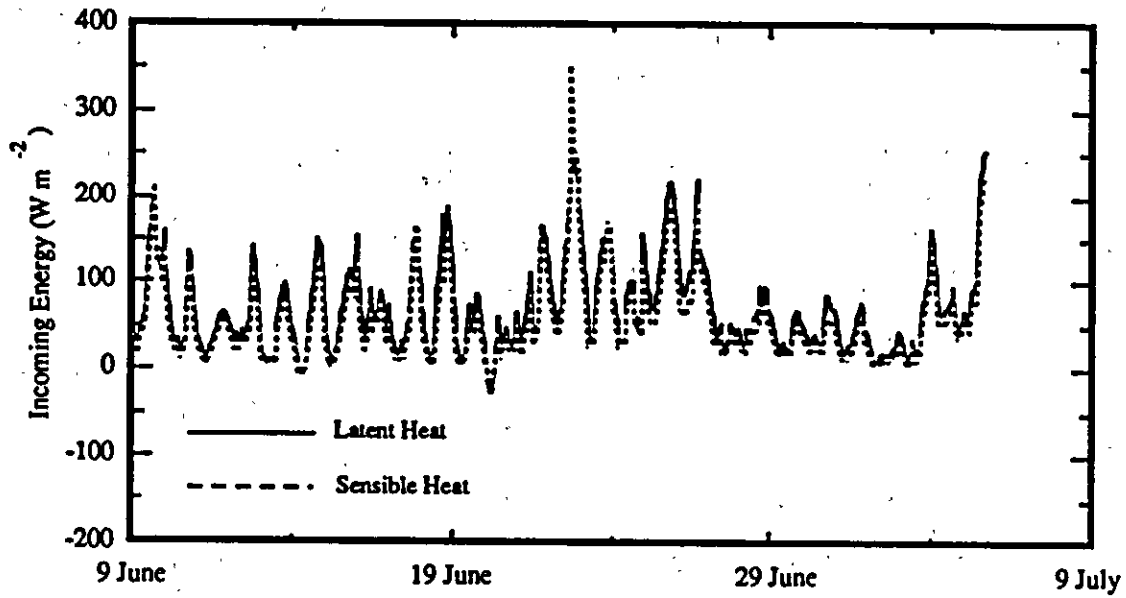


Figure 4. Sensible and latent heat flux off the spray ice.

the influence of the Mackenzie River outflow. Because this temperature is relatively high for the Beaufort Sea it was not considered to be a constant temperature. Therefore the temperature was assumed to increase linearly from 0°C on 23 June to 12°C on 8 July.

RESULTS

Ablation

In order to use the most consistent set of data, the model was run with data from 10 June to 5 July only. Although some ablation occurred before this date, it would be very difficult to measure the ablation processes with the same kind of accuracy as could be achieved from 10 June onwards. Our reference level then became the level of the ice on this date, the first level measurement since radiation and temperature data gathering began at the island.

The energy balance between the different energy components was first calculated at the surface of the island. For unprotected spray ice the albedo was set to 0.8, the emissivity was set to 0.95, and the heat transfer coefficient was set to 0.0014. In the case of gravel and sawdust, the albedo can vary considerably depending if the material is wet or not. For this study the albedo for both materials will be set to 0.35. The emissivity of the materials is also approximately the same and slightly lower than that of ice, 0.9. In order to compensate somewhat for the effects of radiative heating of the thermistor probes, the temperature of the 2 cm probe has been multiplied by 0.9.

Table 1 shows the totals for the various energy components over the 26 day period. Note that these terms are positive incoming to the island, except Longwave Out which is negative incoming. These numbers are fairly rough, especially the latent and sensible heat flux terms, but nonetheless demonstrate the effect of ablation protection on the island. Although the net solar radiation term is higher for the protection materials, due to the lower albedo, the protection materials emit much more longwave radiation and also reverse the sensible and latent heat flux because their surface temperatures can exceed 0°C.

	Net Solar	Longwave In	Longwave Out	Latent	Sensible	Residual
Gravel, Sawdust	113	155	-212	-14	-11	31
Ice	31	149	-185	38	46	79

Table 1. Net totals of the energy balance terms on the surface of the island over the 26 day measurement period in kW m⁻². Positive incoming to the island except for Longwave Out.

In order to generate the terms in Table 1, the heat transfer coefficient was required. Because the differences between the sensible and latent heat flux coefficients are within measurement error, they were taken to be equal for this study. A number of different coefficients were tried in the model to determine the model sensitivity. Figure 5 shows some of these results

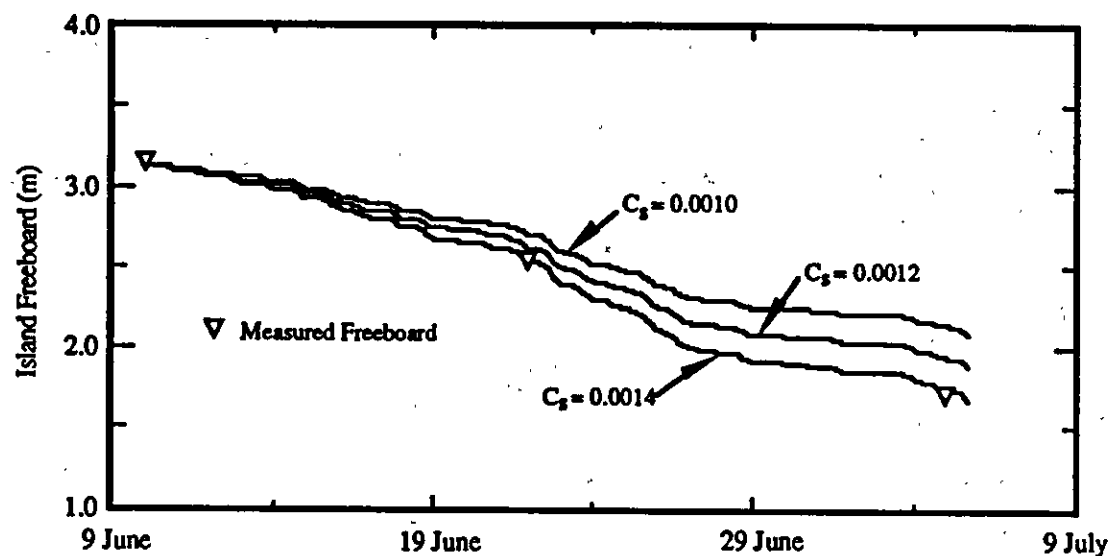


Figure 5. Ablation of the top surface of the ice island compared with measured data.

compared with the data measured on the island. From this figure it appears that 0.0014 provides the best fit to the measured data. This compares favorably with a survey Macklin (1983) has done on drag coefficients of sea ice. For smooth, flat ice the drag coefficients ranged from 0.001 to 0.0024. In a paper investigating the relationship between the drag coefficient and the heat transfer coefficient over open ocean, Kondo (1975) estimates $C_s = 0.9C_d$ where C_d is the drag coefficient. This value for the heat transfer coefficient was then used with the protection materials as well.

The flat parts in the ablation curves correspond to the night time periods when net heat flux is away from the island. Since there is no heat entering the island surface, no ice is melted. Instead, some of the liquid water present in the surface can then be refrozen which requires subsequent energy absorption to melt again. This accounts for the hard crust on the island surface in the mornings.

After the energy balance terms for the island surface were calculated these were input into the heat conduction portion of the model. The results from the sawdust model are shown in Figure 6. The diffusivity used for sawdust was required to be quite low, $2.8 \times 10^{-9} \text{ m}^2 \text{ sec}^{-1}$. Because the diffusivity is inversely proportionate to density and heat capacity, the effects of saturating the sawdust would cause major changes in this term.

A similar situation occurred in the modeling of the ice meltback under gravel as that which was observed with the sawdust. In both cases the model under estimated the meltback under the thinner layers and over estimated the meltback under the thicker layers. Figure 7 shows the meltback under gravel for three different layer thicknesses with the diffusivity of gravel taken to be $1.4 \times 10^{-7} \text{ m}^2 \text{ sec}^{-1}$. Since the surface energy balance terms used for both materials is the same, this may reflect an error

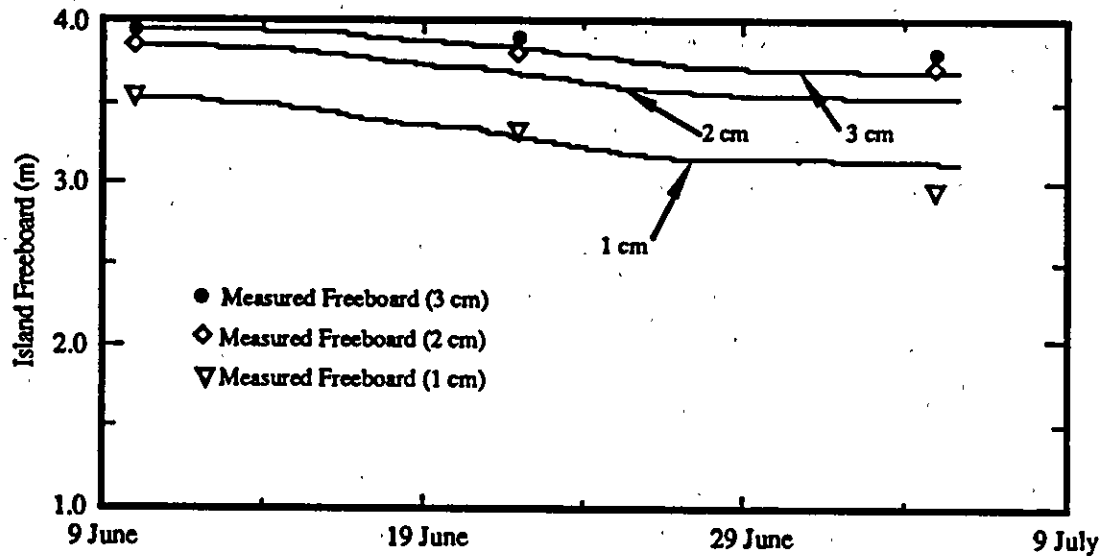


Figure 6. Comparison between measured and modeled ice meltback under sawdust.

in these terms. However, since there doesn't appear to be a consistent over or under estimation for all layers the error may be more a symptom of assuming constant diffusivity through the material as well as consistence through time. The results do appear to be within the bounds of the measurement error, however, and should be viewed as an approximation.

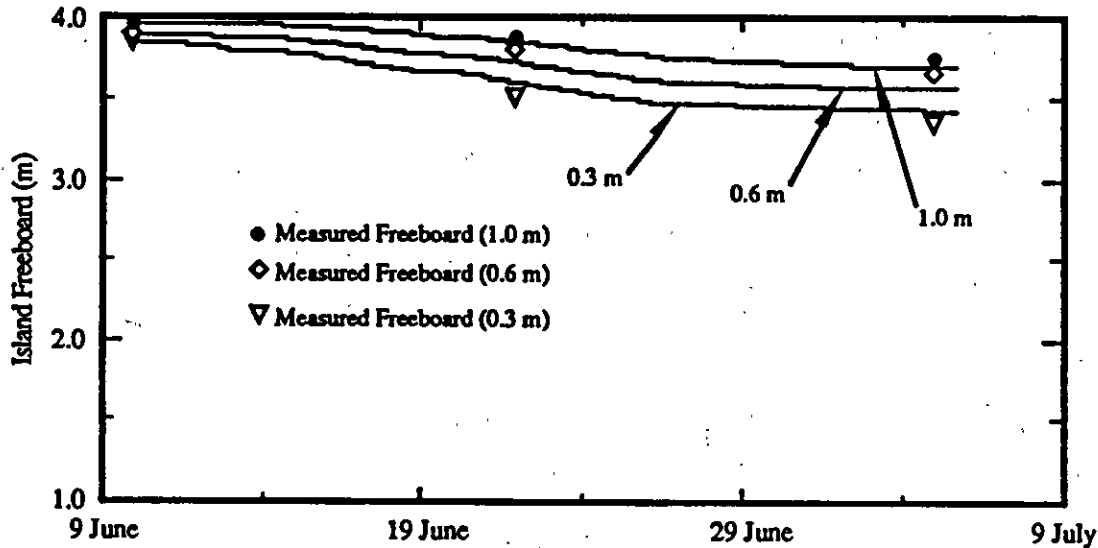


Figure 7. Comparison between measured and modeled ice meltback under gravel.

Erosion

The wave erosion has been distributed evenly around the perimeter of the island so that the island retains the shape of disc. In reality the erosional forces are directional and the island quickly becomes asymmetrical depending on the predominant directions of the forces. However, one of the most important factors in island survivability is sliding friction between the ice and the seabed. Since the sliding friction is a function of area of contact, the shape of the island is not as critical of a term.

Wave height, period, and water temperature are important factors in the erosion model. Since data were sparse concerning these terms, a variety of different wave heights and periods were input into the model to determine the sensitivity of the model. The results are shown in Figure 3. Waves of 0.25m, 0.5m, and 1.0m were input along with periods of 3 and 4 seconds. The model was run from the first day of open water, 23 June, until 5 July.

As can be expected, the higher wave heights and shorter periods cause the greatest amount of erosion. The closest fit to the data is achieved with an average wave height of 0.5m and a period of 4 seconds.

The use of various island edge protection materials has shown definite value in protecting the perimeter of the island from erosion. Although a number of different protective materials were used, it was difficult to

determine from the aerial photos if any showed better results than the others. Another comparison problem arose due to the fact that the protective sheets were only used on a portion of the island. Since the perimeter erosion was asymmetrical it was difficult to determine what erosion would be for an unprotected edge with the same exposure.

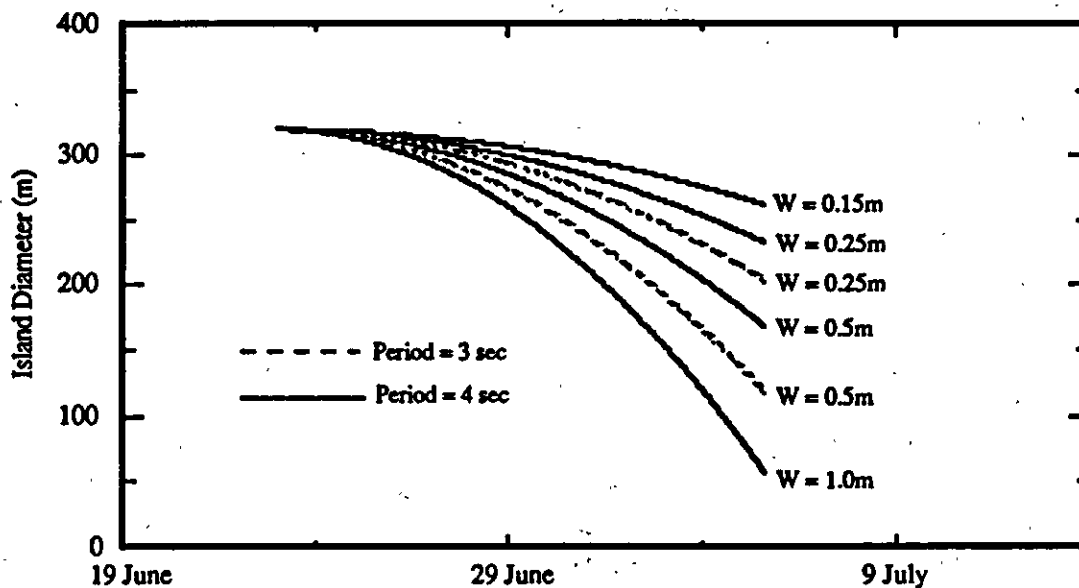


Figure 8. Results of the use of different wave parameters in the perimeter erosion model.

Nevertheless, the island radius was observed to decrease from 160m to 130m where the edge protection was used. The edge protection is seen as a baffle between the waves and the ice, in effect damping out the amplitude of the waves. From the model a diameter of 260m corresponds to an average wave height of 0.2m if the period remains at 4 seconds. Thus, the edge protection effectively attenuates the waves by 40% of their original height.

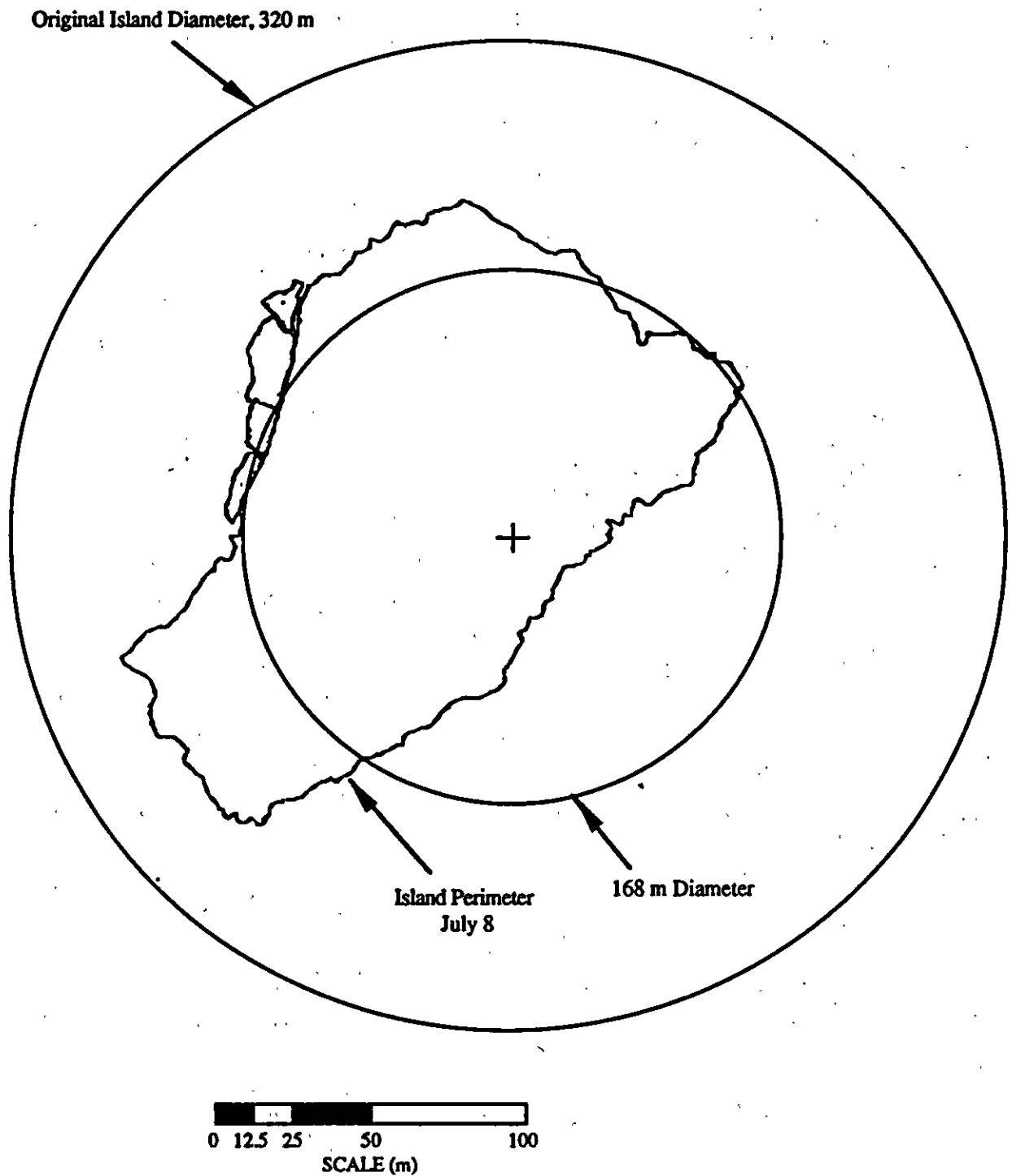


Figure 9. Aerial view of island showing measured perimeter and model results of 8 July.

CONCLUSION

Several changes were made to the original spray ice island model in adapting it for use in this study. Because data were gathered on the island itself, and supplemented with data gathered in the same region, much greater accuracy could be obtained than before. The time scales were reduced from one day to one hour so that greater detail could be observed. Instead of a broad estimate of the sensible and latent heat fluxes, they could be better approximated with air temperature and wind speed. As a result, the output of the model matched the measured data and retained physically meaningful parameters. By retaining a physical basis for the model, the probability for predicting the behavior of hypothetical ice islands improves.

In addition to modeling the deterioration of an unprotected ice island, one major aspect of the study was to observe the effects of various ablation and erosion protection methods. The ablation protection materials change the boundary conditions between the ice and the atmosphere. The albedo decreases, outgoing longwave radiation increases, sensible and latent heat flux reverse from net incoming to net outgoing, and the heat capacity of the surface increases. Naturally, these properties vary from material to material, and with the thickness of the material itself. Because of the environmental forces on the ice, the problem of simulating the effects of ablation protection is more than one of simple insulation.

In addition to the materials tested, other materials such as drilling mud, sea floor sediment, or mylar sheets may be investigated to determine if they may offer improved performance or more economical solutions. As we observed on the island, the plastic sheets offer the best ablation protection per unit thickness but may not be either practical nor economical in covering an entire island. Sawdust outperformed gravel for the same thickness and does not increase the subsidence. All these materials have relatively low albedos which could be improved by using lighter varieties or spraying with a light colored coating.

The effects of the perimeter erosion protection was pronounced. It could not be determined which material offered the best protection, but obviously any material was better than nothing. Since wave action was seen to be the dominating term in the perimeter erosion, the reduction of the wave energy would be the best way to mitigate the effects of the erosion. This was the outcome of using the erosion protection, the net effect being a 40% reduction in average wave height.

We have observed the results of applying various protection materials to the island and have investigated the reasons for these results so that possibility of predicting the behavior of an ice island at a particular location can be reasonably performed. The feasibility of building ice islands in deeper water depths or extending their operating season depends on construction techniques, island design, and environmental conditions. What still determines the longevity of a spray ice island is the weight on bottom and

○ lateral forces. Even if the island could be well preserved through the summer season, if an insufficient amount of ice was used for construction a storm in late summer could result in island break up.

REFERENCES

Macklin, S.A., Wind drag coefficient over first-year sea ice in the Bering Sea, *J. Geophys. Res.*, 88(C5), 2845-2852, 1983.

Connolly, S.T., Artificial ice islands for deep water and production structures, *In Proc. Fourth Intl. Conf. Cold Regions Eng.*, Anchorage, ASCE, 58-68, 1986.

Kondo, J., Air-sea bulk transfer coefficients in diabatic conditions, *Boundary-Layer Meteorol.*, 9, 91-112, 1975.

Jahns, H.O., D.H. Petrie, and A.V. Lockett, CIDS Spray Ice Barrier, *In Proc. of 18th Ann. Offshore Tech. Conf.*, Houston, 575-584, 1986.

White, F.M., M.L. Spalding, and L. Gominho, Theoretical estimates of the various mechanisms involved in iceberg deterioration in the open ocean environment, U.S. Coast Guard Report No. CG-D-62-80, 1980.

Idso, S.B., and R.D. Jackson, Thermal radiation from the atmosphere, *J. Geophys. Res.*, 74, 1969.

Buck, A.L., New equations for computing vapor pressure and enhancement factor, *J. Appl. Meteorol.*, 20, 1527-1532, 1981.

Large, W.G. and S. Pond, Sensible and latent heat flux measurements over the ocean, *J. Phys. Oceano.*, 12, 464-482, 1982.

El-Tahan, M., S. Venkatech, and H. El-Tahan, Validation and quantitative assessment of the deterioration mechanisms of arctic icebergs, *In Proc. ASME Offshore Mech./Arctic Engin. Symp.* New Orleans, ASME, 1984.

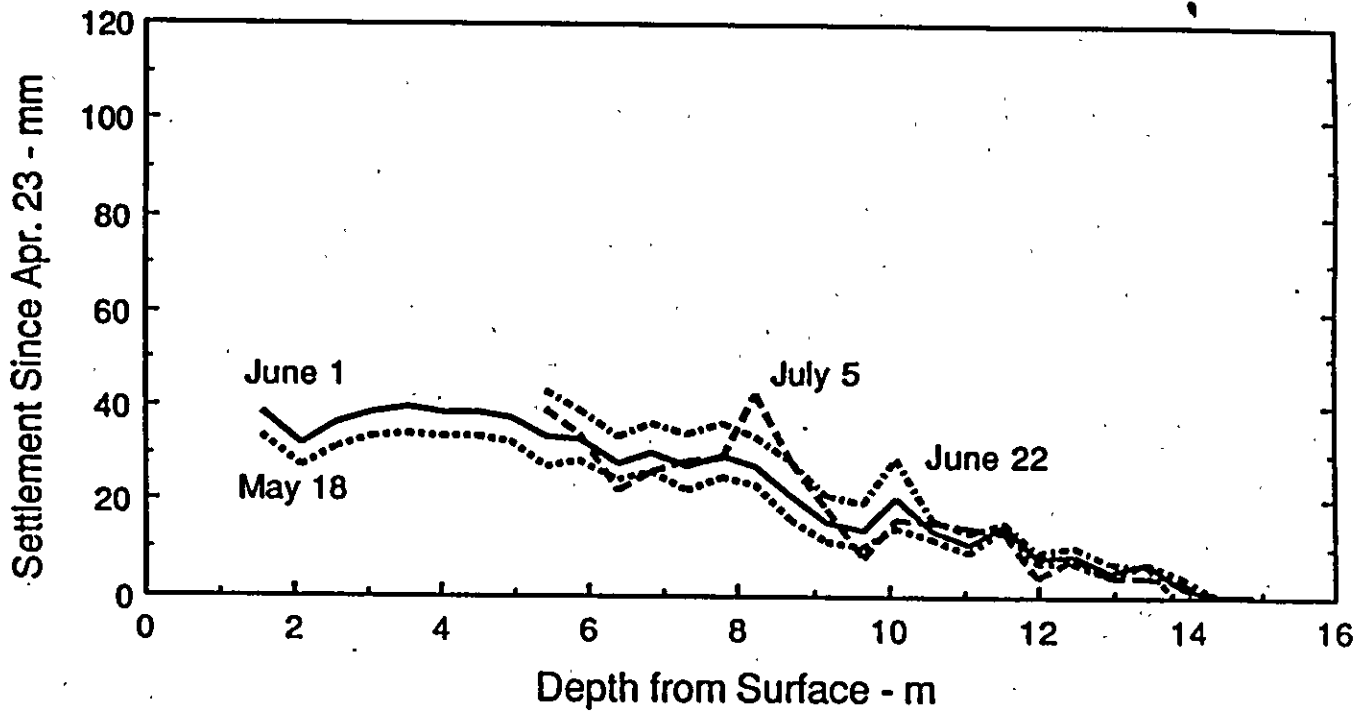
APPENDIX F

SETTLEMENT MEASUREMENTS

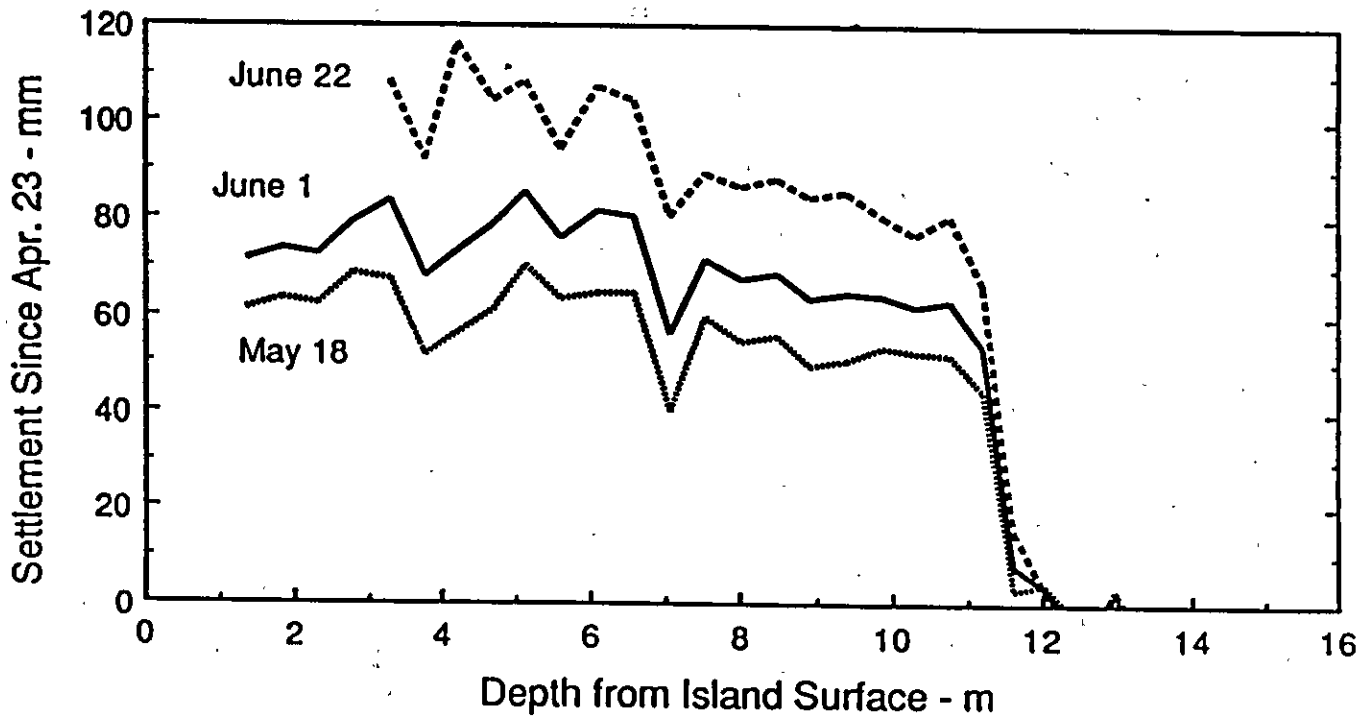
Measurements of surface settlement were performed at as many as five locations during the experiment. Sensing rings were originally mounted to the outside of the Sondex casing at approximately 0.5 m intervals. Settlement surveys were conducted at varying frequencies and locations during the experiment. Settlement data are available throughout the experiment period for locations near the edge of the island working surface.

In addition to the raw settlement data, settlement profiles are also provided. Note that the June 1 profiles are based on an interpolation of actual field data. The seabed is at a depth of about 10.5 to 11 m whereas the submerged spray ice is represented by the level 4.5 m below the surface to the seabed. Because of spray ice ablation, the uppermost 2 m of Sondex casing had to be removed on June 22 due to the height of stick up. Consequently, settlement data for the upper 3-4 m of the island were not collected after the June 22 survey.

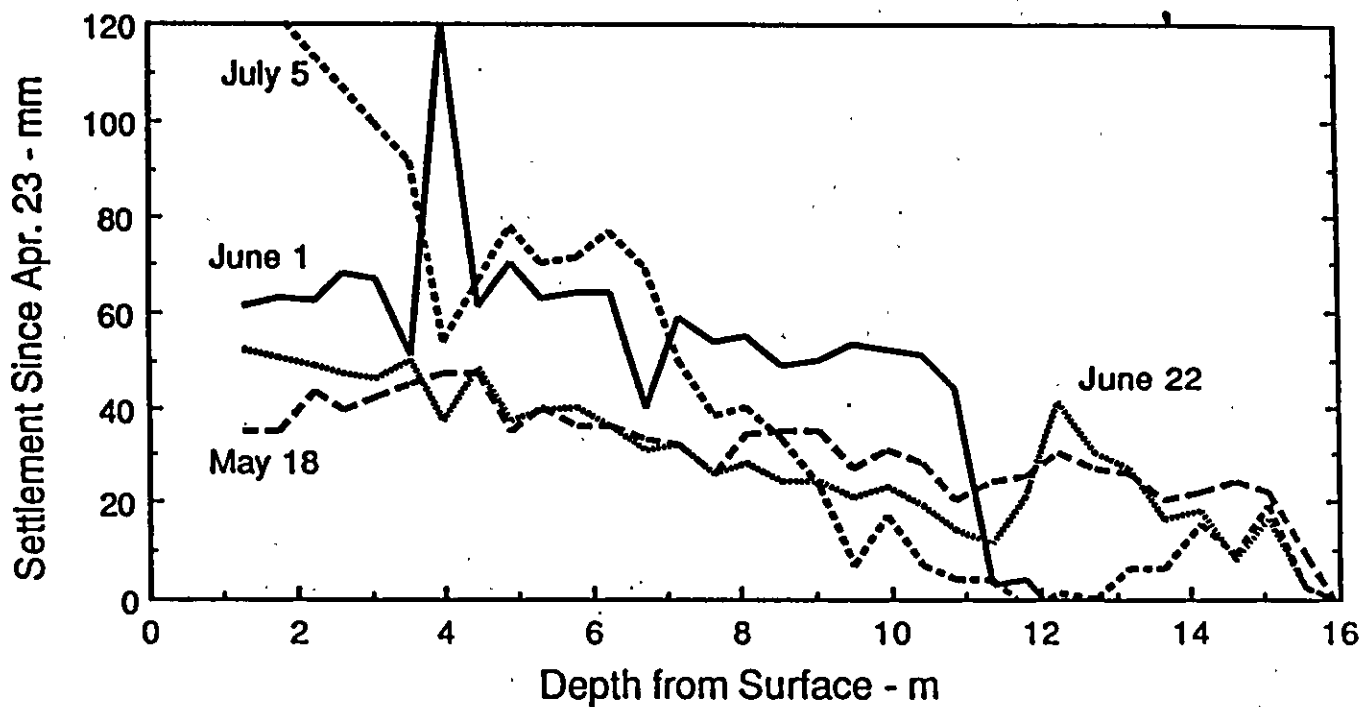
An extrapolation of settlement data was performed for June 1 for each of the three drilling pad settlement monitoring stations. The extrapolation may be a bit conservative in that it does not take into account the below freezing air temperatures prevalent throughout most of May.



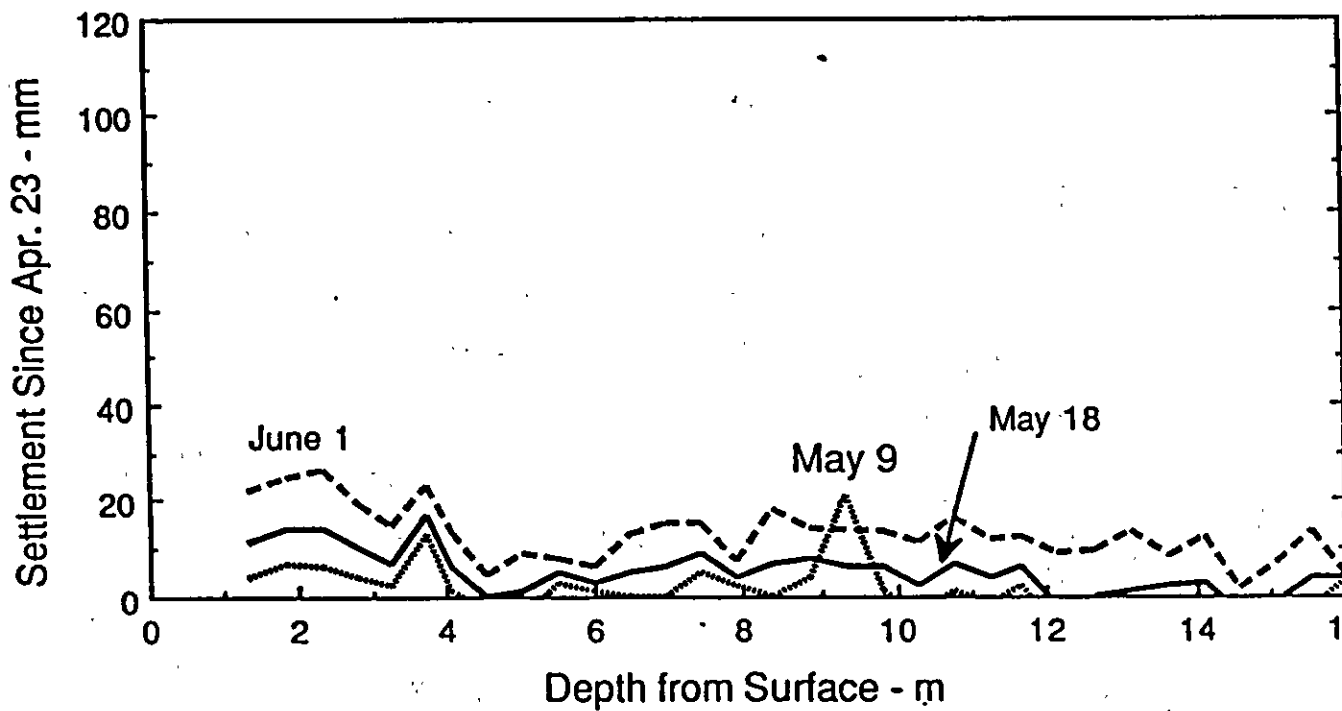
Spray Ice Settlement at North Survey Station



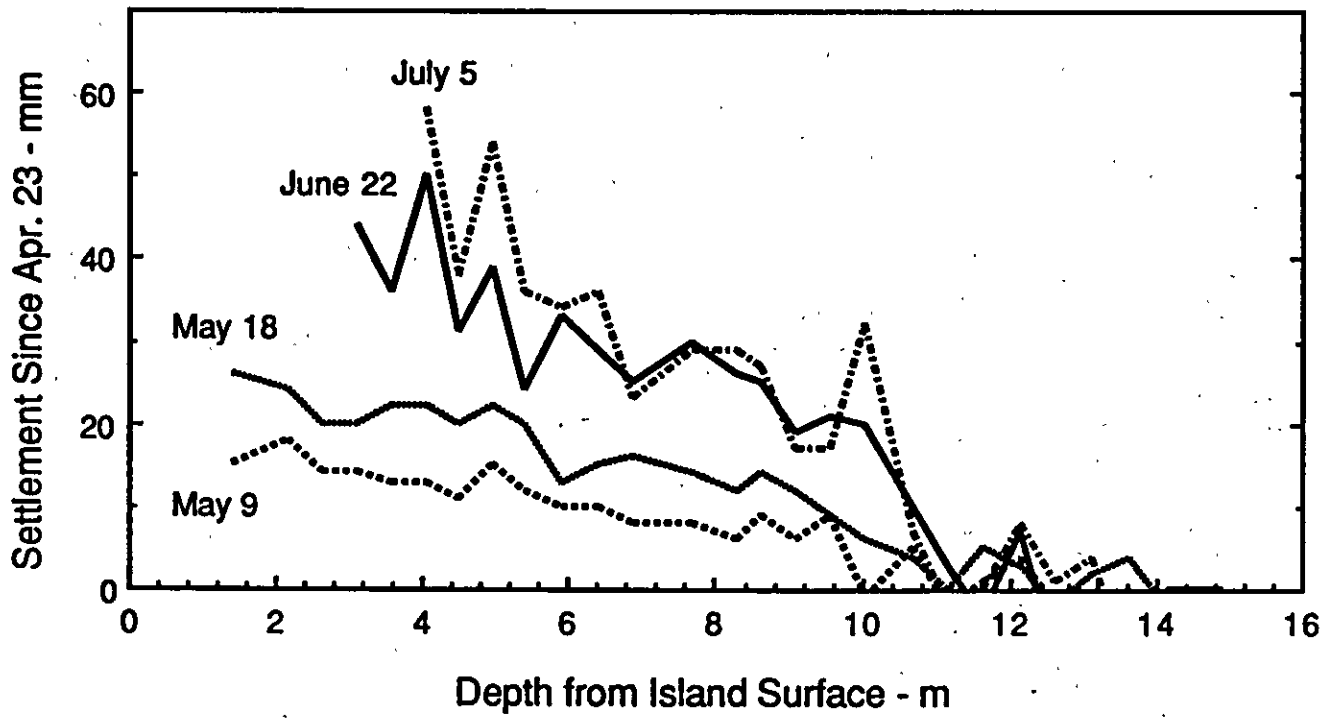
Spray Ice Settlement at North Northeast Survey Station



Spray Ice Settlement at Southeast Survey Station



Spray Ice Settlement at South Southwest Survey Station



Spray Ice Settlement at Southwest Survey Station

Settlement Data from Sondex Survey Stations						
Southeast Station				North Northeast Station		
Depth on				Depth on		
April 23	18-May	22-Jun	5-Jul	April 23	18-May	22-Jun
(m)	(mm)	(mm)	(mm)	(m)	(mm)	(mm)
1.296	35			1.361	61	
1.783	35			1.845	63	
2.267	43			2.328	62	
2.632	39			2.803	68	
3.090	42	46		3.295	67	108
3.554	45	50		3.752	51	92
4.016	47	37	80	4.208		116
4.472	47	48	92	4.679	61	104
4.909	35	37	104	5.142	70	108
5.337	40	39	96	5.629	63	94
5.802	36	40	97	6.105	64	107
6.263	36	36	103	6.563	64	104
6.733	33	31	95	7.066	40	80
7.193	32	32	76	7.551	59	89
7.666	26	26	64	8.020	54	86
8.124	34	28	66	8.489	55	88
8.592	35	24	59	8.958	49	84
9.058	35	24	49	9.423	50	85
9.517	27	21	33	9.886	53	80
9.973	31	23	43	10.337	52	76
10.447	28	19	33	10.798	51	80
10.903	20	14	30	11.223	44	66
11.362	24	11	4	11.627	3	15
11.819	25	21	-2	12.060	4	3
12.271	30	41	1	12.521	-4	-11
12.727	27	30	0	12.983	-2	3
13.190	26	27	6	13.444	0	-8
13.673	20	16	6	13.914	-9	-11
14.142	22	18	15	14.388	0	0
14.615	24	8	9			
15.080	22	16	19			

Settlement Data from Sondex Survey Stations

South Southwest Station			
Depth on			
April 23	9-May	18-May	
(m)	(mm)	(mm)	
1.346	4	11	
1.834	7	14	
2.312	6	14	
2.792	4	10	
3.252	2	7	
3.729	13	17	
4.070	1	6	
4.551	-3	0	
5.021	-4	1	
5.494	3	5	
5.981	1	3	
6.459	0	5	
6.941	0	6	
7.428	5	9	
7.905	2	4	
8.378	0	7	
8.855	4	8	
9.337	21	6	
9.817	1	6	
10.293	-4	2	
10.773		7	
11.262		4	
11.660		6	
12.153		-2	
12.637		0	
13.128			
13.619			
14.107			
14.595			
15.077			
15.560			

APPENDIX G

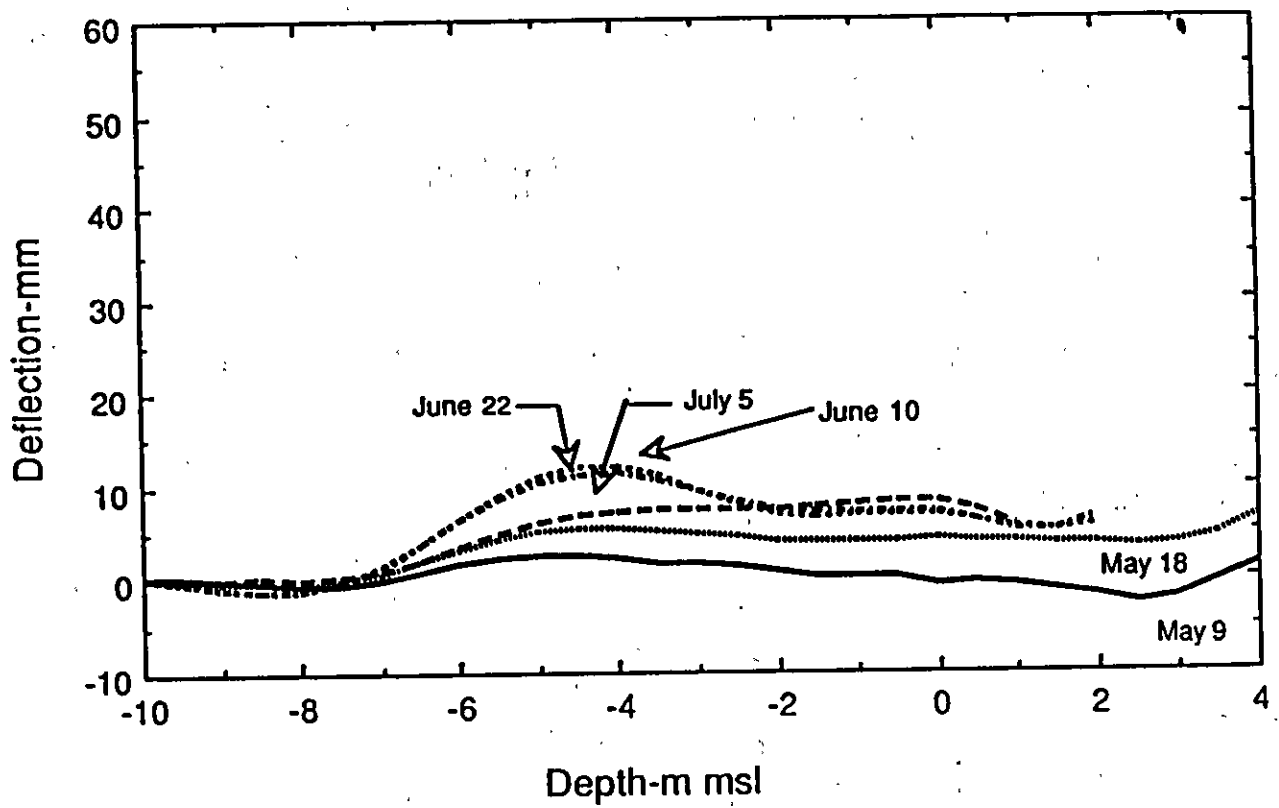
ISLAND HORIZONTAL MOVEMENT MEASUREMENTS

Five manually read inclinometers (slope indicators) were installed in January as part of the winter island stability monitoring program. Three of the five were at the periphery of the drilling pad whereas the other two were near the edge of the island. Inclinometer casings were installed inside Sondex casings which in turn were anchored at different depths below the seabed. These stations were left intact at the conclusion of the drilling program so that measurements could be continued.

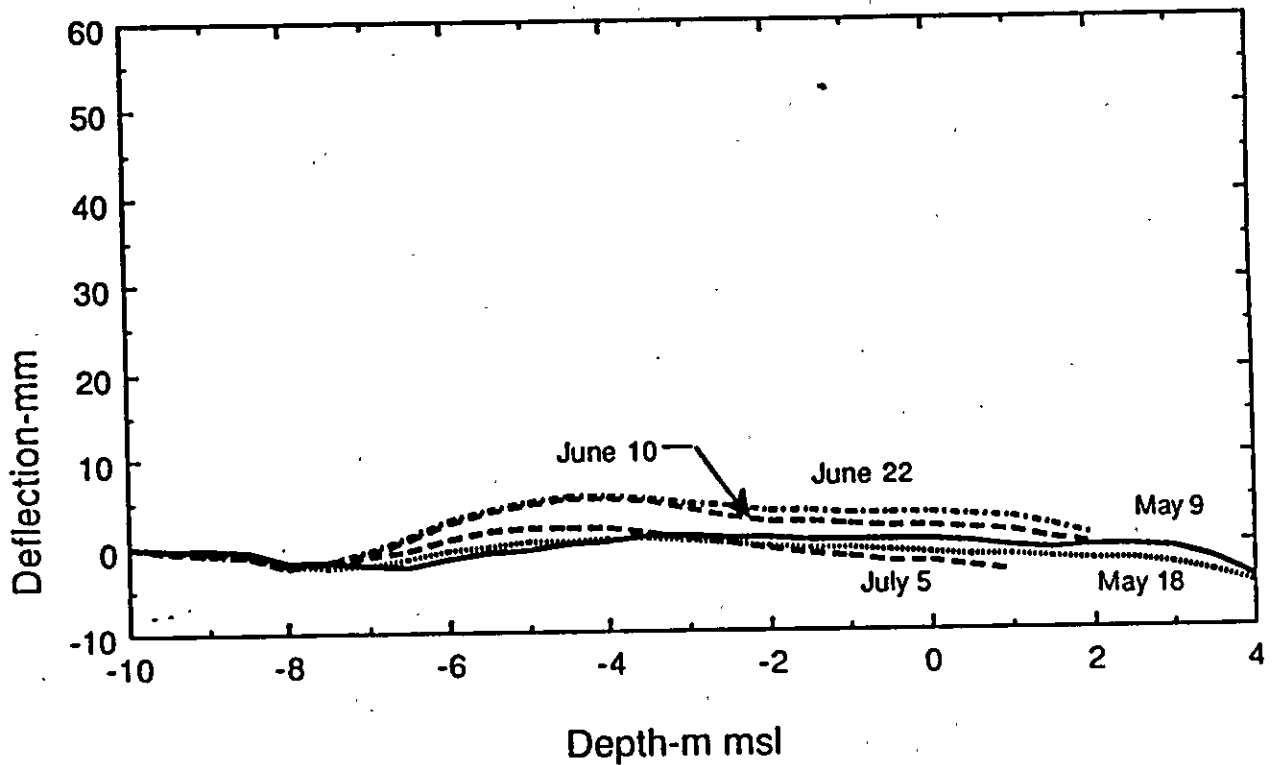
Inclinometer data were collected using the SINCO Recorder Printer Processor (RPP) System. The RPP collected, stored, processed and displayed the digitized data in terms of deflection versus depth profiles.

Slope indicator surveys were undertaken during each complete site survey except at the south-southwest survey station where the casing deformed to the point that surveys could not be performed after May 18. An initial (reference) slope indicator survey was carried out on April 22 and data from subsequent surveys were compared relatively.

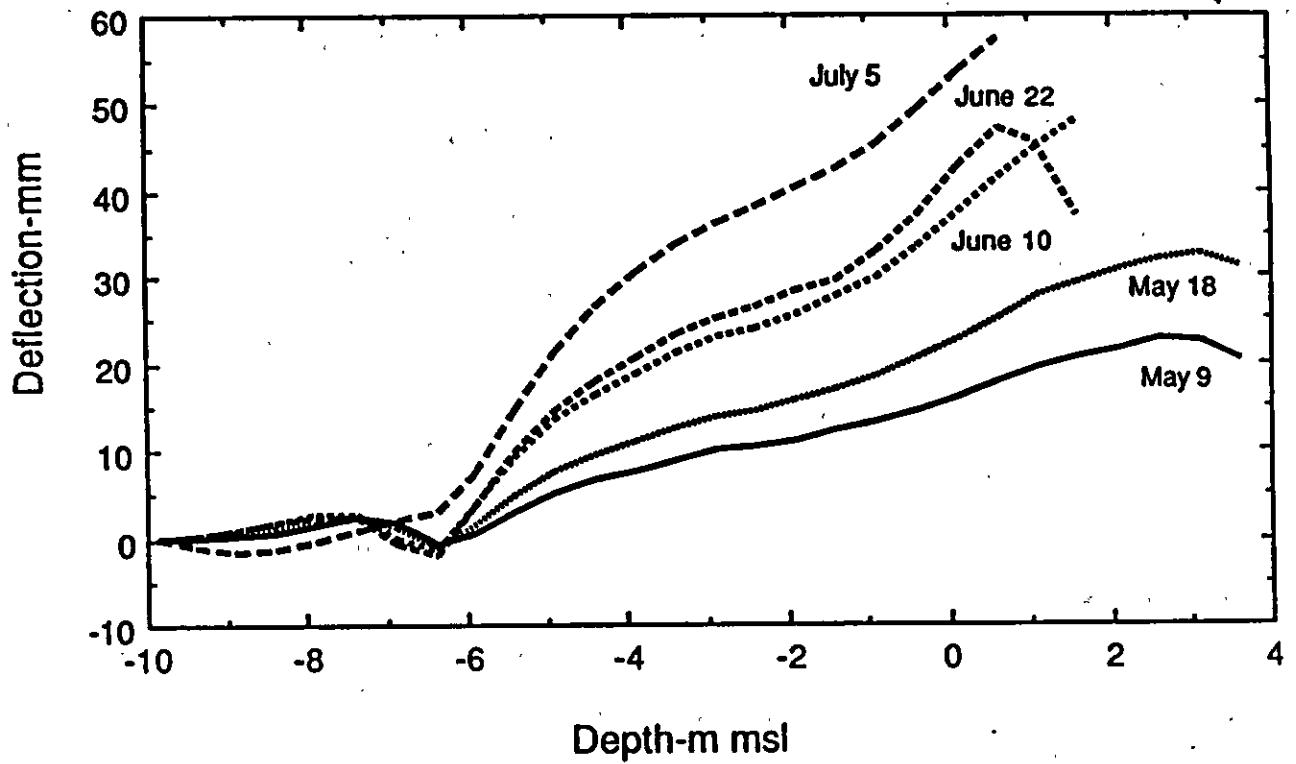
Slope indicator readings were taken at 0.5 m intervals. The readings were taken each time in four geographic directions and are shown as positive values in the north and east directions and negative values in the south and west directions. The island deformations computed from the inclinometer readings are plotted in the Figures.



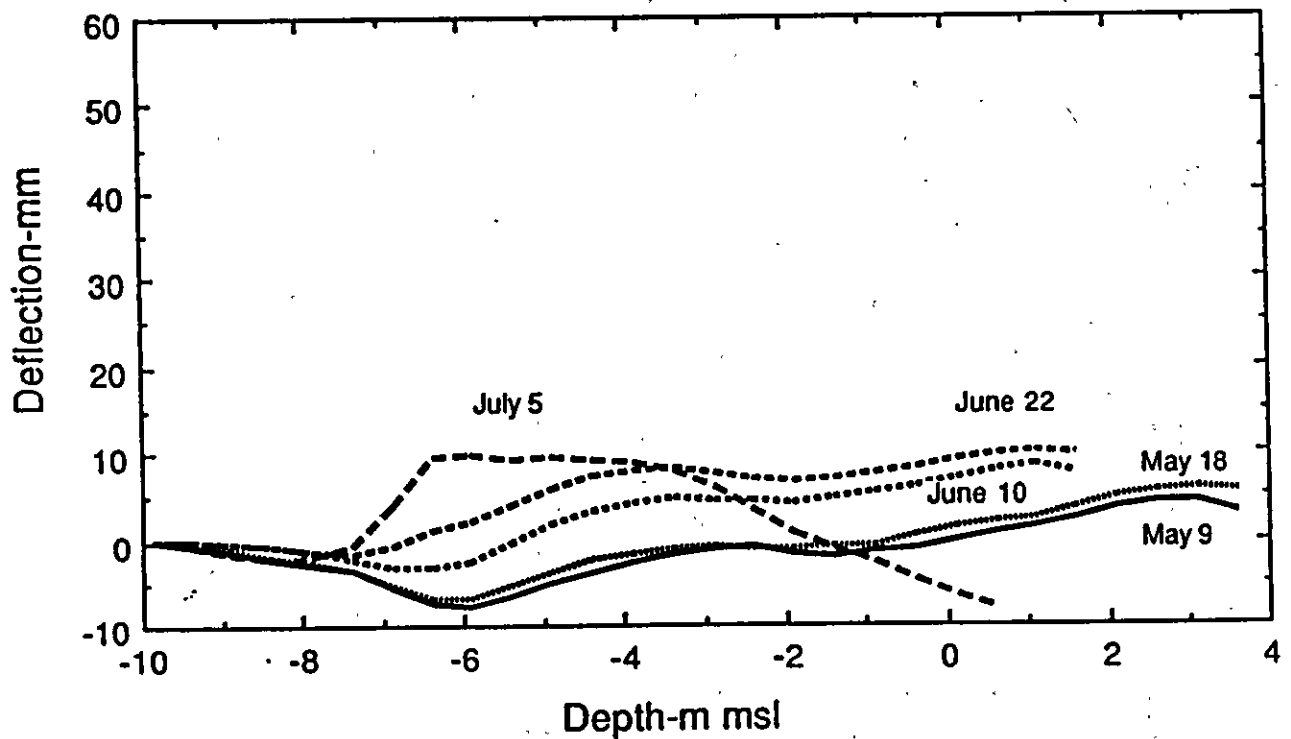
North Slope Indicator Station Deformation Profiles
(North-South Direction)



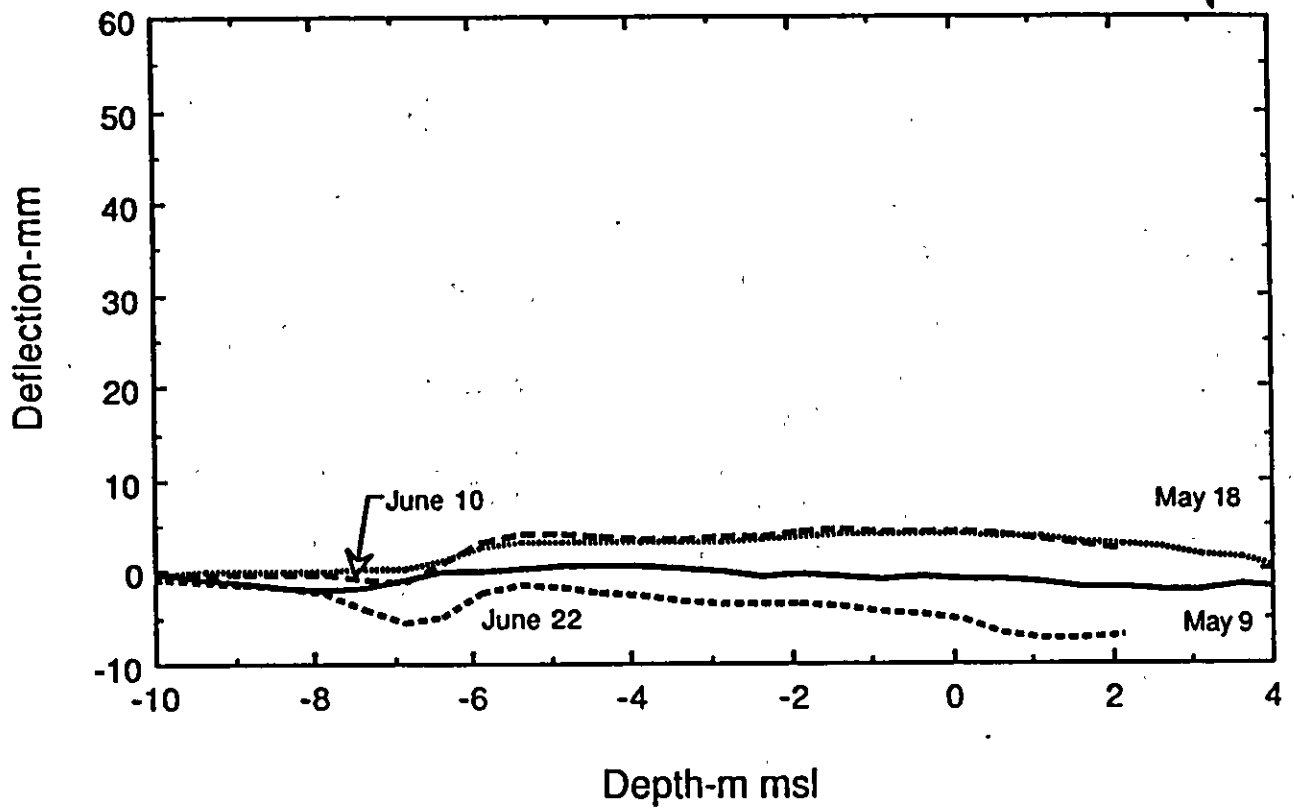
North Slope Indicator Station Deformation Profiles
(East-West Direction)



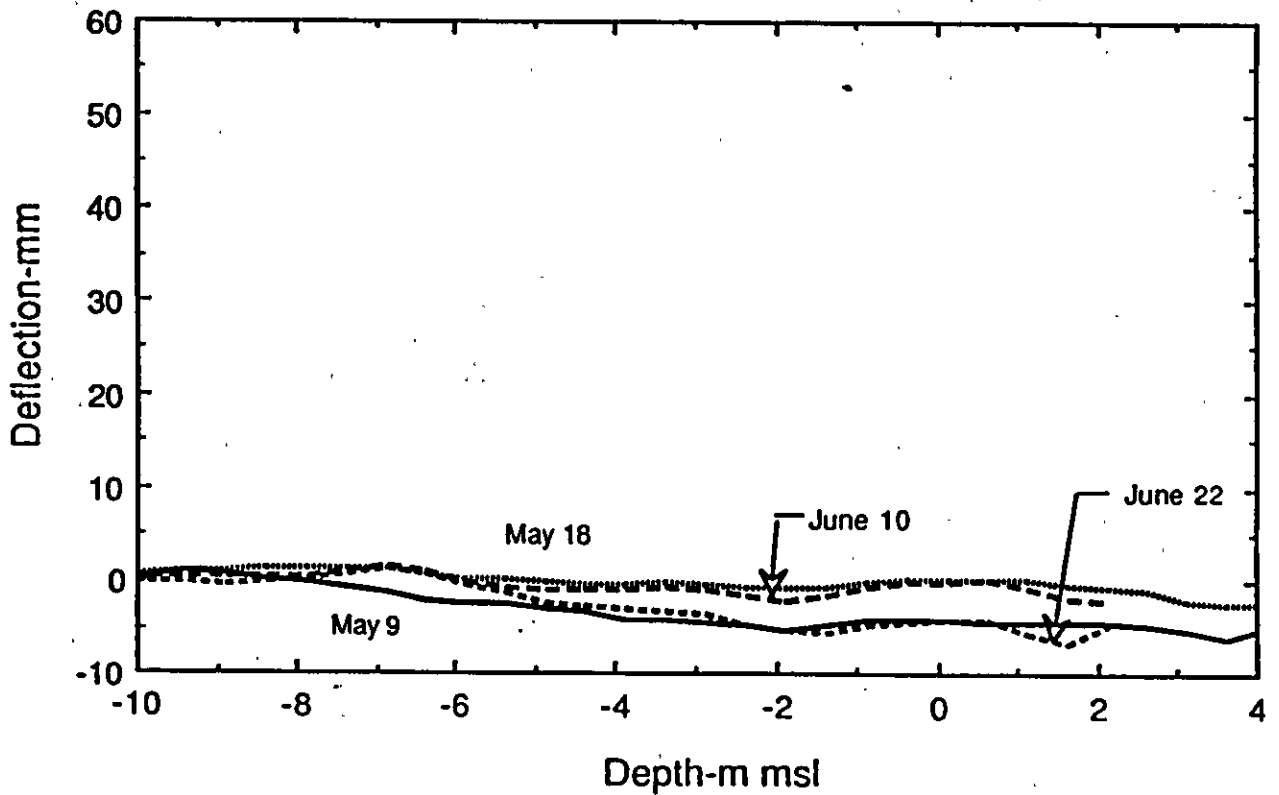
North-Northeast Slope Indicator Station Deformation Profiles
(North-South Direction)



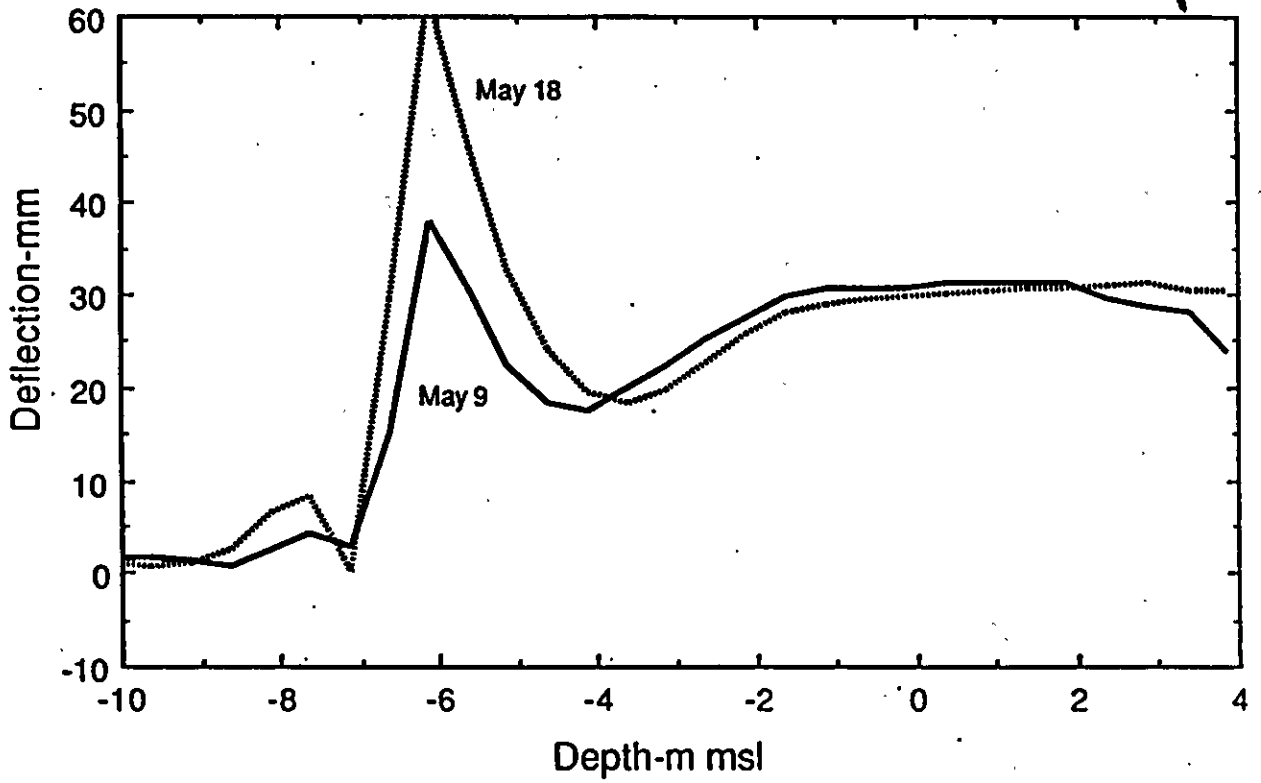
North-Northeast Slope Indicator Station Deformation Profiles
(East-West Direction)



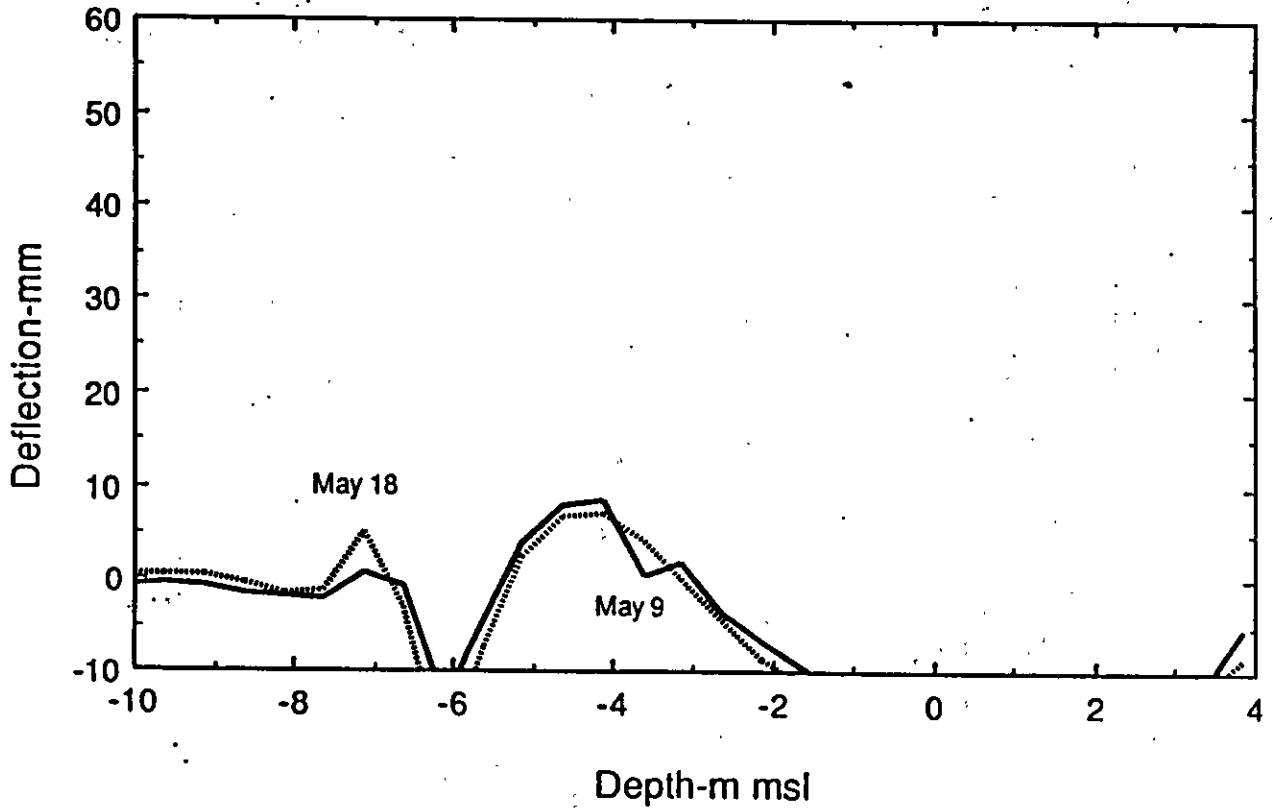
Southeast Slope Indicator Station Deformation Profiles
(North-South Direction)



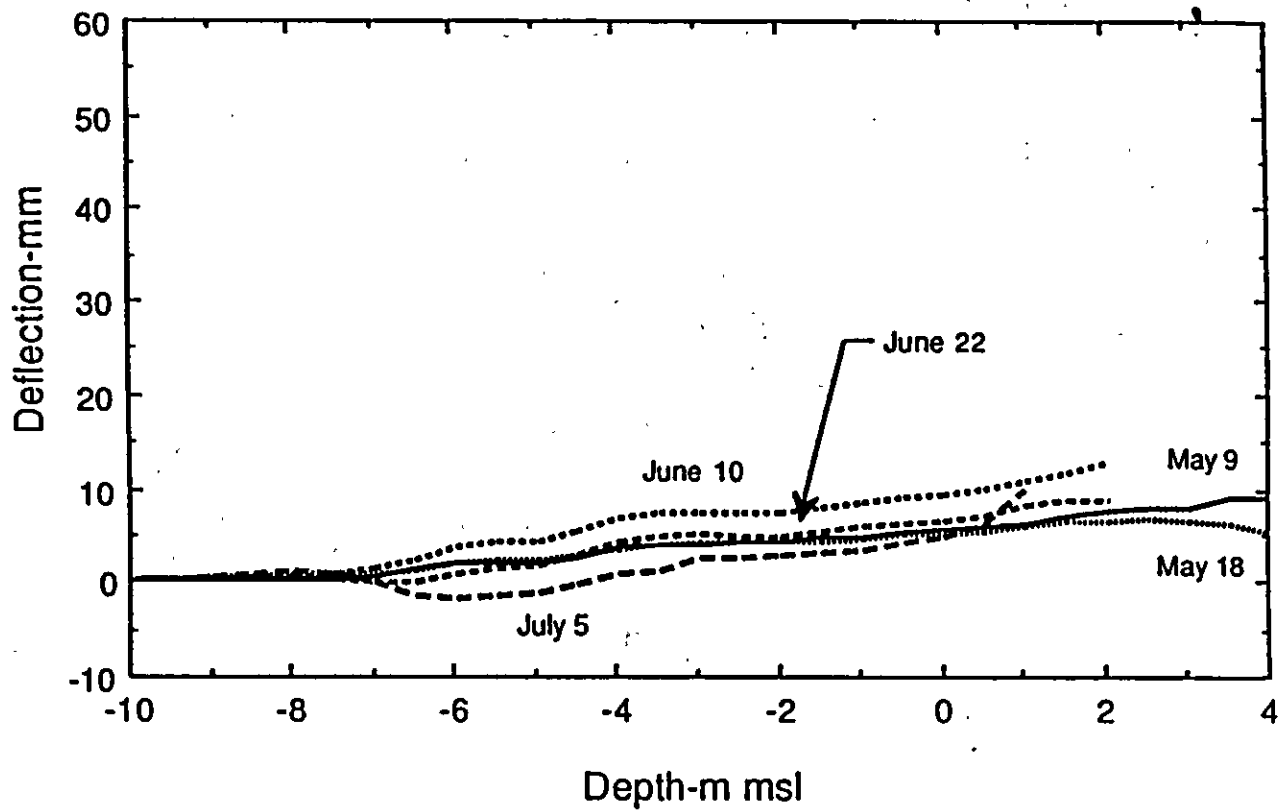
Southeast Slope Indicator Station Deformation Profiles
(East-West Direction)



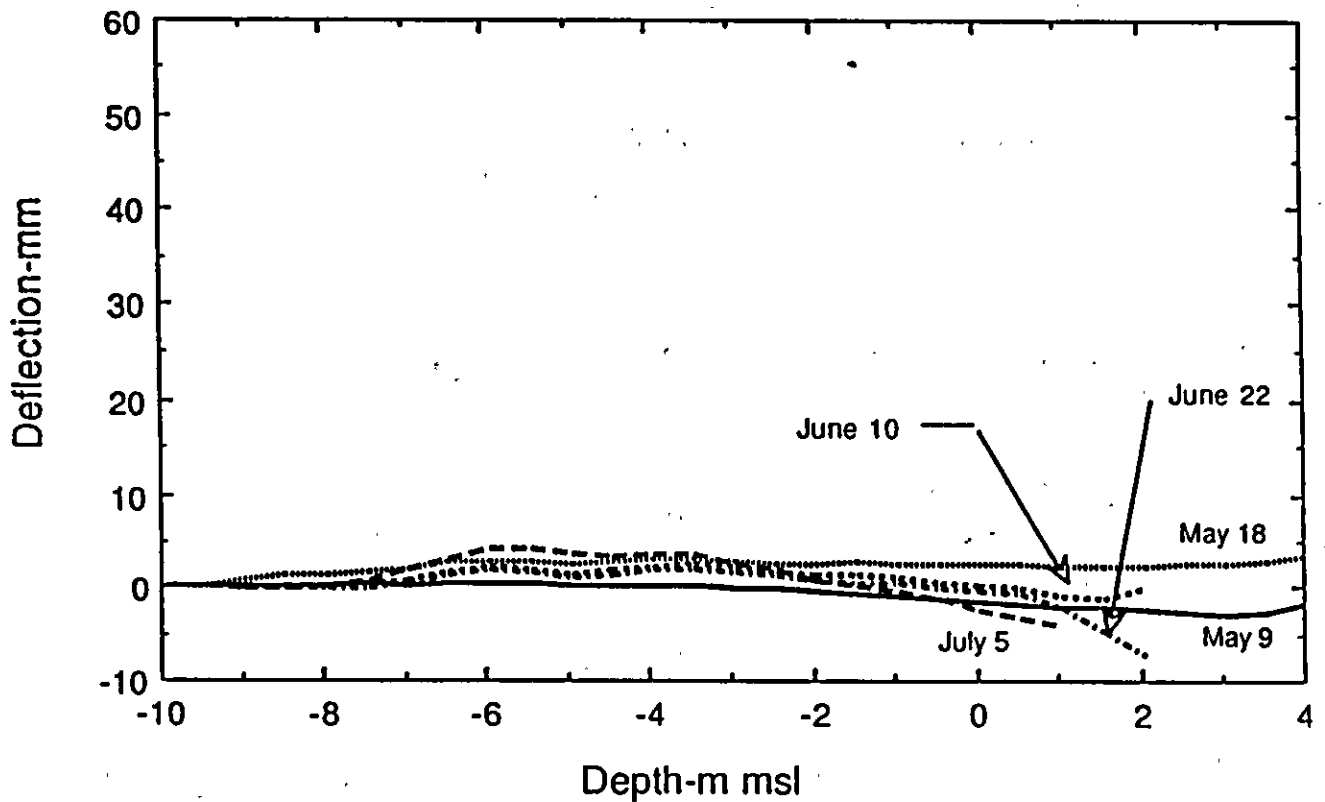
South-Southwest Slope Indicator Station Deformation Profiles
(North-South Direction)



South-Southwest Slope Indicator Station Deformation Profiles
(East-West Direction)



Southwest Slope Indicator Station Deformation Profiles
(North-South Direction)



Southwest Slope Indicator Station Deformation Profiles
(East-West Direction)

North Slope Indicator Readings

West
291
320
343
345
273
277
270
260
210
175
176
142
97
33
-20
-30
57
132
192
280
334
397

North Northeast Slope Indicator

		Deformation				Deformation				Deformation							
Depth	North	East	South	West	North	East	South	West	North	East	South	West	Depth	North	East	South	West
0.5	709	228	-756	-416	658	224	-603	-287	0.5	620	280	-697	0.5	620	280	-697	-333
1	744	211	-786	-304	734	241	-762	-287	1	775	210	-817	1	775	210	-817	-310
1.5	790	158	-839	-253	848	209	-891	-281	1.5	868	193	-893	1.5	868	193	-893	-290
2	843	158	-888	-242	891	244	-932	-287	2	910	227	-953	2	910	227	-953	-317
2.5	782	173	-823	-247	837	234	-880	-290	2.5	870	226	-900	2.5	870	226	-900	-318
3	612	208	-658	-290	690	252	-733	-308	3	730	236	-768	3	730	236	-768	-308
3.5	408	285	-458	-354	503	343	-533	-390	3.5	542	311	-573	3.5	542	311	-573	-413
4	180	351	-224	-430	272	425	-298	-466	4	305	408	-333	4	305	408	-333	-472
4.5	-17	331	-20	-411	49	343	-71	-413	4.5	87	390	-118	4.5	87	390	-118	-465
5	-147	310	103	-378	-90	365	61	-395	5	-68	324	38	5	-68	324	38	-403
5.5	-115	286	71	-364	-60	293	23	-327	5.5	-44	308	5	5.5	-44	308	5	-379
6	-104	241	60	-331	-64	235	29	-269	6	-50	243	13	6	-50	243	13	-313
6.5	-23	230	-20	-322	6	273	-41	-313	6.5	15	234	-53	6.5	15	234	-53	-320
7	68	340	-113	-433	118	405	-156	-438	7	127	339	-169	7	127	339	-169	-442
7.5	43	500	-92	-599	104	553	-145	-628	7.5	126	531	-167	7.5	126	531	-167	-634
8	47	709	-93	-788	108	793	-145	-839	8	120	742	-157	8	120	742	-157	-847
8.5	157	925	-206	-1017	239	1015	-270	-1064	8.5	251	992	-294	8.5	251	992	-294	-1087
9	194	1051	-247	-1132	301	1135	-342	-1210	9	337	1137	-377	9	337	1137	-377	-1228
9.5	89	1149	-136	-1241	217	1231	-243	-1294	9.5	261	1250	-296	9.5	261	1250	-296	-1318
10	-191	1250	141	-1310	-135	1218	93	-1301	10	-65	1243	29	10	-65	1243	29	-1330
10.5	-621	1232	585	-1317	-747	1152	686	-1223	10.5	-714	1148	680	10.5	-714	1148	680	-1245
11	-791	1131	752	-1219	-798	1010	784	-1124	11	-852	1018	822	11	-852	1018	822	-1132
11.5	-632	866	592	-969	-569	851	545	-912	11.5	-594	824	565	11.5	-594	824	565	-913
12	-433	715	395	-803	-396	688	356	-774	12	-388	683	367	12	-388	683	367	-772
12.5	-252	605	210	-686	-226	581	188	-634	12.5	-215	570	183	12.5	-215	570	183	-652
13	-119	524	76	-626	-111	511	70	-546	13	-94	497	62	13	-94	497	62	-590
13.5	-20	461	-22	-548	-19	451	-23	-502	13.5	-8	440	-26	13.5	-8	440	-26	-520

North Northeast Slope Indicator

West
-334
-317
-267
-291
-273
-165
-205
-336
-548
-783
-996
-1155
-1211
-1345
-1573
-1407
-990
-802
-646
-570
-491

Southeast Slope Indicator

West
-797
-906
-1001
-1048
-1022
-910
-892
-874
-926
-882
-776
-600
-833
-2579
-3868
-4025
-2872
-1545
-779
-645
-741
-981
-1235
-1315

South Southwest Slope Indicator

SSW S15				
April 22.				
Deformation				
Depth	North	East	South	West
0.5	179	-142	-189	29
1	-42	-68	-50	-90
1.5	-205	5	147	-140
2	-252	28	245	-134
2.5	-243	38	231	-151
3	-193	99	137	-182
3.5	-166	129	123	-229
4	-174	152	110	-258
4.5	-276	199	238	-286
5	-257	323	210	-405
5.5	-217	320	175	-445
6	-123	283	79	-368
6.5	-64	348	23	-434
7	131	317	-173	-419
7.5	468	146	-515	-266
8	631	-94	-676	-9
8.5	828	-347	-891	242
9	1061	-713	-1113	593
9.5	1311	-1097	-1357	1002
10	1604	-1563	-1640	1500
10.5	2029	-2288	-2078	2191
11	2025	-2472	-2089	2355
11.5	1124	-1461	-1180	1424
12	410	-609	-459	521
12.5	113	-135	-156	28
13	64	47	-113	-134
13.5	96	138	-143	-233
14	106	107	-151	-189
14.5	65	84	-111	-169
15	42	68	-88	-152
15.5	13	49	-63	-136
16	-3	37	-47	-120
16.5	40	18	-86	-103
17	50	-1	-97	-82
17.5	89	-20	-134	-68
18	107	-41	-151	-45
18.5	161	-69	-206	-21

Southwest Slope Indicator

SW S12 April 22.	Deformation						SW S12 May 9.	Deformation						SW S12 May 18.	Deformation					
	North	East	South	West	Depth	North		East	South	West	Depth	North	East		South	West	Depth	North	East	South
0.5	-142	-836	84	724	0.5	-66	-816	84	714	0.5	-107	-720	126	718						
1	-165	-685	82	612	1	-100	-703	67	665	1	-124	-643	98	622						
1.5	-109	-654	72	571	1.5	-113	-659	93	605	1.5	-121	-642	80	556						
2	-124	-628	84	539	2	-115	-624	95	580	2	-98	-619	78	549						
2.5	-278	-599	244	491	2.5	-275	-594	239	543	2.5	-258	-609	240	499						
3	-247	-538	198	505	3	-229	-595	184	533	3	-229	-594	203	503						
3.5	-202	-490	149	483	3.5	-187	-562	181	458	3.5	-177	-552	159	476						
4	-200	-528	149	458	4	-184	-546	164	464	4	-186	-540	158	460						
4.5	-185	-532	136	456	4.5	-173	-531	147	496	4.5	-174	-547	149	459						
5	-136	-520	93	465	5	-130	-553	107	479	5	-112	-559	100	475						
5.5	-203	-545	156	463	5.5	-197	-563	190	477	5.5	-194	-553	159	468						
6	-218	-554	178	475	6	-212	-567	189	537	6	-196	-526	185	494						
6.5	-229	-581	185	498	6.5	-225	-574	195	518	6.5	-228	-584	197	510						
7	-193	-625	146	530	7	-190	-614	165	553	7	-191	-633	160	543						
7.5	-126	-701	76	599	7.5	-124	-686	86	643	7.5	-120	-712	86	611						
8	-17	-796	-33	703	8	-2	-797	-38	733	8	-1	-813	-38	730						
8.5	36	-813	-72	715	8.5	60	-822	-95	787	8.5	72	-836	-95	745						
9	-1	-773	-34	693	9	19	-788	-47	739	9	28	-775	-47	715						
9.5	-43	-745	-4	653	9.5	-42	-739	27	667	9.5	-45	-742	15	668						
10	112	-762	-157	690	10	127	-776	-130	662	10	119	-790	-153	711						
10.5	308	-832	-351	750	10.5	345	-856	-371	801	10.5	342	-868	-375	778						
11	345	-840	-384	752	11	373	-857	-395	776	11	401	-816	-401	758						
11.5	267	-746	-304	642	11.5	284	-745	-287	672	11.5	291	-731	-313	643						
12	171	-627	-215	540	12	182	-630	-222	533	12	193	-616	-217	534						
12.5	109	-527	-151	437	12.5	114	-524	-133	439	12.5	143	-552	-144	441						
13	84	-434	-125	350	13	88	-431	-135	373	13	139	-379	-122	359						
13.5	93	-384	-133	299	13.5	96	-376	-134	304	13.5	149	-390	-127	296						
14	49	-360	-96	276	14	59	-354	-101	278	14	66	-371	-96	276						

Southwest Slope Indicator

SW SI2	Deformation						SW SI2	Deformation						SW SI2	Deformation					
	North	East	South	West	Depth	North		East	South	West	Depth	North	East		South	West	Depth	North	East	South
June 10.							June 22.							July 5.						
0.5	286	-1886	-1240	2505	0.5	-59	0.5	-59	14	-10495	16383	3.5	-104	3.5	-104	-722	143			
1	540	-1165	-366	1324	1	-31	1	-31	21	1435	707	4	-194	4	-194	-618	168			
1.5	201	-976	-213	905	1.5	56	1.5	56	16	-429	-152	4.5	-211	4.5	-211	-574	167			
2	33	-772	-120	640	2	-299	2	-299	-98	-170	606	5	-156	5	-156	-579	117			
2.5	-205	-628	158	544	2.5	-361	2.5	-361	-669	382	568	5.5	-227	5.5	-227	-574	174			
3	-235	-553	171	502	3	-338	3	-338	-656	307	566	6	-244	6	-244	-577	199			
3.5	-209	-572	162	496	3.5	-227	3.5	-227	-599	190	529	6.5	-264	6.5	-264	-595	220			
4	-206	-552	161	478	4	-194	4	-194	-565	159	491	7	-226	7	-226	-652	176			
4.5	-189	-540	144	475	4.5	-184	4.5	-184	-546	149	474	7.5	-141	7.5	-141	-740	91			
5	-138	-573	96	495	5	-138	5	-138	-569	100	484	8	-9	8	-9	-833	-45			
5.5	-199	-575	149	489	5.5	-201	5.5	-201	-569	157	484	8.5	77	8.5	77	-851	-114			
6	-218	-579	174	509	6	-222	6	-222	-574	182	507	9	6	9	6	-809	-46			
6.5	-242	-582	197	511	6.5	-244	6.5	-244	-586	202	514	9.5	-67	9.5	-67	-755	24			
7	-209	-614	166	535	7	-212	7	-212	-626	165	544	10	135	10	135	-768	-177			
7.5	-138	-692	86	608	7.5	-132	7.5	-132	-713	83	620	10.5	346	10.5	346	-784	-389			
8	-5	-813	-46	725	8	2	8	2	-818	-53	740	11	363	11	363	-737	-407			
8.5	88	-858	-124	767	8.5	89	8.5	89	-859	-127	768	11.5	286	11.5	286	-657	-335			
9	47	-819	-83	729	9	38	9	38	-808	-72	733	12	191	12	191	-595	-240			
9.5	-57	-755	15	676	9.5	-62	9.5	-62	-757	17	679	12.5	121	12.5	121	-519	-164			
10	114	-785	-155	717	10	118	10	118	-797	-164	717	13	86	13	86	-445	-133			
10.5	363	-877	-408	807	10.5	356	10.5	356	-853	-403	769	13.5	88	13.5	88	-385	-133			
11	398	-860	-442	782	11	383	11	383	-826	-420	744	14	53	14	53	-362	-101			
11.5	293	-747	-334	661	11.5	283	11.5	283	-717	-314	637									
12	187	-635	-229	551	12	175	12	175	-618	-217	529									
12.5	107	-548	-153	445	12.5	105	12.5	105	-525	-145	440									
13	84	-441	-131	366	13	81	13	81	-441	-122	358									
13.5	90	-387	-134	308	13.5	89	13.5	89	-386	-128	301									
14	58	-360	-107	286	14	55	14	55	-358	-97	276									

APPENDIX H

EXTENDED OPERATIONS ON SPRAY ICE

**REPORT PREPARED BY Wm. St. Lawrence Documenting POLAR ALPINE'S
EXPERIENCE WITH EXTENDING OPERATIONS ON SPRAY ICE FEATURES.**



AND OPERATION ON SPRAY

EXTENDED OPERATIONS ON SPRAY ICE

October 25, 1989

Submitted To:

**Mr. James P. Poplin
Research Department
ESSO RESOURCES CANADA LIMITED
339- 50th Avenue S.E.
Calgary, Alberta T2G 2B3
Canada**

POLAR ALPINE, INC.

**1442A Walnut Sr. #236
Berkeley, CA 94709
(415) 524-1271**

TABLE OF CONTENTS

	PAGE
TABLE OF CONTENTS	i
LIST OF PHOTOGRAPHS	ii
LIST OF FIGURES	iii
LIST OF TABLES	iv
INTRODUCTION	1
SPRAY ICE CONSTRUCTION	3
Nome	3
Red Dog Seaport	6
OVER ICE OPERATIONS	8
STRESS ANALYSIS	13
ABLATION PROTECTION AND SURFACE PREPARATION	22
SPRAY ICE REMOVAL AND EXCAVATION	23
SUMMARY	27
RECOMMENDATIONS	30
REFERENCES	31

LIST OF PHOTOGRAPHS

	page
PHOTOGRAPH 1. An aerial view of the dredge Bima and the Aquamarine behind the spray ice barrier constructed at the causeway at Nome.	4
PHOTOGRAPH 2. An aerial view of the spray ice causeway and protective berm constructed at the Red Dog Port Site, Alaska.	7
PHOTOGRAPH 3. A D-6 Caterpillar tractor working at the edge of unconsolidated spray ice.	10
PHOTOGRAPH 4. A crane operating a dragline at the edge of well-sintered spray ice.	11
PHOTOGRAPH 5. Manitowoc crane operating on crane mats on a raised spray ice platform.	21
PHOTOGRAPH 6. A closeup view of the spray ice causeway with the gravel surface at the Red Dog Port Site.	24
PHOTOGRAPH 7. Backhoe and crane excavating spray ice at the Nome barrier.	26
PHOTOGRAPH 8. The tug Aquamarine wheelwashing spray ice.	28

LIST OF FIGURES

	page
FIGURE 1. Map showing the location of the Red Dog Port Site and the Port of Nome.	2
FIGURE 2. Effective stress state at failure. This figure is reproduced from the paper by Chen and Gram, (reference 3)	14
FIGURE 3. Material model used for finite element stress analysis	16
FIGURE 4. Results of stress analysis for different loading configurations, (a) stress field due to body force alone, (b) geometry of a 276 kPa load applied over a 6 m region, (c) region of failed spray ice using Chen/Gram failure envelope.	18
FIGURE 5. Failure threshold when the load is moved to the edge of the spray ice. In this instance failure occurred when the ground pressure was raised to 145 kPa.	20

LIST OF TABLES

	page
TABLE I. Ground pressure of different types of equipment and the effect of using crane mats to lower the bearing pressure.	12

INTRODUCTION

This report is the result of experience gained over the past several years operating on spray ice in sub-arctic and marginally arctic conditions. The spray ice structures we have been involved with were constructed at Nome and at the Red Dog Port Site site 6 km south of Kivalina, Alaska. The location of these sites is shown in Figure 1.

The spray ice structures we built differed in several ways from the spray ice structures used as oil drilling platforms. Unlike the fairly massive spray ice islands of the Arctic, the structures built at Nome and at the Red Dog Port Site were relatively small. The quantity of spray ice involved in our structures typically ranged from 150,000 to 300,000 cubic meters. Also the structures tended to be linear as opposed to the quasi-cylindrical nature of spray ice islands. At the Red Dog Port Site a spray ice causeway was constructed which had a length of approximately 250 meters and a working surface width of 15 meters. Over this causeway heavy equipment was moved constantly in temperatures that were often above the freezing point of water.

In the operations at Nome the requirement was to build a protective barrier around the gold dredge Bima and the anchor-handling tug Aquamarine. In addition to providing protection against damage by ice movement, the spray ice barrier at Nome also had to function as work surface over which heavy equipment could be moved. Operations carried out on the spray ice were such that equipment had to be positioned at the edge of over-steepened slopes of the spray ice. In this region work is not usually carried out on spray ice islands.

In both the Nome and Red Dog construction projects it was also necessary that the spray ice structure be removed as soon as possible after the beginning of the open water season. In the Nome operation, any delay in removing the spray ice kept the dredge from operating. In Nome techniques were developed to remove the spray ice by both excavation and agitation of the sea water.

In the case of the Red Dog Seaport project the spray ice causeway disintegrated naturally under the force of wave action on the barrier.

An especially troublesome problem during the course of our work was hardening the surface of the spray ice to enable equipment to operate on it. This was particularly important in the case of the Red Dog project where the spray ice causeway would be utilized as a roadway for dump trucks

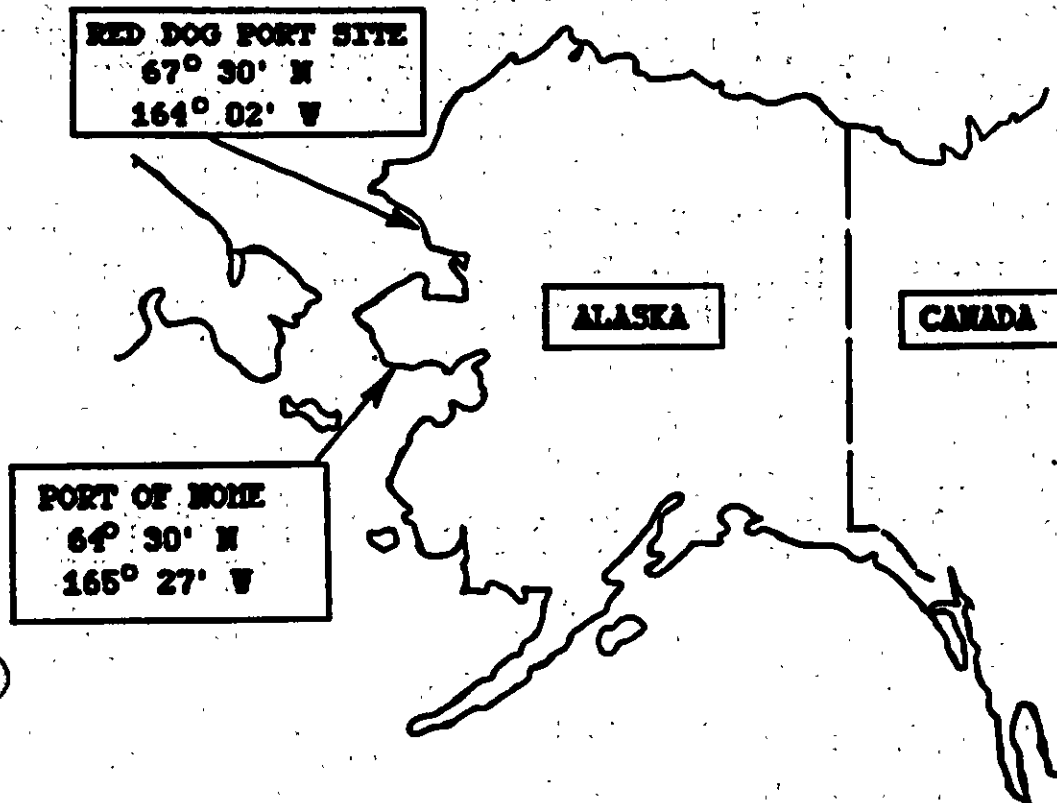


FIGURE 1. Map showing the location of the Red Dog Port Site and the Port of Nome

hauling gravel to construct the permanent port facility. In both the Nome project and the Red Dog project the relatively high ambient air temperatures precluded hardening the surface by spraying water on it and letting it freeze. In the case of the Red Dog site, even if the temperatures were low enough to condition the surface with water, the surface probably would not have survived under the continuous wear and tear imposed by the dump trucks. At the peak of the operation trucks were hauling loads of gravel at three-minute intervals over the spray ice causeway.

In this report we present our experience in working with small spray ice structures in relatively warm environments. The special emphasis in this report is the manner in which we prepared the spray ice surfaces for operation, excavation of spray ice, operating heavy equipment at the edge of spray ice structures and the technique used for removing large quantities of spray ice in a very short time. Preliminary to these discussions, the construction of the spray ice structures that were built is discussed.

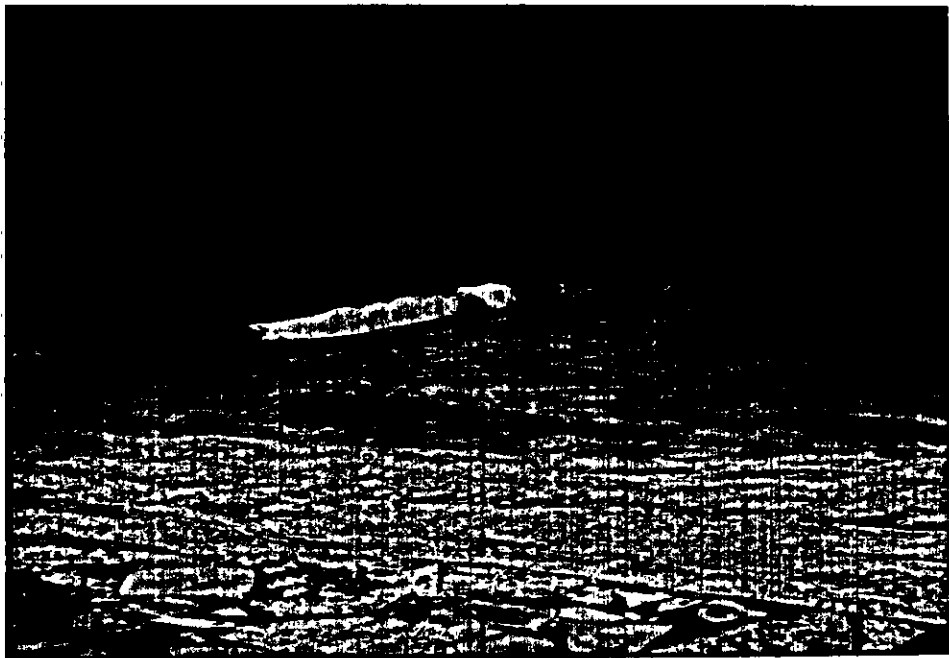
SPRAY ICE CONSTRUCTION

Nome

During the winter of 1987-88 and again during the winter of 1988-89 a spray ice barrier was constructed at Nome, Alaska (64° 30'N, 165° 27'W). The purpose this barrier was to protect the gold dredge Bima and the anchor-handling tug Aquamarine from winter and spring ice movements. This was particularly important since neither vessel was ice reinforced.

The spray ice barrier built during the 1987-88 winter was constructed by spraying water into the air in combination with compressed air (described in Polar Alpine Inc. report to ESSO Resources Canada, June, 1988) and also by hauling snow from around Nome. The hauled snow was dumped in place with dump trucks. Photograph 1 is an aerial view of the Bima and Aquamarine inside the protective barrier built during 1987-88.

To establish a scale for Photograph 1, the dredge Bima has a 110 m length and 31 m beam at the waterline and stands 43 m high above the waterline. The tug Aquamarine is 56 m long and has a beam of 15 m. The vessels were moored against the causeway at Nome for the winter in water depths that ranged from 3 m to 4 m. The spray ice barrier was built in a horseshoe around the vessels. The barrier was approximately 300 m along its center line, 30 m across at the waterline and stood 10 m high in places above the waterline. The volume of material used in constructing the 1987-88 barrier was estimated at 175,000 cubic meters.



PHOTOGRAPH 1. An aerial view of the dredge Bima and the Aquamarine behind the spray ice barrier constructed at the causeway at Nome.

POLAR & POLAR ALPINE, INC.

Photograph 1, taken in the spring of 1988, shows the berm in place around the vessels. The white snow of the barrier is where the spray ice was placed primarily by spraying. The dark material at the bow and stern of the Bima is the region where material was placed from snow scavenged from around Nome. When the snow was initially placed the concentration of foreign particles such as dirt and gravel was relatively light and the snow had a tan color. As melting took place the impurities concentrated on the surface to form a solid layer. Initially the rate of melting in the contaminated snow was greater than non-contaminated snow. As melting progressed and the contaminant layer thickened, the rate of surface ablation decreased dramatically.

We observed that the contaminated surface, in addition to slowing the melting rate, was considerably tougher than the uncontaminated layer. This was particularly evident when heavy equipment was operated over the spray ice.

During the winter and spring of 1988 a number of maintenance operations were carried out on the Bima and Aquamarine. These operations included excavating the spray ice to gain access to the hulls of each vessel and operating cranes and other heavy equipment close to the edge of the excavated ice. Prior to the sea ice around the berm going out, a channel was excavated with a backhoe and a dragline to a point close to the edge of the sea ice-spray ice interface in the vicinity of the Aquamarine. Once the spray ice went out the remainder of the spray ice in the channel was removed and the tug maneuvered outside of the spray ice barrier. The tug (tethered to the Bima) was then used to backwash away the remaining spray ice.

During the winter of 1988-89 the berm around the Bima and Aquamarine was again constructed. Changes made during that season were that the berm was constructed completely with the sprayed water-air system; no material was brought in with trucks. Also, the north end of the berm (the end closest to shore) was left open. Leaving the north end of the berm open was warranted since there could be no significant ice forces generated from this direction due to the proximity of the shoreline. Repair operations were again carried out on the vessels from the spray ice. The spray ice was removed expeditiously in the spring with the Aquamarine.

From our operations at Nome during the 1987-88 season we found that we could build a spray ice structure in the relatively warm climate at Nome; excavate spray ice to contour it to the form we desired; operate heavy equipment close to the edge of the spray ice; harden the surface and slow surface melting with the addition of surface coatings; and remove the spray ice rapidly when required.

Red Dog Port Site

Given the success of the spray ice barrier at Nome during the 1987-88 winter season, we were approached to design and oversee the construction of a spray ice causeway and protective barrier at the Red Dog Port Site (67° 30'N, 164° 02'W) on the Chukchi Sea in Alaska. The purpose of the causeway was to provide a structure over which equipment could be moved to build a sheetpile-encased, gravel-filled "sea cell." The cell to be built was 23 m in diameter and stood 8 m above the sea surface in water 5 m deep. This was the third of three cells to be built and was the farthest of the three from shore. Attempts to construct the cell during the open water season had failed when the cell was destroyed during a storm while under construction.

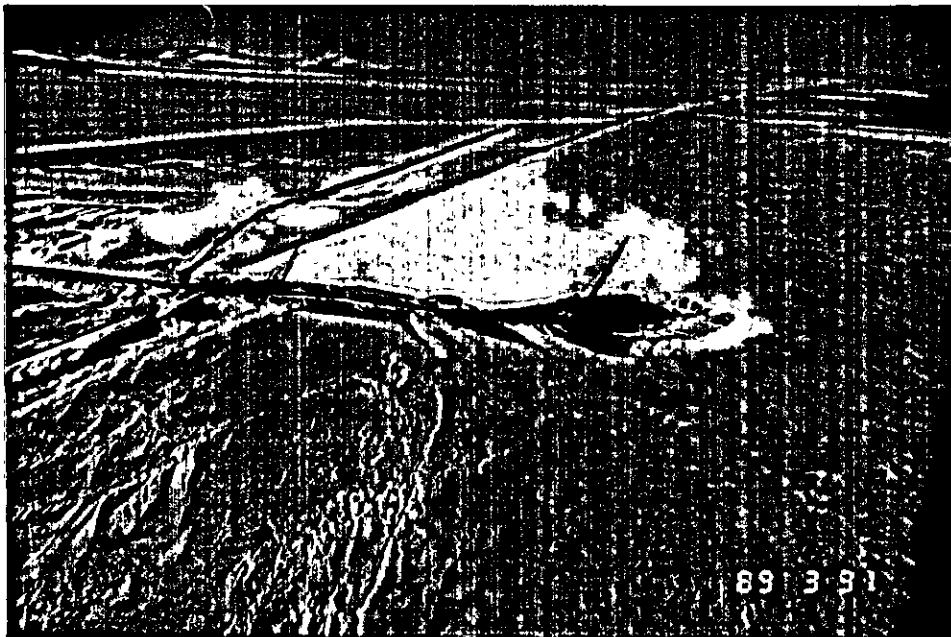
The primary requirements for this operation were that the causeway be constructed with sufficient strength to support a crane with a mass of 225,000 kg driving and extracting piles. In addition, the surface had to be resilient enough to withstand dump trucks hauling gravel to fill cells No. 2 and 3. (Note: Construction on cell No. 2 had to be terminated before completion due to operating conditions the previous summer.)

In addition to constructing the causeway, a barrier had to be constructed around the area of cell No. 3. The purpose of the barrier was to protect the sheet piling structure before it was filled with gravel and before it had sufficient strength to withstand ice loads.

Photograph 2, taken March 31, 1989 shows cell No. 3 under construction. This photograph also shows the protective spray ice berm around cell No. 3 used for spray ice construction and also a portion of the spray ice causeway leading to the construction area. Cell No. 1 is the cylindrical structure at the left side of the photograph. For scale, the boom on the crane in Photograph 2 is 52 m in length.

At the completion of the causeway construction phase of the program temperatures ranged from -4° to +2° C. The spray ice surface was weak and there was little hope of operating large trucks and other heavy equipment over the surface. Drawing on our observations at Nome the previous season, we placed a layer of gravel 150 mm to 300 mm thick on the surface of the spray ice. This gravel layer appears as the brown on the surface of the causeway in Photograph 1.

The causeway and protective barrier was constructed using the water-air spray method employed at Nome. When temperatures dropped below -20° * C, spraying was done with water, but no compressed air.



PHOTOGRAPH 2. An aerial view of the spray ice causeway and protective berm constructed at the Red Dog Port Site, Alaska.

To expedite the construction of the barrier in face of temperatures too high for the water-only spraying system or the air-water spray system, snow was scavenged from snowdrifts around the area. The snow was loaded into dump trucks and deposited in the construction area.

Within a 2 km range of the spray ice construction site we estimated that 20,000 cubic meters of snow was deposited in drifts. Interestingly we found that before we could deplete the supply of drifted snow, storms occurred and the source of snow for hauling was renewed due to new drifting in and around structures in the area. Approximately one-third of the spray ice used for construction was from snow hauled to the site from drifts.

As a construction note, the causeway shown in Photograph 2 was built on a second attempt. Initial construction was started December 19, 1988. A storm on January 6, 1989 broke up the sea ice and on January 7 the causeway washed away with a good deal of the construction equipment.

Given this background we can explore in more detail how our experience on these spray ice structures can be transferred to operations in arctic water.

OVER-ICE OPERATIONS

Major concerns while operating on the spray ice surface involved using heavy equipment on the surface and close to the ice edge. Unlike spray ice islands used for exploratory drilling, the Nome and Red Dog structures were relatively narrow.

The spray ice causeway at the Red Dog site had a designed working surface 15m wide. The largest piece of equipment to be moved over the surface was a Manitowoc model 4100 Series-2 crane. With the crawler extended the width of this unit was 6.4 m. The mass of this crane was estimated at 228,000 kg. The ground pressure exerted by this unit was estimated to be 130 kPa. In addition to the dead-load weight, it was determined that maximum loads would be exerted during pile-extraction operations.

While working the crane would be positioned close to a vertical edge of the spray ice. Other equipment was also operated over the causeway. From our experience in Nome the previous season we were fairly confident that we could operate the equipment on the spray ice with a minimum of problems.

Several examples from our Nome experience the previous season illustrate the strength of the barrier. Photograph 3 shows a Caterpillar D-6 operating very close to edge of the spray

ice. In this case an attempt was being made to start a barrier for the Bima and Aquamarine before the sea ice was formed. It was not successful. It is important to note here that in the case illustrated in Photograph 3 the material was loose snow being trucked onto the gravel jetty at Nome and then bulldozed off the jetty to form the beginnings of the ramp shown.

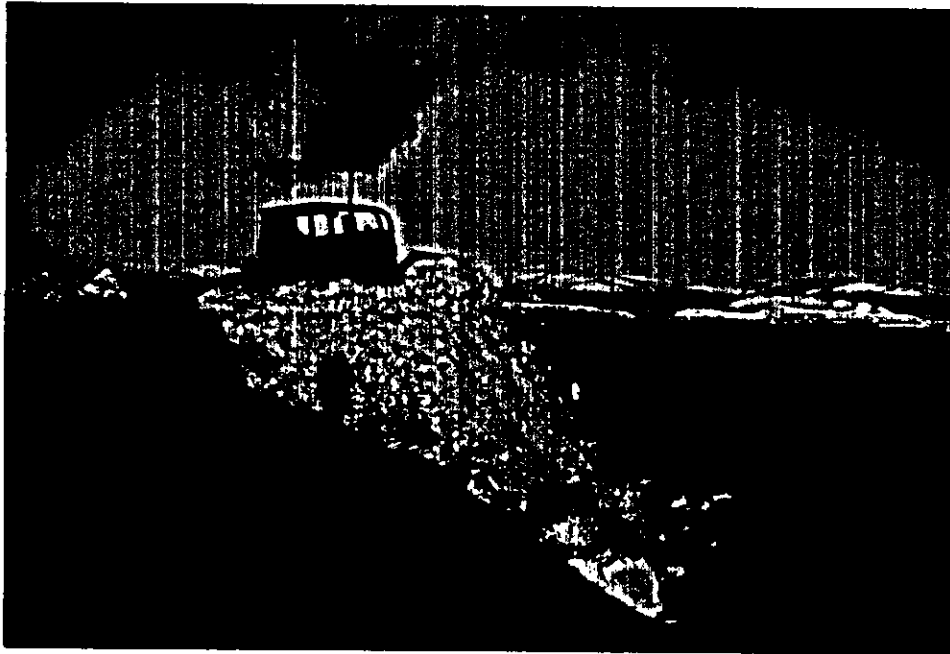
Operating this close to the edge of unsintered spray ice is not recommended. At a latter stage of the operation the toe of the spray ice ramp failed and the cat that was pushing the snow slid down the failed toe and into the water. From Photograph 3 we can see that the material, even though loose and unsintered at the time, had sufficient strength to support an operating D-6.

In contrast to the example of equipment working on loose, unsintered snow, Photograph 4 shows a crane operating on the edge of sintered and seasoned spray ice. As the photo shows, the crane is excavating the spray ice with a dragline. Note that the track of the crawler on the crane is extremely close to the edge of the spray ice. We experienced no spray ice failures operating equipment this close to the edge of seasoned spray ice.

A more conservative approach to operating equipment on spray ice was used on the Red Dog project. Every effort was made to reduce the potential for a material failure while continuing to use the structure. The primary concern was to keep the two Manitowoc cranes from tipping or failing the spray ice.

Table I provides the equipment loads, in terms of ground pressure, that various types of equipment would subject the spray ice to. Cranes were operated off of crane mats (rig mats) to lower the ground pressures. A single section of crane mat consisted of 0.3 m by 0.3 m by 7.3 m timbers fastened together edge to edge. Typically the mats were either 7.3 m by 1.83 m (24'x 6') or 7.3 m by 2.44 m (24'x8'). The mats were used in varied configurations to spread the loads out over the spray ice. The effectiveness of the crane mats in lowering the effective ground pressure is shown in Table I.

As can be noted in Table I, placing the 4100-S2 on a 7.3 m by 7.3 m crane pad reduces the ground pressure by a factor of 3. Considering that a Caterpillar D-8 can be operated on and near the edge of spray ice structures indicates that operating a Manitowoc 4100-S2 crane should present little problem. It should be noted that a D-8 can withstand considerable tipping and operation over rough terrain with little problem. As a last resort a 4100-S2 can be used to extricate a D-8 should it become mired or sunk. However, it would be difficult to remove a 4100-S2 with a D-8 should difficulties arise.



PHOTOGRAPH 3. - A D-6 Caterpillar tractor working at the edge of unconsolidated spray ice.



PHOTOGRAPH 4. A crane operating a dragline at the edge of well-sintered spray ice.

TABLE I. Ground pressure of different types of equipment and the effect of using crane mats to lower the bearing pressure.

EQUIPMENT TYPE	WEIGHT (Newtons)	GROUND PRESSURE (kPa)
Manitowoc 4100-S2	2,223,230	130
Caterpillar D-8	409,074*	100
Manitowoc 4100-S2 on a 6m by 7.3m crane pad	2,223,230	50
Caterpillar D-6 Standard Track	168,965*	50
Manitowoc 4100-S2 on a 7.3m by 7.3m crane pad	2,223,230	42
Caterpillar D6H-LGP (wide pad)	191,198	32
Caterpillar D4H-LGP (wide pad)	111,606	28

* estimated weight

As an aside, in remote operations we have always considered what type of equipment would be required to extract another piece of equipment from a difficult situation. If there is a unit that can not be extracted with the equipment at hand, that unit should be operated in a conservative manner.

STRESS ANALYSIS

To obtain a quantitative understanding of the stresses involved in operating equipment on small spray ice structures a linear elastic finite element analysis is carried out. The purpose of this analysis is to determine in a general way what loads can be expected to cause failure in the spray ice.

If we make the assumption that spray ice can be represented as a linear viscoelastic material we can invoke the correspondence principal (1). The correspondence principal may be stated that if the loads are applied to a structure at time zero and held constant, the stresses will be the same as in the elastic structure and the displacements depend on time. Considering the creep (settlement) that has been observed in spray ice and our general understanding of the viscoelastic properties of high density snow (2), application of the correspondence principal seems reasonable.

The analysis carried out was not extremely detailed. The failure criterion used in this analysis is developed from recent data published by Chen and Gram (3). Figure 2 is reproduced from the Chen/Gram publication. Chen and Gram conducted a number of triaxial test on both above-water and below-water spray ice samples. When presented in terms of the effective stress state at failure, the data appears to be well behaved for both the above- and below-water samples.

To utilize the failure information from Chen and Gram, the equation for the straight line they drew through their data was used as the failure envelope. From measurements that we made from their data, the line they fit to their data appears to be represented by the equation:

$$(1) \quad q = (-9,800) + (0.791)[s(1)' + s(3)']/2$$

In Equation 1 q is the maximum shear stress, $s(1)'$ is the maximum principal stress and $s(3)'$ is the minimum principal stress. The (') associated with the values $s(1)'$ and $s(2)'$ indicates the effective stress state, which includes adjustment in the stress value to include a term for the pore pressure. For the above-water spray ice the pore pressure term is negligible.

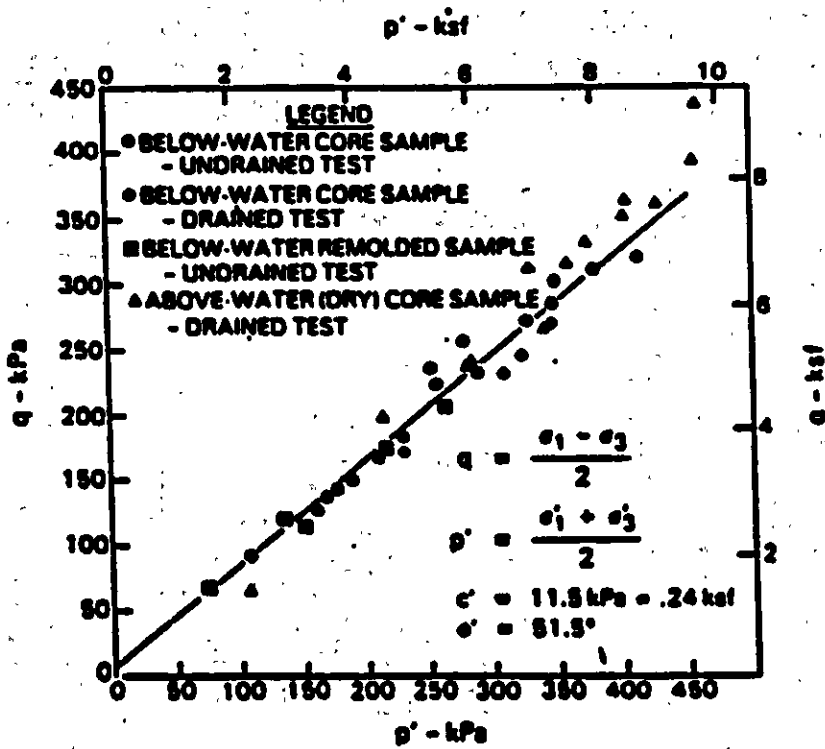


FIGURE 2. Effective stress state at failure. This figure is reproduced from the paper by Chen and Gram, (reference 3)

Equation 1 differs in its representation from that provided by reference (3) in that we admit that spray ice (especially the above-surface spray ice) can support tensional loads. Thus in our application compressional stress is negative and tensional stresses are taken as positive. Mellor (4) suggests that the tensile strength of high-density dry snow is about the same as the shear strength. Also, when operating close to a free surface (such as the equipment shown in Photograph 4) tensional stresses are generated close to the free surface. Typically the tensional stresses are close to an order of magnitude less than the compressional stresses.

As a point of clarification, if the data taken in Figure 2 is interpreted as is presented, it suggests that no matter how low the principle stresses the material will fail. In our analysis we have used a maximum shear stress of 100 kPa (14.5 psi) as the failure stress cut-off value. In the data provided by Chen and Gram our shear stress cut-off excludes all data points except the three lowest. In terms of the above-water spray ice tested, the one low stress failure seemed anomalously low when compared with the other values of above-water strength. We assume the other two data points that fell below this cut off were disturbed samples or represented local weaknesses. Again, our experience with actual loads on spray ice leads to this stress cut-off assumption.

To carry out our analysis we used a four-material model. Figure 3 provides the values used for this model. The values of density for the above-surface and below-surface spray ice were taken from data published by Weaver (4). The moduli values and Poisson's ratio values were taken from data published by Lee et. al. (5) and Mellor (6). The modulus and Poisson's ratio value for sea ice were taken from data published by Croasdale (7). The spray ice was assumed to be resting on a half-meter-thick sheet of sea ice. The sea ice was assumed to be resting on a homogeneous silt layer. The material values used for the silt were taken from Bowles (8). Note that all densities shown in Figure 2 are adjusted for buoyancy.

Only the failure of the spray ice was considered in this analysis. The stress state associated with the silt and sea ice were not considered. In all cases we incorporated the pressures exerted by body forces in the analysis. The finite element analysis conducted was a two-dimensional plane strain analysis.

The initial analysis is carried out on a section of spray ice that is 16 m wide and 6 m thick. The water depth is taken to be 3.5 m. The freeboard of the spray ice is taken to be 3 m. Figure 4a depicts a cross section of the two dimensional plain strain model used.

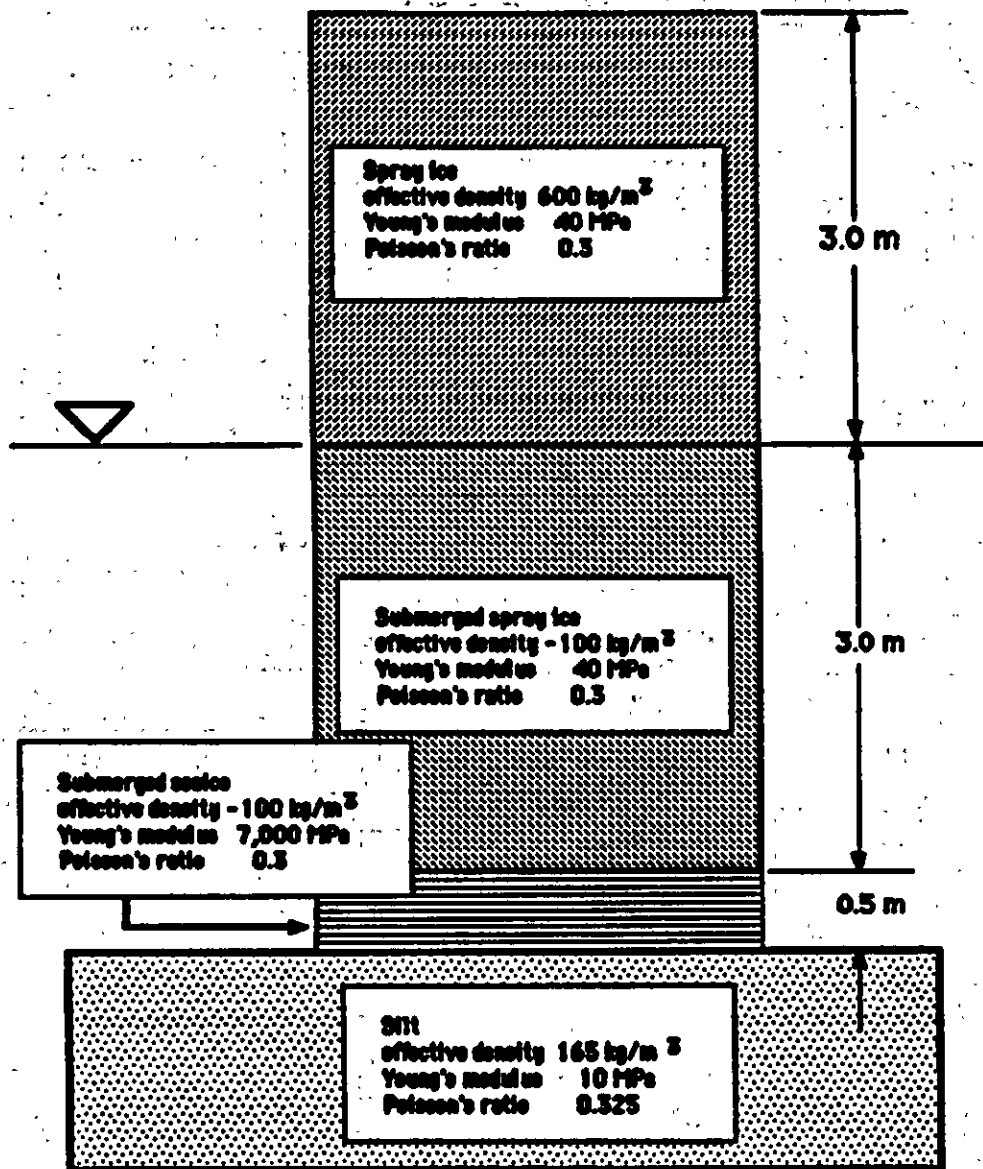


FIGURE 3. Material model used for finite element stress analysis

The first case run (Figure 4a) is for spray ice subjected to overburden pressure only. The purpose of this analysis is to look at the overburden pressure along the section of spray ice and the edge effect present. As predicted from simple analysis of the model used, the maximum overburden pressure should be at the water line. The magnitude of the overburden pressure at the waterline is 17.6 kPa. The overburden pressure at the spray ice/sea ice interface is 14.7 kPa. The effect of the vertical edges on the stress field extends approximately 3 m on each edge. The region of edge effects is shown in Figure 4a. It is noted that the magnitude of the stress variation in the edge zone is 2 kPa.

To examine the loads at which failure would take place a load was applied in the center of the spray ice cross section. The load was spread out over a linear distance of 6m in the center of the cross section. This is depicted schematically in Figure 4b. The intensity of the ground pressure was then increased until failure (according to our failure criterion) took place. We found that failure in the spray ice took place at bearing pressures that exceeded 276 kPa (40 psi). Failure was detected in the subsurface layers when ground pressures exceeded 276 kPa. The pattern of failure that occurred when ground pressure increased is depicted in Figure 4c. The total load applied in this analysis is equivalent to 1,700,000 Newtons (186 tons) per unit of thickness.

It should be noted that the maximum shear stress with an applied bearing pressure of 276 kPa remains below the 100 kPa failure cut-off that we used in the failure criteria. However, the maximum principal stress becomes positive beneath the load. In terms of the data presented on spray ice by Chen and Gram, the failure surface is not defined for positive stresses. The maximum principal stress detected for this loading is a tensile stress of 53 kPa. The minimum principal stress associated with this ground load is a compressional stress of 147 kPa. In carrying out this failure analysis we have assumed that the spray ice can carry a tensile load. For unbonded spray ice, obviously no tensional load can be carried. However, for bonded spray ice we know from past experience that tensional loads can be tolerated. Currently little data exist on the failure of spray ice when the maximum principle stress is tensional.

At this point a conservative approach would suggest that ground pressures for large equipment operating away from the edge of narrow spray ice structures be limited to about 140 kPa. To date we have not experienced failures when operating equipment over narrow spray ice structures with this amplitude of ground pressure.

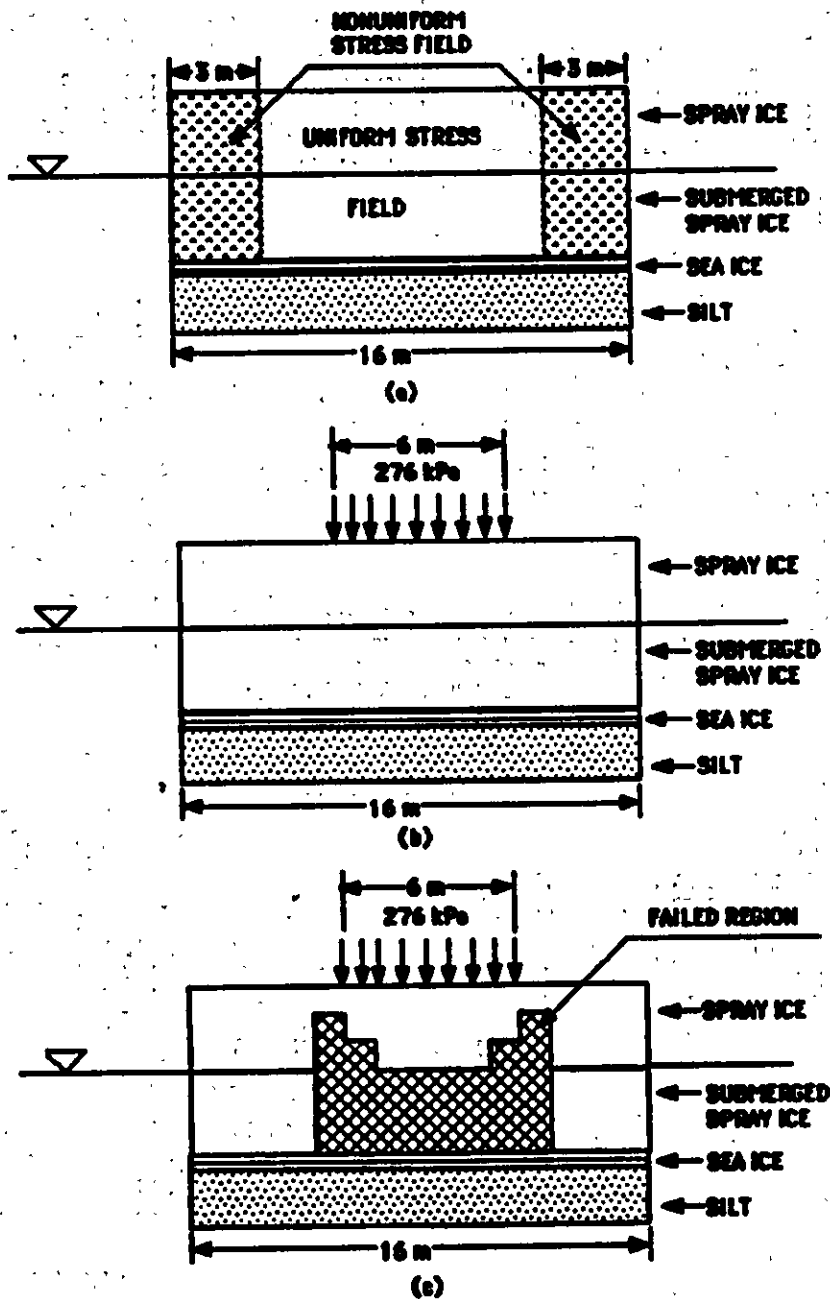


FIGURE 4. Results of stress analysis for different loading configurations, (a) stress field due to body force alone, (b) geometry of a 276 kPa load applied over a 6 m region, (c) region of failed spray ice using Chen/Gram failure envelope.

Having considered operating away from the edge of a narrow spray ice structure, we can look at the magnitude of the loads that can be applied to spray ice when the load is moved to the edge of the structure. To carry out this analysis we used the model in Figure 5. In this case the load was moved to the edge of the spray ice structure. Again the bearing pressure was applied over 6 m. The load was then increased until failure was detected according to the criterion previously established. An edge failure was detected when the bearing pressure reached 145 kPa (21 psi). In this case the failure occurred in the upper edge of the spray ice. When the bearing pressure was lowered to 138 kPa, no failure was indicated. The stress state generated by this loading is close to the stress state generated by the crane operating in Photograph 4.

With all factors considered, we cannot recommend operating equipment with bearing capacities this high close to the edge of a vertical spray ice face. It is feasible, however, to operate heavy equipment at the edge of the spray ice if it is operated off of crane mats or rig mats as described earlier. In the case where a 7.3 m by 7.3 m crane mat is employed with the Manitowoc crane discussed earlier, the bearing pressure drops from 130 kPa to 41 kPa. At this pressure we are operating well away from the failure state for spray ice. It is important to note that when the bearing pressure is dropped to the 41 kPa level the stress field generated in general remains below the failure state defined in (3) without the necessity of imposing a minimum stress cut-off.

The loading configuration shown in Figure 5 should be used only for loading equipment on or off of the spray ice. If the load is moved a short distance from the edge, the edge loading drops significantly. For example, if a 172 kPa load is applied as shown in Figure 5, the maximum shear stress in that vicinity is approximately 122 kPa. If the same load is moved back one meter from the edge, the maximum shear stress drops to 37 kPa at the same point.

Photograph 5 is an example of the application of this principle. In this case a crane pad was built up approximately 1.5 m above the surrounding spray ice. Crane mats were put in place approximately 1 m from the edge and the crane moved onto the mats. The crane worked from this platform for several weeks without the spray ice failing. It should also be noted that the spray ice used was dumped in place. When placed it was a loose material with virtually no cohesion. The strength of this material would fall at the lower end of the failure strengths that Chen and Gram measured.

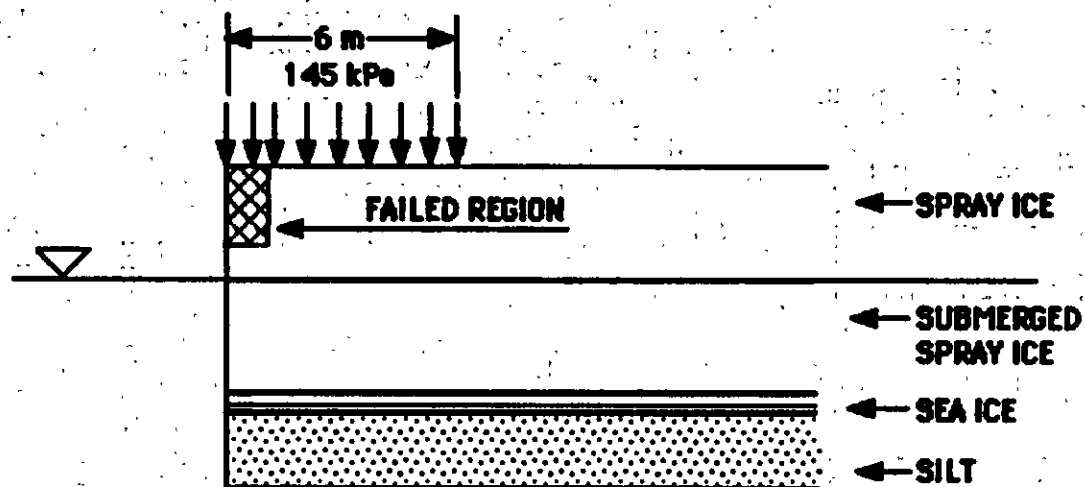
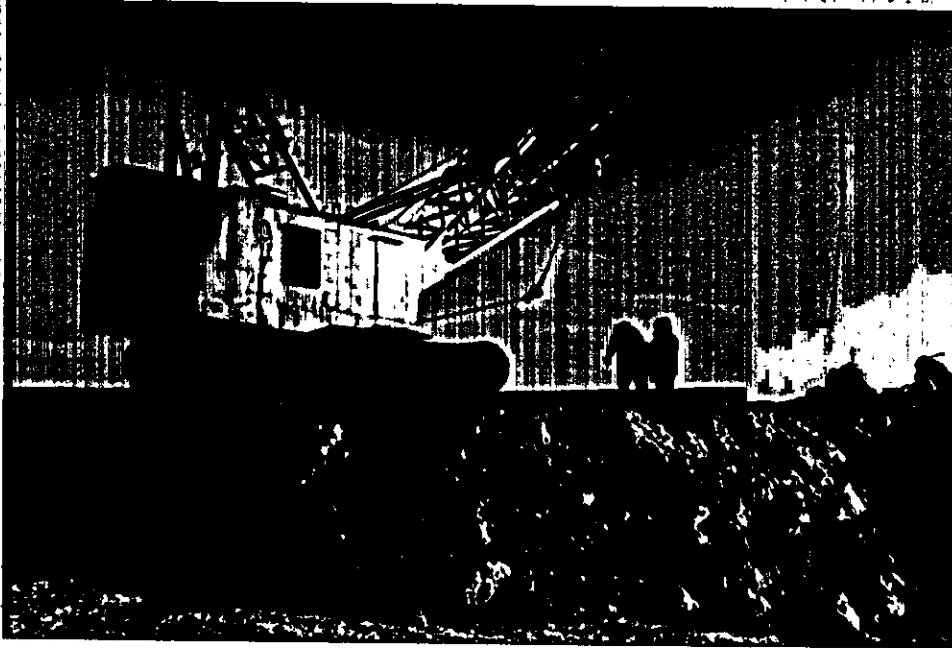


FIGURE 5. Failure threshold when the load is moved to the edge of the spray ice. In this instance failure occurred when the ground pressure was raised to 145 kPa.



PHOTOGRAPH 5. Manitowoc crane operating on crane mats on a raised spray ice platform.

ABLATION PROTECTION AND SURFACE PREPARATION

In the last section we were able to gain a quantitative insight into the strength of spray ice. When we consider how to prepare the surface of spray ice for over-ice operation and how to retard melting we face a less well-defined topic. In general there is little information in the literature on either strengthening spray ice surfaces or attenuating the ablation of these surfaces.

Some information relevant to the strengthening of snow has been presented by Lee et. al. (5). In their work they attempted to strengthen snow runways in Antarctica. The snow densities they were dealing with were in the vicinity of 532 kg per cubic meter. This density is similar to the density of above-water spray ice. From past experience with both snow and spray ice we again emphasize the materials are identical for all practical purposes.

To strengthen the snow and increase its durability the investigators added polystyrene beads in one instance, and sawdust in another. The results of their investigation showed that adding polystyrene was counter-productive. They obtained limited success with the sawdust.

At concentrations of 10% sawdust by volume the investigators found that at strains greater than 12% a noticeable increase in the stress response and the tangent modulus was recorded. In the field they found that the addition of sawdust or wood chips with the snow significantly increased the density, strength and hardness of the snow surface. They also determined that wood additives worked better at higher ambient temperatures.

On the negative side the investigators found that during periods of warm sunny weather the surfaces became more rutted than snow-only sections of road or runway. They attributed the increased surface roughness to increased melting of the snow surface due to a decrease in the albedo of the snow.

Most literature addresses specifically how to decrease the ablation of snow and ice. Some effort has been made in attempts to increase the rate of snow and ice ablation. Recently Colbeck (9) reviewed the work in this area. In attempts to increase snow melt with surface additives such as carbon black it was found that in some instances the rate of melting was decreased. If the surface coating completely covered the surface it was found that surface ablation was inhibited. One explanation provided is that under this condition, not all of the heat that is applied to the surface of the covering layer is transmitted to the snow layer.

In terms of the thickness of surface coatings, it is reported that a layer of sand, gravel or volcanic ash greater than from 1 to 24 mm inhibits surface melting. It was also found that finer materials tend to insulate better than coarse ones.

The information presented by Colbeck (9) is generally in accord with our own observations. When sand or gravel is mixed with the spray ice, even in relatively small concentrations, the resulting mixture appeared to be stronger than the spray ice alone. As the melt season progressed, spray ice that had dirt particles dispersed in it tended to melt more rapidly than uncontaminated spray ice. However, once the surface melted to the point where the impurities formed a solid layer, the melt rate was retarded. It was also noted at this point when the surface was completely covered a much stronger surface resulted.

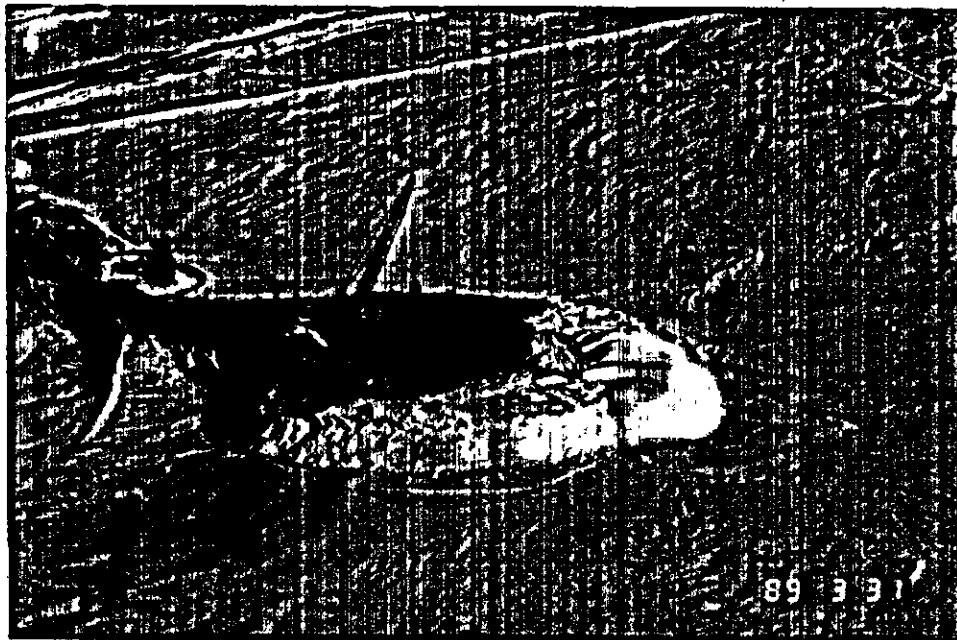
When the Red Dog site was nearing completion the temperatures ranged from -4° C to $+2^{\circ}$ C. Our initial intent was to prepare the surface for operation by spraying water on the surface. Using fresh water at temperatures of -4° C we could not stabilize the surface.

To harden the surface under this condition, a 15- to 30-centimeter layer of gravel was laid down. Using two 12-cubic-yard end dumps (trucks), a surface 200m long and 15m wide was placed in approximately 18 hours. The surface was laid by dumping the gravel and then spreading it with a small bulldozer (D-4). Immediately after the surface layer was placed trucks could operate on it. In fact, to lay the surface the trucks were backed to the edge of the newly spread surface to dump their loads. This causeway was used for a two-month period with virtually no maintenance required to keep the surface intact.

As water and snow mixed with the gravel the surface appeared to harden into a durable operating surface. Over the course of the operation no washboarding of the roadway was experienced. As the work crews became more experienced with operations on the spray ice they also tended to operate the equipment in a more aggressive fashion. At the end of the project in May the cranes were moved onto and off the causeway without the protection of crane mats. Photograph 6 shows a closer view of the spray ice with the gravel surface.

SPRAY ICE REMOVAL AND EXCAVATION

Of some concern in the Nome project and to a lesser extent at the Red Dog Site was how the spray ice could be removed in a timely manner. At the Red Dog Site this did not prove to be



PHOTOGRAPH 6: A closeup view of the spray ice causeway with the gravel surface at the Red Dog Port Site.

a problem. The gravel layer was removed at the end of construction to enhance melting. After the sea ice went out, the wave action against the causeway caused it to break up and wash away. This happened before the first scheduled barges arrived at the seaport.

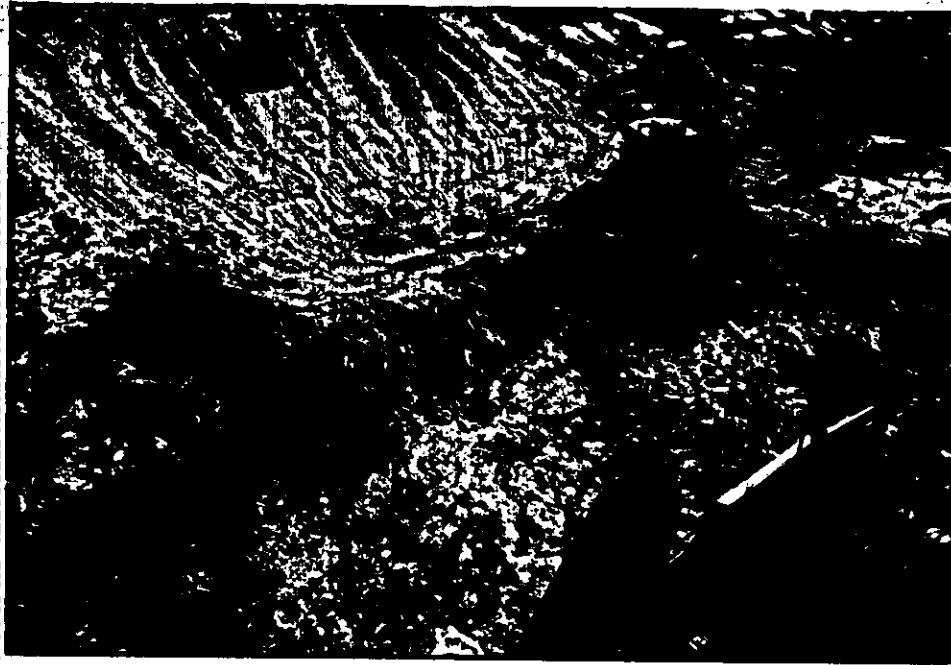
At Nome the problem was more critical: once the sea ice left the vicinity of Nome, the Bima and Aquamarine would be put in use immediately. Each day the vessels were not working revenue was lost.

At the beginning of this project there was no specific information on how to rapidly to remove spray ice. Around the Bima attempts were made to wash away the spray ice with high-pressure water monitors; to remove it with backhoes and draglines; and wheelwash it away with the propwash from the tug Aquamarine. Of the three methods tried, the use of the tug was by far the most efficient.

Attempts to remove the spray ice by directing high-velocity water at the barrier produced only marginal results. A water stream quickly cut a hole or slot in the spray ice. However the effect was very localized. Several days trial proved this technique unsuccessful in clearing away large quantities of spray ice.

The second method involved removing the spray ice with ordinary excavating equipment. Using backhoes and a dragline attached to a crane, a large quantity of spray ice was removed. Photograph 7 shows a backhoe and a dragline-equipped crane excavating spray ice. Although this method proved successful, it was a slow process. The use of this equipment is helpful for excavating where it is necessary to remove material selectively, i.e., to remove spray ice around structures and to contour the side slopes of spray ice for loading and unloading vessels.

In general spray ice offers little resistance to excavation. This is especially true of the upper layers of the material. What is difficult to remove is the natural sea ice layer that is buried at the bottom of the spray ice structure. This layer appears to bond firmly to the bottom and is difficult to break loose with backhoes and draglines. The most successful method found for removing the very bottom layer of material was to remove the spray ice overburden. With enough overburden removed, the base layer would eventually break loose and float to the surface. However, the extent of the overburden that must be removed and the period of time needed for the bottom layer to break loose has not been quantified. In some cases that we observed nearly 100 square meters of overburden was removed from the bottom layer. It sometimes took several days for the bottom layer to break loose and float to the surface.



PHOTOGRAPH 7. Backhoe and crane excavating spray ice at the Nome barrier.

For fast and efficient removal of the spray ice wheelwashing the spray ice with the tug was by far the most effective method. The tug Aquamarine is 56 m in length and has a beam of 12 m. It has three propellers and a rated horsepower of 5700. To remove the spray ice the stern of the tug was attached to a hawser that was tied of to a piling. The tug then worked back and forth while its propwash was directed at the spray ice. In a period of eight to 10 hours over 150,000 cubic meters of spray ice were removed. Photograph 8 is a picture of the tug wheel washing the spray ice.

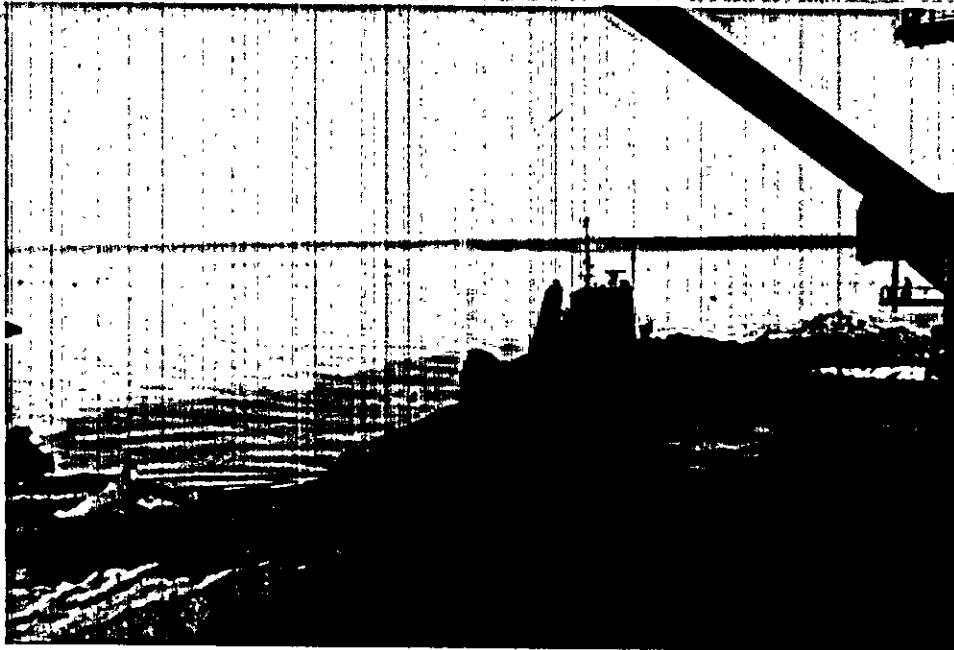
While wheelwashing the spray ice, the propellers operated at relatively low rpm with the boat's engines operating just above idle speed. The exact mechanism by which wheelwashing removes spray ice is not understood. It appears to be a combination of the erosive effects of the water on the spray ice and the thermal degradation of it. Failure of the spray ice takes place when the below water material is sufficiently undercut and the above water portion of the spray ice collapses and was washed away by the propwash. Using this technique there appeared to be no problem removing the bottom layer of natural ice as there was when excavating the material.

SUMMARY

In this report we have outlined our experience operating on spray ice in a somewhat different environment than is usually experienced on spray ice exploration islands in the Arctic. In general, we carried out these operations without prior experience. With minor exception the outcomes were favorable. No equipment was lost and no injuries have occurred. We feel many of the techniques used can be applied to arctic spray ice structures.

Since spray ice structures used for oil exploration are fairly massive, the problems of operating on narrow causeway-type structures are not applicable. However, if plans are made for moving equipment onto or off of spray ice islands onto barges in open water, the experience is directly applicable. Also, to maintain surfaces strong into the melt season surface coatings may be of some use. A landing area for barges loading or off-loading can be prepared with ordinary excavating equipment. If the need should arise to remove a spray ice structure rapidly, a tug boat or icebreaker can be used.

Specifically, to configure the spray ice for a docking operation where equipment can be driven on or off of the structure, ordinary excavating equipment can be used.



PHOTOGRAPH 8. The tug Aquamarine wheelwashing spray ice.

Considering that spray ice can stand vertically without support, we can excavate a docking area into any surface geometry desired. If a new area needs to be built away from the existing spray ice structure, material can be bulldozed into position. It should be noted that when bulldozing spray ice the edgeslope has a much higher angle than when the material is sprayed in place.

For examples of what type of excavations can be carried out in spray ice and the type of equipment that can be used we suggest Mellor's publication of the exploitation of snowfields (10). As indicated earlier in this report, the structure and properties of above-water spray ice are very similar to the structure and properties of snow on polar snowfields. There is a good body of information on the behavior of polar snow, and a reasonable amount of literature exists on engineering projects that have been carried out on the polar snow caps.

Once a barge has been located alongside a spray ice island it should not be difficult to move equipment directly onto and off of the vessel. Care should be taken to operate high ground pressure vehicles on crane mats or rig mats near the edge of the spray ice.

In terms of strengthening the surface of the spray ice islands, our experience with coating the work surface with gravel should be directly applicable. In operating off spray ice islands where a source of material may be difficult to obtain, silt or gravel dredged from the sea bottom might be used.

Finally, if there is a need to remove the spray ice structure, wheelwashing with a tugboat or ice breaker should be employed. In an open water situation an ordinary tug might be used; in ice-overed waters then an ice breaker might be used. A situation where there is a need to remove spray ice in winter is the case where a protective spray ice barrier is built around an offshore structure such as Global Marine's Concrete Island Drilling Structure, and the need arises to remove the barrier so that the structure can be moved to a new location.

RECOMMENDATIONS

The information in this report is based primarily on actual experience. In most instances the work was carried out with little preparation based on our intuition as to how the spray ice would react. We also gained a great deal of information on the behavior of spray ice as we carried out our operations. Considering that we could not locate the information that was needed beforehand in our programs, it would appear that some work should be carried out to explore in a methodical way the parameters in which we can work with spray ice.

It would be useful to extend failure information for spray ice into the region of tensile stresses. We know that the spray ice will take a considerable tensile load. It would be useful if failure criteria could be extended into the tensile regime.

A large-scale test of failure loads would also be useful. In the simplest form, a large-scale test could be carried out by deliberately overloading a section of a spray ice structure. Our experience indicates that on a large scale spray ice is stronger than indicated by small-scale tests.

The addition of foreign substances to the spray ice such as gravel, sand or silt should also be looked at in terms of how various concentrations of impurities affect the strength of the material. Our experience with impurities in the spray ice has indicated that some strengthening of the spray ice occurs.

The effect of surface coatings on slowing the rate of melting should also be considered. This is an area where little or no data exists. In addition to natural coatings such as gravel polystyrene foams have been used to protect spray ice surfaces. The economics of this on a large scale should be considered.

In our work we used a 5,700 horsepower tugboat to remove the spray ice. This tug was used simply because it was available. Indications are that a boat with much less horsepower could be used. Also, the manner in which propwashing affects the spray ice is not understood.

Finally, investigations should be carried out into how to extend the life of spray ice structures into the open water season. Currently the life of spray ice structures is severely limited by the onset of open water. Greater worth would be gained from the use of spray ice structures if they could be utilized during the open water season.

REFERENCES

- (1) Flugge, W. 1967, *Viscoelasticity*, The Blaisdale Publishing Company, Waltham, MA.
- (2) Mellor, M. 1963, *Polar Snow - A Summary of Engineering Properties*. In *Ice and Snow*, Proceedings of a conference held at the Massachusetts Institute of Technology, February 12-16, 1962, M.I.T. Press, Cambridge, MA. pp 528-559
- (3) Chen, A.C.T. and Gram, K.G. 1989, *Strength and Deformation of Spray Ice*, The 10th International Conference on Port and Ocean Engineering under Arctic Conditions, June 12-16, 1989, Lulea Sweden, Vol 2. pp 681-693
- (4) Weaver, J.S., and Gregor, L.C. 1988, *The Design, Construction and Verification of the Angasak Spray Ice Exploration Island*. Proceeding of the Seventh International Conference on Offshore Mechanics and Arctic Engineering. Vol 4. Houston, TX pp 177-183
- (5) Lee, S.M., Haas, W.M., Brown, R.L., Wuori, A.F. 1989, *Improving Snow Roads and Airstrips in Antarctica*, Cold Regions Research and Engineering Laboratory, Hanover, NH. Special Report 89-22
- (6) Mellor, M. 1964, *Properties of Snow*, Cold Regions Science and Engineering, Part III: Engineering, Sect. A: Snow Engineering, Cold Regions Research & Engineering Laboratory, Hanover, NH. Report III-A1.
- (7) Croasdale, K.R. 1980, *Ice Forces on Fixed, Rigid Structures*, In Working Group on Ice Forces on Structures, A State-of-the-Art Report, T. Carstens, Editor. Cold Regions Research and Engineering Laboratory, Hanover, NH, Special report 80-26, pp 34-103.
- (8) Bowles, J.E. 1982, *Foundation Analysis and Design*, McGraw-Hill Book Company, New York, NY
- (9) Colbeck S.C. 1988, *Snowmelt Increase Through Albedo Reduction*, Cold Regions Research and Engineering Laboratory, Hanover NH, Special Report 88-26
- (10) Mellor, M. 1969, *Investigation and Exploitation of Snowfield Sites*. Cold Regions Research and Engineering Laboratory, Hanover, NH, Monograph III-A2B